Università degli Studi di Ferrara

ISTITUTO ITALIANO DI TECNOLOGIA

DOCTORAL COURSE IN
"Translational Neurosciences and Neurotechnologies"

CYCLE XXXIV

COORDINATOR Prof. Luciano Fadiga

"LRRK2 regulates Glucocerebrosidase activity and autophagy in vivo"

Scientific/Disciplinary Sector (SDS) BIO/14

Candidate
Dott. Albanese Federica

_____
(signature)

Supervisor
Prof. Morari Michele

_____
(signature)

Year 2019/2021

ABSTRACT

Mutations in leucine-rich repeat kinase 2 (LRRK2) have been associated with Parkinson's Disease (PD). One of the proposed mechanisms underlying the pathogenic effect of LRRK2 mutants in PD is the modulation of the autophagy-lysosomal pathway (ALP). Indeed, ALP impairment causes aberrant and misfolded α-synuclein (α-syn) accumulation, a common feature of idiopathic and LRRK2-related PD. In the first part of the study, LRRK2 kinase regulation of ALP, its age-dependence and relation with pSer129 α-synuclein inclusions were investigated *in vivo.* Striatal ALP markers were analyzed by Western blotting in 3, 12 and 20-month-old LRRK2 G2019S Knock-in (KI) mice (bearing an increased LRRK2 kinase activity), LRRK2 knock-out (KO) mice, LRRK2 D1994S KI mice (bearing a kinase-dead mutation, KD mice) and WT mice as controls. Striatal gene expression of ALP-related genes was investigated by RT-qPCR. Treatment with the lysosomotrophic compound Chloroquine, CQ, was performed to assess the autophagic flux *in vivo*. The activity of the lysosomal enzyme Glucocerebrosidase (GCase) was measured in the striatum of mice at 3 and 12 months. Finally, immunofluorescence analysis was conducted to evaluate whether LC3B levels and pSer129 α-synuclein accumulate in striatal $MAP2^+$ and nigral TH^+ neurons. The main findings of the first part of the study are that KD mice exhibited age-dependent accumulation of LC3-I, p62, LAMP2 and GAPDH levels, coupled with a reduced p-mTOR levels and *mTOR* and *TFEB* gene expression. Upon CQ treatment, LC3-II/I ratio was reduced in KD mice, indicating a defective autophagic flux. Conversely, G2019S KI mice showed only LAMP2 accumulation and downregulation of several ALP key genes, like *MAP1LC3B*, *p62*, *mTOR* and *TFEB*. Striatal lysosomal GCase activity was found to be increased in both LRRK2-kinase absent genotypes from 3 months of age onwards. Since these data were suggestive of an ALP impairment in aged KD mice, we next investigated whether KD mice were more susceptible to α-synuclein neuropathology *in vivo.* To this aim, AAV2/9 carrying h-α-syn was injected in the substantia nigra of 12-month-old G2019S KI, KD and WT mice. Motor behavior test was performed one, two and three months after injection. At the end, immunohistochemistry analysis was conducted to assess α-synuclein neuropathology and dopaminergic nigrostriatal neurodegeneration. KD mice showed a mild worsening of motor ability in the drag test in the absence of degeneration of dopaminergic nigral neurons or striatal terminals. Nonetheless, KD mice showed enhanced transgene and α-synuclein levels in striatum and substantia nigra. Altogether, these data support the view that LRRK2 kinase silencing causes early deregulation of GCase activity, and late impairment of autophagy and facilitation of α-synuclein neuropathology. Overall, this study contributes to shed lights into the complex modulation exerted by LRRK2 over ALP *in vivo*, demonstrating that a finely tuned LRRK2 kinase activity is needed to preserve ALP function and prevent α-synuclein accumulation in PD.

ABSTRACT

Mutazioni nel gene che codifica per la proteina leucine-rich repeat kinase 2 (LRRK2) sono state associate alla malattia di Parkinson (MP). Uno dei possibili meccanismi attraverso cui LRRK2 esercita la sua azione tossica nella MP è la modulazione del sistema autofagia-lisosoma. Alterazioni del sistema autofagia-lisosoma favoriscono l'accumulo di α-sinucleina, una caratteristica tipica della MP idiopatica e LRRK2-correlata. Nella prima parte di questo studio, è stata investigata la regolazione LRRK2-mediata del sistema autofagia-lisosoma, la sua età dipendenza, la sua correlazione con le inclusioni di α-sinucleina fosforilata alla serina 129 (pSer129) in vivo. I livelli di marcatori del sistema autofagia-lisosoma sono stati misurati mediante la tecnica del Western blotting in topi LRRK2 G2019S KI (esprimenti un'aumentata attività chinasica), LRRK2 KO, LRRK2 D1994S KI (esprimenti un'attività chinasica silenziata; topi kinase-dead, KD) e i WT di controllo, aventi 3, 12 e 20 mei di età. L'espressione di geni associati ad autofagia e lisosomi è stata misurata in striato utilizzando la tecnica della PCR quantitativa. Inoltre, i topi sono stati trattati con clorochina per determinare l'entità del flusso autofagico in vivo. L'attività dell'enzima lisosomiale Glucocerebrosidasi (GCase) è stata misurata nello striato dei topi di 3 e 12 mesi. In fine, analisi in immunofluorescenza è stata condotta per valutare gli accumuli di LC3B e pSer129 α-sinucleina in neuroni striatali MAP2-positivi e neuroni dopaminergici TH-positivi. I risultati salienti di questo primo studio consistono nell'aumento dei livelli di LC3-I, LAMP2, GAPDH, associato ad una riduzione nei livelli di mTOR fosforilato e nell'espressione genica di *mTOR* e *TFEB* nei topi KD a 12 mesi. Dopo trattamento con clorochina, i topi KD hanno dimostrato una riduzione nel rapporto LC3-II/I, a supporto dell'ipotesi di un ridotto flusso autofagico. I topi G2019S KI hanno mostrato solo un accumulo della proteina LAMP2 e una ridotta espressione dei geni *MAP1LC3B*, *p62*, *mTOR* and *TFEB*. I topi KD e KO hanno esibito anche un'elevata attività enzimatica di GCase fin dai 3 mesi d'età. Dal momento che questi dati suggeriscono che il sistema autofagia-lisosomi è inibito nei topi KD di 12 mesi, abbiamo voluto investigare se questo genotipo risultasse più suscettibile all'accumulo di α-sinucleina. Gli animali sono stati iniettati per via stereotassica in sostanza nera con un vettore virale adeno-associato di sierotipo 2/9 (AAV2/9) veicolante α-sinucleina umana mutata A53T (h-α-syn A53T). Sono stati condotti dei test per monitorare l'attività motoria a uno, due e tre mesi dall'iniezione virale. Analisi immunoistochimiche sono state svolte per valutare lo sviluppo della patologia associata all'accumulo di α-sinucleina e i livelli di neurodegenerazione del tratto nigrostriatale. I topi KD mostravano un leggero peggioramento dell'attività motoria nel drag test, in assenza di neurodegenerazione dei neuroni dopaminergici nigrali e delle terminali dopaminergiche striatali. Tuttavia, gli stessi animali presentavano un'elevata espressione del transgene in entrambe le aree, associata ad elevati livelli striatali e nigrali di α-sinucleina murina. Nel complesso, questi dati sostengono l'ipotesi che il silenziamento dell'attività chinasica causi una precoce disinibizione dell'attività di GCase e una tardiva inibizione dell'autofagia e facilitazione della sinucleinopatia. Questo studio contribuisce a fornire nuove evidenze riguardanti il complesso controllo esercitato da LRRK2 nel sistema autofagia-lisosoma *in vivo*, dimostrando come una fine regolazione dell'attività chinasica di LRRK2 risulta necessaria per garantire una normale attività autofagica e, quindi, prevenire l'accumulo di α-sinucleina nella MP.

INDEX

1. INTRODUCTION

1.1. The Autophagy-lysosomal pathway: a general overview

The autophagy-lysosomal pathway (ALP) is a highly conserved bulk degradation process by which long-lived, dysfunctional, misfolded proteins and defective organelles are delivered to lysosomes for elimination (Deter et al., 1967; Mortimore and Schworer, 1977; Galluzzi et al., 2017; Albanese et al., 2019). Beyond its classical role in the bulk elimination of cellular debris and harmful material, ALP function is crucial in maintaining cellular proteostasis, guaranteeing protein quality control and organelle turnover, eventually providing new sources of energy by recycling non-essential, old or harmful material under either physiological or stress conditions. Indeed, autophagy is an adaptive process that can be triggered by a variety of diverse stimuli, such as starvation, amino acid depletion, infection, hypoxia and energy needs (Bingol et al., 2018). Furthermore, not only clearance of aged and useless products provides energy necessary for cell survival but also preserves normal cell morphology and functions. Depending on the type of mechanism through which cellular debris is delivered to lysosomes, three major types of autophagy have been described: macroautophagy, microautophagy and chaperone-mediated autophagy (CMA; **Figure 1**).

1.1.1. Macroautophagy

Macroautophagy is a complex multi-step process that requires autophagosomal biogenesis to deliver the harmful material to the lysosomes (**Figure 1**). This process starts with the nucleation of a small double-membrane structure, named phagophore. Then the phagophore assumes a cup-like shape, by elongating at both ends and sequestering part of the cytoplasm containing cellular debris. The expanding phagophore eventually seals forming the autophagosome that ultimately fuses with lysosomes. The fusion with the lysosome supplies hydrolases that start digesting the autophagosomal content. This entire process is orchestrated by the autophagy-related (ATG) gene-8 family member proteins whose activation relies on upstream key regulators (Tsukada and Ohsumi, 1993; Thumm et al., 1994; Klionsky et al., 2003; Klionsky et al., 2012; Galluzzi et al., 2017).

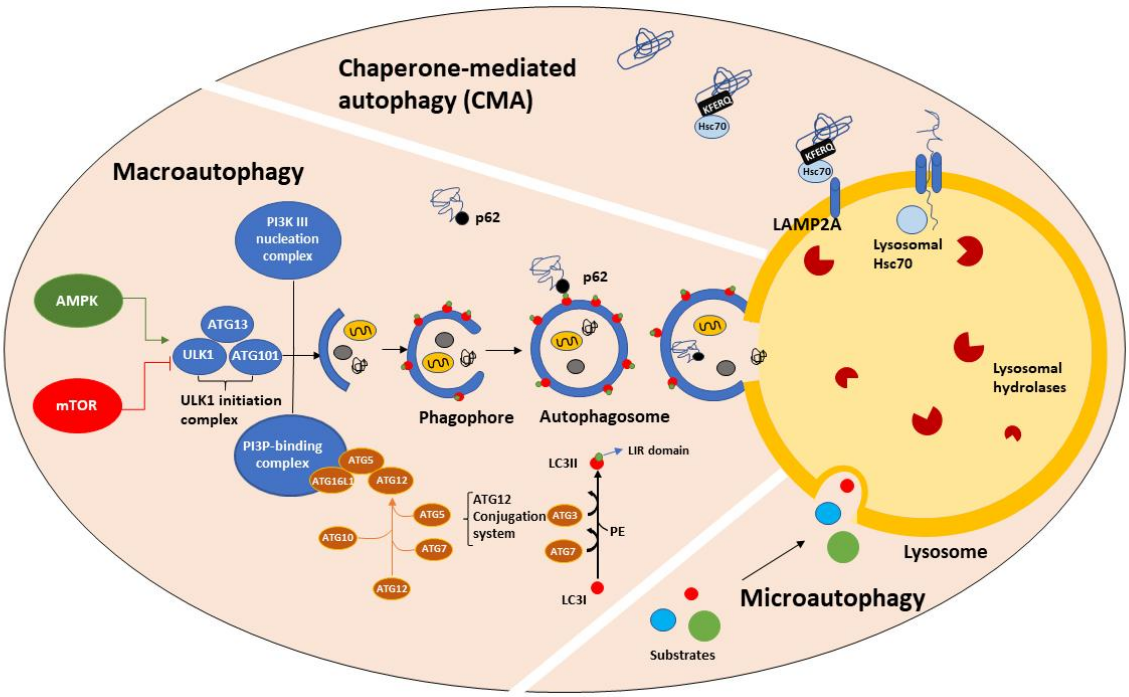

Figure 1. Autophagy-lysosomal pathway. Three major types of autophagy have been described: macroautophagy, microautophagy and chaperone-mediated autophagy (CMA). Macroautophagy is upstream regulated by two actors: AMPK and mTOR. AMPK acts as a promoter and mTOR as an inhibitor of macroautophagy by modulating the ability of ULK1 to form the ULK1 initiation complex. This complex works in association with PI3K III nucleation, and the PI3P-binding complex mediates the formation of the cup-shaped isolation membrane, named phagophore. This structure directly engulfs old/misfolded proteins, dysfunctional organelles and cellular debris, while elongating its terminals to generate autophagosomes. Autophagosomes ultimately fuses with lysosomes, in which the autophagic substrates are degraded by the joint action of the lysosomal hydrolases and the acidic environment. Substrate entry in the autophagosomes can also occur in a more selective fashion through LC3II. LC3I is a cytosolic inactive protein, which is part of the ATG protein family. Upon conjugation with phosphatidylethanolamine (PE), LC3II docks onto the forming autophagosomal membrane, where it binds different cargo proteins, such as p62. p62 binds to both ubiquitinated proteins, via its UBA domain, and LC3II, via its LIR domain, to mediate substrate translocation into the autophagosomal lumen. CMA is a more selective type of autophagy, in which the substrate degradation occurs in a one-by-one fashion. Proteins bearing the KFERQ-like sequence are recognized by the chaperone Hsc70 and shuttled to the lysosomal membrane. Hsc70 interacts with LAMP2A, triggering its multimerization. Upon formation of the LAMP2A translocation complex, the CMA substrate is sequestered into the lysosomal lumen and unfolded by lysosomal Hsc70. Microautophagy does not require the intervention of chaperones or autophagosomes to mediate the substrate entry into the lysosomes. The lysosomal membrane, in fact, directly engulfs the cellular debris to degrade (taken from Albanese et al., 2019).

Autophagy upstream regulation: mTORC1 and AMPK

To allow autophagosome biogenesis to start, autophagy induction is required. One of the key players in the autophagy induction process is the serine-threonine protein kinase uncoordinated-51-like kinase 1 (ULK1). ULK1 acts upstream of autophagy also by mediating the recruitment of complexes involved in the nucleation and elongation processes (Koyama -Honda et al., 2013). ULK1 activation status relies on the activity of two major upstream autophagy regulators: mammalian target of rapamycin complex 1 (mTORC1) and 5'-AMP-activated protein kinase (AMPK).

The mTORC1 complex has been characterized as a major autophagy upstream inhibitor, acting in response to the levels of extracellular and intracellular nutrients and growth factor signaling pathways (Lawrence et al., 2019; **Figure 1**). The abundance of nutrients and the presence of growth factor signals trigger the Rag GTPases-mediated mTORC1 translocation onto the lysosomal membrane and, thus, its activation (Yim et al., 2020). The Rag GTPases are a heterodimer complex constituted by Rag A or B bound to Rag C or D (Sancak et al., 2008). In the case of amino acid enrichment in the cytoplasm or in the lysosomal lumen, RagA/B are bound to GTP and Rag C/D to GDP. In this configuration, they are able to mediate mTORC1 recruitment onto the lysosomal membrane, where mTORC1 is allosterically activated by the GTPase Rheb (Yang et al., 2017; Lawrence et al., 2018). Upon activation, mTORC1 inhibits autophagy through different mechanisms. First, mTORC1 directly phosphorylates ATG13 and ULK1 at Ser757, preventing its association with ATG13 and AMPK (Kim and Guan 2015; Meijer et al., 2015). Second, onto the lysosomal surface, mTORC1 phosphorylates and inhibits the MiT/TFE basic leucine zipper transcription factors, including transcription factor EB (TFEB), which is a master transcriptional regulator of lysosomal and autophagy gene expression (Settembre et al., 2011). mTORC1-mediated phosphorylation of TFEB at Ser142 and Ser211 favors its sequestration by 14-3-3 proteins and prevents its translocation into the nucleus, where it can promote coordinated lysosomal expression and regulation (CLEAR) gene expression (Martina et al., 2012; Roczniak-Ferguson et al., 2012; Settembre et al., 2012). mTORC1 phosphorylates TFEB in the nucleus, regulating its export kinetics in a nutrient availability dependent manner (Napolitano et al., 2018). Third, mTORC1 phosphorylates the histone acetyltransferase p300 at Ser2271, Ser2279, Ser2291, and Ser2315, causing its inhibition. Knockdown of p300 reduces the acetylation of several ATGs, promoting their transcription. Therefore, mTORC1-mediated phosphorylation of p300 regulates starvation-induced autophagy (Wan et al., 2017). Conversely, one of the major mechanisms for mTORC1 repression is mediated by starvation which, in turn, promotes GTP hydrolysis on Rag A by GATOR1 complex, causing the dissociation of mTORC1 from the lysosomal surface (Bar-Peled et al., 2013; Panchaud et al., 2013). mTORC1 is, in fact, a key player in the complex lysosomal nutrient-sensing regulation of ALP. mTORC1 activity can be inhibited also by the AMPK-mediated phosphorylation of ULK1 at Ser317 and Ser777 in conditions of glucose depletion (Kim et al., 2011).

AMPK is considered the cell energy sensor and a key upstream autophagy promoter (**Figure 1**). AMPK heterotrimer complex is composed of a catalytic α subunit and two regulatory β and γ subunits. Upstream kinases (LBK1, CAMKK2, TAK1) as well as the allosteric binding with AMP (and to a much lesser extent with ADP) trigger AMPK α-subunit phosphorylation at Thr172 and its activation (Hawley et al., 2003; Shaw et al., 2004). AMPK complex is, in fact, able to sense the ratio

of AMP/ATP and ADP/ATP in the cell. Under physiological conditions, ATP, which is particularly abundant in the cellular cytoplasm, binds to the γ subunit and mediates AMPK complex suppression. Conversely, in the case of energy need, AMP (and to a lesser extent ADP) binds to the γ subunit and promotes AMPK activation through different ways: stimulation of LBK1-mediated phosphorylation, prevention of protein phosphatase-mediated dephosphorylation of Thr172, and allosteric activation of the complex (Shackelford et al., 2009; Xie et al., 2006; Herrero-Martin et al., 2009). Upon activation, AMPK promotes autophagy through direct and indirect mechanisms. AMPK, in fact, acts as one the major mTORC1 competitors, in terms of autophagy regulation. AMPK inhibits mTORC1 activity by phosphorylating TSC2, thus inhibiting Rheb-dependent mTORC1 activation (Bingol et al., 2018). Furthermore, AMPK directly phosphorylates RAPTOR1 at Ser772 and Ser792, favoring its inactivation by 14-3-3 protein binding (Bingol et al., 2018). Upon glucose and energy deprivation, AMPK promotes autophagy also by phosphorylating ULK1 at Ser317 and Ser777, triggering its assembly to ATG13, ATG101 and focal adhesion kinase family-interacting protein of 200 kDa (FIP200; Egan et al., 2011; Kim et al., 2011). AMPK is also able to regulate autophagy at transcriptional level by phosphorylating FOXO3 at multiple sites and promoting its translocation to the nucleus, under stress conditions (Bowman et al., 2014). FOXO3 activation induces the transcription of several autophagy-related genes, including *ULK1*, *MAP1LC3B*, *BECN1*, *ATG4*, *ATG13*. However, mTORC1 antagonizes FOXO3 activity under nutrient-rich conditions.

Autophagosome nucleation

Upon activation, ULK1 forms a complex with ATG101, FIP200 and ATG13, which recruits nucleation and elongation complexes to the phagophores (Gammoh et al., 2013; Nishimura et al., 2013; **Figure 1**). ULK1 activity is required to initiate the autophagosomes nucleation, a process mediated by the class III phosphatidylinositol-3-phosphate kinase (PI3K III) complex (Ikatura and Mizushima 2010). PI3K III complex phosphorylates and converts phosphatidylinositol (PI) into phosphatidylinositol 3-phosphate (PI3P). PI3P activates the family of the WD-repeat protein Interacting with PhosphoInositides (WIPI), which are involved in the recruitment of downstream autophagy effectors, such as ATG proteins, orchestrating the autophagosomes assembly.

Autophagosome elongation

Recruitment and conjugation of ATG8 proteins with phosphatidylethanolamine (PE) onto the growing phagophores (a process called lipidation) are required for autophagosome elongation (**Figure 1**). The ATG8 protein family can be divided into two main subfamilies: the microtubule-associated protein 1 light chain 3 (LC3) family (LC3A, LC3B, LC3C) and the GABA type A receptor-

associated protein (GABARAP) family (GABARAP, GABARAP-like1, GABARAP like-2) (Kabeya et al., 2000; Shpilka et al., 2011). Specifically, two LC3B isoforms have been identified: LC3-I, inactive and mainly located in the cytoplasm, and its PE-conjugate LC3-II, active and associated with the autophagosomal membranes. LC3-II levels are a common readout of autophagosomal abundancy whereas the LC3-II/ LC3-I ratio is an accepted readout of the autophagic flux (Klionsky et al., 2021). To mediate LC3-I lipidation, two conjugation systems work together. First, LC3 is activated by the cysteine protease ATG4B. ATG4B exposes the C-terminal glycine of LC3, making it suitable for conjugation first to E1-like ATG7, then to E2-like ATG3 (Kabeya et al., 2000; Kauffman et al., 2018; Tanida et al., 2002; Tanida et al., 2004a; Tanida et al., 2004b). Finally, LC3-I is conjugated to PE through the activity of the E3-like complex ATG12-ATG5-ATG16L1 (Kabeya et al., 2000). The formation of the E3-like complex relies on E1-like ATG7 and E2-like ATG10 activity, and its recruitment onto the forming phagophore membrane is mediated by FIP200 (Gammoh et al., 2013; Nishimura et al., 2013). Once lipidated, LC3-II is integrated in the autophagosomal membrane, where it acts as a receptor for selective autophagy. Several cargo proteins are in fact able to interact with LC3 through their LC3-interacting region (LIR), mediating the entry of specific substrates into the autophagosomal lumen (**Figure 1**). The first mammalian cargo protein identified was p62 (Bjorkoy et al., 2005; Pankiv et al., 2007) that contains both the LIR domain to bind LC3-II on the autophagosomal surface and the ubiquitin-associate (UBA) domain to selectively engage ubiquitinated cargoes (Khaminets et al., 2016; **Figure 1**). Indeed, p62 is required to form and deliver ubiquitin-positive aggregates and misfolded proteins to the autophagosomes (Komatsu et al., 2007a). p62 plays a key role in the interplay between the ubiquitin-proteasome system (UPS) and selective autophagy. In fact, under physiological conditions, ubiquitinated misfolded proteins or aggregates are degraded by UPS. However, in the case of proteotoxic stress derived by dysfunctional or overloaded UPS, p62 functions as a cargo protein for selective autophagy, delivering the ubiquitinated burden to the autophagosomes (Danieli et al., 2018). p62 activity is also tightly regulated by oligomerization that stabilizes low-affinity interaction between the LIR domain and LC3 (Ciuffa et al., 2015).

Autophagolysosome formation

The elongation process terminates when the two ends of the phagophore fuse by forming a mature autophagosome, and the SNARE protein syntaxin 17 is recruited (Bingol et al., 2018; **Figure 1**). Microtubules mediate the active transport of the autophagosomes toward the lysosomes. However, prior to the fusion with lysosomes, LC3-II on the outer membrane of the autophagosomes is recycled, while LC3-II bound to the inner membrane is degraded by the lysosomal hydrolases. The fusion of the autophagomes with lysosomes generates autophagolysosomes, in which the V-type ATPase

proton pump works to acidify the lumen to activate lysosomal hydrolases (Oot et al., 2016). This complex process is mediated by the interaction of syntaxin 17 with synaptosome-associated protein 29 (SNAP 29) and the endosomal/lysosomal SNARE vesicle-associated membrane protein 8 (VAMP8) (Itakura et al., 2012).

1.2 CMA

CMA is a more selective type of autophagy that engages and targets substrates for lysosomal degradation in a one-by-one fashion (**Figure 1**). The selectivity associated with this degradation pathway relies on the selective recognition of proteins bearing the KFERQ-like pentapeptide sequence by the cargo protein heat shock cognate 71 kDa protein (Hsc70), also known as HSPA8. Only 40% of cytosolic proteins carry this degradation motif, making them eligible to CMA-mediated degradation (Chiang et al., 1989). However, Hsc70 function is not limited to CMA. Hsc70 contributes to the correct folding of an array of unfolded or misfolded proteins. Upon the engagement with the substrate, Hsc70 carries it to the lysosomal surface where the splicing-isoform of the lysosome-associated membrane protein 2 (LAMP2), LAMP2A, mediates its entry into the lysosomal (Cuervo and Dice, 1996; Cuervo and Wong, 2014). There are two populations of Hsc70: one that shuttles in the cytoplasm and docks to the lysosomal membrane on the cytosolic side (hereafter referred to as membranal Hsc70) and another localized in the lysosomal lumen (hereafter referred to as luminal Hsc70; **Figure 1**).

Luminal Hsc70, in association with co-chaperones, is required for substrate unfolding and release into the lumen and is fundamental for substrate internalization, since the lysosomes devoid of Hsc70 are CMA-incompetent (Kaushik et al., 2018; **Figure 1**). Different from the membranal form, lysosomal Hsc70 is highly stable in acid lysosomal environment, and small variations in the pH are able to affect the protein stability. These changes in lysosomal pH are part of a regulatory mechanism that controls the number of CMA-competent lysosomes in response to intracellular and extracellular stimuli (Cuervo et al., 1997). LAMP2A, LAMP2B and LAMP2C are the three splicing variants of the *LAMP2* gene. All share the same luminal domain but not the transmembrane and the cytosolic domains, suggesting their involvement in different molecular pathways. Only LAMP2A, in fact, participates in CMA. Selective blockage of this isoform represents the most effective way to inhibit it. Through its cytosolic domain, monomeric LAMP2A interacts and recognizes protein substrates bound to membranal Hsc70. The binding with the substrate triggers LAMP2A multimerization to form a 700 kDa multimeric protein that mediates the protein translocation into the lysosomal lumen (Bandyopadhyay et al., 2008). LAMP2A is the rate-limiting step of this process since changes in its levels or dynamics directly affect CMA flux. *LAMP2* transcription, differently from other autophagy-

and CMA-related genes, does not rely on TFEB activity. Starvation, mild oxidative stress, hypoxia and genotoxic damage upregulate *LAMP2* transcription and, thus, CMA activity. During T cell activation, nuclear factor of activated T cells (NFAT1) is the transcriptional factor involved in LAMP2A synthesis (Valdor et al., 2014). CMA is active under both physiological and pathological conditions.

1.3 Lysosomes

For a long time, lysosomes have been considered only as the terminal compartment for degradation at the crossroad of ALP and endocytic pathway (Nixon et al., 2008; **Figure 1**). In fact, lysosomes have always been described as static "garbage-disposal" organelle characterized by a large number of acid hydrolases activated by the acidic pH (4.5-5) in the lumen (Saftig and Klumperman, 2009). Nevertheless, several recent findings have re-evaluated lysosome functions besides degradation, recognizing their crucial role in cellular adaptation mechanisms in response to environmental cues (Ballabio et al., 2020). Lysosomes are indeed able to sense the cellular energetic status and contribute to modulate different cellular functions, such as metabolism, gene regulation, immunity, plasma membrane repair and cell adhesion/migration. Recently, it has been found that lysosomes interact with other cellular components and that their intracellular localization is highly correlated with their activation status (Ballabio et al., 2020).

As the major degradation center of the cell, lysosomes are in the unique position for accessing the quantity of material actively degraded and function as a sensor for the cellular nutritional status (Ballabio et al., 2020). The hub function of lysosomes requires mTORC1, which is dynamically associated with the lysosomal membrane in a nutrient and growth signal dependent-manner. mTORC1 acts as a major regulator for cellular metabolism by promoting anabolism and inhibiting catabolism, e.g. autophagy, in the presence of nutrients and growth factor abundance. Starvation is, in fact, the most efficient method to suppress mTORC1 activity (Hosokawa et al., 2009). As mentioned above, however, the RAG-dependent mTORC1 recruitment onto the lysosomal membrane is key to its activation. Furthermore, mTORC1 is also involved in the lysosome re-formation process, maintaining an adequate pool of functional lysosomal even in case of prolonged starvation (Yu et al., 2010). mTORC1 is also important in mediating the lysosomal transcriptional regulation of CLEAR gene network through TFEB, which is primarily involved in the regulation of the expression of autophagy and lysosomal biogenesis-related genes. TFEB continuously shuttles from the cytoplasm to the nucleus and its subcellular localization is tightly regulated by mTORC1-mediated phosphorylation. Upon nutrient-rich conditions, mTORC1 phosphorylates TFEB at Ser211, favoring its binding by 14-3-3 proteins and preventing its nuclear translocation (Puertollano et al., 2018).

Moreover, mTORC1-mediated phosphorylation of nuclear TFEB at Ser142 and Ser138 induces its nuclear export, thus inhibiting TFEB activity (Napolitano et al., 2018). However, TFEB subcellular localization is co-regulated by lysosomal Ca^{2+} release through the Ca^{2+}-dependent phosphatase calcineurin, which dephosphorylates TFEB and facilitates its nuclear relocation (Medina et al., 2015). Another important mechanism through which lysosomes exert their signaling hub function is the modulation of Ca^{2+} release. Lysosomes are the most important storage of intracellular Ca^{2+}, suggesting that maintaining Ca^{2+} homeostasis is crucial for lysosomal function. Release of Ca^{2+}, indeed, is required for the fusion with other intracellular components, such as autophagosomes, endosomes and plasma membrane, and for lysosomal acidification and recruitment of acidic hydrolases (Morgan et al., 2011; Li et al., 2019; Mindell et al., 2012). Lysosomal Ca^{2+} also triggers contact sites formation with endoplasmic reticulum (ER) to restore lysosomal Ca^{2+} storage in case of shortage of Ca^{2+} levels (Wang et al., 2017). In mammals, three types of Ca^{2+} channels are involved in lysosomal Ca^{2+} release: transient receptor potential cation channels of the mucolipin family (TRPML), two-pore channels (TPC) and the trimeric Ca^{2+} two transmembrane channel $P2X_4$ (Morgan et al., 2011; Li et al., 2019). Various upstream stimuli can activate those channels, among which pH, nutrients, stress, energetic status, phospholipids (Ballabio et al., 2020). Furthermore, the presence of three types of Toll-like receptors (TLR), TLR3, TLR7/8, TLR9, on the lysosomal surface of macrophages and dendritic cells makes them capable of detecting microbial nucleic acids and participating in the proinflammatory transduction response (Matz et al., 2019; Vidya et al., 2018).

1.4 Transcriptional regulation of autophagy

CLEAR gene transcription is regulated by mTORC1 through TFEB in a nutrient and growth factor-dependent fashion. The transcriptional counterpart of TFEB is KRAB and SCAN domains 3 (ZKSCAN3) that represses several autophagy-related genes. Upon activation of autophagy, ZKSCAN3 translocates from the nucleus to the cytoplasm whereas TFEB moves to the nucleus to promote CLEAR gene expression.

The members of Forkhead box O (FOXO) family such as ATG4, ATG12, BECN1, MAP1LC3B, ULK1 are another major regulator of autophagy-related gene expression. FOXOs can act both as inducers and repressors of autophagy depending on their subcellular localization (Mammucari et al., 2007; Zhao et al., 2007). As for TFEB, their phosphorylation status mirrors their activation status. Among the FOXO family, FOXO1 and FOXO3 are transcription factors promoting autophagic flux in the muscle. FOXO1 promotes expression of ATG5 (Xu et al., 2011), ATG14 (Xiong et al., 2012) and PIK3C3 (Li et al., 2009). FOXO1 is also able to enhance autophagy by directly interacting with

cytosolic proteins involved in ALP machinery. FOXO activation can also be mediated by AMPK to enhance the autophagic flux.

p53, a tumor suppressor protein, is another important player in the complex transcriptional regulation of autophagy. It was first characterized as an autophagy enhancer because of its ability to inhibit mTORC1 and promote AMPK activity (Budanov and Karin, 2008). Upon DNA damage, p53 induces autophagy by promoting transcription of several autophagy-related proteins involved in autophagy initiation and autophagosome elongation (Kenzelmann Broz et al., 2013), FOXO3a expression and activity (You et al., 2006; Fu et al., 2011) and TFEB nuclear translocation (Jeong et al., 2018).

The two transcriptional factors E2F1 and NF-kB control the hypoxia-mediated induction of autophagy by regulating the expression of BNIP3. BNIP3 induces autophagy by disrupting the inhibitory interaction between B-cell lymphoma 2 (Bcl-2) and beclin-1, thus allowing beclin-1 to engage with the PI3K-complex (Shaw et al., 2008). Under physiological conditions, NF-kB constitutively occupies the promotor region upstream the *BNIP3* gene, preventing its transcription. In case of hypoxia, NF-kB binding is less efficient, so E2F1 can bind and promote *BNIP3* expression and activity as autophagy enhancer. E2F1 is also able to directly enhance *ULK1*, *MAP1LC3B*, and *ATG5* expression.

The farnesoid X receptor (FXS) is one of the most important autophagy repressors in the liver and operates through two different mechanisms. Upon feeding, FXS inhibits autophagy by preventing the binding of cAMP response element-binding protein (CREB) to its cofactor CRTC2. During starvation, FXS cannot sequester CREB, allowing the binding with CRTC2 and, thus, increasing the expression of key autophagy-related genes, such as ATG7, ULK1, and TFEB (Seok et al., 2014). FXS was also found to compete with Peroxisome Proliferator Activated Receptor alpha (PPARα) for the binding to specific DNA sites. Under starvation conditions, FXS is inhibited whereas PPARα is activated, promoting the transcriptional expression of autophagy genes (Lee et al., 2014). In addition, under low nutrient conditions, TFEB is able to induce PPARα expression (Settembre et al., 2013), suggesting a potential interplay between the FXS-CREB and FXS- PPARα axes.

1.5. ALP and healthy aging

Aging is a biological process that causes a time-dependent decline in cellular and molecular mechanisms affecting the quality of life of all organisms (Leidal et al., 2018). Indeed, aging is considered one of the major risk factors associated with diseases, such as neurodegenerative and cardiovascular diseases, and cancer. However, the intimate causal relationship between aging and diseases is not clear. ALP impairment has been reported as a classical feature of aging across species, (Leidal et al., 2018). In particular, lysosomal activity is progressively reduced over time as testified

by the presence of enlarged lysosomes accumulating lipofuscin, which is mainly composed by residues of highly oxidized cross-linked protein aggregates, carbohydrates and lipids. Furthermore, lipofuscin accumulation facilitates cellular ROS production (Rezzani et al., 2012). In addition to a compromised proteolytic function exerted by lysosomes, aging also affects the delivery of cargoes to lysosomes for degradation by reducing the number of autophagosomes and the rate of their fusion with lysosomes. Studies conducted in flies, rodents and human cells have associated a decreased expression of several important autophagy-related proteins with senescence. In aged flies, *ATG2* and *ATG8a* were found to be reduced. An age-associated decline in *ATG5*, *ATG12* and *BECN1* expression has been reported in the rodent whole brain and hippocampus (Ott et al., 2016; Galluzzi et al., 2017). Consistently, a similar decrease in *ATG5*, *ATG7* and *BECN1* transcripts has been reported in humans. Reduction in *ATG* expression significantly impacts autophagosomes formation and delivery to the lysosomes. On the other hand, a compromised lysosomal activity is thought to be responsible also for the alterations reported in the fusion step and autophagosome clearance (Kenessey et al., 1989; Sitte et al., 2000a, b). To strengthen the link between *ATG* expression, autophagy and life span, selective mutations/knockdown of key autophagy-related genes, such as *ATG8, ATG1, BECN1, ATG7, ATG12, ATG18* in *C. elegans, ATG3 and ATG8a* in *Drosophila* and *ATG5, ATG7* and *BECN1* in mice significantly affects lifespan and quality of life (Leidal et al., 2018; Hansen et al., 2008; Simonsen et al., 2007; Toth et al., 2008). Conversely, knock out of *BECN1, ATG5, ATG9* and *ATG13* in mice leads to embryonic lethality, suggesting the importance of autophagy in development (Kuma et al., 2017). Furthermore, genetic knockdown of the key transcriptional factors *hlh-30* and *daf-16* (*C. elegans* ortholog of TFEB and FOXO, respectively) shortened the lifespan in WT and long-lived *daf-2* mutant worms (Lin et al., 2018). Mutations in the *daf-2* gene, ortholog of the insulin/insulin-like growth (IGF-1) receptor, promotes longevity in worms. In fact, mutations in the *daf-2* gene promote autophagy by inhibiting downstream mTORC1 and inducing *daf-16*/FOXO activities, suggesting for the first time that improvement of the autophagic flux delays aging (Melendez et al., 2003; Hansen et al., 2008). Other genetic and pharmacological strategies widely used to promote the autophagic flux target mTORC1, since elevation of mTORC1 activity is associated with age-dependent autophagy decline. mTORC1 can be efficiently inhibited by two different approaches: calory restriction (CR) and pharmacological inhibitors. CR, which can be defined as a limitation of food assumption without incurring in malnutrition, activates autophagy by inhibiting mTORC1 and activating AMPK and Sirtuin-1. It has been proposed that both reduced IGF pathway and mTORC1 activity mediate extended longevity through abolition of high metabolic rate (Toth et al., 2008). Genetic or pharmacological (via rapamycin or its rapalog derivatives) inhibition of mTORC1, promote life span in *C. elegans* (Vellai et al., 2003), *D. melanogaster* (Kapahi et al., 2004), *S. cerevisiae* (Kaeberlein et

al., 2005), and mice (Harrison et al., 2009). However, knocking out or knocking down ATG-encoding genes abolished the rapamycin-mediated extended longevity, indicating that rapamycin affects mainly autophagy induction and autophagosome formation steps (Moyse et al., 2019). Macroautophagy is not the only type of autophagy contributing to the age-associated cellular phenotype, CMA activity declines along with time as well. Limiting-rate factor in the CMA pathway is LAMP2A abundancy and synthesis. An age-dependent reduction in LAMP2A compensated by an early increased lysosomal and co-chaperones abundancy was first described in senescent cells (Cuervo and Dice, 2006; Ott et al., 2016). However, this compensation is not able to sustain CMA activity over time, suggesting that the loss of LAMP2A levels can be caused by either a reduced recycling from the lysosomal lumen or a decreased stability of the receptor. LAMP2A is usually located in parts of the lysosomal membranes characterized by a low-cholesterol content. Indeed, cholesterol and ceramide levels directly correlate with the membrane fluidity properties. Aging causes cholesterol accumulation at the lysosomal membrane which, in turn, reduces LAMP2A stability by directly preventing its multimerization and inducing its membrane sequestration to mediate its degradation (Rodriguez-Navarro et al., 2012). An age-related autophagy failure impacts on cellular physiology and function also by causing old and dysfunctional organelles accumulation, especially lysosomes, mitochondria, and endoplasmic reticulum (ER). This aging-related feature is particularly relevant in postmitotic cells, such as neurons, which cannot undergo mitosis cycles to dilute the cytotoxic material accumulated over time (Albanese et al., 2019). Consistent with this view, accumulation of swollen, fragmented and dysfunctional mitochondria is one the main contributors to the age-related cellular phenotype. Decreased mitophagy, i.e. the selective type of autophagy responsible for degrading mitochondria, associated with reduced PINK1 expression has been described in mouse lung (Sosulski et al., 2015) but, more in general, has been accepted as a senescence feature (Terman et al., 2010). PINK1 participates in targeting damaged mitochondria by binding their outer membrane, then recruiting the E3 ubuquitin ligase Parkin for autophagome-mediated degradation (Jin and Youle, 2012). Accumulated mitochondria affect cellular function by increasing the production of free radicals and oxidative stress (Rezzani et al., 2012). According to the "free-radical theory" proposed by Harman in 1986, the phenotype of the aging cells is determined by both the increased ROS production and the reduced efficiency in the detoxification processes due to the progressive impairment of mitochondrial function. In particular, the increased ROS burden can be detrimental for cellular functions through multiple mechanisms. Free radicals can attack and damage mtDNA, leading to accumulation of mutations and increased hypoxia in senescent cells. Furthermore, free radicals promote protein oxidation that, in turn, exposes their hydrophobic residues favoring misfolding and aggregation (Miquel et al., 1998; Hohn et al., 2017). Among the

detoxification mechanisms adopted by the cells, autophagy plays a crucial role. Indeed, increased oxidative stress is able to induce autophagy by mediating ATG overexpression and mTORC1 inhibition (Chakraborty et al., 2019). Consistently, both mTORC1-dependent and mTORC1-independent autophagy enhancers have been widely used as effective strategies to promote ROS clearance in the senescent cells (Mizunoe et al., 2018). Indeed, rapamycin promoted ROS elimination in neurons (Ramirez-Moreno et al., 2019) whereas trehalose, a naturally available disaccharide, enhanced the autophagic flux and induces Nrf2 activation and transcription of its target genes (Mizunoe et al., 2018).

1.6. ALP in the nervous system and neurodegeneration

Neurons can be considered as highly specialized, long-lived cells, characterized by high metabolic energy demand. In particular, considering that neurons are postmitotic cells, ALP function in each neuronal compartment, e.g. soma, axons and dendrites, is crucial for cellular proteostasis by promoting elimination of cytotoxic materials and managing diverse stressors. To better address the role of autophagy in CNS and given the fact that complete knockout of core *ATG* genes results in neonatal and embryonic lethality, conditional knockouts of either *ATG5* or *ATG7* in specific neural or glial populations were generated via the Nestin-Cre promoter, (Hara et al., 2006; Komatsu et al., 2006, 2007a). Conditional deletion of *ATG5* and *ATG7* (as well as *FIP200* and *BECN1*) affects early autophagosomal formation, preventing autophagy initiation (Albanese et al., 2019). These models showed neuronal loss and accumulation of ubiquitin-positive inclusions with a different onset and/or progression based on the cell type and nature of the aggregates. For example, targeted deletion of *ATG5* and *ATG7* in cerebellar Purkinje cells led to cell-autonomous degeneration, characterized by early axonal swelling (Komatsu et al., 2007b; Nishiyama et al., 2007). These findings suggest the importance of axonal autophagy in supporting neuronal homeostasis or, more specifically, proteostasis, in response to insults, such as toxic protein aggregation. Furthermore, selective knock-out of *ATG7* in dopaminergic neurons caused neural death, loss of dopaminergic terminals in striatum, formation of ubiquitin-positive and p62-positive aggregates and α-synuclein (α-syn) accumulation in vivo (Ahmed et al. 2012, Sato et al. 2018). Moreover, even targeting late steps of the autophagy process results in protein aggregation and neurodegeneration. Indeed, *Epg5* knockout caused accumulation of p62- and ubiquitin-positive aggregates in brain and spinal cord, and TDP43 (TAR DNA-binding protein 43) in neurons. These features were accompanied by the soma and axonal degeneration of pyramidal and motor neurons (Zhao et al. 2013). The age-associated physiological process of autophagy decline is exacerbated in the context of neurodegenerative disorders of aging, such Parkinson's Disease (PD), Alzheimer's Disease (AD) and Huntington Disease (HD) (Boland et

al., 2018). A common feature of these conditions is the age-dependent accumulation of protein aggregates into the cytoplasm of neurons. Upon accumulation, those proteins are more easily subjected to oxidation, misfolding, and cross-linking by cellular post-translational machinery (Albanese et al., 2019). Due to aberrant post-translational processing, they lose the physiological quaternary structure and function, gaining new "toxic" properties. Protein aggregates might exert their toxic function by interfering with several physiological processes e.g. autophagy and cellular trafficking, thus favoring their accumulation. Moreover, a typical feature of these proteins is that they can act as a "seed" to trigger wild-type proteins to assume the misfolded conformation as well, thus, facilitating their spreading throughout the CNS (Brudin et al., 2010; Brudin and Melki, 2017; Albanese et al., 2019). Furthermore, mutations in several genes associated with the autophagy machinery are considered risk factors or genetic cause of several neurodegenerative disorders of aging, including PD (Ravikumar et al., 2002; Berger et al., 2006; Ravikumar et al., 2006).

1.7. ALP and PD

PD is a multifactorial, progressive and multisystemic neurodegenerative disorder characterized by motor and non-motor symptoms. It usually presents with a late onset and affects 2-3% of the elderly population (above 65 years of age). The neuropathological hallmarks of PD are the degeneration of dopaminergic neurons located in SNpc and the appearance of intracellular accumulation of proteinaceous aggregates, named Lewy Bodies (LB), mainly composed by α-syn (α-syn, Poewe et al., 2017; Balestrino et al., 2020). α-syn is a presynaptic monomeric protein that exists into a dynamic equilibrium with its oligomeric form. It plays an important role at the presynaptic site, where it contributes to neurotransmission. Under unknown triggers, α-syn assumes a misfolded conformation, which promotes its aggregation into higher-molecular weight structures, that, ultimately form LB (Stefanis et al., 2019; Hijaz et al., 2020). α-syn accumulation is a PD feature, suggesting that autophagy impairment can play an important role in PD-related pathology. Indeed, a reduction of lysosomal (e.g. LAMP1) and CMA (e.g LAMP2A, Hsc70 or Cathepsin D) markers and an elevation of autophagy markers (e.g. LC3-II and p62) were detected in the whole brain (Mamais et al., 2018) and SNpc (Chu et al., 2009; Dehay et al., 2010) of idiopathic PD patients (Xilouri and Stefanis, 2015). Furthermore, studies conducted in Dementia with Lewy Bodies (DLB) patients pointed out greater mTOR and LC3-II levels and reduced ATG7 levels compared to AD patients (Crews et al., 2010), consistent with that reported in the idiopathic PD patients (Higashi et al., 2011). However, as observed in idiopathic PD patients, lysosomal LAMP2 levels were diminished in both DLB and AD cases (Higashi et al., 2011). Altogether, this evidence supports a causative relationship between autophagy and PD pathophysiology. Differently from idiopathic PD patients, LRRK2 G2019S PD patients

displayed only a reduced lysosomal content, as supported by the decreased LAMP1 levels compared to age-matched controls, probably suggesting a different pathophysiology underlying the idiopathic versus the G2019S PD forms (Mamais et al., 2018). Consistently, lower insoluble α-syn levels were found in G2019S compared to idiopathic PD brains (Mamais et al., 2013). However, G2019S PD patients showed an increase in the CMA-competent marker LAMP2A, but no changes in LAMP1, in the cholinergic cells of the motor nucleus of the vagal nerve. This increase suggests either a compensatory increase to overcome an impaired CMA activity or an impaired LAMP2A clearance (Orenstein et al., 2013). Furthermore, mutations in genes associated with PD were proven to play a role in autophagy machinery as mutations in autophagy-related genes were associated with PD (Ravikumar et al., 2002; Berger et al., 2006; Ravikumar et al., 2006). Indeed, heterozygous mutations in the gene encoding for the lysosomal hydrolase Glucocerebrosidase (GCase), *GBA1,* are considered a major genetic risk factor for PD (Behl et al., 2021). On the other hand, mutations in the SNCA gene, encoding for α-syn, were the first genetic cause associated to PD. In particular, point mutations as well as multiplications in the *SNCA* gene have been considered as cause of autosomal dominant PD and risk factor for idiopathic PD (Henderson et al., 2019). Mutations in the *LRRK2* gene are considered the most common genetic cause of familial PD (Zimprich et al., 2004; Paisan-Ruiz et al., 2005) and, also, according to GWAS studies (Nalls et al., 2014), single nucleotide polymorphisms (SNPs) in the LRRK2 locus as a genetic risk factor for idiopathic PD. The impact of *GBA1*, *SNCA* and *LRRK2* mutations on PD pathophysiology will be covered in the next paragraphs.

1.8. GCase and PD

1.8.1. GBA1 mutations and PD

The Glycosylceramidase beta (*GBA1*) gene encodes for the lysosomal enzyme Glucocerebrosidase (GCase). GCase hydrolyzes glucose from Glucosylceramide (GlcCer) and glucosylsphingosine (GlcSph), obtaining ceramide (Cer) and sphingosine (Sph) (Do et al., 2019). *GBA1* gene is located in the gene-rich region on the chromosome 1q21, consisting in 11 exons and spanning around 7 kb. Located only 16 kb downstream is the highly homologous, untranslated *GBA1* pseudogene that shares 98% homology in the coding regions (Winfield et al., 1997). GCase is a 497-amino acid membrane-associated protein that is synthesized in the ER and glycosylated. Unlike other lysosomal hydrolases, GCase sorting to the lysosome does not involve the mannose-6-phosphate-dependent pathway but the binding, at a neutral pH, with the lysosomal integral membrane protein-2 (LIMP2), encoded by the *SCARB2* gene (Aerts et al., 1988; Reczek et al., 2007). In fact, LIMP2 transfers the protein through the Golgi, then to late endosomes. Finally, the fusion between late endosomes and lysosomes mediates the release and activation of GCase due to the acidic environment. However, GCase gets

activated also by the coordinated activity of its cofactor Saposin C and negatively charged lipids (Grabowski et al., 2008). Homozygous mutations in the *GBA1* gene are associated with the lysosomal storage disorder Gaucher Disease (GD). These mutations lead to the protein loss-of-function and the accumulation of its substate GlcCer within the lysosomal lumen, which impairs the lysosomal proteolytic function. To date, around 495 *GBA1* mutations have been identified to be associated to GD. The two most common mutations found in patients are c.1226A > G (p.N370S; now referred to as p.N409S) and the c.1448T > C (L444P, now referred to as p.L483P). However, several point, frame shift and splicing mutations as well as and null alleles often resulting from recombination with the homologous pseudogene sequence have been identified in all exons (Tayebi et al., 2003). The association between *GBA1* mutations and PD stemmed from the observation that some GD patients presented parkinsonism-like symptoms (Neudorfer et al., 1996; Tayebi et al., 2001; 2003). However, one study pointed out that although the incidence of developing PD-like symptoms is not different in homozygous and heterozygous *GBA1* mutation carriers, patients with homozygous mutations showed an earlier onset of about 6-11 years compared to the heterozygous carriers (Alcalay et al., 2014). Studies conducted in the past 14 years have identified the heterozygous mutations in *GBA1* gene as the major genetic risk factor associated with PD. In fact, mutations in *GBA1* gene are more frequent than the classical mutations associated with PD, such mutations of *LRRK2*, *SNCA*, *PARK2,* in different PD populations (Horowitz et al., 1989; Winfield et al., 1997). It has been estimated that 7-12% of patients with PD carry a GBA1 mutation, with the frequency varying depending on the population (Sidransky et al., 2009). Occurrence of *GBA1* variants increases by up to 10 folds the risk of PD (Lwin et al., 2004; O'Regan et al., 2017). However, the relationship between PD pathogenesis and GCase does not simply rely on the presence of pathogenic mutations in the *GBA1* gene. In fact, autopsy studies conducted on idiopathic PD patients, carrying no mutations in the *GBA1* gene, showed reduced GCase activity in the same brain tissues affected by α-syn pathology (Mazzulli et al., 2011; Gegg et al., 2012; Murphy et al., 2014). Furthermore, two non-pathogenic GBA1 mutations, E326K (p.E365K) and T369 M (p.T408M), still increase the risk to develop parkinsonism (Mallett et al., 2016; Duran et al., 2012). Therefore, speculation on the complex and, still unexplored, crosstalk between PD and GCase is related but not limited to the reduced lysosomal activity and the GlcCer accumulation (Do et al., 2019).

1.8.2. GCase and PD pathogenesis

The reduced GCase activity associated with *GBA1* mutations has been hypothesized to be potentially linked to several mechanisms: impairment of of GCase transport from either ER or Golgi, failure in binding its transporter LIMP2, reduction of protein stability or protein misfolding that might target it

to proteasomal degradation, failure in activating its cofactor Saposin C, or mutations affecting its active site (Do et al., 2019). Post-mortem studies conducted on PD and GD-PD brains have linked a decreased GCase activity in SN with an increased α-syn overload (Gunder et al., 2019). In keeping with this, Mazzulli and colleagues reported that reduced GCase activity was associated with an impaired clearance of α-syn (Mazzulli et al., 2011). Cholesterol accumulation is another evidence sustaining the GCase impairment in PD brains. GCase has a broad enzymatic profile because it also transfers a glucose from GlcCer to cholesterol, obtaining glycosylated cholesterol (GlcChol). A study pointed out lysosomal accumulation of cholesterol, which in turn interferes with LIMP2 activity in PD fibroblasts expressing the N370S *GBA1* mutation (Franco et al., 2018). Consistently, (Gegg et al., 2015) also demonstrated that GlcCer accumulation can affect α-syn stability and solubility. Nevertheless, there is no evidence of substrate overload in PD brains with heterozygous *GBA1* mutations (Gegg et al., 2015). GCase has been demonstrated to play an important role in α-syn homeostasis, as suggested by the fact that promoting GCase activity reduced α-syn levels in IPSC-derived dopaminergic neurons (Gruschus et al., 2015). Inhibiting GCase activity by conduritol-b-epoxide (CBE) administration causes α-syn accumulation in midbrain dopaminergic neurons (Zunke et al., 2018). *In vitro* studies revealed an interaction between GCase and the C-terminal of α-syn in the acidic lysosomal environment (Yap et al., 2011), but in vivo evidence of GCase-α-syn interaction is still lacking. Another proposed mechanism correlating GCase dysfunction to α-syn aggregation is mediated by the ER stress. Misfolded proteins can accumulate in the ER due to *GBA1* mutations, leading to ER stress and ER-mediated unfolded protein response (UPR). ER engages UPR to control the overload of unfolded proteins and prevents cell death by apoptosis (Hetz et al., 2012). In fact, iPSCs-derived dopaminergic neurons from patients carrying either N370S GBA1 or SNCA triplication showed aberrant autophagy and UPR upregulation (Fernandes et al., 2016; Heman-Ackah et al., 2017). Furthermore, the levels of two UPR markers were found altered in N370S *GBA1* dopaminergic neurons (Fernandes et al., 2016). A secondary effect of a reduced GCase activity might be mitochondria dysfunction, a mechanism that can sustain α-syn misfolding. In vitro studies demonstrated that the reduction of GCase activity was coupled to a loss in mitochondria membrane potential, respiratory complex function, increased ROS production and membrane fragmentation (Gegg and Schapira, 2016). The “lysosomal defect theory” has been proposed to explain the GCase-mediated α-syn aggregation. However, it has been noted that this mechanism is GCase-driven because general inhibition of lysosomal function does not result *per se* in α-syn accumulation. Most likely, the impaired translocation from the Golgi to lysosomes is responsible for the reduced GCase-driven lysosomal function. Consistently, mutations in *SCARB2* gene, encoding for the GCase transporter LIMP2, reduce GCase activity. Two single nucleotide polymorphisms within the *SCARB2* gene have

been associated with PD, but through a mechanism that does not rely on GCase activity (Alcalay et al., 2016). All this evidence suggests that still little is known about the complex mechanism through which *GBA1* mutations cause α-syn neuropathology associated with PD (Do et al., 2019).

1.9. α-syn and PD

1.9.1. α-syn: gene, protein structure and biological functions

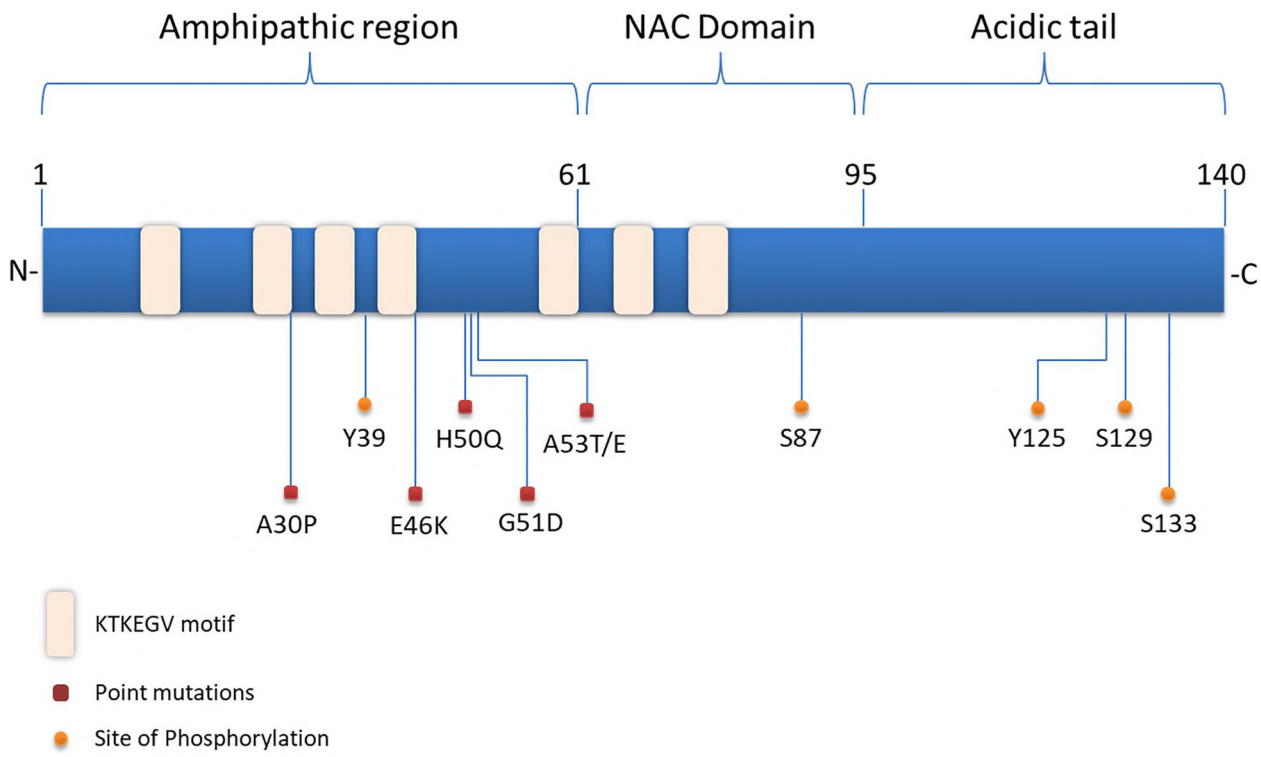

Figure 2. α-syn gene structure, mutations and phosphorylation sites (Fouka et al., 2020). α-syn is a 140 amino acid-long protein, that can be divided into three regions: the N-terminal amphipathic region (1-60 aa), the central NAC region (61-95 aa) and the C-terminal acid tail (96-140 aa). Six point mutations, all located in the N-terminal domain, have been described: A30P, E46K, H50Q, G51D, A53E, A53T. Five phosphorylation sites have been characterized: Y39 in the N-terminus, S87 in the NAC domain and Y125, S129, S133 in the C-terminus. The highly-conserved KTKEGV motif is required for the protein to assume the α-helical conformation, and participates in modulating its ability to bind membranes.

Mutations in the *SNCA* gene were first characterized in monogenic forms of PD. Point mutations, such as A30P, E46K, H50Q, G51D, A53E, A53T (Polymeropoulos et al. 1997; Kruger et al. 1998; Zarranz et al. 2004; Kiely et al. 2013; Proukakis et al. 2013; Pasanen et al. 2014) as well as gene duplications and triplications (Singleton et al. 2003; Ibanez et al. 2004; Ferese et al. 2015) of the *SNCA* gene have been associated with PD (**Figure 2**). Several polymorphisms in regulatory regions upstream the *SNCA* gene are considered risk factors for early-onset PD (Maraganore et al. 2006). α-syn is a small protein, composed by 140 amino acids. Its structure can be divided into three main regions (**Figure 2**). The highly conserved N-terminal domain, comprising 1-60 amino acids, is rich

in positively charged residues that are repeated four times. The central region spanning over the 61-95 amino acids, also called non-amyloid-β component (NAC), contains hydrophobic residues that are responsible for its ability to fibrillate and, thus, assume the β-sheet structure that, eventually, evolves in amyloid fibrils. Disruption and deletion of this region can prevent α-syn misfolding and abnormal aggregation. The unfolded C-terminal domain (96-140 amino acids) is highly acidic and involved in post-translational modifications as well as interactions with cytosolic or membrane-bound proteins (Giasson et al., 2001; Bayer et al., 1999; Guardia-Laguarta et al., 2014; Theillet et al., 2016). LBs contain not only the full-length protein but also several truncated forms of the sole C-terminal domain of α-syn. Interestingly, those truncated forms have been observed also in age-matched healthy controls, suggesting that α-syn cleavage can occur also under physiological conditions (Li et al., 2005). Nevertheless, it has been proposed that the truncated C-terminal domain of α-syn might be more prone to accumulation, acting as a promoter for full-length protein aggregation (Li et al., 2005). As part of an intrinsically disordered protein class, α-syn mainly exists as unorganized soluble monomers that eventually can combine to form oligomers, then protofibrils and fibrils. To date, several factors are believed to trigger changes in α-syn conformation and aggregation status, such as oxidative stress, proteolysis, fatty acid, phospholipids, metal ions, alternative splicing, point mutations and multiplications in the SNCA gene, overload of α-syn or its post-translational modifications (Atik et al., 2016). Indeed, α-syn is subjected to several post-translational modifications, including phosphorylation, ubiquitination, nitration and truncation (Oueslati et al., 2010). Several studies have found that α-syn colocalizes with ubiquitin in both LBs and Lewy neurites. Lysine residues in the N-terminal region are subjected to ubiquitination, and Lys12, Lys21 and Lys23 have been described as the major sites for this post-translational modification in α-syn purified from LBs (Anderson et al., 2006; Oueslati et al., 2010). The presence of ubiquitin-targeted α-syn in LBs might suggest the failure of proteasomal involvement in its degradation. In fact, there is evidence that non-ubiquitinated α-syn undergoes proteasomal and ALP degradation (Stefanis et al., 2019). α-syn has been also found to be nitrated in LBs of PD, AD, LBD and MSA patients. In fact, α-syn is subjected to nitration at several Tyr residues located in both N- and C-terminals, such as Tyr39, Tyr125, Tyr133 and Tyr136, under nitrative stress conditions (Giasson et al., 2000). Although the exact role of nitrate α-syn is still unknown, this post-translational modification has been found to promote oligomer formation, by forming covalently crosslinked Tyr dimers that are insoluble in SDS solutions and highly thermally stable (Souza et al., 2000). Furthermore, nitration reduces the ability of the protein to bind lipids and cellular membranes (He et al., 2019). Hodara and colleagues conducted a study on chromatographically purified nitrated monomers, dimers and oligomers of α-syn, demonstrating that low concentrations of nitrated monomers and dimers promote fibrils rather

than oligomers formation (Hodara et al., 2004). Altogether, these findings sustain the hypothesis that nitration contributes to conferring toxic gain-of-function properties to α-syn. Indeed, nitrate α-syn has been reported to be directly or indirectly cytotoxic, especially for dopaminergic neurons, by promoting neuroinflammation and reactive oxygen and nitrogen species release, that, in turn, further sustain the nitration of α-syn (He et al., 2019). Phosphorylation has been extensively studied as a major factor contributing to α-syn toxicity (**Figure 2**). Under physiological conditions, only 4% of α-syn is phosphorylated at Ser129, whereas this percentage rises up to 90% in LBs, suggesting a putative role in regulating α-syn aggregation and cytotoxic properties (Chen et al., 2005; Fujiwara et al., 2002). Consistent with this view, pSer129 α-syn has been considered neurotoxic and an early marker of aggregation and accumulation (Chen et al., 2005; McFarland et al., 2009; Sato et al., 2013). Nevertheless, further investigation is still needed to fully understand which are the alterations in its biochemical properties and biological functions upon phosphorylation at Ser129, and if this modification enhances or suppresses α-syn neuropathology *in vivo* (Oueslati et al., 2016). Several studies failed to prove whether the phosphorylation at Ser129 can modify α-syn ability to bind cellular membranes. In fact, some in vitro studies reported no influence whereas others described an inhibitory effect of this modification on α-syn association to cellular membranes in yeasts (Fiske et al., 2011), *C. elegans* (Kuwahara et al., 2012), and rats (Azeredo da Silveira et al., 2009). Furthermore, Hara and colleagues reported that Ser129 phosphorylation of α-syn increases dopamine uptake in SH-SY5Y cells without affecting DAT transporter expression (Hara et al., 2013). Another line of research sustains that phosphorylation might influence the protein binding to metallic ions, since Ser129 is in the C-terminal region that is involved in ion binding (Oueslati et al., 2016). In fact, α-syn fibrillization can be driven by interaction with metal ions (Levin et al., 2011). Phosphorylation at Ser129 can also alter α-syn clearance. The first evidence was provided by *in vitro* studies reporting an increase of pSer129 α-syn after proteasomal (Chau et al., 2009) and ALP blockage (Machiya et al., 2010). In addition, the S129A substitution in yeast prevents α-syn degradation by ALP (Tenreiro et al., 2014). Finally, several *in vitro* and *in vivo* studies (Oueslati et al., 2016) have suggested that phosphorylation at Ser129 might reduce α-syn nuclear translocation. Altogether, these data suggest that phosphorylation at Ser129 might alter α-syn biochemical and functional features. Whether this post-translational modification is also required for α-syn aggregation and seeding is still elusive. In fact, a number of *in vitro* studies support the hypothesis that pSer129 α-syn triggers α-syn fibrillization, although such correlation has not been proven *in vivo*. Indeed, Luk et al. (2009) reported that formation of LB-like inclusions occurs even in the absence of phosphorylation *in vitro.* Conversely, the sole addition of the truncated form of α-syn (1-120) was sufficient to induce phosphorylation at Ser129 of the recruited endogenous α-syn (Luk et al., 2009; Volpicelli-Daley et al., 2010), suggesting

that phosphorylation at Ser129 is not likely a limiting factor for the α-syn neurotoxic gain-of-function (Oueslati et al., 2016).

1.9.2. α-syn and ALP

There is evidence that only a small portion of the intracellular α-syn undergoes a proteasomal-dependent degradation, as suggested by the *in vitro* studies reporting no changes in the levels of both higher order α-syn oligomers and monomers upon proteasomal inhibition (Emmanouilidou et al., 2010). ALP has been also largely investigated as the major factor responsible for α-syn clearance, in particular CMA and macroautophagy. The first studies assessed the role of cathepsin D (Sevlever et al., 2008), cathepsin B and cathepsin L (McGlinchey and Lee, 2015) in degrading α-syn, reporting that only cathepsin L was effective on the fibrillar form. Webb and colleagues (Webb et al., 2003) demonstrated that A53T α-syn was degraded by both proteasome and macroautophagy, while WT and A30P α-syn by the proteasome when overexpressed. In the same study, it was also reported that macroautophagy induction by rapamycin promoted the clearance of overexpressed WT, A53T and A30P but not endogenous α-syn. A year later, in partial agreement, Cuervo and colleagues reported that pharmacological inhibition of macroautophagy had no effect on endogenous monomeric and dimeric α-syn that, in fact, was degraded by a one-by-one fashion type of degradation named CMA (Cuervo et al., 2004). α-syn bears the KFERQ-like pentapeptide sequence that is selectively recognized by the Hsc70 chaperone. The first evidence that α-syn is degraded by CMA came from a study in purified lysosomes from rat liver. Not only this study proved that CMA participates in α-syn clearance, but also that A53T and A30P α-syn block CMA. Both mutants bind to the rate-limiting lysosomal receptor LAMP2A with high affinity, inhibiting its function and CMA activity (Cuervo et al., 2004). Similar resistance to CMA-dependent degradation was shown by oligomeric and dopamine modified α-syn in isolated lysosomes (Martinez-Vicente et al., 2008). Consistent with Cuervo et al.(2004) and Webb et al.(2003), other studies confirmed that knocking down LAMP2A leads to α-syn accumulation in primary cortical neurons, ventral midbrain dopaminergic neurons (Vogiatzi et al., 2008) and human dopaminergic neuroblastoma SH-SY5Y cells (Alvarez-Erviti et al., 2010). The same study also reported a reduction in CMA-competent markers LAMP2A and Hsc70 in PD brain regions affected by α-syn neuropathology, as SN (Alvarez-Erviti et al., 2010). In particular, A53T α-syn-dependent blockage of CMA was associated with increased toxicity and compensatory activation of macroautophagy in neuronal cells (Xilouri et al., 2009). Enhancing CMA activity has been also proven neuroprotective *in vivo* (Xilouri et al., 2013). Interestingly, there are studies connecting α-syn degradation with its secretion from the cell and spreading. In an *in vitro* study on Cathepsin D-deficient cells, α-syn displayed an increased propensity to aggregation (Bae et al., 2015). Cell-to-cell

transmission, e.g. secretion and uptake, of aggregated α-syn was enhanced in Cathepsin D-deficient cells, suggesting a lysosomal role in preventing α-syn spreading (Bae et al., 2015). Extracellular α-syn excretion has been described as a protective cellular mechanism to prevent α-syn-mediated blockage of ALP. In fact, α-syn aggregates can resist macroautophagy degradation, which leads to their deposition in the extracellular space (Lee et al., 2004; Tanik et al., 2013). Only a few *in vivo* studies have tried to address the role of proteasome and ALP in α-syn elimination. Ebrahimi-Fakhari and colleagues confirmed that upon proteasomal inhibition superficial cortical tissues showed an accumulation of both endogenous and overexpressed human α-syn in mice (Ebrahimi-Fakhari et al., 2011). Conversely, *in vivo* lysosomal inhibition led to selective accumulation of overexpressed human α-syn, suggesting that ALP involvement occurs exclusively in the case of α-syn aggregation. Ahmed and collaborators reported that mice conditionally lacking *Atg7* in midbrain dopaminergic neurons have increased α-syn levels and ubiquitin-positive inclusions, which were not associated with changes in the aggregation properties of the protein (Ahmed et al., 2012). Consistently, another study using a similar animal model reported accumulation of oxidized α-syn in the swelling nigrostriatal axons of aged animals (Friedman et al., 2012). These studies underlie that important role of axonal macroautophagy in α-syn accumulation. Nevertheless, Mak et al., 2010 showed that, upon application of different stressors, LAMP2A colocalizes with α-syn, and its translocation into the lysosomal lumen is accelerated. Interestingly, knocking out *LAMP2* gene in mice did not alter α-syn or CMA substrate levels (Rothaug et al., 2015). However, further investigations at molecular levels are needed to better define the compensatory mechanisms that can occur to overcome the loss of the three lysosomal isoforms of the LAMP2 receptors *in vivo* (Stefanis et al., 2019). On the contrary, mice lacking Cathepsin D exhibited a preferential accumulation of α-syn oligomeric and aggregated forms, as also reported in human brains displaying lower Cathepsin D levels (Qiao et al., 2008; Cullen et al., 2009). Altogether, these results suggest that α-syn degradation requires the concomitant intervention of several pathways, proteasome, macroautophagy and CMA, under both physiological and pathological conditions. Given that several factors, including the aggregation status, concentration of α-syn, post-translational modification and presence of mutant forms, might influence the main pathway involved, it might be plausible that multiple pathways degrade different α-syn forms at the same time (Stefanis et al., 2019). Mishandling of α-syn clearance can facilitate α-syn secretion from cells and its spreading throughout the CNS as a "seed" for misfolding of native endogenous α-syn.

1.10. LRRK2 and PD

1.10.1. LRRK2 gene and protein

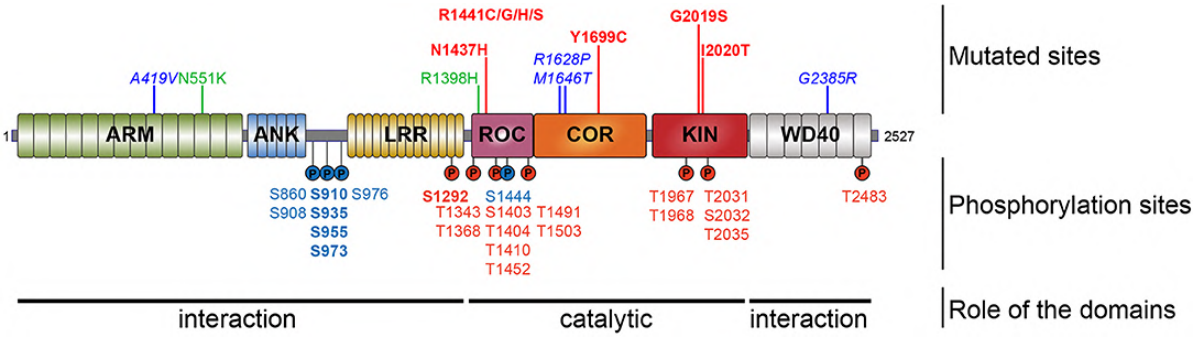

Figure 3. LRRK2 gene structure, mutations and phosphorylation sites (Marchand et al., 2020)**.** LRRK2 is a large multidomain protein with a catalytic core composed by GTPase Ras-of-Complex (ROC) and kinase domains separated by a C-terminal of ROC (COR) domain. The central core is surrounded by several protein-protein interacting motives, such as armadillo (ARM), ankyrin (ANK), LRR (N-terminal region), and WD40 (C-terminal) domains. A handful of pathogenic mutations have been identified: N1437H, R1441C/G/H/S, Y1699C, G2019S, I2020T (in red). In the upper part of the figure, the risk variants (A419V, M1646T, R1628P, G2385R) are depicted in blue and the two protective variants (N551K, R1398H) are indicated in green. In the lower part, the heterologous phosphorylation sites are depicted in blue, the autophosphorylation sites in red. In bold, the most characterized (auto)/phosphorylation sites.

Mutations in the leucine-rich repeat kinase 2 (*LRRK2)* gene cause autosomal dominant PD (Zimprich et al., 2004; Paisan-Ruiz et al., 2005), but according to genome-wide association studies (GWAS), the LRRK2 locus also represents a risk factor for idiopathic PD (Nalls et al., 2014). GWAS also linked SNPs in the *LRRK2* gene to three chronic inflammatory conditions, such the Crohn's Disease (CD) (Hui et al., 2018; Kumar et al., 2013; Witoelar et al., 2017), leprosy (Zhang et al., 2009) and tuberculosis (Wang et al., 2018). The association with cancer remains controversial (Berwick et al., 2019). LRRK2-related PD is a pleomorphic pathology, presenting with degeneration of dopaminergic neurons in SNpc and LB formation (Marras et al., 2011; Kalia et al., 2015). The *LRRK2* gene encodes for a large multidomain protein encompassing a central catalytic core composed by the GTPase Ras-of-Complex (ROC) and serine-threonine kinase domains separated by a C-terminal of ROC (COR) domain (**Figure 3**). The catalytic core is surrounded by protein-protein interaction motives, including the armadillo, ankyrin, LRR (N-terminal region), and WD40 (C-terminal) domains (Mata et al., 2006; Cookson et al., 2010; Mills et al., 2014). Eight mutations in the *LRRK2* gene have been pathogenically linked to PD: the G2019S and I2020T mutations in the kinase domain, the N1437H and R1441C/G/H/S in the ROC domain, and Y1699C in the COR domain (**Figure 3**). The most prevalent mutation in the *LRRK2* gene is the c.6055G>A transition resulting in the serine to glycine substitution in position 2019 of the protein. The G2019S mutation is present in 4% of familial and 1% of idiopathic PD cases, with frequencies up to 40% in specific ethnic groups (Gasser, 2009; Okubadejo et al., 2018). This pathogenic mutation is attractive not only due to the highest prevalence among LRRK2

mutations but also because it causes an increase of LRRK2 kinase activity, making it an ideal target for pharmacological intervention. LRRK2 has been found to interact with several substrates, including LRRK2 itself at Ser1292 (Sheng et al., 2012) and at least 20 sites that have been identified *in vitro* (Marchand et al., 2020), 14-3-3 proteins, and a subset of Rab small GTPases (e.g. Rab3A/B/C/D, Rab8A/B, Rab10, Rab12, Rab29, Rab35, Rab43) (Steger et al., 2016). Initially, the discovery of the G2019S mutation has led to hypothesize that all pathogenic mutations occurring within the *LRRK2* gene would cause neurotoxicity through increased kinase activity-mediated mechanism. In fact, hyperactivation of the kinase domain has been proven neurotoxic in a plethora of *in vitro* and *in vivo* models (West et al., 2005; Smith et al., 2006; Greggio et al., 2006; Heo et al., 2010; Yao et al., 2010). Nonetheless, the precise mechanism through which the increased LRRK2 kinase activity exerts its toxic action, ultimately triggering PD-like neuropathology, is still unclear. Lately, it has been proposed that all LRRK2 pathogenic mutations ultimately result in hyperactivation of LRRK2 kinase activity. Mutations occurring in the RoC and COR domains lead to either an increased affinity for the binding to GTP or a slower hydrolysis rate of the GTP (o both), resulting in a higher amount of LRRK2-GTP. Consistent with this view, the R1398H variant, showing protection from PD and CD, has been associated with lesser GTP-bound and a higher rate of GTP hydrolysis (Hui et al., 2018; Nixon-Abell et al., 2016). The precise mechanism leading to LRRK2-mediated GTP hydrolysis and recycle is still elusive. This is supported by the fact that neither GEFs nor GAPs have been found in the RoC domain (Mills et al., 2018; Liao et al., 2014), whereas the leading model associated with LRRK2 GTPase activity has been the "GTPase Activated by Dimerisation". According to this model, LRRK2 GTPase activity requires the formation of a homodimer by the interaction between the two RoC domains facing each other (Wauters et al., 2019). However, studies conducted on the truncated RocCoR domains reported that their dimerization occurs when they both bind to GDP, whereas the substitution of the GDP with a GTP promotes their disassembly. Therefore, the hydrolysis of GTP is mediated by the monomeric RocCoR domain (Deyaert et al., 2017; Wauters et al., 2019). These results should be taken with caution because they do not consider the involvement of other protein-protein interaction domains that might participate in the dimer assembly. The fact that LRRK2 GTPase effectors have not been identified yet does not rule out the possibility that in addition to modulating the adjacent kinase activity, the GTPase activity exerts downstream independent functions (Berwich et al., 2019). LRRK2 dimerization has also been linked to a different subcellular localization of the protein. LRRK2 dimers, exhibiting an increased kinase activity, were predominantly found to be associated with intracellular membranes, while LRRK2 monomers, characterized by a lower kinase activity, were mostly located in the cytoplasm (Berger et al., 2010; Sen et al., 2009; Civiero et al., 2017; James et al., 2012). It is still not clear whether mutations in the

CoR domain stabilize the dimeric or the monomeric form. Those mutations weaken the dimer interaction in the isolated RocCor fragments (Nixon-Abell et al., 2016; Klein et al., 2009; Law et al., 2014). According to the mechanism proposed by Deyaert and colleagues, the mutations do not decrease GTPase activity but reduce the rate of the dimers disassembly, thus "blocking" LRRK2 in a GTP-bound state (Deyaert et al., 2017). However, to allow LRRK2 physiological function, the ankyrin domain and Rab29-GTP participate in the membrane recruitment of a pool of LRRK2 monomers, facilitating their assembly into dimers. Upon membrane-binding, LRRK2 becomes active and phosphorylates its substrates. The presence of Rab29-GTP is not required for LRRK2 recruitment, dimerization and increase in kinase activity but stabilizes LRRK2 dimers preventing their dissociation and monomerization. The increased phosphorylation of LRRK2 substrates associated with pathogenic mutations is mediated by the interplay between the mutant LRRK2 and the Rab29 activity. In particular, mutations in the RocCoR domain increase LRRK2 dimer stability, whereas G2019S mutation augments the intrinsic kinase activity (Berwick et al., 2019). Furthermore, a reciprocal regulation between the GTPase and kinase domains has been hypothesized, as suggested by the presence of several autophosphorylation sites in both regions. The detailed mechanism for this mutual control is still poorly understood, as is the role of the WD40 domain in the dimerization process (Zhang et al., 2019). Phosphorylation at serine residues within the ankyrin and LRR domains plays an important role in the regulation of LRRK2 activity. Different kinases were identified to directly phosphorylate LRRK2, such as casein kinase 1α (CK1α) (Chia et al., 2014), the IκB family kinases IKKα, IKKβ, IKKε and TANK-binding kinase 1 (TBK1) (Dzamko et al., 2012), the protein kinase A (PKA) (Li et al., 2011; Muda et al., 2014). The phosphatase responsible for LRRK2 dephosphorylation is, instead, protein phosphatase PP1, whose activity is induced by arsenite or hydrogen peroxide (Lobbestael et al., 2013; Mamais et al., 2014). The phosphorylation mediated by these kinases triggers LRRK2 binding and sequestration by 14-3-3 proteins (Stark et al., 2006; Dzamko et al., 2010) which might influence dimer formation, and LRRK2 subcellular localization and activity (Berwick et al., 2019). Modulation of this interaction rescued some PD-related alterations, such as the reduction of neurite outgrowth mediated by R1441G and G2019S overexpression *in vitro* (Lavalley et al., 2016).

1.10.2. LRRK2 mutations and PD

To further investigate the causative relationship between LRRK2 enzymatic activity and PD neuropathology, the first approach adopted was the overexpression of LRRK2 pathogenic mutations G2019S, I2020T, R1441C or Y1699C in primary neurons, leading to neurite shortening, cell death and impaired cellular functions (Lee et al., 2010; West et al., 2005; Biosa et al., 2013; Greggio et al.,

2006; Smith et al., 2006; MacLeod et al., 2006; Wang et al., 2012). Pharmacological inhibition or genetic inactivation of the LRRK2 kinase domain and the GTPase domain were able to rescue PD-related phenotypes in most cases (Lee et al., 2010; Ramsden et al., 2011). For example, deletion of *LRRK2* promoted an increase in neurite length and branching in primary cortical neurons (Lee et al., 2010; West et al., 2005; Smith et al., 2006; MacLeod et al., 2006). The pathogenicity of those mutations was also studied in several transgenic (Tg) animal models. *Drosophila* models expressing human G2019S, R1441C, Y1699C, or I2020T LRRK2 recapitulated some PD features, such as age-dependent dopaminergic neurons loss, altered dopamine homeostasis, impairment in locomotor activity or shortened life span (Lin et al., 2010; Venderova et al., 2009; Hindle et al. 2013; Ng et al., 2009; Liu et al., 2011). Also *C.elegans* expressing human LRRK2 G2019S and R1441C showed degeneration of dopaminergic neurons, reduced dopamine release and locomotor dysfunction (Liu et al., 2011; Yao et al., 2010). Pharmacological inhibition of LRRK2 activity proved effective in rescuing some PD-related features (Liu et al. 2011) suggesting that targeting LRRK2 kinase activity would represent a novel therapeutic strategy for PD pharmacotherapy. In rodents, viral overexpression of LRRK2 G2019S in the striatum of mice and rats caused the loss of dopaminergic neurons in SNpc (Lee et al., 2010; Tsika et al., 2015) although most studies in Tg animals failed in replicating this phenotype (Chen et al., 2012; Chou et al., 2014; Maekawa et al., 2012; Weng et al., 2016; Xiong et al., 2018). Likewise, knock-in (KI) models expressing *LRRK2* pathogenic mutations at endogenous levels did not show nigral neurodegeneration (Maewaka et al., 2012; Longo et al., 2017; Tong et al., 2009; Li et al., 2010; Herzig et al., 2011; Yue et al., 2015; Volta & Melrose, 2017). However, aged G2019S KI mice exhibited dopamine synaptic dysfunctions and mild behavioral deficits, which would make them a suitable model for studying the prodromal phase of PD (Giesert et al., 2017; Longo et al., 2017). This is also supported by the fact that G2019S KI mice show enhanced susceptibility to parkinsonian toxins or triggers (Karuppagounder et al., 2016; Arbez et al., 2020), particularly at an advanced age (Novello et al, 2018). All these studies suggest that manifestation of a pathological phenotype is highly dependent on the age of the animals, the expression levels of LRRK2 and the animal model used.

1.10.3. LRRK2 mutations and α-syn neuropathology

Postmortem analysis on PD brains detected LRRK2 in LBs, suggesting that LRRK2 might sustain α-syn neuropathology (Greggio et al., 2006; Miklossy et al., 2006; Zhu et al., 2006a; Zhu et al., 2006b). Nonetheless, a subset of LRRK2 PD patients did not show LBs or α-syn accumulation, even in presence of nigral neurodegeneration (Schneider et al., 2017; Poulopoulos et al., 2012; Kalia et al., 2015). However, since high α-syn levels were found in the cerebrospinal fluid (CSF) of asymptomatic

LRRK2 carriers, LRRK2 might play an important role in the early formation of toxic oligomers (Aasly et al., 2014). Different LRRK2 models were employed to investigate whether LRRK2 facilitates age-dependent α-syn neuropathology. Age-dependent accumulation of Venus fluorescent protein-tagged α-syn was reported in WT worms, which was rescued by the deletion of *lrrk1* (*LRRK1* and *LRRK2* ortholog in *C.elegans*) (Bae et al., 2018). Deposition of α-syn oligomers along with aging was also described in the striatum and cortex of R1441G KI mice at 15 and 18 months of age (Ho et al., 2020). Tg mice overexpressing LRRK2 G2019S under the TH promoter, exhibited an age-dependent loss of both dopaminergic and norepinephrinergic neurons and increased levels of high molecular weight pSer129-positive α-syn levels in striatum and SN at 15 and 24 months (Xiong et al., 2018). In keeping with the view that LRRK2 kinase activity facilitates α-syn deposition, mice co-overexpressing the kinase dead mutation D1994S with the pathogenic mutation G2019S did not display any sign of synucleinopathy. Although overexpression of LRRK2 in Tg rodents did not always lead to neurodegeneration, co-overexpression of either human WT or G2019S LRRK2 with A53T α-syn in mice exacerbated the α-syn neuropathology and toxicity in striatum and cortex (Lin et al., 2009). Nevertheless, other studies in Tg mice failed to prove this synergistic toxic action *in vivo* (Daher et al., 2012; Herzig et al., 2011). In a rat model of synucleinopathy, the AAV2/1-mediated overexpression of WT α-syn resulted in an increased loss of dopamine neurons and microgliosis (Daher et al., 2014; Daher et al., 2015). Consistent with this report, Novello and colleagues showed that AAV2/9-mediated nigral overexpression of human A53T α-syn caused greater pSer129 α-syn accumulation and neurodegeneration in the striatum and SN of aged G2019S KI mice (Novello et al., 2018). These studies corroborate the hypothesis that LRRK2 mutations facilitate the emergence of synucleinopathy. Consistently, studies conducted in mice injected with preformed fibrils (PFFs) of α-syn, a recently developed etiological model of PD, showed that overexpression of human G29019S LRRK2 was associated with accelerated α-syn deposition and aggregation and greater neural loss in SNpc neurons and neuroinflammation (Bieri et al., 2019). α-syn PFFs have been developed as a powerful tool to test the prion-like properties of α-syn, which would act as a seed in the conversion of endogenous α-syn into its pathogenic forms, facilitating their spreading in CNS *via* cell-to-cell transmission and accumulation of toxic α-syn (Volpicelli-Daley et al., 2016). In the study of Bieri and colleagues, rats were injected in the vagus nerve with AAV vectors carrying human α-syn in to test long-distance α-syn spreading (Bieri et al., 2019). Consistent with a facilitatory LRRK2 role in α-syn cell-to-cell transmission, the immunohistochemical analysis revealed that the number of the α-syn-positive axons were significantly lower in the medulla, midbrain and forebrain of LRRK2 KO rats compared to WT controls. To confirm this view, a PFF-based transmission assay carried out in iPSCs-derived neurons obtained from PD patients revealed that the G2019S mutation enhanced PFF-

mediated α-syn aggregation, which was abolished by LRRK2 knockout (Bieri et al., 2019). Despite of the recognized role of LRRK2 in the α-syn spreading, the exact mechanism underlying this interplay is still unknown. One of the possible mechanisms is the LRRK2-mediated regulation of Rab35 activity. Indeed, Rab35 might contribute to LRRK2-related neurodegeneration (Jeong et al., 2018) and A53T α-syn release and aggregation in SH-SY5Y cells (Chiu et al., 2016). Given the involvement of LRRK2 and Rab35 in endosomal recycling, it seems plausible that interfering with the LRRK2-Rab35 interplay would prevent the degradation of α-syn-positive inclusions and facilitate α-syn transmission. However, no proof of this causative mechanism has been provided yet, leaving the possibility open that other Rabs might be involved in this regulation.

1.10.4. LRRK2 cellular functions

A number of studies have been conducted in order to identify the LRRK2 substrates *in vivo* and, thus, the cellular pathways in which LRRK2 and its kinase activity are involved. A group of LRRK2 substrates, including endophilin A1, snapin, synaptojanin-1 and NSF, is involved in synaptic transmission. Postmortem analysis of PD brains has suggested that synaptic dysfunction is an early event in PD pathogenesis. In particular, these studies suggest that LRRK2 plays an important role in the endocytosis and recycling of synaptic vesicles (Matta et al., 2012; Arranz et al., 2015). To date, LRRK2 has been found to phosphorylate 14 Rab GTPases: Rab3a/b/c/d, Rab5a/b/c, Rab8a/b, Rab10, Rab12, Rab29, Rab35, and Rab43. All PD-associated LRRK2 mutations resulted in increased phosphorylation of these proteins at their conserved residue. The Rab proteins are part of the Ras-like small GTPase superfamily, which consists of 66 genes in the human genome. Rab GTPases cycle from a GTP-bound to a GDP-bound state and play a crucial role in intracellular vesicle trafficking, acting as a molecular switch (Stenmark et al., 2009). Each Rab targets a specific organelle or pathway, regulating endocytosis or exocytosis, vesicle recycling, fusion, and transport along cytoskeleton. The LRRK2-mediated phosphorylation and activation of several Rabs have led to hypothesize a possible involvement of LRRK2 in the vesicle trafficking pathway. Consistent with this view, LRRK2 has been found to be associated with intracellular membranes, including Golgi apparatus, ER, mitochondria, lysosomes, endosomal vesicles, autophagosomes (Bonet-Ponce et al., 2021). Therefore, further investigations are needed to understand whether an altered vesicle trafficking due to Rab GTPase aberrant modulation is the pathogenic event triggering LRRK2-related PD. Indeed, several studies focused on the characterization of the impact of LRRK2 mutations on the vesicle trafficking involved in the endolysosomal and autolysosomal pathways (Boecker et al., 2021; Manzoni et al., 2018; Herzig et al., 2011; Wallings et al., 2019).

1.10.5. LRRK2 and Autophagy

Autophagy is a complex multi-step process in which several actors are involved as parts of different canonical and non-canonical pathways aimed at the clearance of cellular debris, old/misfolded proteins, dysfunctional organelles or pathogens (Deter et al., 1967; Mortimore and Schower, 1977). LRRK2 participates in this process, acting at different levels (Bonet-Ponce et al., 2021). Indeed, ALP alterations have been widely recognized to be associated with misfolded protein accumulation and aggregation (Galluzzi et al., 2017; Boland et al., 2018; Albanese et al., 2019; Madureira et al., 2020). The involvement of LRRK2 in several autophagic steps has extensively been documented (Albanese et al., 2019; Madureira et al., 2020).

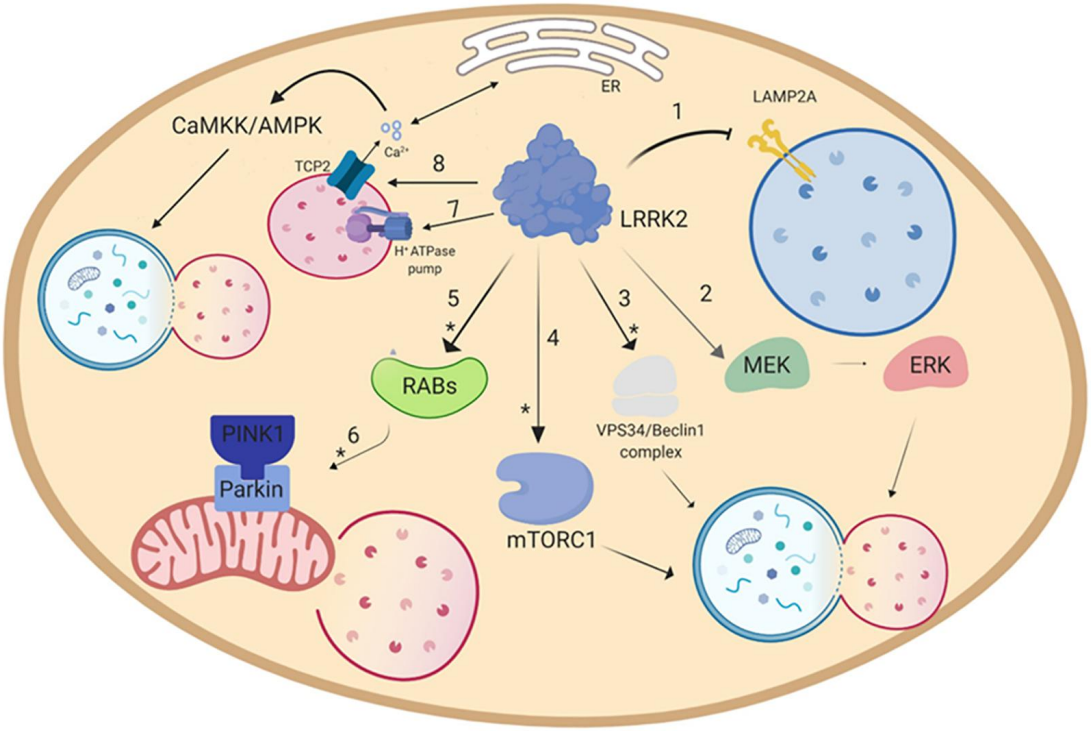

Figure 4. Putative mechanism through which LRRK2 regulates autophagy (Albanese et al., 2019). **1)** Blockage of CMA (Orenstein et al., 2013); modulation of **2)** MEK/ERK pathway (Bravo-San Pedro et al., 2013), **3)** VPS34/beclin1 complex (Manzoni et al., 2016), 4) mTOR pathway (Imai et al., 2008; Ho et al., 2018), 8) Ca^{2+}/CaMKK/AMPK pathway (Gomez-Suaga et al., 2012b). Regulation of mitophagy via **5)** Rabs (Wauters et al., 2020), **6)** PINK1/Parkin (Saez-Atienzar et al., 2014; Schapansky et al., 2014; Yakhine-Diop et al., 2014; Bonello et al., 2019). Furthermore, LRRK2 can modify lysosomal pH via **(7)** lysosomal H+-ATPase pump (Wallings et al., 2019). Asterisk (∗) indicates the putative pathways modulated by pharmacological LRRK2 kinase inhibitors.

Autophagy induction. The canonical pathway of autophagic induction starts with mTORC1 inhibition and/or AMPK activation. In mouse primary astrocytes it has been reported that pharmacological inhibition of LRRK2 kinase activity with LRRK2-IN-1 promotes autophagy through Beclin-1-mediated PI3P upregulation, which does not involve the canonical mTORC1/ULK1 pathway (Manzoni et al., 2016; **Figure 4**). However, in the same *in vitro* model, prolonged LRRK2 kinase inhibition resulted in autophagy repression through an mTORC1-independent increased ULK1 phosphorylation at Ser758 (Manzoni et al., 2018). In keeping with Manzoni et al. (2016) and Bravo-

San Pedro et al. (2013), the G2019S-mediated increase in basal autophagy flux was reversed by the MAPK1/3 inhibitor UO126, indicating the involvement of the MEK/ERK/Beclin-1 pathway (**Figure 4**). Consistently, Plowey and colleagues showed that the MAPK1/3 inhibitor UO126, but not 3-Methyladenine (that acts through the mTOR pathway) rescued the G2019S-induced neurite shortening phenotype (Plowey et al., 2008). Moreover, overexpression of WT or I2020T LRRK2 in *Drosophila melanogaster* hyperphosphorylated 4E-PB (a downstream mTORC1 substrate) without affecting mTOR protein levels or phosphorylation (Imai et al., 2008; **Figure 4**). These results suggest that LRRK2 might play a role in autophagy induction through an mTOR-independent noncanonical mechanism. In contrast, in RAW264.7 or murine microglial cells activated via TLR4, LRRK2 phosphorylates and translocates onto autophagosomal membranes, promoting autophagy via an mTOR-dependent activation (Schapansky et al., 2014). A possible LRRK2-mediated modulation of mTORC1 was also investigated in LRRK2 mutant mice. Herzig and colleagues reported an increase of mTOR protein levels in the kidney of 5-month-old G2019S KI and LRRK2 KO mice and a decrease in LRRK2 D1994S KI mice (bearing a kinase dead mutation). However, no change in the downstream S6K1 phosphorylation levels, readout of mTORC1 kinase activity, was observed (Herzig et al., 2011).

Autophagosome formation and flux. Several studies have attempted to address the role of LRRK2 in autophagosome formation *in vitro*, obtaining inconsistent results. Neuronal or macrophage cultures obtained from LRRK2 KO mice showed an increase of LC3II levels and autophagic flux (Manzoni et al., 2016; Hartlova et al., 2018; Wallings et al., 2019), while KO mice showed a striking kidney pathology (Tong et al., 2010, 2012; Hinkle et al., 2012; Fuji et al., 2015). Tong and colleagues reported a biphasic change in ALP along with α-syn aggregation properties: reduction of both LC3-II/LC3-I ratio and insoluble α-syn forms at 7 months, and elevation of LC3-II/LC3-I ratio and insoluble α-syn deposition while at 20 months (Tong et al., 2012). Although some studies failed in observing α-syn accumulation in the kidney (Herzig et al., 2011; Hinkle et al., 2012), all agreed in finding alterations of p62 levels (Tong et al., 2010,2012; Herzig et al., 2011; Hinkle et al., 2012; Baptista et al., 2013; Fuji et al., 2015). However, these studies did no detect changes in α-syn and ALP in the brain of mice lacking LRRK2. Differently, it has been reported that knocking out both *LRRK1* and *LRRK2* resulted in age-dependent increase of p62 and LC3II levels along with the autophagic vacuole number and a reduction of LC3I levels, suggesting an impairment of autophagy and a compensatory role of LRRK1 to maintain autophagy homeostasis (Giaime et al., 2017).
Different lines of evidence sustain that hyperactivation of LRRK2 kinase activity enhances autophagy. For example, overexpression of G2019S LRRK2, but neither WT LRRK2 nor the kinase

dead K1906M LRRK2 mutant, increased the number and size of neuritic and somatic autophagic vacuoles in SH-SY5Y cells (Plowey et al., 2008). As a support of the autophagy involvement in this mechanism, this effect was amplified by rapamycin and abolished by RNAi-mediated knockdown of LC3 or Atg7 (Plowey et al., 2008). More *in vitro* studies support this view (Gomez-Suaga et al., 2012b; Bravo-San Pedro et al., 2013; Orenstein et al., 2013; Su and Qi, 2013; Yakhine-Diop et al., 2014; Su et al., 2015). On the contrary, other *in vitro* studies led to the opposite conclusion that LRRK2 kinase activity inhibits autophagy causing autophagosome accumulation (Alegre-Abarrategui et al., 2009; Sanchez-Danes et al., 2012; Manzoni et al., 2016; Wallings et al., 2019; **Figure 4**). For example, co-application of LRRK2-IN-1 and bafilomycin A1 caused additive elevation of LC3-II levels, suggesting that the inhibition of LRRK2 kinase activity promotes autophagosome formation (Manzoni et al., 2013a). Also in worms, the expression of human G2019S or R1441G LRRK2 reduced the autophagic flux, which was restored by expression of either WT LRRK2 or a KD mutant of LRRK2 (Saha et al., 2015). In keeping with this view, Walling and colleagues showed an accumulation of LC3B puncta due to an autophagy impairment in rat primary cortical neurons overexpressing human WT and G2019S LRRK2. This was confirmed by the reduction in LC3B puncta upon treatment with the autophagy inducer trehalose (Wallings et al., 2019). This finding is consistent with the autophagy inhibition observed in G2019S Tg LRRK2 mice, which was associated with an increased ER stress *in vivo*, resulting in elevated LC3-II and p62 levels (Ho et al., 2018; **Figure 4**). As for the G2019S mutation, studies aimed at elucidating the effect of R1441C/G mutations over ALP led to inconsistent data. Neither (Tsika et al., 2014) or (Liu et al., 2014) showed changes in LC3-II or p62 levels in aged R1441C Tg and R1441G KI mice, respectively. Only Wallings and colleagues demonstrated that LC3 puncta accumulated in cortex and nigral neurons from BAC R1441C rats (Wallings et al., 2019). To better address LRRK2 kinase-mediated role in autophagy, several studies have been conducted employing pharmacological LRRK2 kinase inhibitors. First and second generation LRRK2 kinase inhibitors, such as LRRK2-IN1, GSK2578215A and CZC25146, were able to promote (Manzoni et al., 2013a, 2016) or block (Saez-Atienzar et al., 2014; Schapansky et al., 2014) the autophagosome formation. However, data might be affected by the lack of selectivity of this class of drugs. In fact, third generation LRRK2 inhibitors MLi-2 and PF-06447475 caused an increase of the autophagy flux (Wallings et al., 2019). The inconsistency of these results could be due to the different cell lines or animal model used, LRRK2 expression (endogenous vs viral-mediated overexpression), class of LRRK2 inhibitors, and techniques adopted to study autophagy. It becomes crucial to keep in mind that levels of autophagy-related protein, such as LC3-I, LC3-II and p62, reflect the status of a "streaming" process, rather than just a static condition. Hence, it is critical to establish ground rules in the field to distinguish between

a flux enhancement and a flux impairment, like the employment of ALP enhancers (e.g. rapamycin and trehalose) or inhibitors (e.g. Bafilomycin A1 or chloroquine, CQ; Klionsky et al., 2021). However, only few studies adopted this strategy to correctly interpret their data. Those exceptions are represented by the work of Manzoni and colleagues that demonstrated that G2019S LRRK2 mutation promoted the autophagosome formation in H4 cells, as confirmed by the increase in LC3-II levels after Bafilomycin A1 treatment (Manzoni et al., 2016). Nonetheless, these results need to be taken with caution because H4 neuroblastoma cells showed upregulated autophagy at basal levels (Zhou et al., 2016). Indeed, studies in different models suggest that the G2019S-mediated higher LC3-II levels are related to autophagosome accumulation. For example, LC3-II levels and LC3B puncta were found to accumulate in SH-SY5Y overexpressing G2019S LRRK2 upon CQ treatment due to a G2019S-mediated alteration of lysosomal morphology and proteolytic activity (Obergasteiger et al., 2020).

Autophagosome-lysosome fusion and lysosomal function. The fusion between autophagosomes and lysosomes is an important step in the autophagy process. A decreased colocalization between LC3 puncta and LAMP1 was observed in rat primary cortical neurons expressing BAC R1441C LRRK2, suggesting a reduced autolysosomes formation (Wallings et al., 2019). Nevertheless, a conditional expression of the LRRK2 R1441C mutation in rat midbrain dopaminergic neurons did not affect p62 and LC3 in vivo (ex-vivo) (Tsika et al., 2014). Similar reduction in autolysosomal formation was observed also in iPCS-derived G2019S LRRK2 astrocytes (di Domenico et al., 2019). Conversely, pharmacological inhibition of LRRK2 kinase activity in SH-SY5Y cells with GSK2578215A led to decreased fusion events between autophagosomes and lysosomes (Saez-Atienzar et al., 2014). Furthermore, G2019S-mediated reduction in autolysosome formation was associated with enlarged autophagic vacuoles *in vitro* (Plowey et al., 2008; Alegre-Abarrategui et al., 2009; Gomez-Suega et al., 2012b; Sanchez-Danes et al., 2012) and *in vivo* (Ramonet et al., 2011) and enlarged and swollen lysosomes *in vitro* (MacLeod et al., 2006,2013; Yahine-Diop et al., 2014). Interestingly, similar autophagic vacuole accumulation was observed in yeast after treatment with fragments of human LRRK2 (Xiong et al., 2010). Conversely, no changes in LAMP1 homolog lmp-1 were detected in G2019S mutant worms (Saha et al., 2015). Alteration of lysosomal homeostasis is one of the proposed mechanisms underlying the decreased fusion observed between autophagosomes and the altered lysosomal morphology. Indeed, maintenance of the correct lysosomal acidic environment (pH 4.5-5.0) is required for lysosomal enzymatic function, fusion with autophagosomes and recycling (Hu et al., 2015). First evidence of PD-related lysosomal impairment came from autopsy analysis conducted in whole-brains (Mamais et al., 2018) and nigral tissues (Chu et al., 2009; Dehay et al., 2010) from idiopathic PD patients in which lysosomal-associated markers, such as LAMP1, Cathepsin D and

HSP73 were reduced and ALP protein levels, such as LC3-II and p62, were elevated. Despite of the different biochemical properties exhibited by α-syn in idiopathic and G2019S LRRK2 PD, both conditions share the reduction in LAMP1 immunoreactivity (Mamais et al., 2013). Similar impairment of LAMP2 levels was also observed in DLB and AD patients, underlying the important role of the lysosomal function in aberrant protein accumulated-related disorders (Higashi et al., 2011). In the context of LRRK2-related PD, a growing body of evidence suggests that LRRK2 might play a crucial role in preserving lysosomal homeostasis. Evidence supporting this hypothesis derives from studies in LRRK2 KO flies and mice. *D. melanogaster* lacking the *Lrrk2* homolog, *Lrrk,* presented abnormally large Rab7-positive structures containing undegraded material, elevated number of autophagosomes and enlarged early-endosomes (Dodson et al., 2012, 2014). Curiously, restoration of LRRK2 expression (by overexpressing either WT or G1914S *Lrrk*, a mutant with enhanced kinase activity) rescued the aberrant phenotype (Dodson et al., 2014). LRRK2 KO kidneys showed an age-dependent impairment in α-syn clearance associated with lysosomal dysfunction (Tong et al., 2010, 2012; Baptista et al., 2013; Fuji et al., 2015). In particular, Tong and colleagues showed that high molecular weight proteins and lipofuscin accumulate in aged kidneys (Tong et al., 2010). Later, they also reported an early upregulation of LAMP1, LAMP2 and Cathepsin B levels after the first month of age and an increase of Cathepsin D levels at both 7 and 20 months. EM analysis showing the kidney-specific lipofuscin deposition confirmed the age-related lysosomal dysfunction caused by the loss of LRRK2 (Tong et al., 2012). Consistently, lipofuscin staining, which appears already at 3 months, becomes more prominent in LRRK2 KO mice along with aging (Hinkle et al., 2012; Fuji et al., 2015), albeit not associated with changes in α-syn levels (Hinkle et al., 2012). In keeping with these findings, LRRK2 KO rats showed progressive lipofuscin accumulation, LAMP1 and LAMP2 abundancy starting from 4 months of age (Baptista et al., 2013). Also, increased lamellar bodies in lung type II pneumocytes has been reported in LRRK2 KO mice (Fuji et al., 2015). Although kidney and lungs appeared markedly affected by the loss of LRRK2, no brain pathology was observed in either *LRRK1* or *LRRK2* KO mice (Albanese et al., 2019). These results corroborate the hypothesis that LRRK2 is important for lysosomal homeostasis and loss of LRRK2 leads to lysosomal dysfunction especially in kidney and lungs *in vivo*. However, enlarged lysosomes have been observed not only in LRRK2 KO models, but also in G2019S carriers PD patients and different G2019S models, such as SH-SY5Y, transgenic rodents, primary cortical neurons, primary astrocytes (MacLeod et al., 2006, 2013; Higashi et al., 2009; Ramonet et al., 2011; Dodson et al., 2014; Henry et al., 2015; Hockey et al., 2015; Bang et al., 2016). Fibroblasts carrying G2019S LRRK2 mutation exhibited enlarged and aggregated lysosomes located perinuclearly, and LRRK2 kinase inhibition was able to rescue this aberrant phenotype (Hockey et al., 2015). Also, primary cortical neurons

obtained from G2019S KI mice displayed similar aberrant lysosomes characterized by higher pH (Schapansky et al., 2018; Wallings et al., 2019). G2019S-mediated lysosomal disruption was evident also in G2019S-expressing primary neurons where the increased number and decreased size of perinuclear and distal lysosomes was coupled with an accumulation of endogenous, detergent-insoluble α-syn and increased α-syn release (Schapansky et al., 2018). Consistently, overexpression of G2019S LRRK2 in HEK-293T cells inhibits the activity of Cathepsin B and L (McGlinchey and Lee, 2015). However, this regulation was later proven to be kinase-independent (Hu et al., 2018). Similarly, overexpression of G2019S LRRK2, but not WT LRRK2, in SH-SY5Y cells increased lysosomal pH, while both were able to alter mRNA levels of *CTSB*, encoding for Cathepsin B, by transcriptomic analysis (Obergasteiger et al., 2020). To strengthen the correlation between LRRK2 and lysosomal function, WT LRRK2 interacts with the subunit a1 of the vacuolar ATPase (vATPase) proton pump and this binding as well as protein levels are significantly affected by R1441C mutation, leading to an impaired lysosomal degradative function (Wallings et al., 2019). vATPase is endoced by the *ATP6V0A1* gene whose mutations have been linked to higher risk to develop PD (Chang et al., 2017). Therefore, as a result of this aberrant interaction, and in keeping with Obergasteiger et al. (2020) and Schapansky et al. (2018), primary cortical neurons from BAC R1441C mice showed abnormally increased lysosomal pH. This was also associated with a decreased Ca^{2+} release from the lysosomal TRPML1 channels, which is required for a proper fusion between autophagosomes and lysosomes (Walling et al., 2019). Lysosomes are the major site for intracellular Ca^{2+} storage, and cytosolic Ca^{2+} release is known to modulate autophagy at different levels (Bootman et al., 2018). Another proposed mechanism for LRRK2-mediated upregulation of autophagy involves the lysosomal two-pore receptors (TCPs). LRRK2 kinase activity, whose action was mimicked by the nicotinic acid adenine nucleotide diphosphate (NAADP), triggers the TCP2-dependent release of lysosomal Ca^{2+}, which in turn can promote further release of Ca^{2+} from the ER, thus promoting autophagy via the CaMKK/AMPK cascade. Indeed, the LRRK2-mediated activation of autophagy was reversed by genetic and pharmacological inhibition of TCP2 (Gomez-Suaga et al., 2012b). The central role of lysosomes in PD pathology is also revealed by the finding that mutations in genes encoding for the lysosomal proteins ATP13A are associated with familial PD, and mutations in different lysosomal-related genes (*GBA*, *GALC, CTSB*, and *TMEM175*) have been identified as risk factors for idiopathic PD. Only in the last years, it has been found that LRRK2 docks on the lysosomal membrane (Eguchi et al., 2018; Bonet-Ponce et al., 2020). LRRK2 recruitment occurs along with that of Rab8a, in response to an insult to the lysosomal membrane. This was first observed in RAW264.7 cells treated with a lysosomotrophic agent LLOME (L-leucyl-l-leucine methyl ester). Lysosomotrophic agent-mediated lysosomal membrane damage is normally repaired by a cellular

process mediated by the ESCRT-III complex. This process is activated to prevent cell death. In the case of a prolonged damage, Galectin 3 (Gal3) mediates the ubiquitination of different lysosomal proteins. Upon activation, Gal3 is also able to induce lysophagy by recruiting ULK1 and ATG16L1 to the lysosomal membrane (Chauhan et al., 2016). Herbst and colleagues demonstrated a modest translocation of LRRK2 and Rab8a on the lysosomal membrane after a short exposure to LLOME. Moreover, constitutive deletion or pharmacological inhibition of LRRK2, as well constitutive deletion of Rab8a resulted in a decreased level of CHMP4A/B, which is a component of the ESCRT-III complex, and Gal3, and an increased time to recover Lysotracker after LLOME washout in vitro. This was also confirmed by Ponce-Bonet et al. (2020) in a subset of damaged lysosomes in resting primary mouse astrocytes, suggesting that LRRK2 is recruited and activated on the lysosomal membrane, phosphorylates Rab8a and contributes to the repair of the lysosomal membrane. Consistently, Eguchi and colleagues reported that CQ enhanced the Rab29-mediated LRRK2 recruitment at the stressed lysosomal membrane in HEK293T and RAW264.7 cells. LRRK2 phosphorylates Rab10 (at Thr73) and Rab8a, which in turn mediates the lysosomal exocytosis and release of non-degraded material in the extracellular space (Eguchi et al., 2018). The mechanisms of action of LLOME and CQ are different, and changes in lysosomal pH is not sufficient to induce LRRK2 translocation to the lysosomes, as suggested by the lack of effects on LRRK2 translocation upon Bafilomycin A treatment *in vitro* (Eguchi et al., 2018). Further investigations are necessary to better understand which stimuli trigger the Rab29-mediated LRRK2 enrichment onto damaged lysosomes and the reason why only a subset of lysosomes are LRRK2-positive in resting astrocytes. Moreover, upon translocation on the lysosomal surface, LRRK2 phosphorylates Rab35 at Thr72 and Rab10 at Thr73, which in turn, brings the motor adaptor protein JIP4 (JNK-interacting protein 4) to lysosomes. This process is strictly kinase-dependent, since it is promoted by the G2019S mutation and inhibited by MLi-2 (Bonet-Ponce et al., 2021). According to these observations, Holzbaur and colleagues recently showed an increased recruitment of JIP4 proteins to the autophagosomes in G2019S neurons, leading to an altered and less efficient retrograde transport of the autophagosomes (Boecker et al., 2021). Altogether, these results suggest that LRRK2 is likely involved in lysosomal homeostasis, albeit the precise mechanism is still unresolved. In fact, why both the increase of LRRK2 kinase activity and the loss of LRRK2 are detrimental for lysosomal function is puzzling. It might be possible that LRRK2 regulates lysosomes depending on the cell line/tissue investigated (Gomez-Suaga et al., 2012a). However, growing evidence is linking the hyperactive kinase activity mainly to alterations of the lysosomal pH, Ca^{2+} release and hydrolase expression. Dysregulation of lysosomal function might also be the mechanism through which LRRK2 affects ALP. In fact, the loss

of functional lysosomes prevents normal fusion with the autophagosomes, impairs the degradative capacity and induces substrate accumulation.

CMA. Similar to α-syn, also LRRK2 bears the KFERQ-like sequence that recognizes LAMP2A, suggesting that its degradation can occur via CMA. Furthermore, (Orenstein et al., 2013; **Figure 4**) showed that either WT LRRK2 or G2019S LRRK2 overexpression can block the assembly of CMA translocation complex, consistent with that observed in the case of high levels or mutant (A53T) α-syn (Cuervo et al., 2004). Although G2019S LRRK2 overexpression was reported to inhibit CMA activity, macroautophagy was upregulated, possibly to overcome CMA deficit (Orenstein et al., 2013). Similar changes were observed in human fibroblasts from G2019S patients (Bravo-San Pedro et al., 2013; Yakhine-Diop et al., 2014). A comprehensive study conducted on mouse embryonic fibroblasts pointed out an age-dependent decline in CMA activity in R1441G KI mice (Ho et al., 2020). The reduced CMA activity was accompanied by accumulation of α-syn oligomers as well as the CMA substrate GAPDH, which was evident at 18 months. In particular, the impaired α-syn clearance was associated with lysosome organization in perinuclear clusters and a modest increase of LAMP2A and Hsc70 abundancy in striatal neurons. CMA enhancement was able to restore the impaired α-syn turnover (Ho et al., 2020). Loss of *Lrrk2 in vivo* results in lysosomal dysregulation in kidney and lungs of mice, which has been also linked to CMA dysregulation. In fact, two independent studies reported upregulated levels of LAMP2A in the kidney of 7-month-old LRRK2 KO mice (Tong et al., 2012) and 12-month-old LRRK2 KO rats (Baptista et al., 2013). These results can suggest either an upregulation of CMA activity to overcome the macroautophagy impairment or an accumulation of the key CMA receptor LAMP2A linked to the aberrant lysosomal function. Further investigation needs to be conducted to clarify the mechanism causing the LRRK2-mediated elevation of LAMP2A content.

2. AIM OF THE STUDY

Autophagy dysfunction has been linked to aberrant and misfolded protein accumulation, a common feature of neurodegenerative disorders of aging, among which PD. *LRRK2* mutations have been associated with PD. LRRK2-related PD is a pleomorphic condition, that shares with idiopathic PD the two key hallmarks: neural loss of dopaminergic neurons in SNpc and intracellular accumulation of LBs. The most common *LRRK2* mutation, i.e. G2019S, occurs in the kinase domain and confers a higher kinase activity to the protein, which has been proven neurotoxic in various *in vitro* and *in vivo* models. A growing body of literature supports the hypothesis that LRRK2 contributes to PD by modulating autophagy. *In vitro* studies, however, failed to ultimately prove whether LRRK2 acts as a promoter or an inhibitor of ALP (Albanese et al., 2019; Madureira et al., 2020). A few *in vivo* studies reported that deletion of LRRK2 causes ALP impairment in the lung and kidney in rodents (Baptista et al., 2013; Fuji et al., 2012; Herzig et al., 2011; Hinkle et al., 2012; Tong et al., 2012; Tong et al., 2010) and KD mice (Herzig et al., 2011). Similar autophagy inhibition, as confirmed by the increase in LC3-II and p62 and reduction of LC3-I, was reported in the mouse brain at 15 months when both *LRRK1* and *LRRK2* were knocked out (Giaime et al., 2017). However, not only loss of LRRK2, but also hyperactive LRRK2 kinase activity inhibited ALP *in vivo*. Indeed, 15-20 month-old G2019S KI mice (Shapansky et al., 2018; Yue et al., 2015) and BAC G2019 rats (Wallings et al., 2019) showed increased LC3-II or LC3B puncta correlated with a reduction of LC3-I and LAMP1. Nevertheless, these results do not lead to a conclusive picture, because these studies did not measure the autophagy flux *in vivo*, as recommended by (Klionsky et al., 2021). Higher autophagic proteins levels can, in fact, be predictive of either a promoted or an impaired autophagic flux.

Therefore, this study sought to investigate the role of LRRK2 in regulating ALP through its kinase activity *in vivo*, and how this modulation changes along with aging. To this aim, G2019S KI mice (bearing hyperactive kinase domain), LRRK2 D1994S KI mice (bearing a KD mutation), LRRK2 KO mice and wild-type (WT) mice of 3, 12 and 20 months of age were used. Western blotting (WB) and RT-qPCR analysis were performed to investigate the striatal levels and expression of macroautophagy markers LC3-I, LC3-II, p62, mTOR and its Ser2448 phosphorylated, active form (p-mTOR), AMPK and its Thr182 phosphorylated, active form (p-AMPK), lysosomal marker LAMP2, and CMA marker GAPDH. Gene expression levels of the transcript levels of Transcription factor EB (TFEB) a master regulator of autophagy and lysosome biogenesis (Sardiello et al., 2009; Settembre et al., 2013) were also monitored. Subacute administration of CQ, a lysosomotropic agent, was performed to modulate the autophagic flux *in vivo.* The activity of the lysosomal hydrolases GCase and *GBA1* gene expression were also measured in the striatum at 3 and 12 months of age.

Furthermore, pharmacological inhibition of LRRK2 kinase activity *in vivo* was evaluated via subacute administration of MLi-2. Finally, in order to correlate LC3B puncta with the levels of phosphorylated α-syn (pSer129 α-syn), immunofluorescence analysis has been conducted in nigral TH^+ and striatal $MAP2^+$ neurons at 12 months of age.

The second part of this study aimed to investigate whether striatal ALP alteration associated to 12-month-old KD mice might contribute to promote α-syn neuropathology *in vivo*. We previously reported that nigral AAV vector serotype 2/9 injection of human A53T α-syn caused greater striatal and nigral degeneration in G2019S KI mice compared to WT at 12 months, but not at earlier stages (Novello et al., 2018). To this aim, we injected recombinant AAV 2/9 carrying h-A53T-α-syn or GFP as a control (Bourdex et al., 2015) in SNpc of 12-month-old G2019S KI, KD and WT mice. Motor behavioral performance was evaluated 4, 8 and 12 weeks after viral injection. Immunohistochemistry analyses were performed to assess α-syn neuropathology in striatum and SNpc, as well as degeneration of nigral dopaminergic somas and terminals 12 weeks post viral injection.

3. MATERIALS AND METHODS

3.1. Animals

All procedures involving animals were in accordance with the ARRIVE guidelines and the EU Directive 2010/63/EU for animal experiments and were approved by the Ethical Committee of the University of Ferrara and the Italian Ministry of Health (license 714/2017-PR). Male homozygous LRRK2 G2019S KI and KD mice backcrossed for at least 9 generations on a C57BL/6J background, were used. Founders were obtained from Mayo Clinic (Jacksonville, FL, USA) (LRRK2 KO mice) and from Novartis Institutes for BioMedical research (Novartis Pharma AG, Basel, Switzerland) (G2019S KI and KD mice). A colony of non-transgenic wild-type (WT) mice was initially set from heterozygous breeding of G2019S KI mice, then control WT male mice used in all experiments. Colonies were grown at the vivarium (LARP) of the University of Ferrara and kept under regular lighting conditions (12 h light/dark cycle), with free access to food (4RF21 standard diet; Mucedola, Settimo Milanese, Milan, Italy) and water. Animals were housed in groups of 5 for a 55x33x20 cm polycarbonate cage (Tecniplast, Buguggiate, Varese, Italy) with a Scobis Uno bedding (Mucedola, Settimo Milanese, Milan, Italy) and environmental enrichments.

3.2. Western Blotting

Striatal tissue was dissected, snap-frozen and stored at −80 °C until use. Tissue was lysed on ice in 1× RIPA lysis buffer supplemented with 1× Halt protease and phosphatase Inhibitor Cocktail (ThermoFisher Scientific, Waltham, Massachusetts, US). RIPA lysates were centrifuged at 15,000 g for 10 min at 4 °C to remove cellular debris. The pellet was discarded and total protein content of each sample was quantified by using a bicinchoninic acid (BCA) assay (ThermoFisher Scientific). For p62, LAMP2, p-mTOR, mTOR, p-S6K1, S6K1, p-AMPK, AMPK immunoblotting, 30 µg of proteins per sample mixed with 4X LDS Sample buffer, 10X Reducing Agent and ddH_2O up to 30 µl as final volume were loaded in 4-12% Bis-Trisglycine gels. For LC3-I, LC3-II and GAPDH immunoblotting, 10 µg of proteins per sample mixed with SDS, 10X Reducing Agent and ddH_2O up to 20 µl as final volume were loaded in 16% Trisglycine gels. After electrophoresis gel running, separated proteins were transferred to polyvinyl fluoride (PVDF) membranes (Bio-rad, Hercules, California, USA).

Protein	Protein content	Volume loaded in gel wells	Gel	Running buffer	Volt (Running)	Transfer buffer
p62, LAMP2, p-mTOR, mTOR, p-S6K1, S6K1, p-AMPK, AMPK	30 µg	30 µl	4 – 12% Bis-Trisglycine (Thermo Fisher Scientific)	(20X) MOPS (Thermo Fisher Scientific)	90 V	1X Transfer Buffer
LC3-I, LC3-II, GAPDH	10 µg	20 µl	16% Trisglycine (Thermo Fisher Scientific)	Trisglycine (Thermo Fisher Scientific)	60 V	1X Transfer Buffer + 20% MeOH

Table 1. Experimental setting for Western Blotting

Membranes were first blocked with 5% milk, 2% or 5% BSA in tris-buffered saline with 0.1% Tween (TBST) and immunoblotted overnight at 4°C for the detection of endogenous LC3, p62, LAMP2, mTOR, phospho-mTOR (Ser2448), AMPK, phospho-AMPK (Thr172), phospho-S6K1 (Thr389), S6K1, β-actin, listed in **Table 2**. Following incubation, appropriate horseradish peroxidase (HRP)-conjugated anti-Rabbit (1:4000; 12–34, Merck Millipore, Burlington, Massachusetts, US) and anti-Rat (1:4000, AP136P, Merck Millipore) secondary antibodies, and an ECL kit (ThermoFisher Scientific) were used to detect protein signals. Multiple exposures and images were acquired by the ChemiDoc MP System (Bio-Rad) and analyzed by using the ImageLab Software (Bio-Rad). β-actin bands were used for normalization. To minimize experimental variability, each blot was replicated twice and data averaged.

Protein	Molecular weight	Blocking Solution	HPR-conjugated Primary antibody	Dilution
β-actin	42 kDA	BSA 2%	Anti-beta Actin antibody (ab8227, Rb, Abcam, Cambridge, Massachusetts, US)	1:3000
LC3-I, LC3-II	16 kDa, 14 kDa	No fat milk 5%	Anti-LC3 antibody (ab51520, Rb, Abcam)	1:3000
p62	55 kDa	No fat milk 5%	Anti-SQSTM1/p62 antibody (ab91526, Rb, Abcam)	1:1000

LAMP2	75 kDa	BSA 5%	Anti-LAMP2 antibody [GL2A7] (ab13524, Rb, Abcam)	1:1000
mTOR	289 kDa	No fat milk 5%	Anti-mTOR antibody (#2983, Rb, CST)	1:1000
p-mTOR	289 kDa	BSA 5%	Anti-Phospho-mTOR (Ser2448) antibody (#2971, Rb, CST)	1:1000
AMPK	62 kDa	BSA 5%	Anti-AMPKα (D5A2) antibody (BK8531S, Rb, CST)	1:1000
p-AMPK	62 kDa	BSA 5%	Anti-Phospho-AMPKα (Thr172) antibody (BK2535S, Rb, CST)	1:1000
S6K1	70 kDa	BSA 5%	Anti-p70 S6 Kinase antibody (BK9202S, Rb, CST)	1:1000
p-S6K1	70 kDa	BSA 5%	Anti-Phospho-p70 S6 Kinase (Thr389) antibody (BK9205S, Rb, CST)	1:1000
p-Ser1292 LRRK2	220 kDa	No fat milk 5%	Anti-phosphoSer1292-LRRK2 antibody (ab203181, Rb, Abcam)	1:300
LRRK2	220 kDa	No fat milk 5%	Anti-LRRK2 antibody (ab133474, Rb, Abcam)	1:300

Table 2. Antibodies used

3.3. Tissue processing

Mice were anesthetized with isofurane and transcardially perfused with Phosphate Buffer Solution (PBS) solution, then fixed with 4% paraformaldehyde (PFA) solution pH 7.4 at 4 °C (Sigma Aldrich, Saint Louis, Missouri, USA). Brains were dissected out and post-fixed in 4% PFA for 24 h. Brains were then transferred in 30% sucrose in 1×PBS at 4 °C and then stored at −80 °C. PFA-fixed brains were sectioned at 50 μm (coronal sections) with a cryo-microtome (Leica, Buffalo Grove, Illinois, US) and stored in cryoprotective medium (30% glycerol, 30% ethylene glycol) at −20 °C.

3.4. α-syn and pSer129 α-syn immunohistochemistry

Tissue processing and immunohistochemistry were performed on free-floating sections according to standard published techniques (Duraiyan et al., 2012). Coronal sections of striatum (AP from +1.0 to −1.25 mm from bregma; Paxinos and Franklin, 2001) and SNpc (AP from -3.16 to -3.52 mm from bregma) were used. Two sections per animal were placed in the same well, rinsed 3 times in PBS, pre-treated with 3% H_2O_2 and 0.3% Triton X-100 (Sigma Aldrich) in PBS, rinsed 3 times in PBS again, then blocked in 2% BSA in PBST (PBS + 0,3% Triton). The following rabbit polyclonal antibodies were used in BSA 1% PBST: Rb anti-TH (ab112; 1:1000, Abcam, Cambridge, Massachusetts, US), Rb anti-total α-syn (ab52168; 1:200, Abcam), Rb anti hα-syn (ab138501; 1:150,

Abcam) and Rb anti pSer129-α-syn (ab51253; 1:250, Abcam). After overnight incubation at 4 °C, sections were rinsed and incubated for 1 h with an anti-rabbit HRP-conjugated secondary antibody (1:500; ab6721, Abcam) in 1% BSA in PBST and revealed by using a DAB substrate kit (ab64238, Abcam). Only for pSer129-α-syn and human-α-syn staining, sections were pre-incubated with an antigen retrieval solution. Sections were mounted on gelatinized slides, dehydrated and coverslipped using a xylene-based mounting medium. Slides were then scanned using a Leica DM6B motorized microscope and the representative immunostaining surface for each striatal and nigral section was determined by a color threshold using Fiji Software (NIH, Bethesda, Maryland, US).

3.5.LC3, pSer129 α-syn and MAP2/TH immunofluorescence

Tissue processing and immunohistochemistry were performed on free-floating sections according to standard published techniques (Duraiyan et al., 2012). Coronal sections of striatum (AP from +1.0 to −1.25 mm from bregma; Paxinos and Franklin, 2001) and SNpc (AP from -3.16 to -3.52 mm from bregma) were collected. Sections were rinsed 3 times in PBST and blocked in 5% normal goat serum and PBST for 1 h. The following primary antibodies were used: anti-LC3B (1:3000; Rb ab51520, Abcam), anti-pSer129 α-syn (1:2000; Ms ab184674, Abcam), anti-MAP2 (1:1000; Ck ab5392, Abcam) and anti-TH (1:1000; Ck ab76442, Abcam). After overnight incubation at 4 °C, the primary antibody staining was revealed using donkey anti-Rabbit Secondary Antibody Alexa Fluor 488 (A-21206), donkey anti-Mouse Secondary Antibody Alexa Fluor 555 (A31570), goat Anti-Chicken IgY H&L Alexa Fluor 647 (ab150171). Sections were rinsed three times in PBS, incubated in DAPI solution for 30 min and then rinsed again 3 times. Finally, they were mounted on Superfrost Plus slides (ThermoFisher Scientific) and coverslipped using antifade mounting medium (Fluoromount G, ThermoFisher Scientific). Images were collected using 63X Leica SP8-X Confocal microscope, and unbiased estimations of LC3B puncta and pSer129^{+} inclusions in MAP2^{+} and TH^{+} cells were performed by investigators blinded to genotype and experimental conditions using Fiji (NIH) and Cell Profiler software (Cambridge, Massachusetts, US).

3.6. Gcase activity assay

GCase activity was assessed according to published protocol (Ambrosi et al., 2015). Mouse striatal and cortical tissues (∼15 mg and ∼25 mg, respectively) were dissected out and rapidly homogenized in 150µl and 250µl of ice-cold RIPA buffer. Tissue lysates were centrifuged at 16,000 g at 4°C for 10 min, then the supernatant was collected. Ten micrograms of protein lysates for each sample were diluted in 100µl of assay buffer (0.1 M sodium citrate phosphate, pH 5.6, 0.1% Triton X-100, 0.25%

sodium taurocholate and 2.5mM 4-4-Methylumbelliferyl β-D-glucopyranoside or 4-MUG) in a 96-Well Black Clear Bottom plate (Corning 3603).

Six-point standard curve (25 µM – 0 µM, **Table 3**) was also prepared by serial dilutions of 4-methylumbelliferyl (4-MU, M1381 Sigma Aldrich) in ddH_20.

STD A	275 µL of Stock solution + 725 µL of ddH2O	**25 µM**
STD B	500 µL of A + 500 µL of ddH2O	**12.5 µM**
STD C	500 µL of B + 500 µL of ddH2O	**6.25 µM**
STD D	200 µL of C + 100 µL of ddH2O	**4.16 µM**
STD E	500 µL of C + 500 µL of ddH2O	**3.125 µM**
STD F	200 µL of E + 100 µL of ddH2O	**2.08 µM**
STD G	500 µL of E + 500 µL of ddH2O	**1.562 µM**
STD H	500 µL of G + 500 µL of ddH2O	**0.78 µM**
STD I	500 µL of ddH2O	**0 µM**

Table 3. Dilution scheme for 4-MU standard curve

After incubation with the substrate for 1 h at 37 °C, the reaction was terminated adding 150µl of stop solution (0.25 M Glycine, pH 10.4). Plates were read (Ex 360/Em 460) in Ensight Perkin Elmer, a fluorescent plate reader using Kaleido software. Enzymatic activity was assessed from a 4-methylumbelliferyl standard curve, whereas protein quantification was determined using a BCA assay (ThermoFisher Scientific). A CBE solution (3 mM) was used as negative control for GCase activity.

3.7. RNA extraction

Total RNA was extracted from the striatal tissue (15 mg) of 12-month-old C57BL/6J WT, G2019S KI, KO and KD mice (n=8/group) using TRIzol reagent (ThermoFisher Scientific), following the manufacturer's recommended protocol. Fifteen milligrams of fresh samples were homogenized in 100 µl of TRIzol reagent and stored at -20°C. For RNA extraction, 400 µl of chloroform were added to the TRIzol solution. Then, the tube was shaken and incubated at room temperature for 2 min before the centrifugation at 12,000 g for 15 min at 4 °C. The supernatant was transferred into a new tube and 500 µl of cold isopropanol added. After mixing, the obtained solution was incubated in ice for 20 min to facilitate RNA precipitation and, then centrifuged at 12,000 g for 10 min at 4 °C. The RNA pellet obtained was washed with 1 ml of ice-cold 75% ethanol and centrifuged at 12,000 g for 5 min at 4 °C. The supernatant was then removed, the RNA pellet briefly air-dried and re-suspended in 25-30 µl of RNase-free water. All RNA samples were stored at -80 °C. Total RNA content and its quality

were measured using a NanoDrop1000 spectrophotometer (ThermoFisher Scientific). Samples were considered pure if the A260/A280 and A230/A260 ratios were close to 2.

Potential DNA contamination was removed from the RNA eluate using the DNase I (ThermoFisher Scientific), following the manufacturer's recommended protocol. One microgram of total RNA, diluted in RNase-free water up to a final volume of 8 µl, was treated with 1 µl of DNase I enzyme (1 U/µl) and 1 µl of 10X Reaction Buffer with $MgCl_2$. The solution was mixed gently and incubated at 37 °C for 15 min. The reaction was stopped by adding 1 µl of EDTA (50 mM) at 70 °C for 10 min.

3.8. Synthesis of cDNA

RevertAid First Strand cDNA Synthesis Kit (ThermoFisher Scientific) was used to synthesize cDNA. The cDNA synthesis was carried out in 20 µl reactions, according to the manufacturer's instructions: 1 µg of total RNA after DNAse I treatment (10 µl) was mixed with 1 µl of Random Primers and, then, incubated at 65°C for 5 min to resolve any RNA secondary structure. After incubation, the following reagents were added: 4 µl of 5X Reaction Buffer, 2 µl dNTP Mix (10 µM), 1 µl reverse transcriptase (RT) enzyme (200 U/µl) and 1 µl of RiboLock RNase Inhibitor (200 U/µl). The reaction mixture was incubated at 25°C for 5 min, followed by 60 min at 42°C. Reaction was terminated by incubating the tubes at 70 °C for 5 min. The synthesised cDNA was subsequently diluted (1:5) and used as a template in PCR reactions.

3.9. Quantitative real-time PCR

Quantitative real time PCR (qPCR) was performed using a CFX Connect Real-Time PCR Detection System (Bio-Rad) in a 12 µl reaction mixture containing 1.6 µl of 1:5 diluted cDNA, 6 µl SsoAdvanced Universal SYBR Green Supermix (Bio-Rad), 0.4 µl forward primer (10 µM), 0.4 µl reverse primer (10 µM) and 3.6 µl nuclease free water. Thermal cycling condition protocol was set at 95 °C for 2 min, 40 cycles at 95 °C for 15 s and 60 °C for 20 s. After the cycling protocol, a melting-curve analysis from 55 °C to 95 °C was conducted. Gene expression of *MAP1LC3*, *TFEB*, *mTOR*, *LAMP2*, *p62* and *GBA1*, was normalized using *ACTB* and *HPRT* as reference genes, using the QBase+ algorithm (Hellemans et al., 2007). Gene-specific primers (**Table 4**) were used and eight independent biological replicates, made in triplicate, were performed for each sample.

MAP1LC3	*Forward:* 5'-ACGGCTTCCTGTACATGGTTT - 3' *Reverse*: 5'- GGAGTCTTACACAGCCATTGC - 3'
TFEB	*Forward*: 5'- GACTCAGAAGCGAGAGCTAACA - 3'

	Reverse: 5'- GTGATTGTCTTTCTTCTGCCG - 3'
mTOR	*Forward*: 5'- AGAAGGGTCTCCAAGGACG - 3' *Reverse:* 5'- CAGGACACAAAGGCAGCAT - 3'
LAMP2	*Forward:* 5'- TAGGAGCCGTTCAGTCCAAT - 3' *Reverse*: 5'- GTGTGTCGCCTTGTCAGGTA - 3'
p62	*Forward:* 5'- GCTGCCCTATACCCACATCT - 3' *Reverse:* 5'- CGCCTTCATCCGAGAAAC - 3'
GBA1	*Forward:* 5'- GACCAACGCTTGCTGCTAC - 3' *Reverse:* 5'- ACAGCAATGCCATGAACGTA - 3'
ACTB	*Forward:* 5'- GCTGTATTCCCCTCCATCG-3' *Reverse:* 5'- CCAGTTGGTAACAATGCCATG-3'
HPRT	*Forward:* 5'- AGTGTTGGATACAGGCCAGAC -3' *Reverse:* 5'- CGTGATTCAAATCCCTGAAGT - 3'

Table 4. qPCR primers used

3.10. Drugs

The lysosomotropic autophagy inhibitor CQ was purchased from Sigma Aldrich (CC6628) and it was dissolved in PBS solution. The LRRK2 inhibitor, MLi-2 was purchased from Carbosynth (Commpton, Bershire, UK) and was dissolved in 4% DMSO and 30% hydroxypropyl β-cyclodextrin.

3.11. CQ treatment

CQ was administered intraperitoneally once daily for three consecutive days to assess the autophagic flux (Mauthe et al., 2018). Mice were sacrificed 4 and 24 h after the last injection and striatal tissues were dissected out to perform WB analyses. To prove protocol efficacy in blocking the autophagolysosomal formation, the 50 mg/kg dose was first tested in six 3-month-old WT mice. After confirming LC3-II accumulation, six 12-month-old WT and KD mice were treated with the same dose of CQ to assess the autophagic flux.

3.12. MLi-2 treatment

Seven 12-month-old WT and G2019S KI mice were treated with MLi-2 to inhibit LRRK2 kinase activity. MLi-2 (5 mg/kg) was administered intraperitoneally once daily for 7 days. Animals were sacrificed 4 h after the last injection and striata were collected to perform WB analysis.

3.13. AAV2/9-hα-syn vector production and injection

Recombinant AAV2/9 vectors carrying A53T-human-α-syn (AAV-hα-syn) were obtained from Prof E. Bezard at the University of Bordeaux (Bourdenx et al., 2015). Mice were anesthetized with isoflurane and placed in a stereotaxic apparatus. Mice were injected bilaterally in the SNpc (coordinates in mm from bregma: antero-posterior -3.3, medio-lateral ± 1.25; dorso-ventral -4.6) with the AAV2/9-hα-syn (2.35×10^{13} genome containing particles/ µl; 1 µl) or the control vector AAV2/9-GFP. Viral vectors were injected using a glass pipette at 0.5 µl/min, that was left in place for 4 min after injection to prevent from leakage during withdrawal.

3.14. Behavioral tasks

Drag test

Modification of the "wheelbarrow test", this test measures the ability of the animal to balance its body posture with the forelimbs in response to an externally imposed dynamic stimulus (backward dragging; Marti et al., 2005; Marti et al., 2004; Viaro et al., 2008). It gives information regarding the time to initiate (akinesia) and execute (bradykinesia) a movement. Animals were gently lifted from the tail leaving the forepaws on the table, and then dragged backwards at a constant speed (about 20 cm/s) for a fixed distance (100 cm). The number of steps made by each paw was recorded. Five determinations were collected for each animal. The test was performed before and 1, 2 and 3 months after AAV2/9-hα-syn injection.

3.15. TH, total α-syn, human α-syn and pSer129 α-syn immunohistochemistry

Coronal free-floating sections of striatum (AP from +1.0 to −1.25 mm from bregma; Paxinos and Franklin, 2001) and SN (AP from -3.16 to -3.52 mm from bregma) were rinsed three times in PBS, then incubated with 3% H_2O_2 in PBS for 10 min to inhibit endogenous peroxidases. After 3 washes in PBS, sections were first blocked in 5% BSA solution in PBST, then incubated overnight with the following primary antibodies: Rb anti-TH (ab112; 1:1000, Abcam, Cambridge, UK), Rb anti-total α-syn (ab52168; 1:200, Abcam), Rb anti hα-syn (ab138501; 1:150, Abcam) and Rb anti pSer129-α-syn (ab51253; 1:250, Abcam). Sections were rinsed in PBS and incubated for 1 h with a rabbit HRP-conjugated secondary antibody (ab6721, 1:500, Abcam). DAB substrate kit (ab64238, Abcam) was then used to reveal the staining. Sections were mounted onto gelatin coated slides, dehydrated and

coverslipped. Only for pSer129 α-syn and human-α-syn staining, sections were pre-incubated with an antigen retrieval solution. Images were acquired by using a Leica DM600B motorized microscope and analyzed with Fiji ImageJ Software (NIH).

3.16. Stereology and neuronal counting

Stereological analysis was performed using an unbiased stereological sampling method based on optical fractionator stereological probe (Novello et al., 2018; Arcuri et al., 2016; Larsen et al., 1998). TH^+ neurons in SNpc were counted on 5 serial slices cut 50-µm thick and 200-µm apart and magnified at 60×. Stereo Investigator software (MBF Europe, Delft, The Netherlands) was used to estimate the total number of neurons calculated from the number of neurons counted within a Systematic Randomly Sampled set of unbiased virtual counting areas covering the entire region of interest with a uniform distance between unbiased virtual counting in spaces in directions X, Y, and Z. Images were acquired using a Leica DM600B motorized microscope. Neural counting was performed by investigators blinded to the experimental condition.

3.17. Data presentation and statistical analysis

Data are expressed as mean ± SEM (standard error of mean) of n mice. Statistical analysis was implemented on GraphPad Prism 8. Differences upon CQ or MLi-2 treatment in the same genotype were established using an unpaired Student's t test (two-tailed). For experiments with n>2 groups, one-way ANOVA followed by Bonferroni post-hoc test for multiple comparisons was used. QBase+ analysis was performed to quantify fold change in gene expression (Hellemans et al., 2007). qPCR data were analyzed by one-way ANOVA followed by Bonferroni test. Motor performance in the drag test was presented as absolute values (calculated as number of steps) and analyzed by two-way repeated measure (RM) ANOVA followed by the Bonferroni test. Number of neurons obtained from stereological counting was expressed as absolute values, density of striatal TH^+ terminals was expressed as absolute data (mean absolute value of grey scale between the two striata), density of human, total and pSer129 α-syn levels were expressed as percentage of area of threshold. Statistical significance was set at $p < 0.05$.

4. RESULTS

4.1. PART I: Constitutive silencing of LRRK2 kinase activity leads to early glucocerebrosidase deregulation and late impairment of autophagy in vivo

4.1.1. Effect of aging on expression of ALP markers in LRRK2 mice

To evaluate whether age-related dysfunction in striatal macroautophagy and CMA machineries is associated with LRRK2 kinase activity, immunoblot analysis was performed in striatal tissues from 3, 12 and 20-month-old G2019S KI, KO, KD and WT mice. No marker changes across genotypes were observed in 3-month-old mice (Fig. 5). Conversely, changes of LC3-I ($F_{3,28} = 18.03$, $p < 0.0001$; Fig. 6A), LC3-II ($F_{3,28} = 2.85$, $p = 0.055$, Fig. 6B), p62 ($F_{3,20} = 5.37$, $p = 0.0071$, Fig. 6D), p-mTOR ($F_{3,28} = 12.94$, $p < 0.0001$; Fig. 6E), LAMP2 ($F_{3,28} = 8.50$, $p = 0.0004$; Fig. 6G) and GAPDH ($F_{3,20} = 11.69$, $p = 0.0001$; Fig. 6H) were detected in 12-month-old mice. KD mice showed a ~2-fold increase in the abundancy of LC3-I and p62, an 80% elevation of LC3-II and a 72% reduction of p-mTOR with respect to controls. This was associated with an increase of lysosomal marker LAMP2 (+46%) and CMA marker GAPDH (+70%). As far as KO and G2019S KI mice were concerned, a 45% increase of LAMP2 levels was only observed. As AMPK is a functional antagonist of mTOR and promotes autophagy in most systems, AMPK levels were investigated in 12-month-old mice (Fig. 7). AMPK levels were significantly affected across genotypes ($F_{3,20} = 3.62$, $p = 0.0308$), being a 50% elevation observed in KD mice.

Immunoblot analysis at 20 months (Fig. 8) showed significant changes of LC3-II ($F_{3,20} = 5.49$, $p = 0.0065$; Fig. 8B), p62 ($F_{3,20} = 8.53$, $p = 0.0008$; Fig. 8D), p-mTOR ($F_{3,20} = 8.91$, $p = 0.0006$; Fig. 8E), mTOR ($F_{3,20} = 22.28$, $p < 0.0001$; Fig. 8F) and LAMP2 ($F_{3,20} = 4.93$, $p = 0.0100$; Fig. 8G) across genotypes. Again, KD mice were most affected, showing increases of LC3-II (+30%), p62 (+80%) and mTOR (+95%) levels along with a 50% reduction of p-mTOR levels. At variance with that observed in younger mice, significant elevations of p62 (+47%), mTOR (+73%) and LAMP2 (+30%) levels were found in KO mice. Conversely, no changes in macroautophagy or lysosomal markers were observed in G2019S KI mice. To investigate whether the increase of mTOR levels corresponded to an increase of its activity, the phosphorylation levels of the mTOR substrate, S6K1 were investigated (Fig. 9). No changes in p-S6K1 and S6K1 levels were found (Fig. 9B, C). p-AMPK and AMPK levels were also investigated (Fig. 9D, E). Only p-AMPK levels were significantly affected across genotypes ($F_{3,20} = 6.93$, $p = 0.0022$). Both KO and KD mice showing marked increases (+443% and +300% respectively), being this effect just above the limit of significance in KD mice ($p = 0.059$).

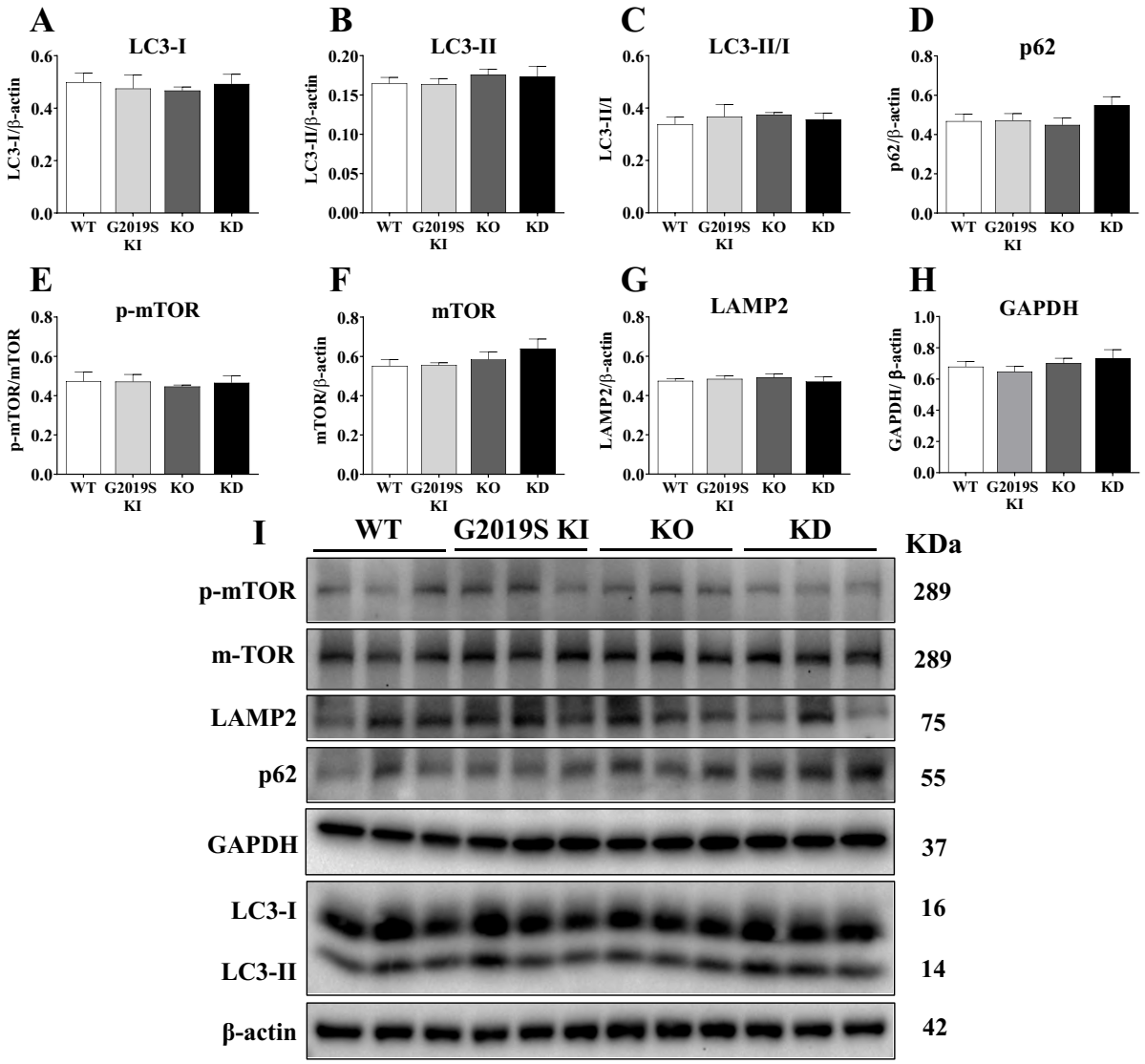

Figure 5. Immunoblot analysis of autophagy and lysosomal markers in 3-month-old LRRK2-mutant mice. Striatal lysates from 3-month-old WT, G2019S KI, KO and KD mice. Semi-quantitative analysis of macroautophagy markers levels: LC3-I (A), LC3-II (B), LC3-II/I (C), p62 (D), p-mTOR normalized on total mTOR (E) and total mTOR (F). Semi-quantitative analysis of chaperone-mediated autophagy marker levels: LAMP2 (G) and GAPDH (H). Representative immunoblots of macroautophagy and chaperone-mediated autophagy markers in 3-month-old LRRK2-mutant mice (I). β-actin was used as housekeeping protein. Data are mean ± SEM of 6 mice per group and were analyzed using one-way ANOVA followed by the Bonferroni's test for multiple comparisons.

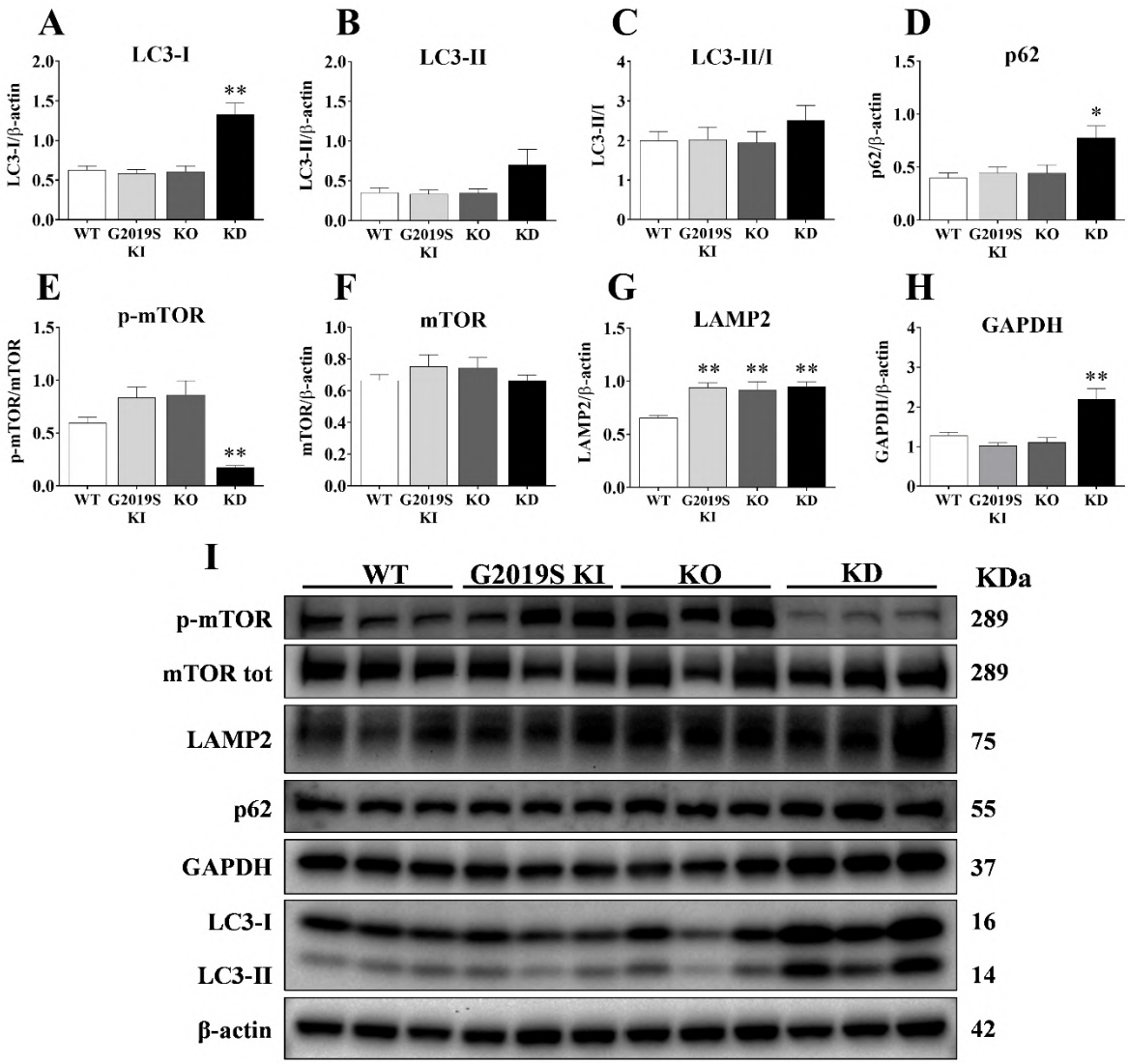

Figure 6. Immunoblot analysis of autophagy-lysosomal pathway (ALP) markers in 12-month-old LRRK2 mice. Striatum lysates from 12-month-old WT, G2019S KI, KO and KD mice. Semi-quantitative analysis of macroautophagy markers levels: LC3-I (A), LC3-II (B), LC3-II/I (C), p62 (D), p-mTOR (normalized to total mTOR) (E) and total mTOR (F). Semi-quantitative analysis of lysosomal and CMA marker levels: LAMP2 (G) and GAPDH (H). Representative immunoblots of ALP markers in 12-month-old LRRK2-mutant mice (I). β-actin was used as housekeeping protein. Data are mean ± SEM of 8 mice per group and were analyzed using one-way ANOVA followed by the Bonferroni's test for multiple comparisons. *$p < 0.05$, **$p < 0.01$ different from WT mice.

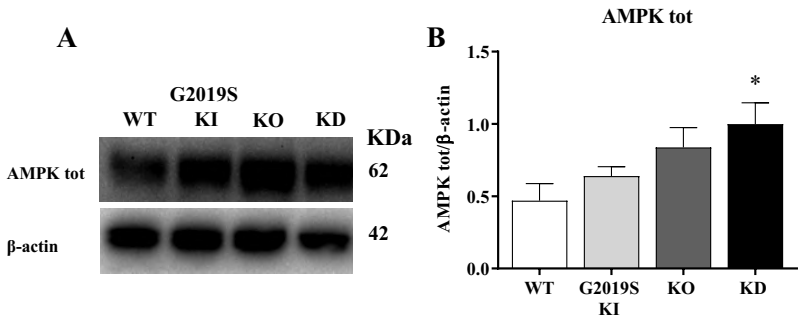

Figure 7. Immunoblot analysis of AMPK levels in 3-month-old LRRK2-mutant mice. Striatum lysates from 12-month-old WT, G2019S KI, KO and KD mice were collected to perform WB analysis. A) Representative immunoblots of AMPK markers. B) Semi-quantitative analysis of total AMPK levels. β-actin was used as housekeeping protein. Data are mean ± SEM of 6 mice per group and were analyzed using one-way ANOVA followed by the Bonferroni's test for multiple comparisons. *p<0.05 different from WT mice.

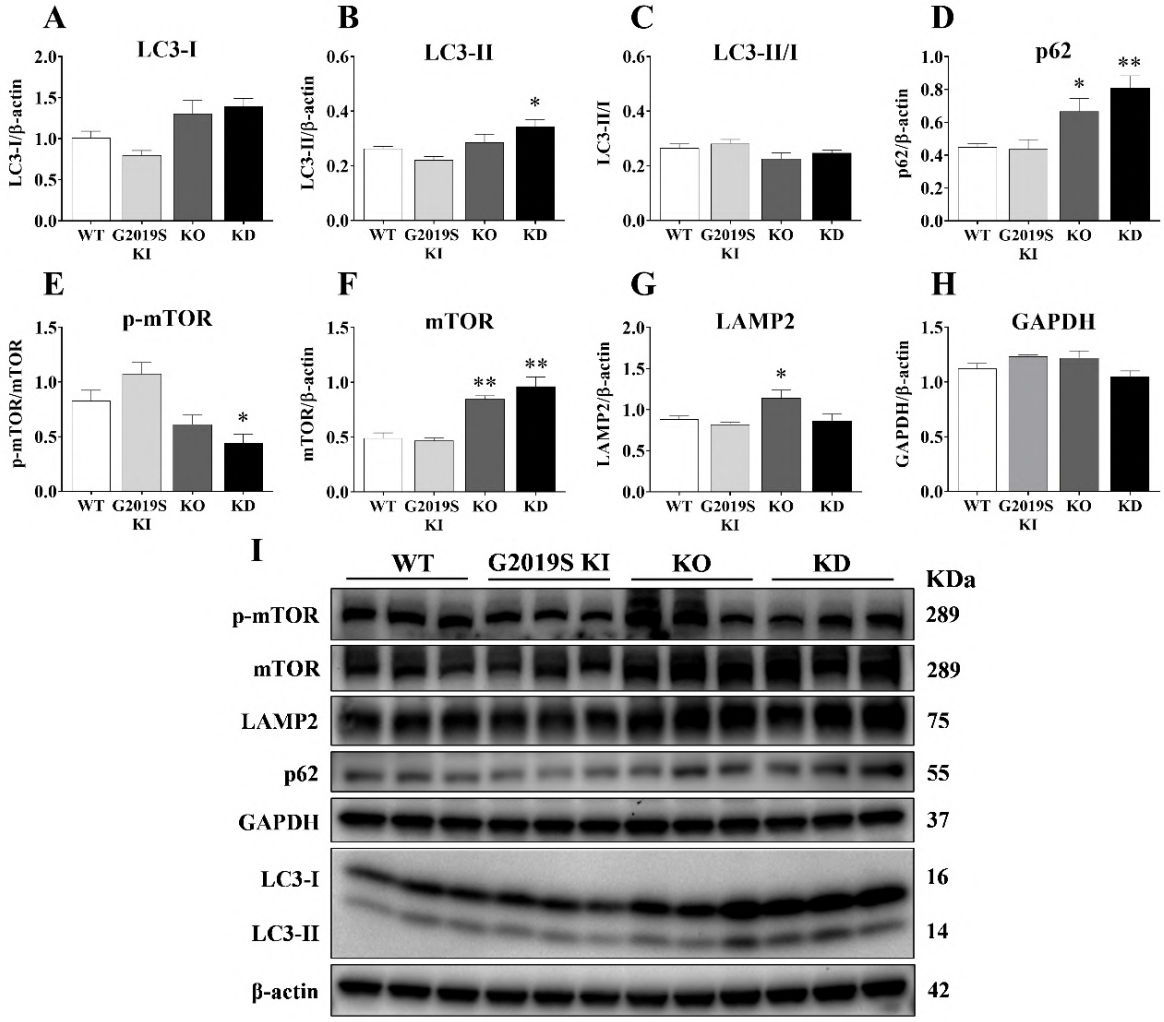

Figure 8. Immunoblot analysis of autophagy-lysosomal pathway (ALP) markers in 20-month-old LRRK2 mice. Striatum lysates from 20-month-old WT, G2019S KI, KO and KD mice. Semi-quantitative analysis of macroautophagy marker levels: LC3-I (**A**), LC3-II (**B**), LC3-II/I (**C**), p62 (**D**), p-mTOR normalized on total mTOR (**E**) and total mTOR (**F**). Semi-quantitative analysis of lysosomal and CMA marker levels: LAMP2 (**G**) and GAPDH (**H**). Representative immunoblots of ALP markers in 20-month-old LRRK2-mutant mice (**I**). β-actin was used as housekeeping protein. Data

are mean ± SEM of 8 mice per group and were analyzed using one-way ANOVA followed by Bonferroni's test for multiple comparisons. *$p < 0.05$; ** $p < 0.01$ different from WT mice.

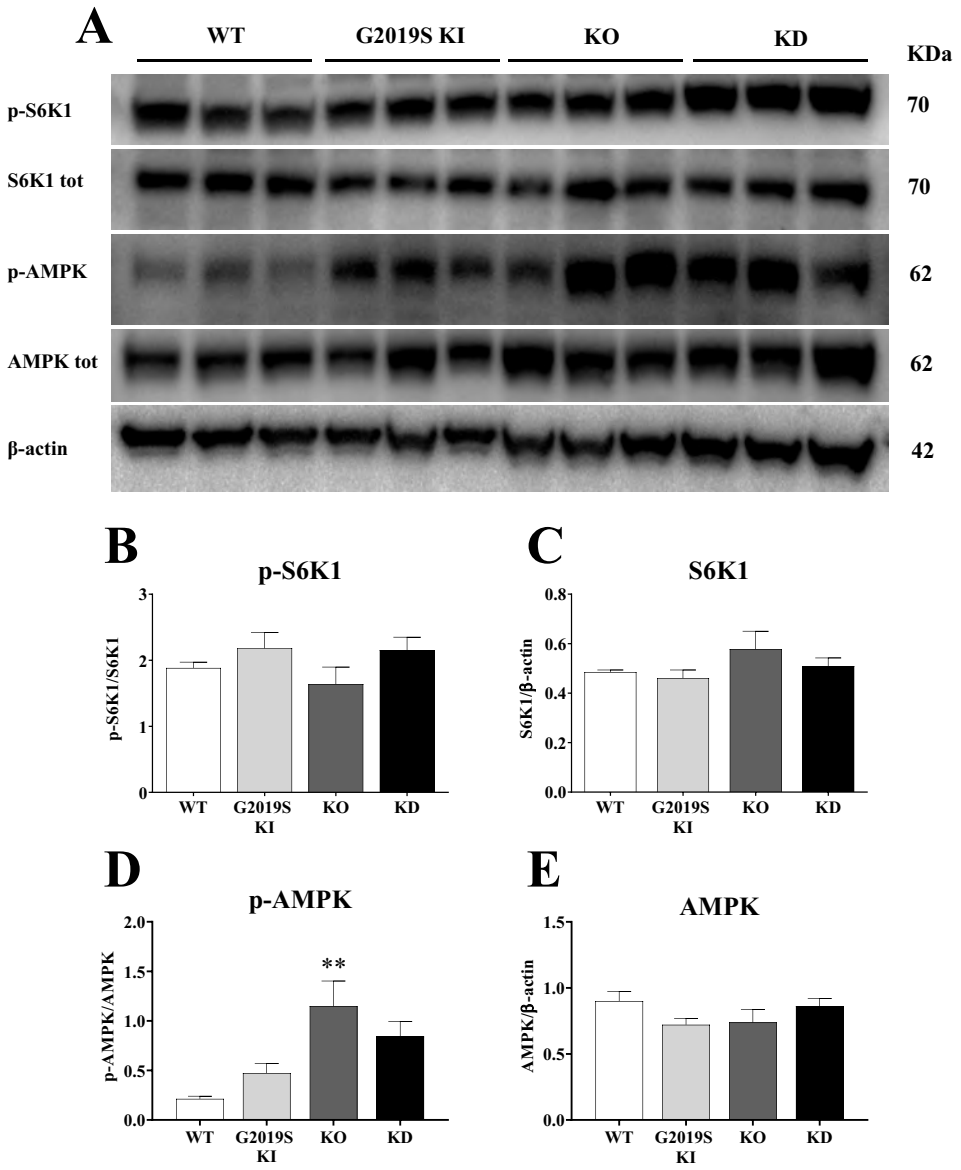

Figure 9. Immunoblot analysis of autophagy in 20-month-old LRRK2-mutant mice. Striatum lysates from 20-month-old WT, G2019S KI, KO and KD mice were collected to perform WB analysis. A) Representative immunoblots of macroautophagy markers. B) Semi-quantitative analysis of p-S6K1 normalized on total S6K1 levels C) Semi-quantitative analysis of total S6K1 levels D) Semi-quantitative analysis of p-AMPK normalized on total AMPK levels. E) Semi-quantitative analysis of AMPK levels. β-actin was used as housekeeping protein. Data are mean ± SEM of 6 mice per group and were analyzed using one-way ANOVA followed by Bonferroni test for multiple comparisons. **p<0,01 different from saline-treated mice.

4.1.2. Gene expression analysis of autophagy-related markers at 12 months

To investigate whether changes in protein levels correlated with changes in gene expression, RT-qPCR was performed in striatal extracts from 12-month-old mice (Fig. 10). Changes were observed in mRNA levels of *MAP1LC3B* ($F_{3,28} = 5.23$, $p = 0.0054$; Fig. 10A), *LAMP2* ($F_{3,27} = 13.44$, $p < 0.0001$;

Fig. 10C), *mTOR* ($F_{3,28} = 5.39$, $p = 0.0047$; Fig. 10D) and *TFEB* ($F_{3,28} = 3.40$, $p = 0.0315$; Fig. 10E) whereas mRNA levels of *p62* were unaffected (Fig. 10B). KD mice showed a ~20% reduction of *mTOR* and *TFEB* mRNA whereas KO mice a 20% reduction of *MAP1LC3B* mRNA. Conversely, G2019S KI mice appeared largely impaired at transcriptional level due to the significant ~20% downregulation of *MAP1LC3B*, *LAMP2*, *TFEB* and *mTOR* gene transcripts.

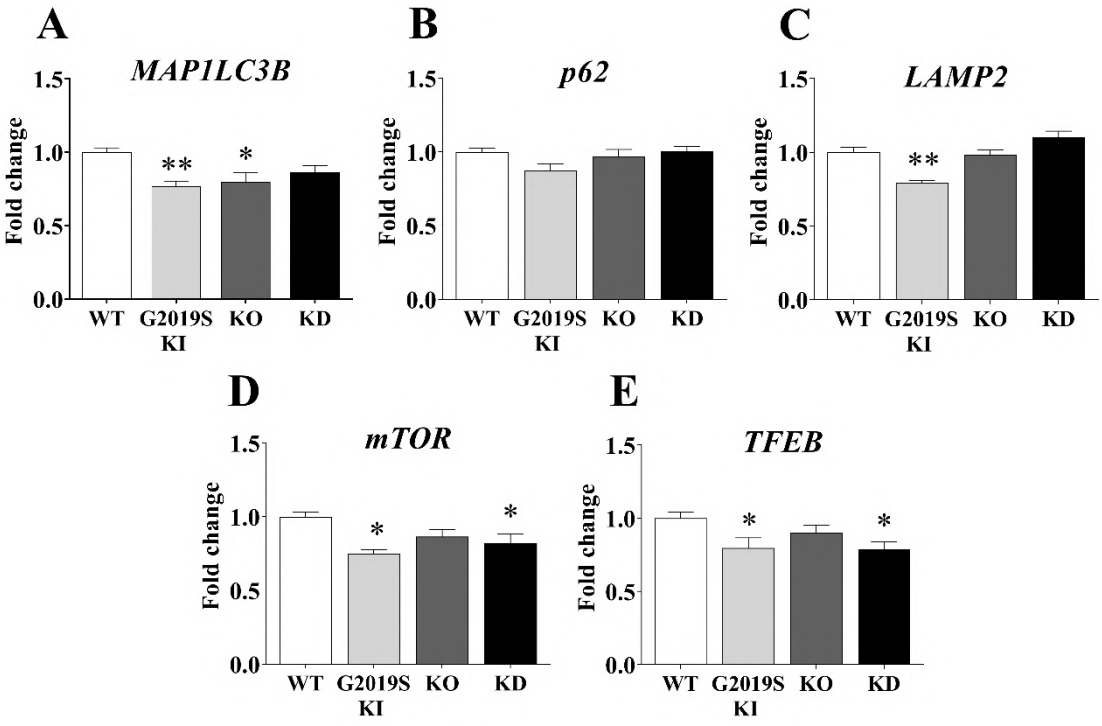

Figure 10. RT-qPCR analysis of autophagy-related gene expression in 12-month-old LRRRK2 mice. RNAs were isolated from striatal tissue of 12-month-old WT, G2019S KI, KO and KD mice. RT-qPCR analysis was performed to analyze the mRNA expression levels of *MAP1LC3B* (**A**), *p62* (**B**), *LAMP2* (**C**), *mTOR* (**D**), *TFEB* (**E**) among genotypes. *ACT* and *HPRT* were used as reference genes (Gong et al., 2016). Data are mean ±SEM of 8 mice per genotype. Statistical analysis was performed using one-way ANOVA followed by the Dunnett's test for multiple comparison. * $p < 0.05$, ** $p < 0.01$ different from WT mice.

4.1.3. Autophagic flux assessment in LRRK2 KD mice at 12 months of age

The lysosomotropic autophagy inhibitor CQ was employed to determine whether the LC3-I and LC3-II changes were due to increased or impaired ALP (Klionsky et al., 2021). To validate the administration protocol, CQ (50 mg/Kg, i.p.) (Vodicka et al., 2014) was administered daily for three consecutive days in 3-month-old WT mice, and animals were sacrificed 24 hours after the last injection (Fig. 11). A significant ~30% increase was found in LC3-II levels (df = 10, $t = 2.88$, $p = 0.0165$) and LC3-II/I ratio (df = 10, $t = 2.44$, $p = 0.0350$), which is considered an index of effective blockage of autophagosome-lysosome fusion (Fig. 11A) (Klionsky et al., 2021). CQ treatment did not alter the levels of other macroautophagy or lysosomal markers, such as p62, LAMP2, p-mTOR and mTOR in 3-month-old WT mice (Fig. 11B). The same protocol was then applied to assess the

autophagic flux in 12-month-old WT, G2019S KI, KO and KD mice (Fig. 11C). CQ administration significantly reduced the levels of LC3-I (-60%, df = 10, t = 4.20, p = 0.0018), LC3-II (-80%, df = 10, t = 5.70, p = 0.0002) and p62 (-40%, df = 10, t = 3, p = 0.0065) in KD mice (Fig 11C), and elevated LC3-I levels in WT (+60%; df = 10, t = 3, p = 0.0107) and G2019S KI (+110%; df = 10, t = 3, p = 0.0110) mice (Fig. 11C). However, the LC3-II /I ratio was significantly reduced by ~40% in G2019S KI (df = 10, t = 6.11, p = 0.0001), KO (df = 10, t = 5.22, p = 0.0004), KD (df = 10, t = 4.66, p = 0.0009) and WT (df = 10, t = 10, p = 0.0040) mice, suggesting an impairment of the autophagic flux in all genotypes (Fig. 11C). This was accompanied by a consistent elevation of p-mTOR levels across all CQ-treated LRRK2 mutants, that was most dramatic in KD mice: G2019S KI (+150%, df = 10, t = 2.55, p = 0.0288), KO mice (+110%, df = 10, t = 3.72, p = 0.0040), KD mice (+1630%; df = 10, t = 3.74, p = 0.0038). KD mice also showed a 60% reduction of mTOR levels (df = 10, t = 3.41, p = 0.0066). LAMP2 levels were found 57% elevated only in WT mice after CQ treatment (df = 10, t = 3, p = 0.0096; Fig.11C). These results, in particular the lack of an increase of LC3-II and LC3-II/I ratio in CQ-treated WT mice, led us to hypothesize that these changes were due to a tardive feedback mechanism occurring in all genotypes as a consequence of the CQ-mediated blockage of the autophagic flux, as previously reported in WT mice (Vodicka et al., 2014). Therefore, CQ administration was replicated anticipating WB analysis at 4 h after the last CQ injection, i.e. when the ALP blockage is still effective. This new administration protocol was performed only in 12-month-old KD mice, i.e. the only genotype showing alterations in LC3-I and LC3-II levels. At this time-point, LC3-I levels were unchanged (Fig. 12A) whereas LC3-II levels (df = 10, t = 5.63, p = 0.0002; Fig. 12B) and the LC3-II/I ratio (df = 10, t = 10.35, p < 0.0001; Fig. 12C) were 2.5-fold elevated in WT mice, likely due to the inhibition of autolysosome formation. Conversely, CQ-treated KD mice exhibited a 30% reduction of LC3-II levels (df = 10, t = 2.31, p = 0.0432) and LC3-II/I ratio (df = 10, t = 2.61, p = 0.0258), indicating a defective autophagic flux (Fig. 12B, C). Consistently, the cargo protein p62 accumulated in CQ-treated WT mice (+78%, df = 10, t = 4.30, p = 0.0016) but not in KD mice (Fig. 12D). Conversely, p-mTOR levels were elevated by 2.5-fold in WT mice (df = 10, t = 6.32, p < 0.0001) and by 12-fold in KD mice (df = 10, t = 19.57, p < 0.0001; Fig. 12E) suggesting a marked mTOR activation in both genotypes. This enhancement of mTOR activation was coupled to a 44% reduction in total mTOR levels in KD mice (df = 9, t = 4.18, p = 0.0024; Fig. 12F). LAMP2 levels were elevated by CQ administration in both WT (+28%, df = 10, t = 2.60, p = 0.0265) and KD mice (+52% df = 10, t = 5.89, p = 0.0002; Fig. 12G).

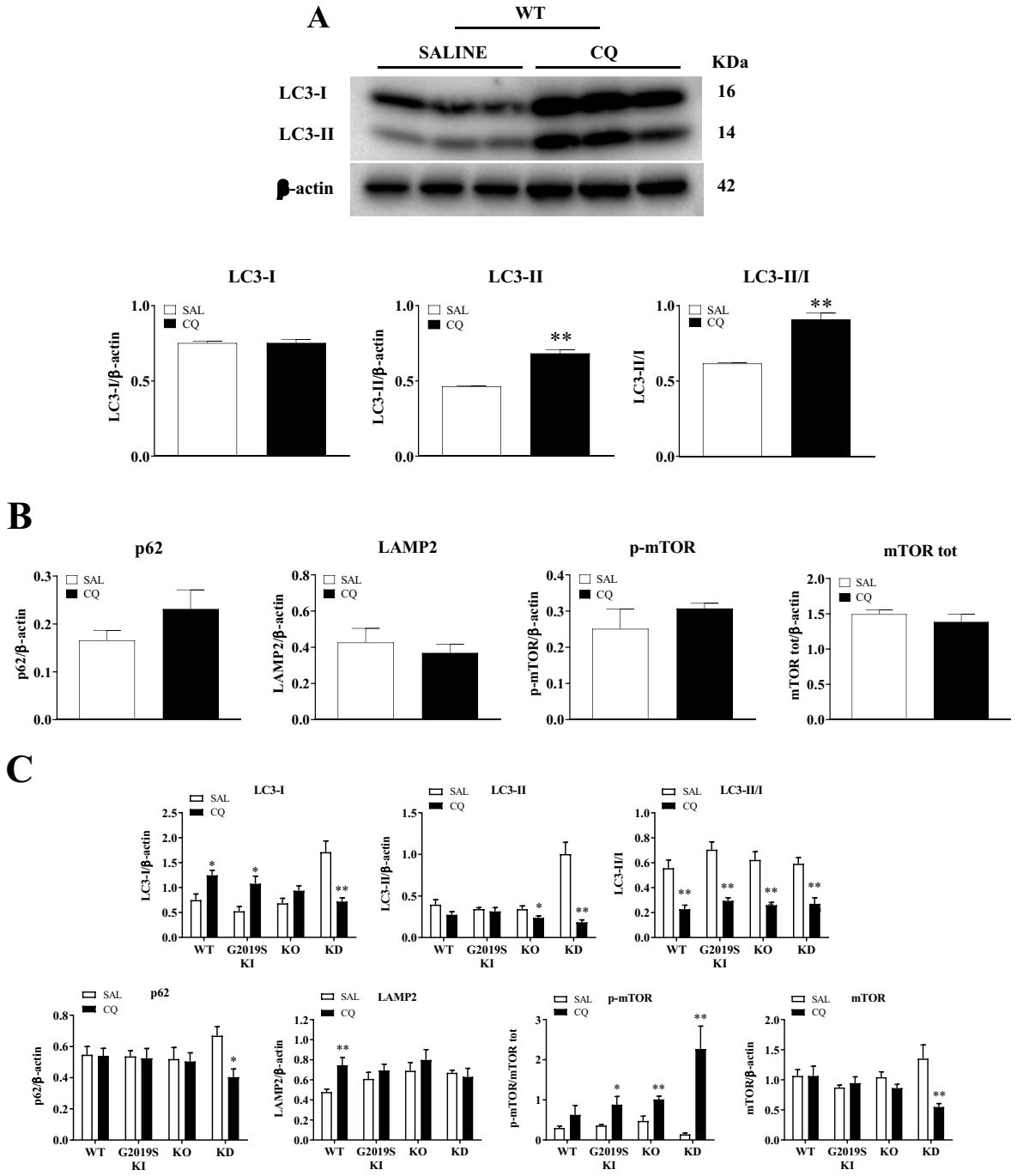

Figure 11. Autophagic flux assessment using chloroquine in 3-month-old WT and 12-month-old LRRK2 mice. A) Validation of CQ administration protocol in 3-month-old WT mice. Representative immunoblots and semi-quantitative analysis of LC3-I, LC3-II and LC3-II/I ratio in 3-month-old WT mice (n=6) after CQ and saline administration. B) Semi-quantitative analysis of p62, LAMP2, p-mTOR (normalized to total mTOR levels) and total mTOR levels. C) CQ administration in 12-month-old LRRK2-mutant mice. Semi-quantitative analysis of LC3-I, LC3-II, LC3-II/I ratio, p62, LAMP2, p-mTOR (normalized to total mTOR levels) and total mTOR levels upon CQ treatment. β-actin was used as housekeeping protein. Data are mean ± SEM. Statistical analysis was performed using the Student's t-test, two tailed for unpaired data. *p<0.05, ** p<0.01 different from saline-treated mice.

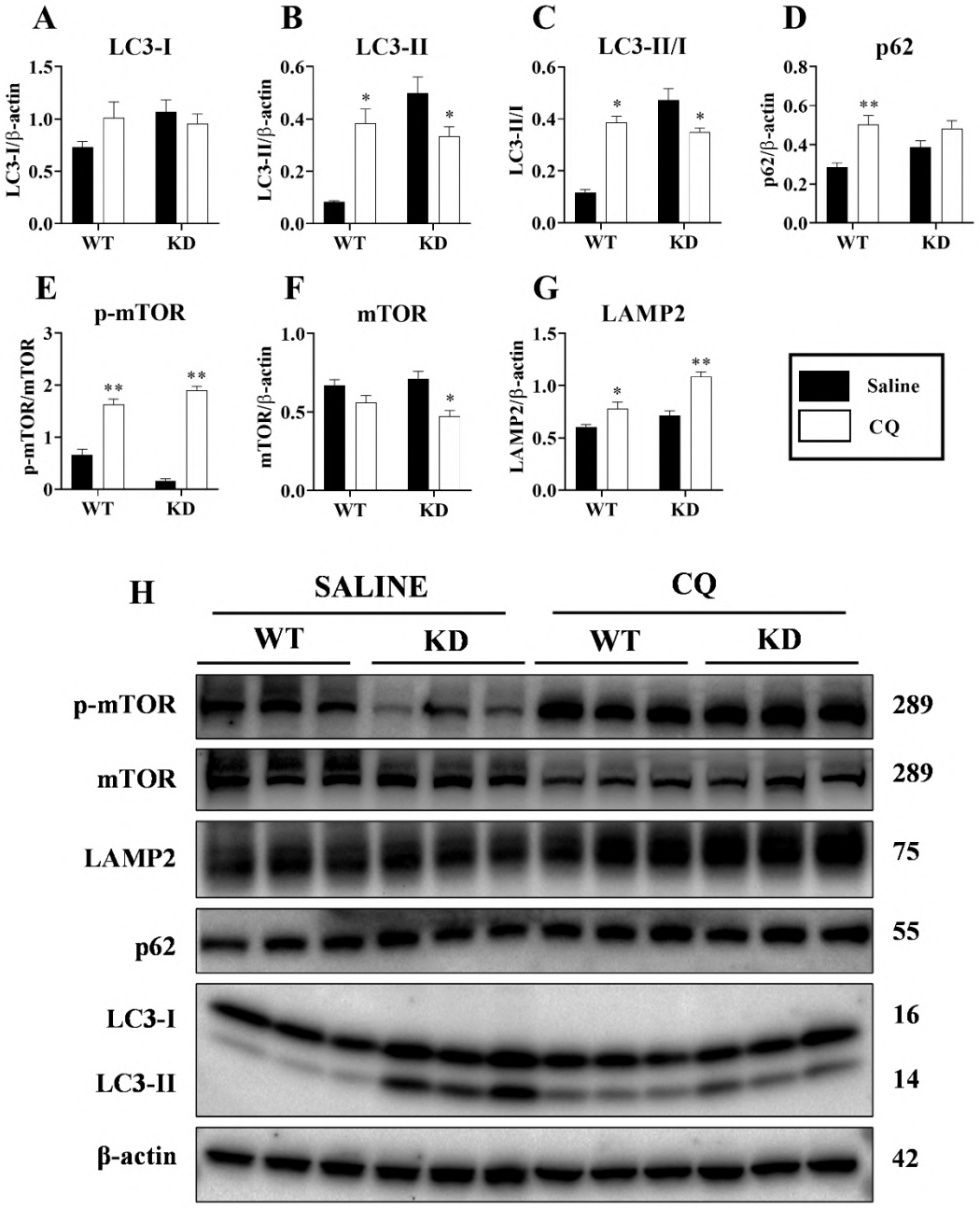

Figure 12. Autophagic flux assessment in 12-month-old WT and KD mice. Semi-quantitative analysis of macroautophagy marker levels: LC3-I (**A**), LC3-II (**B**), LC3-II/I (**C**), p62 (**D**), p-mTOR normalized on total mTOR (**E**) and total mTOR (**F**). Semi-quantitative analysis of lysosomal marker levels LAMP2 (**G**). Representative immunoblots of macroautophagy, mTOR activation and lysosomal markers (n=6) after CQ and saline administration (**H**). β-actin was used as housekeeping protein. Data are mean ± SEM. Statistical analysis was performed using Student's t test, two-tailed for unpaired data. * p <0.05, ** p <0.01 different from saline-treated mice.

4.1.4. Changes in GCase activity and GBA1 expression in LRRK2 mice

Since data pointed to a reduced autophagic flux in KD mice, we investigated whether also the activity of lysosomal GCase was affected in LRRK2 mice (Fig. 13). Significant changes were observed both at 3 months ($F_{3,20}$ = 8.46, p = 0.0008; Fig 13A) and 12 months ($F_{3,24}$ = 14.97, p < 0.0001; Fig 13B).

When compared to WT controls, KD mice showed an enhancement at both ages (+80% and +32%, respectively) whereas KO mice only at 12 months (+47%), although such increase was significant when the comparison was made against 3-month-old G2019S KI mice ($p < 0.05$). Conversely, no changes of GCase activity were detected in G2019S KI mice. RT-qPCR analysis interrogated whether changes in GCase activity were accompanied by changes of *GBA1* transcript levels in 12-month-old LRRK2-mutant mice. No significant change in *GBA1* gene expression was detected across genotypes ($F_{3,28} = 2.45$, $p = 0.0844$; Fig. 13C) although a tendency towards a reduction (15%) was observed in G2019S KI mice.

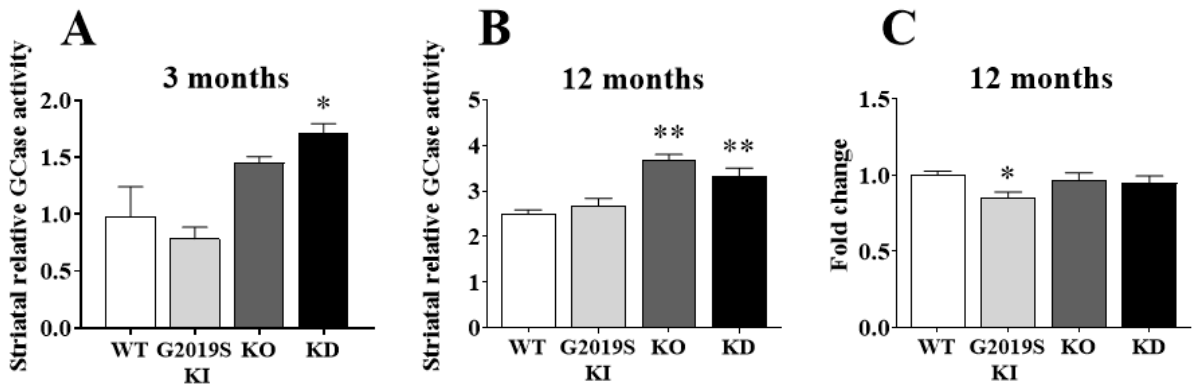

Figure 13. Relative striatal GCase activity in 3 and 12-month-old LRRK2 mice. Striatal tissue lysates isolated from 3-month-old (**A**) and 12-month-old (**B**) WT (n=6-8), G2019S KI (n=6-8), KO (n=6) and KD (n=6) mice were used to measure Relative GCase activity. Striatal *GBA1* gene expression was assessed (n=8) at 12 months (**C**). *ACT* and *HPRT* were used as reference genes for RT-qPCR analysis. Data are mean ± SEM of n mice per group. For GCase activity assay, data were analyzed using one-way ANOVA followed by Bonferroni's test for multiple comparisons. *p<0.05, **p<0.01 different from WT mice. For RT-qPCR analysis, data were analyzed using one-way ANOVA followed by the Dunnett's test for multiple comparison. * p <0.05, ** p <0.01 different from WT mice.

4.1.5. Subacute pharmacological inhibition of LRRK2 kinase activity

To test whether pharmacological LRRK2 kinase inhibition replicates the ALP impairment associated with the constitutive kinase silencing *in vivo*, MLi-2, a potent and brain penetrant LRRK2 kinase inhibitor, was administered subacutely for 7 days in 12-month-old WT and G2019S KI mice. Levels and expression of macroautophagy and lysosomal markers were evaluated 4 h after the last injection. Target engagement was confirmed by immunoblot analysis of pSer1292 LRRK2 levels, a readout of LRRK2 kinase activity (Kluss et al., 2018), in G2019S KI mice. In a pilot experiment, 10 mg/Kg (i.p.) b.i.d. for 7 days was administered, since this protocol was well tolerated in 3-month-old mice (unpublished data). After a few doses, however, lethality was observed in some 12-month-old mice of both genotypes prompting us to lower the dosage to 5 mg/Kg (i.p.), once a day for 7 days. Under these conditions, no signs of distress or mortality were noticed. WB analysis revealed a 42% reduction

of pSer1292 LRRK2 levels in G2019S KI mice (Fig. 14), indicating effective targeting of LRRK2 *in vivo*.

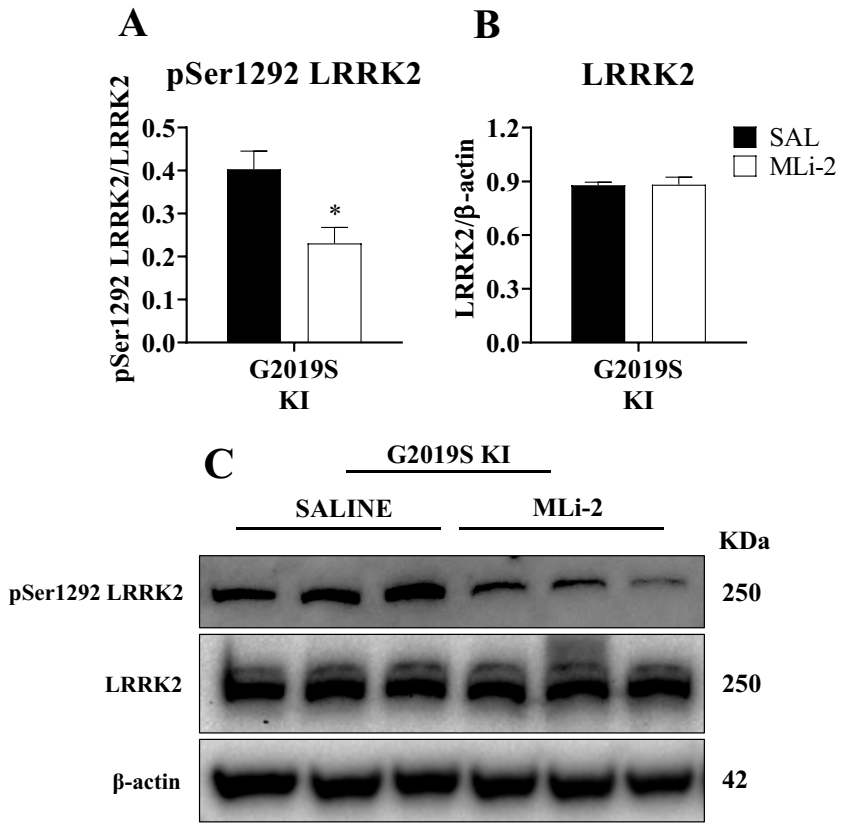

Figure 14. In vivo LRRK2 targeting of MLi-2. Striatum lysates were collected from 12-month-old G2019S KI mice administered with saline or MLi-2 (5 mg/Kg i.p.) once a day for seven days, and processed for WB analysis. A) Semi-quantitative analysis of pSer1292 LRRK2 normalized to total LRRK2 levels. B) Semi-quantitative analysis of total LRRK2 levels. C) Representative immunoblots. β-actin was used as housekeeping protein. Data are mean ± SEM. Statistical analysis was performed using the Student's t-test, two tailed for unpaired data. *p<0.05 different from saline.

MLi-2 caused a 50% elevation of LC3-I in WT mice (df = 10, t = 2.35, p = 0.00406) but not in G2019S KI mice, and no changes in LC3-II or LC3-II/ I ratio in both genotypes (Fig. 15A). p62 levels were elevated in both WT and G2019S KI mice, although the increase was significant only in G2019S KI mice (+80%, df = 10, t = 2.52, p = 0.0303) whereas LAMP2 levels remained unaffected (Fig. 15A). Interestingly, p-mTOR was reduced by ~32% (df = 10, t = 2.58, p = 0.00272) and mTOR levels enhanced by ~30% (df=10, t = 2.51, p = 0.0306; Fig. 15A) in G2019S KI mice, whereas no changes were observed in WT mice. RT-qPCR analysis showed that MLi-2 increased MAP1LC3B (+35%, df = 10, t = 2.62, p = 0.00257), and reduced mTOR (-25%, df = 10, t = 3.66, p = 0.0044) and TFEB (-20%, df = 10, t = 2.71, p = 0.00218) transcripts in WT mice (Fig. 15B). Moreover, MLi-2 reduced mTOR transcripts in G2019S KI mice (-25%, df = 10, t = 3.86, p = 0.0032) and left unaffected p62 and LAMP2 transcript levels in both genotypes (Fig. 15B).

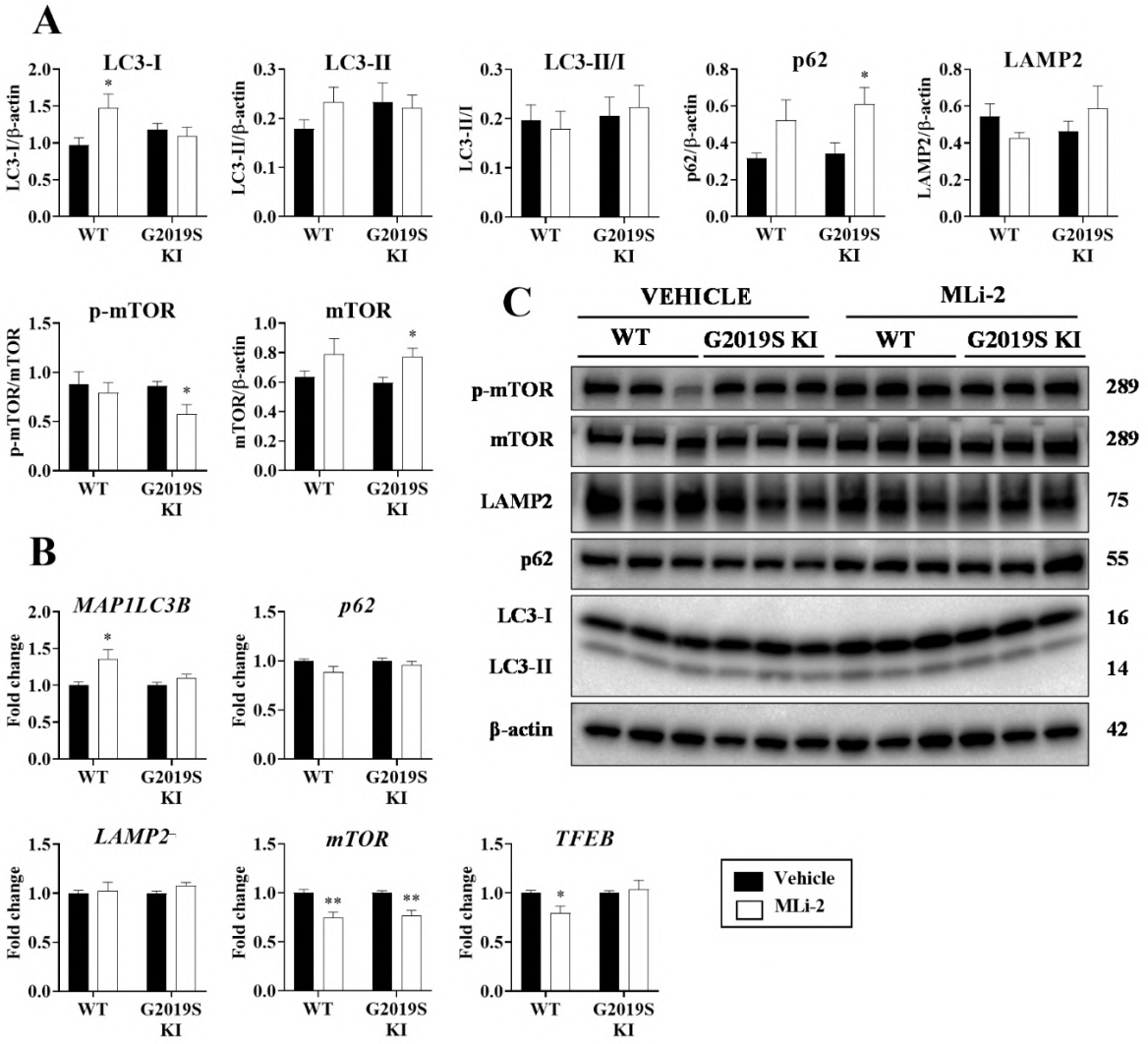

Figure 15. Sub-acute pharmacological inhibition of LRRK2 kinase activity in 12-month-old WT and G2019S KI mice. Mice were subacutely administered with the LRRK2 kinase inhibitor MLi-2 (5 mg/Kg i.p., once daily for 7 days) and sacrificed 4 hours after the last injection. **A**) Semi-quantitative analysis of macroautophagy markers (LC3-I, LC3-II, LC3-II/I ratio, p62, p-mTOR, mTOR) and lysosomal marker (LAMP2) levels, and representative immunoblots. **B**) RT-qPCR analysis of mRNA levels of *MAP1LC3B, p62, LAMP2, mTOR* and *TFEB* genes. β-actin was used as housekeeping protein and *ACT* and *HPRT* were used as reference genes. Data are mean ± SEM of 6 mice per group. Protein levels were analyzed using one-way ANOVA followed by the Bonferroni's test for multiple comparisons * p <0.05, ** p <0.01 different from saline-treated mice. Transcript levels were analyzed using one-way ANOVA followed by the Dunnett's test for multiple comparison. * p <0.05, ** p <0.01 different from saline-treated mice.

4.1.6. Immunofluorescence analysis of LC3B puncta and pSer129 α-syn in striatum and substantia nigra

We previously reported accumulation of pSer129 α-syn soluble forms in the striatum and SN of 12-month-old G2019S KI mice (Novello et al., 2018). To investigate whether changes in ALP markers were associated with significant increase of neuronal pSer129 α-syn inclusions, immunofluorescence analysis in the striatum and SN of 12-month-old WT, KD, KO and G2019S KI mice was carried out (Fig. 16). Significant changes in LC3 puncta were observed across genotypes ($F_{3,28}$ = 5.40, p = 0.0046). Consistent with the increase in LC3B-I and LC3B-II detected by WB analysis, LC3B puncta

were more abundant (+78%) in striatal MAP2$^+$ neurons of KD mice compared to WT mice (Fig. 16A, B) whereas no alterations were observed in KO or G2019S KI mice. On the contrary, pSer129 α-syn signal was elevated in striatal MAP2$^+$ neurons of G2019S KI mice (+60%) but not KD and KO mice ($F_{3,28}$ = 3.68, p = 0.0237) (Fig. 16A, C). LC3B changes were also detected in TH$^+$ neurons of SN ($F_{3,29}$ = 12.47, p < 0.0001), with KD and KO mice showing an increase (2.5-fold and 2-fold, respectively) and G2019S KI mice no change (Fig. 16D, E). However, no changes in pSer129 α-syn signal were observed in TH$^+$ neurons across genotypes (Fig. 16F).

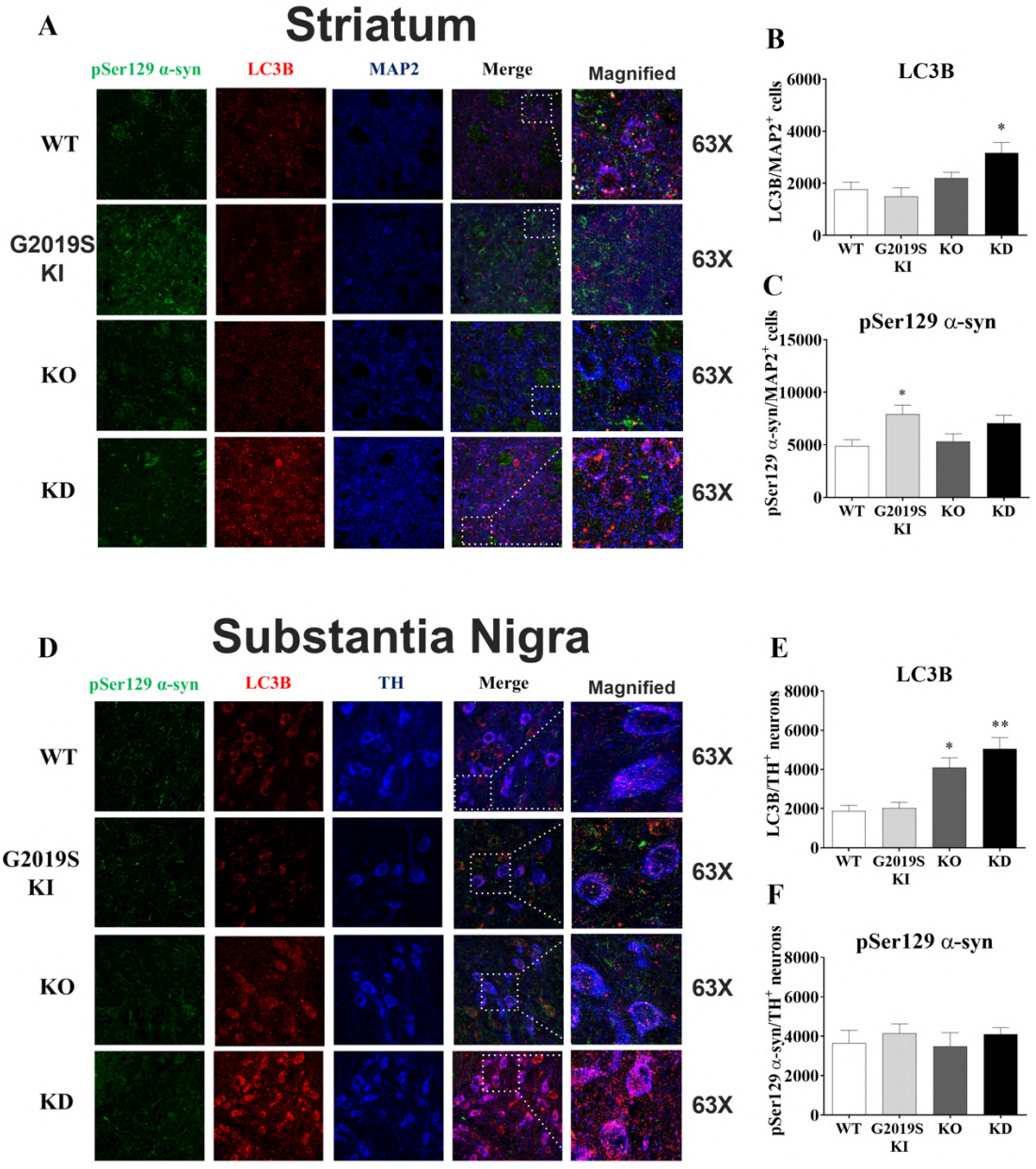

Figure 16. Immunofluorescence analysis of LC3B puncta and pSer129 α-syn inclusions in striatal MAP2$^+$ and nigral TH$^+$ neurons of 12-month-old LRRK2 mice. **A)** Representative immunofluorescence images and quantification of **B)** LC3B expression and **C)** pSer129 α-syn inclusions in striatal MAP$^+$ cells. **D)** Representative immunofluorescence images and quantification of **E)** LC3B expression and **F)** pSer129 α-syn inclusions in nigral TH$^+$ cells. Higher magnifications of insets drawn in merged images were also shown. The number of LC3B puncta was quantified within a mask image made by the TH or MAP2 staining. Data are mean ± SEM of 6-8 mice per group and were analyzed using one-way ANOVA followed by the Bonferroni's test for multiple comparisons. * p <0.05, ** p <0.01 different from WT mice.

4.2. PART II: AAV2/9-hα-syn treatment of 12-month-old WT, G2019S KI and KD mice

Immunoblot of striatal autophagy markers in LRRK2 mice revealed that 12-month-old KD mice have an impaired autophagic flux. We therefore sought to investigate whether overexpression of α-syn could accelerate the appearance of a parkinsonian phenotype in these mice. In the drag test (Fig 17), no difference in basal stepping activity was observed across genotypes (WT 8.33±0.51, G2019S KI 8.36±0.41, KD 8.27±0.29). Two-way ANOVA revealed an overall effect of treatment in all injected genotypes (WT $F_{1,16}$=18.50, p=0.0005; G2019S KI $F_{1,18}$= 4.73 p = 0.043; KD $F_{1,16}$ = 20.77 p = 0.0003) and an effect of time in KD mice only ($F_{3,48}$ = 6.30, p = 0.0011). In any genotype, however, time X treatment interaction reached the limit of significance although in KD mice this was just above the threshold ($F_{3,48}$ = 2.63, p = 0.0574), overall suggesting that AAV2/9-hα-syn injection reduced motor performance in KD mice.

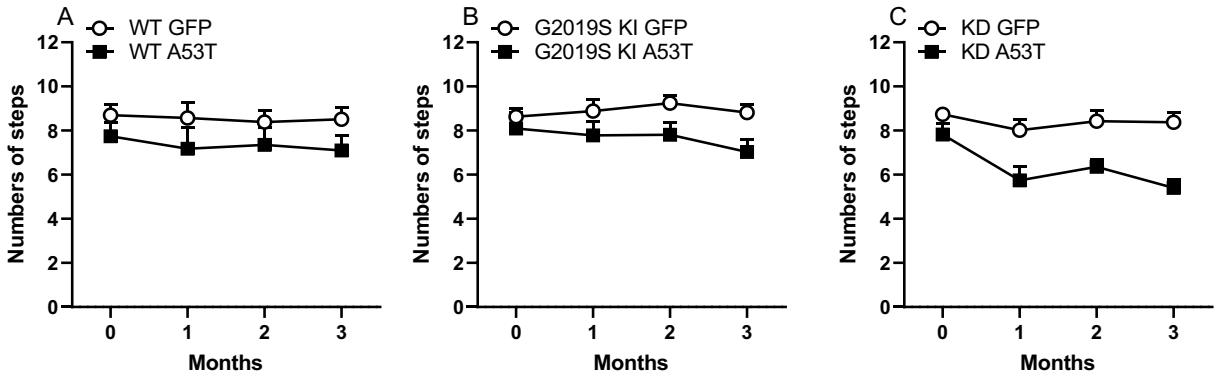

Figure 17. Behavioral motor tests. Stepping activity was evaluated using the Drag test in AAV2/9-hα-syn A53T- and GFP-treated 12-month-old WT (A), G2019S KI (B) and KD (C) mice at the baseline (time 0) and 1, 2, 3 months after surgery. Data are expressed as number of steps and are mean ± SEM of 10 mice per group and were analyzed using two-way ANOVA followed by Dunnett's test for multiple comparisons.

To test the efficiency of transgene expression after AAV2/9 injections, hα-syn levels were measured in SN and striatum (Fig. 18). As expected, two-way ANOVA revealed that only mice injected with AAV2/ 9-hα-syn had high levels of hα-syn staining in SN (Fig. 18A, C), suggesting transgene expression and A53T α-syn transport from nigral dopaminergic neurons (i.e. the site of injection) to the striatal projection area (treatment $F_{1,49}$ = 239.9, p < 0.0001, genotype $F_{2,49}$ = 5.88, p = 0.005, treatment X genotype interaction $F_{2,49}$ = 4.75, p = 0.013). In addition, a higher nigral hα-syn load (71%) was detected in AAV2/9-hα-syn-injected KD mice compared to the WT (46%) and G2019S KI (50%) counterparts. In keeping with this result, a stronger hα-syn staining was found in the striatum of KD mice (85%) (Fig. 18B, D) injected with A53T hα-syn compared to WT (52%) and

G2019S KI (56%) mice subjected to the same treatment (treatment $F_{1,45} = 242.7$, $p < 0.0001$, genotype $F_{2,45} = 8.66$, $p = 0.0007$, treatment X genotype interaction $F_{2,45} = 7.10$, $p = 0.022$).

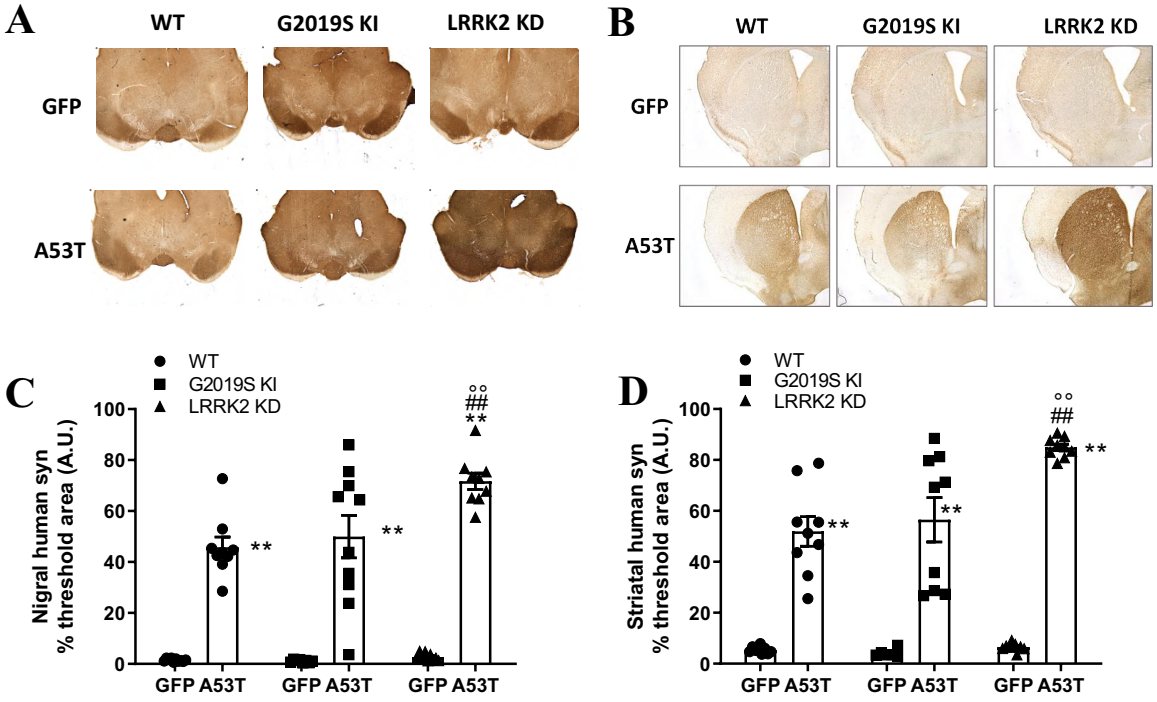

Figure 18. Expression of hα-syn in 12-month-old mice. Transgene expression was evaluated 3 months after the AAV2/9-A53T and GFP injection. Representative IHC images and quantification of hα-syn in SN (A, C) and striatum (B, D). Data are expressed as mean percentage ± SEM of n = 10 mice per group. Statistical analysis was performed by two-way ANOVA followed by the Dunnett's test for multiple comparisons. $^{**}p < 0.01$ different from respective GFP controls. $^{\circ\circ}$ $p < 0.01$ different from WT A53T. ## $p < 0.01$ different from G2019S KI A53T.

Next, the integrity of the nigrostriatal pathway was investigated (Fig. 19). Stereological analysis revealed no differences in the number of nigral TH^+ neurons between AAV2/9-hα-syn and GFP-injected mice, regardless of genotype considered (Fig. 19A, C). Likewise, no loss of striatal TH^+ nerve terminals was observed in all three genotypes injected with AAV2/9-hα-syn compared to their respective controls (Fig. 19B, D).

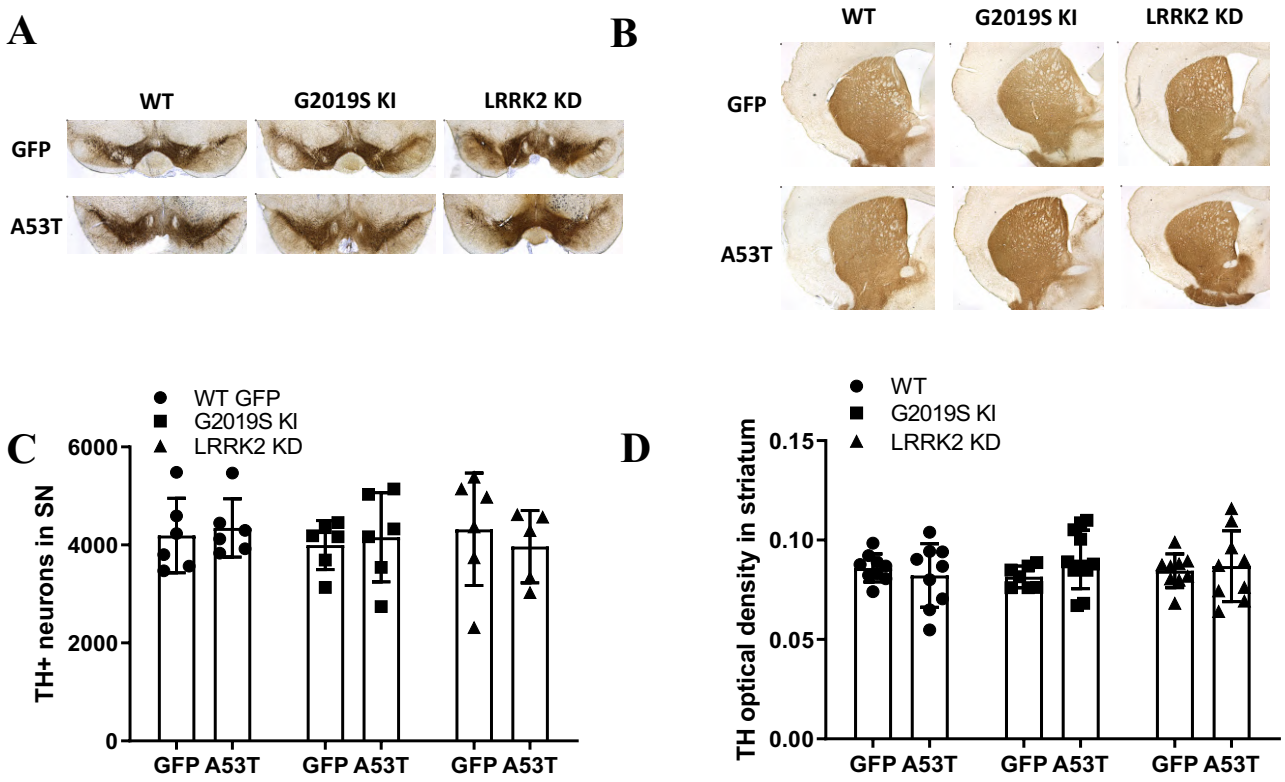

Figure 19. Stereological counting of nigral TH$^+$ neurons and optical density of TH$^+$ terminals. Stereological count of nigral neurons and optical density (grey scale arbitrary units were analyzed in 12-month-old WT, G2019S KI and KD mice 3 months after AAV2/9-A53T and GFP injection. Representative IHC images and quantification of TH$^+$ neurons in SN (A, C) and terminals in striatum (B, D). Data are expressed as mean percentage ± SEM of n = 10 mice per group. Statistical analysis was performed by two-way ANOVA followed by the Dunnett's test for multiple comparisons.

To investigate whether hα-syn overexpression was able to facilitate the phosphorylation of α-syn, total syn and pSer129 α-syn levels were measured in SN and striatum (Fig 20-21). In SN (Fig. 20A, C), two-way ANOVA on total α-syn levels revealed a significant effect of treatment ($F_{1,48} = 11.44$, $p = 0.0014$), genotype ($F_{2,48} = 11.82$, $p < 0.0001$) and a significant treatment X genotype interaction ($F_{2,48} = 6.98$, $p = 0.0022$). Total α-syn inclusions were more abundant in AAV2/9-hα-syn-injected KD and G2019S KI mice compared to the WT counterparts. Moreover, GFP-treated G2019S KI mice trended to higher α-syn levels compared to GFP-treated WT mice ($p = 0.075$). Nigral pSer129 α-syn staining (Fig. 20B, D) was significantly reduced in AAV2/9-hα-syn-treated G2019S KI mice compared to their GFP-treated controls (treatment $F_{1,49} = 7.93$, $p = 0.0070$, genotype $F_{2,49}=1.49$, $p = 0.23$, treatment X genotype interaction $F_{2,49} = 4.11$, $p = 0.0224$).

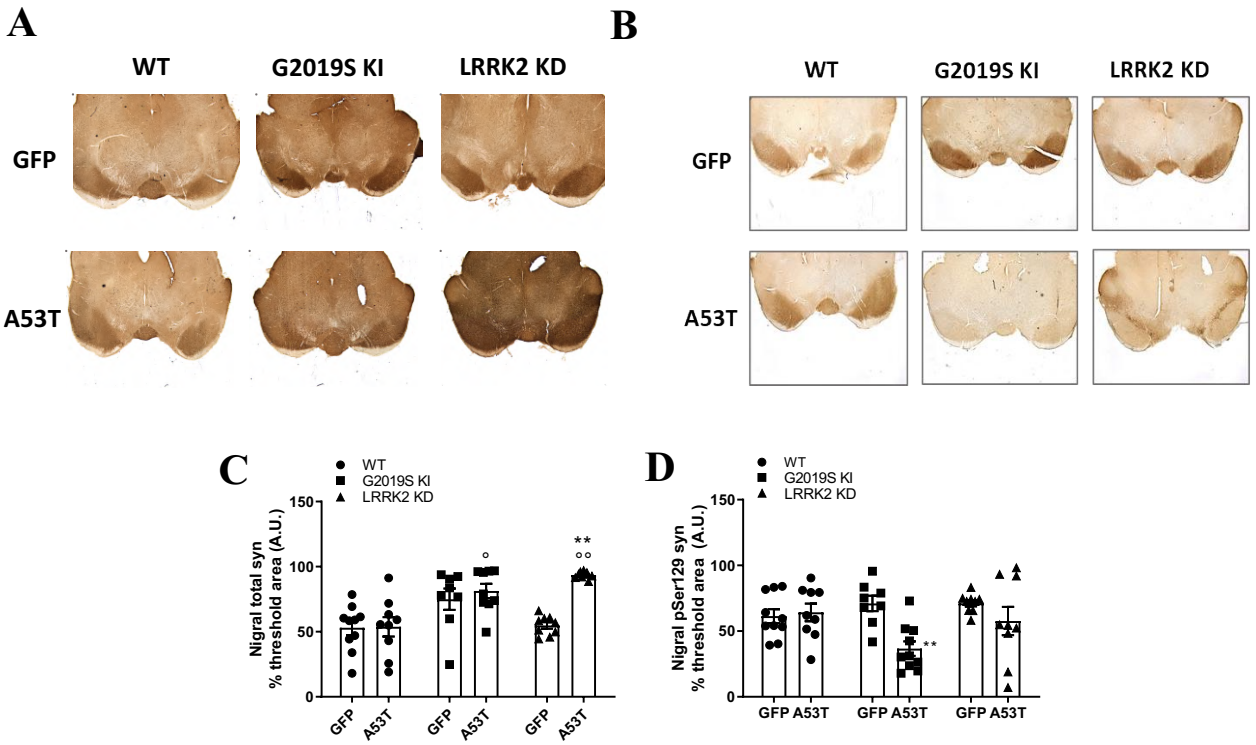

Figure 20. Expression of total α-syn and pSer129 α-syn in SNpc. Immunohistochemistry analysis was conducted to analyze levels of total α-syn and pSer129 α-syn in the SNpc of 12-month-old WT, G2019S KI and KD mice 3 months after AAV2/9-A53T or GFP injection. Representative IHC images and quantification of nigral total α-syn (A, C) and pSer129 α-syn (B, D). Data are expressed as immunopositive surface of the structure of interest of 10 mice per group Statistical analysis was performed by two-way ANOVA followed by the Dunnett's test for multiple comparisons. $^{**}p < 0.01$ different from respective GFP controls. $^{\circ\circ}$ $p < 0.01$ different from WT A53T.

In striatum (Fig. 21A, C), an overall effect of treatment was found on total α-syn levels ($F_{1,49} = 8.42$, $p = 0.0056$) but no significant effect of genotype ($F_{2,49} = 1.61$, $p = 0.2096$) or treatment X genotype interaction ($F_{2,49} = 2.47$, $p = 0.09$). Instead, no significant effect of treatment on pSer129 α-syn levels (Fig. 21B, D) was found ($F_{1,49} = 0.57$, $p = 0.45$) but a significant effect of genotype ($F_{2,49} = 8.43$, $p = 0.0007$) and a significant treatment X genotype interaction ($F_{2,49} = 4.32$, $p = 0.0188$). pSer129 α-syn levels were increased in AAV2/9-hα-syn-injected KD mice compared to WT and G2019S KI counterparts (Fig. 21B, D).

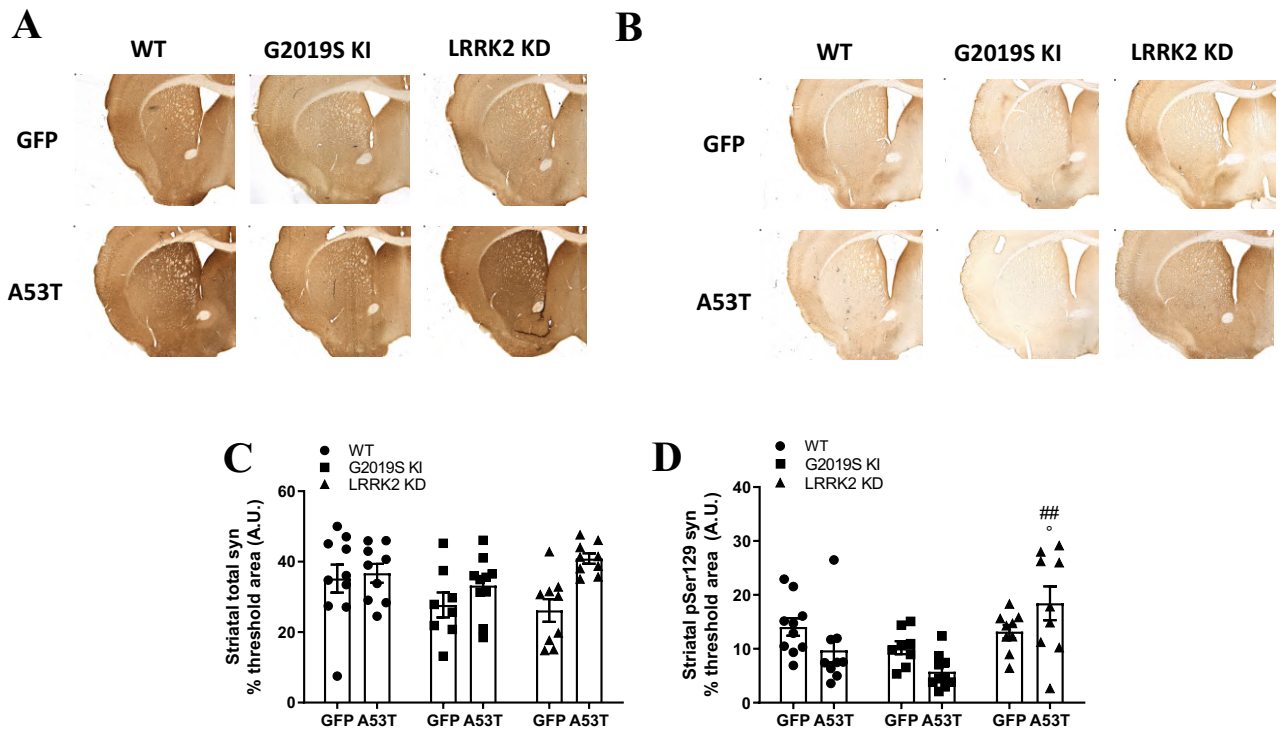

Figure 21. Expression of total α-syn and pSer129 α-syn in striatum. Immunohistochemistry analysis was conducted to analyze levels of total α-syn and pSer129 α-syn in the striatum of 12-month-old WT, G2019S KI and KD mice 3 months after AAV2/9-A53T or GFP injection. Representative IHC images and quantification of striatal total α-syn (A, C), pSer129 α-syn (B, D). Data are expressed as immunopositive surface of the structure of interest of 10 mice per group Statistical analysis was performed by two-way ANOVA followed by the Dunnett's test for multiple comparisons. $^{\circ\circ}$ $p <$ 0.05 different from WT A53T. $^{\#\#}$ $p < 0.01$ different from G2019S KI A53T.

5. DISCUSSION

5.1. PART I: Constitutive silencing of LRRK2 kinase activity leads to early glucocerebrosidase deregulation and impairment of autophagy *in vivo*

The first part of this study aimed to investigate whether LRRK2 kinase activity modulates striatal autophagy, lysosomal activity, GCase activity and pSer129 α-syn levels *in vivo.*

5.1.1. Constitutive LRRK2 kinase silencing impairs ALP in an age-dependent manner

No alterations in ALP markers were observed in the striatum of 3-month-old mice, suggesting that autophagy dysfunction occurs along with aging (Rubinzstein et al., 2011). Consistently, (Herzig et al., 2011) reported no changes in Akt, mTOR and its downstream substrate, TSC2, levels in the kidney of G2019S KI, KO and KD mice at 6 months.

Twelve-month-old KD mice showed increased levels of LC3-I, the autophagosomal marker LC3-II (Mizushima et al., 2010), p62, associated with accumulation of LC3B-I and LC3B-II puncta in striatal $MAP2^+$ and nigral TH^+ neurons. Different lines of evidence led us to hypothesize that ALP changes observed are related to a defective ALP rather than an upregulation of the autophagic flux occurring in aged striatal neurons bearing the LRRK2 KD mutation. First, CQ was administered in 12-month-old WT and KD mice. In fact, CQ is a lysosomotrophic agent able to prevent lysosomal acidification, thus leading to impaired autophagolysosomal formation. Therefore, if the autophagic flux were normal or upregulated, LC3-II/I ratio would be increased after CQ treatment (Vodicka et al., 2014), as observed in WT mice. If the flux were defective, following CQ administration, a reduction in LC3-II/I ratio would be expected, suggesting that CQ probably further blocks the autophagolysosome fusion step, as observed in KD mice. Second, p62 levels accumulated in KD mice. Upon CQ, p62 levels were elevated in WT mice, but no KD mice. Third, mRNA levels of *MAP1LC3B* and *p62* were unchanged in KD mice, supporting the view that increased levels of LC3-I, LC3-II and p62 were associated with a reduced clearance. Moreover, expression of *TFEB,* a master regulator of autophagy, was reduced in striatum of KD mice (Sardiello et al., 2009; Settembre et al., 2013).

If we hypothesize that striatal ALP is impaired in KD mice, the reduction in p-mTOR levels (i.e. mTOR active levels) might be caused by a compensatory mechanism possibly recruited to counteract the defective autophagic flux. In fact, KD mice also exhibited increased AMPK levels, and, opposite to mTOR, AMPK stimulates the activity of the autophagy initiator ULK1 (Kim et al., 2011). The

robust elevation of p-mTOR levels observed following CQ treatment in KD and WT mice might indicate a general feedback mechanism aimed to block ALP in response to lysosomal stress (Wang et al., 2018). Nevertheless, the reduction of p-mTOR levels observed at 20 months was not associated with a reduction in phosphorylation of S6K1, an mTOR downstream substrate. Even though we did not assess the phosphorylated levels of another mTOR substrate, 4EBP1, and so we cannot rule out the possibility that a differential regulation might occur, we concluded that changes in p-mTOR levels do not reflect alteration in its activity. In fact, mTOR is involved in a number of molecular pathways aimed to regulate cellular survival, metabolism and homeostasis (Liu and Sabatini., 2020). In keeping with this view, previous *in vitro* (Manzoni et al., 2013a; Manzoni et al., 2018) and *in vivo* (Herzig et al., 2011) studies indicated that LRRK2 might control ALP in an mTOR-independent manner.

Impairment of CMA can also be hypothesized to occur in 12-month-old KD mice, based on the finding of increased levels of the lysosomal receptor LAMP2 and the CMA substrate GAPDH, even though *LAMP2* transcript levels were unchanged in the striatum (Cuervo et al., 2004; Kaushik and Cuervo, 2011). Altogether, these observations led us to hypothesize a lysosomal accumulation and a reduced GAPDH turnover in KD mice. Differently, the increased LAMP2 levels upon CQ treatment might be sign of the impaired autophagosome-lysosome fusion, leading to lysosomal overload.

At 20 months, KD mice still show a similar ALP defective profile, as confirmed by the enhanced levels of the macroautophagy markers LC3-II and p62. This was associated with a decreased levels of p-mTOR but not of its substrate p-S6K1, and an increase of p-AMPK levels (e.g. the AMPK active form). Lysosomal marker LAMP2 and CMA substrate GAPDH were unchanged at 20 months, indicating a normalization of lysosomal activity. Similar to KD mice, 20-month-old KO mice showed elevated p62 and reduced mTOR levels, coupled to a mild decrease in p-mTOR levels, suggesting a late ALP impairment in the striatum of *LRRK2* deficient mice. A previous study has reported the lack of ALP changes in the brain of 15-month-old LRRK KO mice (Giaime et al., 2017). The discrepancy might be explained by the different age analyzed. Our findings, instead, are consistent with the striking age-dependent kidney pathology observed in KO mice, characterized by lysosomal and lipofuscin accumulation and ALP deficits (Baptista et al., 2013; Fuji et al., 2015; Herzig et al., 2011; Hinkle et al., 2012; Tong et al., 2012; Tong et al., 2010). However, the higher *LRRK2* gene expression in the kidney compared to the brain might explain the earlier onset and more severe course associated with the kidney pathology compared to the alterations reported in the brain. LAMP2 levels were also higher in 20-month-old striatum of KO mice, but this was not coupled to changes in GAPDH protein levels and *LAMP2* mRNA levels, making it impossible to formulate any hypothesis concerning lysosomal and CMA activity in these mice. Differently from the reduction of LC3-I and p62 levels observed in the cerebral cortex of 20-month-old G2019S KI mice (Schapansky et al., 2018), but in

line with what reported in the basal ganglia of G2019S PD patients (Mamais et al., 2018), macroautophagy markers were unaltered in the striatum of 3, 12 and 20-month-old G2019S KI mice. Increased LAMP2 but not GAPDH levels exhibited by 12-month-old G2019S KI mice are in partial agreement with the elevated levels of LAMP2 and GAPDH proteins reported in R1441G KI mice, supporting the view that CMA is impaired in these mice (Ho et al., 2020). However, the presence of two different LRRK2 mutations might explain the inconsistency related to the GAPDH levels between the two studies (Wallings et al., 2019). Nevertheless, robust downregulation of several ALP-related genes, such as *MAP1LC3B*, *LAMP2*, *mTOR* and *TFEB*, was observed in the striatum of 12-month-old G2019S KI mice, likely indicating an impaired transcription associated with a compensatory post-translational regulation.

5.1.2. LRRK2 inhibits GCase activity in vivo through its kinase activity

Consistent with the increased GCase activity reported in whole brain and primary astrocytes from KO mice (Ferrazza et al., 2016), the current study reported higher GCase activity in the striatum of LRRK2 KO and KD mice, suggesting an inverse correlation between GCase and LRRK2 kinase activity. In line with this view, MLi-2 treatment restored the reduced GCase activity observed in iPSCs-derived dopaminergic neurons and fibroblasts from G2019S, R1441G, R1441C LRRK2 carriers (Nguyen et al., 2018; Fujiwara et al., 2002; Ysselstein et al., 2019). In agreement with this study, the enhanced GCase activity observed in both LRRK2 kinase-absent genotypes was not associated with changes in *GBA1* mRNA levels, possibly indicating that intracellular trafficking of GCase might be impaired in these mice (Ysselstein et al., 2019). Only a trend toward inhibition in the enzymatic activity and *GBA1* gene expression levels was reported in the striatum of 12-month-old G2019S KI mice, in keeping with a mild downregulation of GBA1 transcript levels observed in the human PD brain (Murphy et al., 2014). This suggests that the LRRK2 inhibitory regulation of GCase is already maximal under basal conditions and further enhancement of LRRK2 kinase activity, associated with G2019S mutation, does not result in an additional reduction of GCase activity. It is noteworthy that increased GCase activity was measured in the striatum of KD mice at both 3 and 12 months, indicating that alterations in lysosomal activity might precede ALP changes observed in these mice.

5.1.3. Pharmacological inhibition of LRRK2 kinase activity

To better understand whether LRRK2 kinase inhibition impacts ALP under basal and hyperactive kinase activity conditions, subacute MLi-2 administration was performed in 12-month-old WT and G2019S KI mice. Aged mice showed increased susceptibility to high doses of MLi-2 (10 mg/Kg b.i.d.) as testified by some deaths in both WT and G2019S KI cohorts. Adopting a safer MLi-2

administration protocol (5 mg/Kg once a day), which resulted in a 42% reduction of striatal pSer1292 LRRK2 levels, elevation of p62 and mTOR levels, coupled to a reduction in p-mTOR levels and *mTOR* gene expression was observed in G2019S KI mice. Conversely, WT mice were less affected showing only an increase of LC3-I protein and MAP1LC3B mRNA levels. Nonetheless, neither WT nor G2019S KI mice treated with MLi-2 were able to replicate the KD-associated ALP phenotype observed at 12 months, possibly due to the difference degree of kinase inhibition existing between the constitutive kinase silencing and a mild pharmacological inhibition achieved with a subacute protocol. Different in vitro studies reported that pharmacological LRRK2 kinase inhibition, e.g. MLi-2 treatment, was effective in restoring a defective autophagic flux or lysosomal function associated with G2019S mutation (Boecker et al., 2021; Manzoni et al., 2013b; Obergasteiger et al., 2020; Saez-Atienzar et al., 2014; Schapansky et al., 2018; Wallings et al., 2019), whereas other reported the opposite (Schapansky et al., 2014). Our findings cannot either support or confute this view, given the controversial results obtained: increase in p62 protein but not transcript levels, together with *TFEB* downregulation might suggest an ALP blockage whereas increase in LC3-I and *MAP1LC3B* expression points to the opposite. Even though subacute inhibition of LRRK2 kinase activity did not fully recapitulate the ALP impairment observed in the striatum of KD mice it might help identify the ALP targets more susceptible to LRRK2 kinase inhibition. In fact, the hyperactive LRRK2 kinase activity associated with the G2019S mutation brings mTOR function under a stronger LRRK2 modulation. To date, different LRRK2 inhibitors are employed in clinical trials as disease modifying agents in PD (Tolosa et al., 2020). Although our results do not allow any conclusions on whether the MLi-2 toxicity observed in aged mice is LRRK2 related, they support the view that dosage of LRRK2 inhibitors in older subjects requires fine titration in order to prevent profound LRRK2 kinase inhibition (Tolosa et al., 2020). Furthermore, further investigation is needed to assess the effect of long-term treatment with LRRK2 inhibitors on ALP, especially in the elderly animals.

5.1.4. Relationship between ALP impairment and pSer129 α-syn

Recent studies have associated increased α-syn inclusions with CMA impairment in 18-month-old R1441G LRRK2 mice (Ho et al., 2020) or ALP deficits in 15-month-old LRRK double KO mice (Giaime et al., 2017), supporting the hypothesis of an existing link between ALP dysfunction and synucleinopathy. pSer129 α-syn levels are considered as an early sign of synucleinopathy (Oueslati et al., 2016), given the evidence that pSer129 α-syn promotes α-syn ability to aggregate and spread (Samuel et al., 2016). Furthermore, pSer129 α-syn colocalizes with markers associated with LB pathology in animal models of PD progression (Luk et al., 2012; Niu et al., 2018) and is highly expressed in LB (Anderson et al., 2006; Fujiwara et al., 2002). Considering previous findings that

G2019S LRRK2 facilitated α-syn phosphorylation at Ser129 and degeneration of nigrostriatal tract (Novello et al., 2018; Volpicelli-Daley et al., 2016), we decided to investigate whether pSer129 α-syn levels correlates with ALP dysfunction. We previously reported that G2019S KI mice showed increased soluble pSer129 α-syn levels in striatum and SNpc at 12 months (Longo et al., 2017; Novello et al., 2018). In the current study, we measured pSer129 α-syn inclusions in striatal $MAP2^+$, likely GABAergic neurons (Gerfen et al., 1992) of 12-month-old G2019S KI and KD mice. Consistently with immunoblot data, no changes in pSer129 α-syn and LC3B puncta were observed in striatal G2019S neurons, whereas an increase of LC3B but not pSer129 α-syn levels was reported in striatal KD neurons. Therefore, ALP alterations and pSer129 α-syn inclusions might occur in different cell types. Based on these results, we should conclude that the higher nigrostriatal degeneration associated with G2019S KI mice upon viral injection of mutant human α-syn is due to ALP-independent neuronal mechanisms. However, it is possible that the G2019S-related increase of pSer129 α-syn levels is not linked to the greater susceptibility to parkinsonism showed by this genotype. In keeping with this view, a recent study demonstrated the existence of presynaptic pools of pSer129 α-syn that are unrelated to LB pathology (Weston et al., 2021). Altogether, these observations suggest that the increased deposition of pSer129 α-syn in the striatum of aged G2019S KI mice under basal conditions might be linked to neuronal dysfunctions reported in these mice (Longo et al., 2017). However, it cannot be ruled out that the ALP deficits observed in KD mice also facilitate synucleinopathy in response of α-syn overload, due to an α-syn mishandling.

5.2. PART II: AAV2/9-mediated A53T α-syn overexpression causes increased α-syn overload, but no neurodegeneration in LRRK2 kinase-dead mice

Since in the first part of the study we provided evidence that 12-month-old KD mice have an impaired autophagic flux, we next investigated whether these mice also show increased susceptibility to α-syn pathology *in vivo.* To this aim we injected G2019S KI, KD and WT mice with AAV2/9 carrying h-α-syn. To measure the efficiency of transgene transduction, hα-syn levels were monitored both in SN, the site of injection, and the striatum, to analyze the hα-syn diffusion along the nigrostriatal tract. Interestingly, KD mice showed significantly higher hα-syn protein levels in both SN and striatum compared to the G2019S and WT counterparts, suggesting either a higher viral transduction or a reduced clearance of hα-syn. Since there is no evidence supporting that the D1994S LRRK2 KD mutation can promote hα-syn viral overexpression, these results would confirm the hypothesis that silencing of LRRK2 kinase activity significantly impairs striatal and nigral autophagy *in vivo*, as shown in the first part of this study. In keeping with this view, KD mice also showed higher total α-syn levels in SN, with a trend to increase in striatum, upon AAV2/9-hα-syn injection, possibly

suggesting greater endogenous α-syn accumulation or impaired clearance in KD mice. Interestingly, such an increase of α-syn burden was associated with a mild motor decline in the drag test in the absence of nigral degeneration. Consistently, behavioral alterations were observed also in the case of AAV-induced synucleinopathy not associated with nigrostriatal damage (Koprich et al., 2011). This is in contrast with human PD pathology, in which the nigrostriatal neurodegeneration anticipates the onset of motor symptoms (Kordower et al., 2013; Cheng et al., 2010).

Perhaps not too surprisingly, the increase in α-syn was paralleled by an increase in pSer129 α-syn levels in striatum, resulting in no change in α-syn phosphorylation rate. On the contrary, a reduction in pSer129 α-syn levels, resulting in a reduction of α-syn phosphorylation rate, was observed in SNpc. The reasons for such a different response are not clear but might be based on area-dependent factors among which the much lower levels of α-syn in SN compared to striatum, the higher transgene expression in SN (the injection area) and the likely presence of different LRRK2 interactors in the two areas.

Different α-syn patterns were observed in WT and G2019S KI mice. Different from KD mice, G2019S KI and WT mice did not exhibit changes in total α-syn levels in SN and striatum upon AAV2/9-h-α-syn injection when compared with their GFP controls. Nonetheless, A53T G2019S mice showed higher α-syn levels than A53T WT mice. Such difference was also observed under basal conditions (i.e. in GFP-injected mice) although it was just above the limit of significance ($p = 0.0768$). The higher pSer129 α-syn nigral staining of 12-month-old G2019S KI mice was also reported by Novello et al. (2018) although in that study G2019S KI mice also showed higher pSer129 α-syn staining following AAV-hα-syn injection, which was not observed in the present study. This inconsistency might be explained by the different level of nigrostriatal neurodegeneration, since in that study the increase of striatal and nigral pSer129 α-syn staining was associated with a marked nigral cell loss whereas in the present study no cell loss was observed. Therefore, the reduction of pSer129 α-syn staining observed in striatum and SN of G2019S KI mice might represent an early posttranslational modification of α-syn, preceding the appearance of neurodegeneration. It remains matter for speculation why with the same vector type, titer and genetic model such a different response was observed 3 months after injection.

5.3. Concluding remarks

In conclusion, Part I of this study pointed out that constitutive silencing of LRRK2 kinase activity in LRRK2 KD mice leads to early deregulation of GCase activity and late alteration of the macroautophagy and lysosomal homeostasis *in vivo*. Consistently, Part II of this study revealed that AAV-mediated overexpression of human α-syn in aged LRRK2 KD causes human and endogenous

α-syn accumulation and mild motor deficits. Although longer time might be necessary to allow nigrostriatal degeneration to appear, this result corroborates the hypothesis that constitutive silencing of LRRK2 kinase activity *in vivo* impairs autophagy and facilitate α-syn accumulation at a stage that precede the onset of nigrostriatal degeneration. Surprisingly, hyperactive LRRK2 kinase activity, associated with the pathogenic G2019S mutation, did not alter macroautophagy markers but downregulated several key autophagy and lysosomal genes, as also reported in PD brain (Decressac et al., 2013) perhaps revealing a stronger control on lysosomal *vs* autophagic activity by endogenous LRRK2. This study contributes to shed lights on the complex LRRK2-mediated regulation of ALP *in vivo*, highlighting the importance of LRRK2 kinase activity to maintain a proper ALP function during aging.

6. REFERENCES

Aasly, J.O., et al., 2014. Elevated levels of cerebrospinal fluid alpha-synuclein oligomers in healthy asymptomatic LRRK2 mutation carriers. *Front. Aging Neurosci.* 6, 248.

Aerts, J.M., et al., 1988. Glucocerebrosidase, a lysosomal enzyme that does not undergo oligosaccharide phosphorylation. *Biochim. Biophys. Acta.* 964: 303-308.

Ahmed, I., et al., 2012. Development and characterization of a new parkinson's disease model resulting from impaired autophagy. *J. Neurosci.* 32: 16503–16509.

Albanese, F., et al., 2019. Autophagy and LRRK2 in the aging brain. *Front. Neurosci.* 13, 1352.

Alcalay, R.N., et al., 2014. Comparison of Parkinson risk in Ashkenazi Jewish patients with Gaucher disease and GBA heterozygotes. *JAMA*. 71(6): 752–757.

Alcalay, R. N., et al., 2016. SCARB2 variants and glucocerebrosidase activity in Parkinson's disease. *npj Parkinson's Disease* 2.1: 1-4.

Alegre-Abarrategui, J., et al., 2009. LRRK2 regulates autophagic activity and localizes to specific membrane microdomains in a novel human genomic reporter cellular model. *Hum. Mol. Genet.* 18: 4022–4034.

Alvarez-Erviti, L., et al., 2010. Chaperone-mediated autophagy markers in Parkinson disease brains. *Archiv. Neur.* 67: 1464–1472.

Ambrosi, G., et al., 2015. Ambroxol-induced rescue of defective glucocerebrosidase is associated with increased LIMP-2 and saposin C levels in GBA1 mutant Parkinson's disease cells. *Neurobiol. Dis.* 82: 235–242.

Anderson, J.P., et al., 2006. Phosphorylation of Ser-129 is the dominant modification of α-synuclein in familial and sporadic Lewy body disease. *J. Biol. Chem.* 281: 29739–29752.

Arbez, N., et al., 2020. G2019S-LRRK2 mutation enhances MPTP-linked Parkinsonism in mice. *Hum. Mol. Genet.* 29: 580–590.

Arcuri, L., et al., 2016. Genetic and pharmacological evidence that endogenous nociceptin/orphanin FQ contributes to dopamine cell loss in Parkinson's disease. *Neurobiol. Dis*. 89: 55-64.

Arranz, A.M., et al., 2015. LRRK2 functions in synaptic vesicle endocytosis through a kinase-dependent mechanism. *J. Cell Sci.* 128: 541–552.

Atik, A., et al., 2016. α-Synuclein as a biomarker for Parkinson's disease. *Brain Pathol.* 26: 410–418.

Azeredo Da Silveira, S., et al., 2009. Phosphorylation does not prompt, nor prevent, the formation of alpha-synuclein toxic species in a rat model of Parkinson's disease. *Hum. Mol. Genet*. 18: 872–887.

Bae, E. J., et al., 2015. Loss of glucocerebrosidase 1 activity causes lysosomal dysfunction and alpha-synuclein aggregation. *Exp. Mol. Med.* 47, e153.

Bae, E. J., et al., 2018. LRRK2 kinase regulates α-synuclein propagation via RAB35 phosphorylation. *Nat. Commun.* 9, 3465.

Balestrino, R., et al., 2020. Parkinson disease. *Eur. J. Neurol.* 27: 27–42.

Ballabio, A. & Bonifacino, J.S., 2020. Lysosomes as dynamic regulators of cell and organismal homeostasis. *Nat. Rev. Mol*. 21: 101–118.

Bandyopadhyay, U., et al., 2008. The Chaperone-mediated autophagy receptor organizes in dynamic protein complexes at the lysosomal membrane. *Mol. Cell. Biol*. 28: 5747–5763.

Bang, Y., et al., 2016. LRRK2 interferes with aggresome formation for autophagic clearance. *Mol. Cell. Neurosci.* 75: 71–80.

Baptista, M.A. et al., 2013. Loss of leucine-rich repeat kinase 2 (LRRK2) in rats leads to progressive abnormal phenotypes in peripheral organs. *PLoS One*. 8, e80705.

Bar-Peled, L., et al., 2013. A Tumor suppressor complex with GAP activity for the Rag GTPases that signal amino acid sufficiency to mTORC1. *Science*, 340: 1100-1106.

Bayer, T.A., et al., 1999. α-synuclein accumulates in Lewy bodies in Parkinson's disease and dementia with Lewy bodies but not in Alzheimer's disease β-amyloid plaque cores. *Neurosci. Lett.* 266: 213–216.

Behl, T., et al., 2021. Cross-talks among GBA mutations, glucocerebrosidase, and α-synuclein in GBA-associated Parkinson's disease and their targeted therapeutic approaches: a comprehensive review. *Transl. Neurodegener.* 10, 4.

Berger, Z., et al., 2006. Rapamycin alleviates toxicity of different aggregate-prone proteins. *Hum. Mol. Genet*. 15: 433–442.

Berger, Z., et al., 2010. Membrane localization of LRRK2 is associated with increased formation of the highly active LRRK2 dimer and changes in its phosphorylation. *Biochem*. 49(26): 5511–5523.

Berwick, D.C., et al., 2019. LRRK2 biology from structure to dysfunction: research progresses, but the themes remain the same. *Mol. Neurodegener*. 14, 49.

Bieri, G., et al., 2019. LRRK2 modifies α-syn pathology and spread in mouse models and human neurons. *Acta Neuropathol.* 137: 961–980.

Bingol, B., et al., 2018. Autophagy and lysosomal pathways in nervous system disorders. *Molecular and Cellular Neuroscience.* 91: 167–208.

Biosa, A., et al., 2013. GTPase activity regulates kinase activity and cellular phenotypes of Parkinson's disease-associated LRRK2. *Hum. Mol. Genet.* 22: 1140–1156.

Bjørkøy, G., et al., 2005. p62/SQSTM1 forms protein aggregates degraded by autophagy and has a protective effect on huntingtin-induced cell death. *J. Cell. Biol*. 171(4): 603–614.

Boecker, C.A., et al., 2021. Increased LRRK2 kinase activity alters neuronal autophagy by disrupting the axonal transport of autophagosomes. *Curr. Biol.* 31: 2140-2154.

Boland, B., et al., 2018. Promoting the clearance of neurotoxic proteins in neurodegenerative disorders of ageing. *Nat. Rev. Drug Discov.* 17: 660–688.

Bonello, F., et al., 2019. LRRK2 impairs PINK1/Parkin-dependent mitophagy via its kinase activity: pathologic insights into Parkinson's disease. *Hum. Mol. Genet.* 28: 1645–1660.

Bonet-Ponce, L., et al., 2021. LRRK2 recruitment, activity, and function in organelles. *FEBS J.* 1–20.

Bonet-Ponce, L., et al., 2020. LRRK2 mediates tubulation and vesicle sorting from lysosomes. *Sci. Adv.* 6. eabb2454.

Bootman, M. D., et al., 2018. The regulation of autophagy by calcium signals: do we have a consensus? *Cell Calcium.* 70: 32–46.

Bourdenx, M., et al., 2015. Lack of additive role of ageing in nigrostriatal neurodegeneration triggered by alpha-synuclein overexpression. *Acta Neuropathol. Commun.* 3, 46.

Bowman, C., et al., 2014. Foxk proteins repress the initiation of starvation-induced atrophy and autophagy programs. *Nat. Cell. Biol.* 16: 1202–1214.

Bravo-San Pedro, J. M., et al., 2013. The LRRK2 G2019S mutant exacerbates basal autophagy through activation of the MEK/ERK pathway. *Cell. Mol. Life Sci.* 70: 121–136.

Brundin, P., et al., 2010. "Prion-like transmission of protein aggregates in neurodegenerative diseases." *Nat. Rev. Mol. Cell. Biol.* 11.4: 301-307.

Brundin, P., and Melki, R., 2017. Prying into the prion hypothesis for Parkinson's disease. *J. Neurosci*. 37: 9808–9818.

Budanov, A.V. & Karin, M., 2008. p53 target genes sestrin1 and sestrin2 connect genotoxic stress and mTOR signaling. *Cell.* 134: 451–460.

Chakraborty, D., et al., 2019. Enhanced autophagic-lysosomal activity and increased BAG3-mediated selective macroautophagy as adaptive response of neuronal cells to chronic oxidative stress. *Redox Biol.* 24, 101181.

Chang, D., et al., 2017. A meta-analysis of genome-wide association studies identifies 17 new Parkinson's disease risk loci. *Nat. Genet.* 49: 1511–1516.

Chau, K. Y., et. al., 2009. Relationship between alpha synuclein phosphorylation, proteasomal inhibition and cell death: relevance to Parkinson's disease pathogenesis. *J. Neurochem*. 110: 1005–1013.

Chauhan, S., et al., 2016. TRIMs and galectins globally cooperate and TRIM16 and galectin-3 co-direct autophagy in endomembrane damage homeostasis. *Dev. Cell*. 39: 13–27.

Chen, C.-Y., et al., 2012. (G2019S) LRRK2 activates MKK4-JNK pathway and causes degeneration of SN dopaminergic neurons in a transgenic mouse model of PD. *Cell Death Differ.* 19: 1623–1633.

Chen, L. and Feany, M.B., 2005. Alpha-synuclein phosphorylation controls neurotoxicity and inclusion formation in a *Drosophila* model of Parkinson disease. *Nat. Neurosci.* 8: 657–663.

Cheng, H. C., et al., 2010. Clinical progression in Parkinson disease and the neurobiology of axons. *Ann. Neurol.* 67: 715–725.

Chia, R., et al., 2014. Phosphorylation of LRRK2 by casein kinase 1alpha regulates trans-Golgi clustering via differential interaction with ARHGEF7. *Nat. Commun*. 5, 5827.

Chiang, H. L., et al., 1989. A role for a 70-kilodalton heat shock protein in lysosomal degradation of intracellular proteins. *Science.* 246: 382–385.

Chiu, C.C., et al., 2016. Increased Rab35 expression is a potential biomarker and implicated in the pathogenesis of Parkinson's disease. *Oncotarget*. 7: 54215–54227.

Chou, J.S., et al., 2014. (G2019S) LRRK2 causes early-phase dysfunction of SNpc dopaminergic neurons and impairment of corticostriatal long-term depression in the PD transgenic mouse. *Neurobiol. Dis.* 68: 190–199.

Chu, Y., et al., 2009. Alterations in lysosomal and proteasomal markers in Parkinson's disease: relationship to alpha-synuclein inclusions. *Neurobiol. Dis.* 35: 385–398.

Ciuffa, R., et al., 2015. The selective autophagy receptor p62 forms a flexible filamentous helical scaffold. *Cell Rep.* 11: 748–758.

Civiero, L., et al., 2017. Molecular Insights and Functional Implication of LRRK2 Dimerization. *Adv Neurobiol*. 14: 107–121.

Cookson, M.R., 2010. The role of leucine-rich repeat kinase 2 (LRRK2) in Parkinson's disease. *Nat. Rev. Neurosci.* 11: 791–797.

Crews, L., et al., 2010. Selective molecular alterations in the autophagy pathway in patients with Lewy body disease and in models of alpha-synucleinopathy. *PLoS One.* 5:e9313.

Cuervo, A. M. and Wong, E., 2004. Chaperone-mediated autophagy: roles in disease and aging. *Cell Res*. 24: 92–104.

Cuervo, A. M., et al., 1997. A population of rat liver lysosomes responsible for the selective uptake and degradation of cytosolic proteins. *J. Biol. Chem.* 272: 5606–5615.

Cuervo, A.M. & Dice, J.F., 2006. A receptor for the selective uptake and degradation of proteins by lysosomes. *Science.* 273: 501–503.

Cuervo, A.M., et al., 2004. Impaired degradation of mutant alpha-synuclein by chaperone-mediated autophagy. *Science*. 305: 1292-1295.

Cullen, M., et al., 2009. Cathepsin D expression level affects alpha-synuclein processing, aggregation, and toxicity in vivo. *Mol. Brain*, 2, 5.

Daher, J.P., et al., 2012. Neurodegenerative phenotypes in an A53T α-synuclein transgenic mouse model are independent of LRRK2. *Hum. Mol. Genet.* 21: 2420–2431.

Daher, J.P., et al., 2015. Leucine-rich repeat kinase 2 (LRRK2) pharmacological inhibition abates alpha-synuclein gene-induced neurodegeneration. *J. Biol. Chem.* 290: 19433–19444.

Daher, J.P.L., et al., 2014. Abrogation of α-synuclein-mediated dopaminergic neurodegeneration in LRRK2-deficient rats. *Proc. Natl. Acad. Sci. U.S.A.* 111: 9289–9294.

Danieli, A., et al., 2018. P62-mediated phase separation at the intersection of the ubiquitin-proteasome system and autophagy. *J. Cell Sci.* 131, 214304.

Decressac, M., et al., 2013. TFEB-mediated autophagy rescues midbrain dopamine neurons from alpha-synuclein toxicity. *Proc. Natl. Acad. Sci. U.S.A.* 110: E1817-E1826.

Dehay, B., et al., 2010. Pathogenic lysosomal depletion in Parkinson's disease. *J. Neurosci*. 30: 12535–12544.

Deter, R.L., et al., 1967. Participation of lysosomes in cellular autophagy induced in rat liver by glucagon. *J. Cell Biol.* 35: C11–C16.

Deyaert, E., et al., 2017. A homologue of the Parkinson's disease-associated protein LRRK2 undergoes a monomer-dimer transition during GTP turnover. *Nat. Commun*. 8(1), 1008.

di Domenico, A., et al., 2019. Patient-specific iPSC-derived astrocytes contribute to non-cell-autonomous neurodegeneration in parkinson's disease. *Stem Cell Rep*. 12: 213–229.

Do, J., et al., 2019. Glucocerebrosidase and its relevance to Parkinson disease. *Mol. Neurodegener.* 14.1 (2019): 1-16.

Dodson, M., et al., 2012. Roles of the *Drosophila*LRRK2 homolog in Rab7-dependent lysosomal positioning. *Hum. Mol. Genet.* 21: 1350–1363.

Dodson, M., et al., 2014. Novel ethyl methanesulfonate (EMS)-induced null alleles of the *Drosophila* homolog of LRRK2 reveal a crucial role in endolysosomal functions and autophagy in vivo. *Dis. Model. Mech.* 7: 1351–1363.

Duraiyan, J., et al., 2012. Applications of immunohistochemistry. *J. Pharm. Bioallied. Sci*. 4: S307–S309.

Duran, R., et al., 2012. The glucocerobrosidase E326K variant predisposes to Parkinson's disease, but does not cause Gaucher's disease. *Mov Disord*. 28(2): 232–6.

Dzamko, N., et al., 2010. Inhibition of LRRK2 kinase activity leads to dephosphorylation of Ser (910)/Ser (935), disruption of 14-3-3 binding and altered cytoplasmic localization. *The Biochem J.* 430(3): 405–413.

Dzamko N., et al., 2012. The IkappaB kinase family phosphorylates the Parkinson's disease kinase LRRK2 at Ser935 and Ser910 during Toll-like receptor signaling. *PloS One*. 7(6), e39132.

Ebrahimi-Fakhari, D., et al., 2011. Distinct roles *in vivo* for the ubiquitin-proteasome system and the autophagy-lysosomal pathway in the degradation of α-synuclein. *J. Neurosci.* 31, 14508–14520.

Egan, D.F., et al., 2011. Phosphorylation of ULK1 (hATG1) by AMP-activated protein kinase connects energy sensing to mitophagy. *Science*. 331: 456–461.

Eguchi, T., et al., 2018. LRRK2 and its substrate Rab GTPases are sequentially targeted onto stressed lysosomes and maintain their homeostasis. *Proc. Natl. Acad. Sci. USA*. 115: E9115–E9124.

Emmanouilidou, E., et al., 2010. Cell-produced α-synuclein is secreted in a calcium-dependent manner by exosomes and impacts neuronal survival. *J. Neurosci.* 30: 6838–6851.

Ferese, R., et al., 2015. Four copies of SNCA responsible for autosomal dominant Parkinson's disease in two Italian siblings. *Parkinsons Dis.* 546462.

Fernandes, H.J., et al., 2016. ER stress and Autophagic perturbations lead to elevated extracellular alpha-Synuclein in GBA-N370S Parkinson's iPSC-derived dopamine neurons. *Stem Cell Reports*. 6(3): 342–56.

Ferrazza, R., et al., 2016. LRRK2 deficiency impacts ceramide metabolism in brain. *Biochem. Biophys. Res. Commun.* 478: 1141–1146.

Fiske, M., et al., 2011. Contribution of alanine-76 and serine phosphorylation in alpha-synuclein membrane association and aggregation in yeasts. *Parkinsons Dis*. 392180.

Fouka, M., et al., 2020. Search of Effective Treatments Targeting alpha-Synuclein Toxicity in Synucleinopathies: Pros and Cons. *Front Cell Dev. Biol.* 8, 559791.

Franco, R., et al., 2018. Glucocerebrosidase mutations and synucleinopathies. Potential role of sterylglucosides and relevance of stuying both GBA1 and GBA2 genes. *Front Neuroanat*. 12, 52.

Friedman, L.G., et al., 2012. Disrupted autophagy leads to dopaminergic axon and dendrite degeneration and promotes presynaptic accumulation of α-synuclein and LRRK2 in the brain. *J. Neurosci.* 32: 7585–7593.

Fu, G., et al., 2011. Nodal enhances the activity of FoxO3a and its synergistic interaction with Smads to regulate cyclin G2 transcription in ovarian cancer cells. *Oncogene.* 30: 3953–3966.

Fuji, R.N. et al., 2015. Effect of selective LRRK2 kinase inhibition on nonhuman primate lung. *Sci. Transl. Med*. 7, 273.

Fujiwara, H., et al., 2002. α-Synuclein is phosphorylated in synucleinopathy lesions. *Nat Cell Biol.* 4: 160–164.

Galluzzi, L., et al., 2017. Pharmacological modulation of autophagy: therapeutic potential and persisting obstacles. *Nat. Rev. Drug Discov.* 16: 487–511.

Gammoh, N., et al., 2013. Interaction between FIP200 and ATG16L1 distinguishes ULK1 complex–dependent and –independent autophagy. *Nat. Struct. Mol. Biol.* 20: 144–149.

Gasser, T., et al., 2009. Molecular pathogenesis of Parkinson disease: insights from genetic studies. *Expert Rev. Mol. Med.* 11, e22.

Gegg, M., and Schapira, A.H., 2016. Mitochondrial dysfunction associated with glucocerebrosidase deficiency. *Neurobiol. Dis*. 90: 43–50.

Gegg, M.E., et al., 2012. Glucocerebrosidase deficiency in substantia nigra of parkinson disease brains. *Ann. Neurol*. 72(3): 455–463.

Gegg, M.E., et al., 2015. No evidence for substrate accumulation in Parkinson brains with GBA mutations. *Mov. Disord*. 30(8): 1085–1089.

Gerfen, C.R., et al., 1992. The neostriatal mosaic: multiple levels of compartmental organization. *Trends Neurosci.* 15: 133-139.

Giaime, E., et al., 2017. Age-dependent dopaminergic neurodegeneration and impairment of the autophagy-lysosomal pathway in LRRK-deficient mice. *Neuron*. 96: 796–807.

Giasson, B.I. and Lee, V.M., 2011. Parkin and the molecular pathways of Parkinson's disease. *Neuron.* 31: 885–888.

Giasson, B.I., et al., 2000. Oxidative damage linked to neurodegeneration by selective α-synuclein nitration in synucleinopathy lesions. *Science.* 290: 985–989.

Giesert, F., et al., 2017. The pathogenic LRRK2 R1441C mutation induces specific deficits modeling the prodromal phase of Parkinson's disease in the mouse. *Neurobiol. Dis.* 105: 179–193.

Gomez-Suaga, P., et al., 2012a. LRRK2 as a modulator of lysosomal calcium homeostasis with downstream effects on autophagy. *Autophagy*. 8: 692–693.

Gomez-Suaga, P., et al., 2012b. Leucine-rich repeat kinase 2 regulates autophagy through a calcium-dependent pathway involving NAADP. *Hum. Mol. Genet.* 21: 511–525.

Gong, H., et al., 2016. Evaluation of candidate reference genes for RT-qPCR studies in three metabolism related tissues of mice after caloric restriction. *Sci. Rep*. 6, 38513.

Grabowski, G.A., et al., 2008. Phenotype, diagnosis, and treatment of Gaucher's disease. *Lancet* 372: 1263–1271.

Greggio, E., et al., 2006. Kinase activity is required for the toxic effects of mutant LRRK2/dardarin. *Neurobiol. Dis*. 23: 329-341.

Gruschus, J.M., et al., 2015. Did alpha-Synuclein and glucocerebrosidase coevolve? Implications for Parkinson's Disease. *PLoS One*. 10(7): 1–21.

Guardia-Laguarta, C., et al., 2014. alpha-Synuclein is localized to mitochondria-associated ER membranes. *J. Neurosci.* 34: 249–259.

Gunder, A.L., et al., 2019. Path mediation analysis reveals GBA impacts Lewy body disease status by increasing alpha-synuclein levels. *Neurobiol. Dis*. 121: 205–213.

Hansen, M., et al., 2008. A Role for Autophagy in the Extension of Lifespan by Dietary Restriction in *C. elegans*. *PLOS Gen.* 4(2), e24.

Hara, S., et al., 2013. Serine 129 phosphorylation of membrane-associated alpha-synuclein modulates dopamine transporter function in a G protein-coupled receptor kinase-dependent manner. *Mol. Biol. Cell.* 24: 1649–1660.

Hara, T., et al., 2006. Suppression of basal autophagy in neural cells causes neurodegenerative disease in mice. *Nature*. 441: 885–889.

Harrison, D.E., et al., 2009. Rapamycin fed late in life extends lifespan in genetically heterogeneous mice. *Nature*. 460: 392–395.

Hartlova, A., et al., 2018. LRRK2 is a negative regulator of *Mycobacterium tuberculosis* phagosome maturation in macrophages. *EMBO J.* 37, e98694.

Hawley, S.A., et al., 2003. Complexes between the LKB1 tumor suppressor, STRADα/β and MO25 /β are upstream kinases in the AMP-activated protein kinase cascade. *J. Biol.* 2, 28.

He, Y., et al., 2019. Alpha-Synuclein nitration and its implications in Parkinson's disease. *ACS Chem. Neurosci.* 10: 777–782.

Hellemans, J., et al., 2007. qBase relative quantification framework and software for management and automated analysis of real-time quantitative PCR data. *Genome Biol.* 8, R19.

Heman-Ackah, S.M., et al., 2017. Alpha-synuclein induces the unfolded protein response in Parkinson's disease SNCA triplication iPSC-derived neurons. *Hum. Mol. Genet.* 26: 4441–4450.

Henderson, M. X., et al., (2019). LRRK2 inhibition does not impart protection from alpha-synuclein pathology and neuron death in non-transgenic mice. *Acta Neuropathol. Commun*. 7, 28.

Henry, A. G., et al., 2015. Pathogenic LRRK2 mutations, through increased kinase activity, produce enlarged lysosomes with reduced degradative capacity and increase ATP13A2 expression. *Hum. Mol. Genet.* 24: 6013–6028.

Heo, H.Y., et al., 2010. LRRK2 enhances oxidative stress-induced neurotoxicity via its kinase activity. *Exp. Cell Res.* 316: 649-656.

Herrero-Martin, G., et al., 2009. TAK1 activates AMPK-dependent cytoprotective autophagy in TRAIL-treated epithelial cells. *EMBO J.* 28: 677–685.

Herzig, M.C., et al., 2011. LRRK2 protein levels are determined by kinase function and are crucial for kidney and lung homeostasis in mice. *Hum. Mol. Genet*. 20: 4209-4223.

Hetz, C., et al., 2012. The unfolded protein response: controlling cell fate decisions under ER stress and beyond. *Nat Rev. Mol. Cell. Biol.* 13: 89–102.

Higashi, S., et al., 2009. Abnormal localization of leucine-rich repeat kinase 2 to the endosomal-lysosomal compartment in lewy body disease. *J. Neuropathol. Exp. Neurol.* 68: 994–1005.

Higashi, S., et al., 2011. Localization of MAP1-LC3 in vulnerable neurons and Lewy bodies in brains of patients with dementia with Lewy bodies. J. *Neuropathol. Exp. Neurol*. 70: 264–280.

Hijaz, B.A., et al., 2020. Initiation and propagation of alpha-synuclein aggregation in the nervous system. *Mol. Neurodegener.* 15, 19.

Hindle, S., et al., 2013. Dopaminergic expression of the Parkinsonian gene LRRK2-G2019S leads to non-autonomous visual neurodegeneration, accelerated by increased neural demands for energy. *Hum. Mol. Genet*. 22, 2129-2140

Hinkle, K.M., et al., 2012. LRRK2 knockout mice have an intact dopaminergic system but display alterations in exploratory and motor co-ordination behaviors. *Mol. Neurodegener.* 7, 25.

Ho, D.H., et al., 2018. LRRK2 impairs autophagy by mediating phosphorylation of leucyl-tRNA synthetase. *Cell Biochem. Funct.* 36: 431–442.

Ho, P.W.L., et al., 2020. Age-dependent accumulation of oligomeric SNCA/α-synuclein from impaired degradation in mutant LRRK2 knockin mouse model of Parkinson disease: role for therapeutic activation of chaperone-mediated autophagy (CMA). *Autophagy.* 0: 1–24.

Hockey, L. N., et al., 2015. Dysregulation of lysosomal morphology by pathogenic LRRK2 is corrected by TPC2 inhibition. *J. Cell Sci.* 128: 232–238.

Hodara, R., et al., 2004. Functional consequences of alpha-synuclein tyrosine nitration: diminished binding to lipid vesicles and increased fibril formation. *J. Biol. Chem.* 279: 47746–47753.

Hohn, A., et al., 2017. Happily (n)ever after: aging in the context of oxidative stress, proteostasis loss and cellular senescence. *Redox Biol*. 11: 482–501.

Horowitz, M., et al., 1989. The human glucocerebrosidase gene and pseudogene: structure and evolution. *Genomics*. 4: 87-96.

Hosokawa, N., et al., 2009. Atg101, a novel mammalian autophagy protein interacting with Atg13. *Autophagy.* 5: 973–979.

Hu, D., et al., 2018. LRRK2 G2019S mutation inhibits degradation of α-synuclein in an in vitro model of Parkinson's Disease. *Curr. Med. Sci.* 38: 1012–1017.

Hu, Y. B., et al., 2015. The endosomal-lysosomal system: from acidification and cargo sorting to neurodegeneration. *Transl. Neurodegener.* 4: 1–10.

Hui, K.Y., et al., 2018. Functional variants in the *LRRK2* gene confer shared effects on risk for Crohn's disease and Parkinson's disease. *Sci. Transl. Med*. 10, eaai7795.

Ibanez, P., et al., 2004. Causal relation between α-synuclein gene duplication and familial Parkinson's disease. *Lancet.* 364: 1169–1171.

Imai, Y., et al., 2008. Phosphorylation of 4E-BP by LRRK2 affects the maintenance of dopaminergic neurons in *Drosophila*. *EMBO J.* 27: 2432–2443.

Itakura, E., et al., 2010. Characterization of autophagosome formation site by a hierarchical analysis of mammalian Atg proteins. *Autophagy*. 6(6): 764-776.

Itakura, E., et al., 2012. The hairpin-type tail-anchored SNARE syntaxin 17 targets to autophagosomes for fusion with endosomes/lysosomes. *Cell*. 151: 1256–1269.

James, N.G., et al., 2012. Number and brightness analysis of LRRK2 oligomerization in live cells. *Biophys J.* 102(11): L41–L43.

Jeong, G.R., et al., 2018. Dysregulated phosphorylation of Rab GTPases by LRRK2 induces neurodegeneration. *Mol. Neurodegener.* 13, 8.

Jin, S. M., and Youle, R. J., 2012. PINK1- and Parkin-mediated mitophagy at a glance. *J. Cell Sci.* 125: 795–799.

Kabeya, Y., et al., 2000. LC3, a mammalian homologue of yeast Apg8p, is localized in autophagosome membranes after processing. *EMBO J*. 19: 5720-5728.

Kaeberlein, M., et al., 2005. Regulation of yeast replicative life span by TOR and Sch9 in response to nutrients. *Science*. 310: 1193–1196.

Kalia, L.V., et al., 2015. Clinical correlations with Lewy body pathology in LRRK2-related Parkinson disease. *JAMA Neurol.* 72: 100–105.

Kapahi, P., et al., 2004. Regulation of lifespan in Drosophila by modulation of genes in the TOR signaling pathway. *Curr. Biol*. 14: 885–890.

Karuppagounder, S.S., et al., 2016. LRRK2 G2019S transgenic mice display increased susceptibility to 1-methyl-4-phenyl-1,2,3,6-tetrahydropyridine (MPTP)-mediated neurotoxicity. *J. Chem. Neuroanat.* 76: 90–97.

Kauffman, K.J., et al., 2018. Delipidation of mammalian Atg8-family proteins by each of the four ATG4 proteases. *Autophagy*. 14: 992-1010.

Kaushik, S. et al., 2018. The coming of age of chaperone-mediated autophagy. *Nat. Rev. Mol. Cell. Biol.* 19: 365–381.

Kaushik, S. and Cuervo, A.M., 2012. Chaperone-mediated autophagy: a unique way to enter the lysosome world. *Trends Cell Biol.* 22: 407-417.

Kenessey, A., et al., 1989. Increase in cathepsin D activity in rat brain in aging. *J. Neurosci. Res.* 23: 454–456.

Kenzelmann Broz, D., et al., 2013. Global genomic profiling reveals an extensive p53-regulated autophagy program contributing to key p53 responses. *Genes Dev.* 27: 1016–1031.

Khaminets, A., et al., 2016. Ubiquitin-dependent and independent signals in selective autophagy. *Trends Cell Biol*. 26: 6–16.

Kiely, A.P., et al., 2013. α-Synucleinopathy associated with G51D SNCA mutation: a link between Parkinson's disease and multiple system atrophy? *Acta Neuropathol*. 125, 753-769

Kim, Y.C., and Guan, K.L. 2015. mTOR: a pharmacologic target for autophagy regulation. *J. Clin. Invest*. 125: 25–32.

Kim, J., et al., 2011. AMPK and mTOR regulate autophagy through direct phosphorylation of Ulk1. *Nat. Cell Biol.* 13: 132-141.

Klein, C.L., et al., 2009. Homo- and heterodimerization of ROCO kinases: LRRK2 kinase inhibition by the LRRK2 ROCO fragment. *J. Neurochem*. 111(3): 703–715.

Klionsky, D.J., et al., 2012. Look people, "Atg" is an abbreviation for "autophagy related." That's it. *Autophagy*. 8: 1281–1282.

Klionsky, D.J., et al., 2003. A unified nomenclature for yeast autophagy-related genes. *Developmental Cell.* 5: 539–545.

Klionsky, D.J., et al., 2021. Guidelines for the use and interpretation of assays for monitoring autophagy. *Autophagy*. 1: 1–32.

Kluss, J.H., et al., 2018. Detection of endogenous S1292 LRRK2 autophosphorylation in mouse tissue as a readout for kinase activity. *NPJ Parkinsons Dis*. 4.

Komatsu, M., et al., 2006. Loss of autophagy in the central nervous system causes neurodegeneration in mice. *Nature*. 441: 880–884.

Komatsu, M., et al., 2007a. Homeostatic levels of p62 control cytoplasmic inclusion body formation in autophagy-deficient mice. *Cell*. 131: 1149–1163.

Komatsu M., et al., 2007b. Essential role for autophagy protein Atg7 in the maintenance of axonal homeostasis and the prevention of axonal degeneration. *Proc. Natl. Acad. Sci. U.S.A.* 104, 14489–14494.

Koprich, J.B., et al., 2011. Progressive neurodegeneration or endogenous compensation in an animal model of Parkinson's disease produced by decreasing doses of α-synuclein. *PLoS ONE*. 6, e17698.

Kordower, J.H., et al., 2013. Disease duration and the integrity of the nigrostriatal system in Parkinson's disease. *Brain*. 136: 2419–2431.

Koyama-Honda, I., et al., 2013. Temporal analysis of recruitment of mammalian ATG proteins to the autophagosome formation site. *Autophagy*. 9(10): 1491-1499.

Kruger, R., et al., 1998. Ala30Pro mutation in the gene encoding alpha-synuclein in Parkinson's disease. *Nat. Genet.* 18: 106–108.

Kuma, A., et al., 2017. Autophagy-monitoring and autophagy-deficient mice. *Autophagy.* 13.10:1619-1628.

Kumar, V., et al., 2013. Genome-wide association study signal at the 12q12 locus for Crohn's disease may represent associations with the MUC19 gene. *Inflamm. Bowel Dis*. 19, 1254-1259

Kuwahara, T., et al., 2012. Phosphorylation of alpha-synuclein protein at Ser-129 reduces neuronal dysfunction by lowering its membrane binding property in *Caenorhabditis elegans*. *J. Biol. Chem*. 287: 7098–7109.

Larsen, J.O., et al., 1998. Global spatial sampling with isotropic virtual planes: estimators of length density and total length in thick, arbitrarily orientated sections. *J. Microsc.* 191: 238-24.

Lavalley, N.J., et al., 2016. 14-3-3 Proteins regulate mutant LRRK2 kinase activity and neurite shortening. *Hum. Mol. Genet*. 25(1): 109–122.

Law, B.M., et al., 2014. A direct interaction between leucine-rich repeat kinase 2 and specific beta-tubulin isoforms regulates tubulin acetylation. *The J Biol Chem*. 289(2): 895–908.

Lawrence, J., et al., 2018. The role of the mammalian target of rapamycin (mTOR) in pulmonary fibrosis. *Int. J. Mol. Sci*. 19, 778.

Lawrence, R. E., et al., 2019. The lysosome as a cellular centre for signalling, metabolism and quality control. *Nat. Cell. Biol*. 21: 133–142.

Lee, B., et al., 2010. Inhibitors of leucine-rich repeat kinase-2 protect against models of Parkinson's disease. *Nat. Med.* 16: 998–1000.

Lee, H.J., et al., 2004. Clearance of α-synuclein oligomeric intermediates via the lysosomal degradation pathway. *J. Neurosci.* 24: 1888–1896.

Lee, J.M., et al., 2014. Nutrient-sensing nuclear receptors coordinate autophagy. *Nature.* 516: 112–115.

Leidal, A.M., et al., 2018. Autophagy and the cell biology of age-related disease. *Nat Cell Biol.* 20: 1338–1348.

Levin, J., et al., 2011. Generation of ferric iron links oxidative stress to α-synuclein oligomer formation. *J. Parkinsons Dis.* 1: 205–216.

Li, P., et al., 2019. Lysosomal ion channels as decoders of cellular signals. *Trends Biochem. Sci.* 44: 110–124.

Li, W., et al., 2005. Aggregation promoting C-terminal truncation of α-synuclein is a normal cellular process and is enhanced by the familial Parkinson’s disease-linked mutations. *Proc. Natl. Acad. Sci. USA.* 102: 2162–2167.

Li, X., et al., 2010. Enhanced striatal dopamine transmission and motor performance with LRRK2 overexpression in mice is eliminated by familial Parkinson’s disease mutation G2019S. *J. Neurosci.* 30: 1788–1797.

Li, X., et al., 2011. Phosphorylation-dependent 14-3-3 binding to LRRK2 is impaired by common mutations of familial Parkinson's disease. *PloS One*. 6(3): e17153.

Li, Y., et al., 2009. Mutant LRRK2(R1441G) BAC transgenic mice recapitulate cardinal features of Parkinson’s disease. *Nat. Neurosci*. 12: 826–828.

Liao, J., et al., 2014. Parkinson disease-associated mutation R1441H in LRRK2 prolongs the "active state" of its GTPase domain. *Proc. Natl. Acad. Sci. USA*. 111(11): 4055–4060.

Lin, C.H., et al., 2010. LRRK2 G2019S mutation induces dendrite degeneration through mislocalization and phosphorylation of tau by recruiting autoactivated GSK3beta. *J. Neurosci.* 30: 13138–13149.

Lin, X., et al., 2009. Leucine-rich repeat kinase 2 regulates the progression of neuropathology induced by Parkinson's-disease-related mutant α-synuclein. *Neuron.* 64: 807–827.

Lin, X.X., et al., 2018. DAF-16/FOXO and HLH-30/TFEB function as combinatorial transcription factors to promote stress resistance and longevity. *Nat. Commun.* 9, 4400.

Liu, H.F., et al., 2014. LRRK2 R1441G mice are more liable to dopamine depletion and locomotor inactivity. *Ann. Clin. Transl. Neurol.* 1: 199–208.

Liu, Z., et al., 2011. The kinase LRRK2 is a regulator of the transcription factor NFAT that modulates the severity of inflammatory bowel disease. *Nat. Immunol.* 12: 1063–1070.

Liu, G.Y. and Sabatini, D.M., 2020. mTOR at the nexus of nutrition, growth, ageing and disease. *Nat. Rev. Mol. Cell Biol.* 21: 183-203.

Lobbestael, E., et al., 2013. Identification of protein phosphatase 1 as a regulator of the LRRK2 phosphorylation cycle. *The Biochem J.* 456(1): 119–128.

Longo, F., et al., 2017. Age-dependent dopamine transporter dysfunction and Serine129 phospho-alpha-synuclein overload in G2019S LRRK2 mice. *Acta. Neuropathol. Commun.* 5, 22.

Luk, K.C., et al., 2009. Exogenous α-synuclein fibrils seed the formation of Lewy body-like intracellular inclusions in cultured cells. *Proc. Natl Acad. Sci. USA.* 106: 20051–20056.

Luk, K.C., et al., 2012. Pathological alpha-synuclein transmission initiates Parkinson-like neurodegeneration in nontransgenic mice. *Science*. 338: 949-953.

Lwin, A., et al., 2004. Glucocerebrosidase mutations in subjects with parkinsonism. *Mol. Genet. Metab.* 81: 70–73.

Machiya, Y., et al., 2010. Phosphorylated alpha-synuclein at Ser-129 is targeted to the proteasome pathway in a ubiquitin-independent manner. *J. Biol. Chem.* 285: 40732–40744.

MacLeod, D., 2006. The familial Parkinsonism gene LRRK2 regulates neurite process morphology. *Neuron.* 52: 587–593.

MacLeod, D. A., et al., 2013. RAB7L1 interacts with LRRK2 to modify intraneuronal protein sorting and Parkinson's Disease risk. *Neuron.* 77: 425–439.

Madureira, M., et al., 2020. LRRK2: Autophagy and lysosomal activity. *Front. Neurosci.* 14, 498.

Maekawa, T., et al., 2012. The I2020T Leucine-rich repeat kinase 2 transgenic mouse exhibits impaired locomotive ability accompanied by dopaminergic neuron abnormalities. *Mol. Neurodegener.* 7, 15.

Mak, S.K., et al., 2010. Lysosomal degradation of alpha-synuclein *in vivo*. *J. Biol. Chem.* 285: 13621–13629.

Mallett, V., et al., 2016. GBA p.T369M substitution in Parkinson disease: Polymorphism or association? A meta-analysis. *Neurol. Genet*. 2(5), e104.

Mamais, A., et al., 2013.Divergent alpha-synuclein solubility and aggregation properties in G2019S LRRK2 Parkinson's disease brains with Lewy Body pathology compared to idiopathic cases. *Neurobiol. Dis.* 58: 183–190.

Mamais, A., et al., 2014. Arsenite stress down-regulates phosphorylation and 14-3-3 binding of leucine-rich repeat kinase 2 (LRRK2), promoting self-association and cellular redistribution. *The J. Biol. Chem*. 289(31): 21386–21400.

Mamais, A., et al., 2018. Analysis of macroautophagy related proteins in G2019S LRRK2 Parkinson's disease brains with Lewy body pathology. *Brain Res*. 1701: 75–84.

Mammucari, C., et al., 2007. FoxO3 controls autophagy in skeletal muscle *in vivo*. *Cell Metab.* 6: 458–471.

Manzoni, C., et al., 2013b. Pathogenic Parkinson's disease mutations across the functional domains of LRRK2 alter the autophagic/lysosomal response to starvation. *Biochem. Biophys. Res. Commun.* 441: 862–866.

Manzoni, C., et al., 2016. mTOR independent regulation of macroautophagy by Leucine Rich Repeat Kinase 2 via Beclin-1. *Sci. Rep.* 6, 35106.

Manzoni, C., et al., 2013a. Inhibition of LRRK2 kinase activity stimulates macroautophagy. *Biochim. Biophys. Acta*. 1833: 2900-2910.

Manzoni, C., et al., 2018. mTOR independent alteration in ULK1 Ser758 phosphorylation following chronic LRRK2 kinase inhibition. *Biosci. Rep.* 38.

Maraganore, D.M., et al., 2006. High-resolution whole-genome association study of Parkinson disease. *Am. J. Hum. Genet.* 77: 685–693.

Marchand, A., et al., 2020. LRRK2 phosphorylation, more than an epiphenomenon. *Front. Neurosci.* 14: 527.

Marras, C., et al., 2011. Phenotype in parkinsonian and nonparkinsonian LRRK2 G2019S mutation carriers. *Neurology.* 77: 325–333.

Marti, M., et al., 2004. Blockade of nociceptin/orphanin FQ receptor signaling in rat substantia nigra pars reticulata stimulates nigrostriatal dopaminergic transmission and motor behavior. *J. Neurosci*. 24: 6659-6666.

Marti, M., et al., 2005. Blockade of nociceptin/orphanin FQ transmission attenuates symptoms and neurodegeneration associated with Parkinson's disease. *J. Neurosci.*, 25: 9591-9601.

Martina, J.A., et al., 2012. MTORC1 functions as a transcriptional regulator of autophagy by preventing nuclear transport of TFEB. *Autophagy*. 8(6): 903-914.

Martinez-Vicente, M., et al., 2008. Dopamine-modified alpha-synuclein blocks chaperone-mediated autophagy. *J. Clin. Invest.* 118: 777–788.

Mata, I.F., et al., 2006. LRRK2 in Parkinson's disease: protein domains and functional insights. *Trends Neurosci.* 29: 286–293.

Matta, S. et al., 2012. LRRK2 controls an EndoA phosphorylation cycle in synaptic endocytosis. *Neuron*. 75, 1008-1021

Matz, K.M., et al., 2019. The role of nucleic acid sensing in controlling microbial and autoimmune disorders. *Int. Rev. Cell Mol. Biol.* 345: 35–136.

Mauthe, M., et al., 2018. Chloroquine inhibits autophagic flux by decreasing autophagosome-lysosome fusion. *Autophagy*. 14(8): 1435-1455.

Mazzulli, J.R., et al., 2011. Gaucher disease glucocerebrosidase and alpha-synuclein form a bidirectional pathogenic loop in synucleinopathies. *Cell.* 146: 37–52.

McFarland, N.R., et al. 2009. Alpha-synuclein S129 phosphorylation mutants do not alter nigrostriatal toxicity in a rat model of Parkinson disease. *J. Neuropathol. Exp. Neurol.* 68: 515–524.

McGlinchey, R.P. and Lee, J.C, 2015. Cysteine cathepsins are essential in lysosomal degradation of α-synuclein. *Proc. Natl. Acad. Sci. USA.* 112: 9322–9327.

Medina, D.L., et al., 2015. Lysosomal calcium signalling regulates autophagy through calcineurin and TFEB. *Nat. Cell Biol.* 17: 288–299.

Meijer, A.J., et al., 2015. Regulation of autophagy by amino acids and MTOR-dependent signal transduction. *Amino Acids*. 47: 2037–2063.

Melendez, A., et al., 2003. Autophagy genes are essential for dauer development and life-span extension in *C. elegans*. *Science*. 301: 1387–1391.

Miklossy, J., et al., 2006. LRRK2 expression in normal and pathologic human brain and in human cell lines. *J. Neuropathol. Exp. Neurol.* 65: 953–963.

Mills, R.D., et al., 2014. Prediction of the repeat domain structures and impact of parkinsonism-associated variations on structure and function of all functional domains of leucine-rich repeat kinase 2 (LRRK2). *Hum. Mutat.* 35: 395–412.

Mills, R.D., et al., 2018. The Roc-COR tandem domain of leucine-rich repeat kinase 2 forms dimers and exhibits conventional Ras-like GTPase properties. *J. Neurochem.* 147(3): 409–428.

Mindell, J.A., et al., 2012. Lysosomal acidification mechanisms. *Annu. Rev. Physiol*. 74: 69–86.

Miquel, J., et al., 1998. An update on the oxygen stress-mitochondrial mutation theory of aging: genetic and evolutionary implications. *Exp. Gerontol*. 33: 113–126.

Mizunoe, Y., et al., 2018. Trehalose protects against oxidative stress by regulating the Keap1-Nrf2 and autophagy pathways. *Redox Biol*. 15: 115–124.

Mizushima, N., et al., 2010. Methods in mammalian autophagy research. *Cell*. 140: 313-326.

Morgan, A. J., et al., 2011. Molecular mechanisms of endolysosomal Ca^{2+} signalling in health and disease. *Biochem. J.* 439: 349–374.

Mortimore, G.E., and Schworer, C.M., 1977. Induction of autophagy by amino-acid deprivation in perfused rat liver. *Nature.* 270: 174–176.

Moyse, E., et al., 2019. Brain region-specific effects of long-term caloric restriction on redox balance of the aging rat. *Mech. Ageing Dev*. 179: 51–59.

Muda, K., et al., 2014. Parkinson-related LRRK2 mutation R1441C/G/H impairs PKA phosphorylation of LRRK2 and disrupts its interaction with 14-3-3. *Proc. Natl. Acad. Sci. USA.* 111(1): E34-E43.

Murphy, K.E., et al., 2014. Reduced glucocerebrosidase is associated with increased alpha-synuclein in sporadic Parkinson's disease. *Brain*. 137, 834.

Nalls, M. A., et al. 2014. Large-scale meta-analysis of genome-wide association data identifies six new risk loci for Parkinson's disease. *Nat. Genet.* 46: 989–993.

Napolitano, G., et al., 2018. mTOR-dependent phosphorylation controls TFEB nuclear export. *Nat. Commun.* 9:3312.

Neudorfer, O., et al., 1996. Occurrence of Parkinson's syndrome in type I Gaucher disease. *Q. J. Med.* 89: 691–694.

Ng, C.H., et al., 2009. Parkin protects against LRRK2 G2019S mutant-induced dopaminergic neurodegeneration in *Drosophila J. Neurosci*. 29, 11257-11262.

Nguyen, M., et al., 2018. LRRK2 phosphorylation of auxilin mediates synaptic defects in dopaminergic neurons from patients with Parkinson's disease. *Proceedings of the National Academy of Sciences.* 115.21: 5576-5581.

Nishimura, T., et al., 2013. FIP200 regulates targeting of Atg16L1 to the isolation membrane. *EMBO Rep*.14: 284–291.

Nishiyama, J., et al., 2007. Aberrant membranes and double-membrane structures accumulate in the axons of Atg5-null Purkinje cells before neuronal death. *Autophagy.* 3: 591–596.

Niu, H., et al., 2018. Alpha-synuclein overexpression in the olfactory bulb initiates prodromal symptoms and pathology of Parkinson's disease. *Transl. Neurodegener.* 7, 25.

Nixon, R.A., et al., 2008. Neurodegenerative lysosomal disorders: a continuum from development to late age. *Autophagy.* 4: 590–599.

Nixon-Abell, J., et al., 2016. Protective LRRK2 R1398H variant enhances GTPase and Wnt gignaling activity. *Front. Mol. Neurosci*. 9, 18.

Novello, S., et al., 2018. G2019S LRRK2 mutation facilitates alpha-synuclein neuropathology in aged mice. *Neurobiol. Dis.* 120: 21-33.

Obergasteiger, J. et al., 2020. Kinase inhibition of G2019S-LRRK2 enhances autolysosome formation and function to reduce endogenous alpha-synuclein intracellular inclusions. *Cell Death Dis.* 6, 45.

Okubadejo, N.U., et al., (2018). Leucine rich repeat kinase 2 (LRRK2) GLY2019SER mutation is absent in a second cohort of Nigerian Africans with Parkinson disease. *PLoS One* 13, e0207984.

O'Regan, G., et al., 2017. Glucocerebrosidase mutations in Parkinson disease. *J. Parkinsons Dis.* 7: 411–422.

Orenstein, S.J., et al., 2013. Interplay of LRRK2 with chaperone-mediated autophagy. *Nat. Neurosci.* 16: 394–406.

Ott, C., et al., 2016. Reduced autophagy leads to an impaired ferritin turnover in senescent fibroblasts. *Free Radic. Biol. Med.* 101: 325–333.

Oueslati, A., et al., 2016. Implication of alpha-Synuclein phosphorylation at S129 in synucleinopathies: what have we learned in the last decade? *J. Parkinsons Dis.* 6: 39–51.

Oueslati, A., et al., 2010. Role of post-translational modifications in modulating the structure, function and toxicity of α-synuclein: implications for Parkinson's disease pathogenesis and therapies. *Prog. Brain Res.* 183: 115–145.

Paisan-Ruiz, C., et al., 2005. LRRK2 gene in Parkinson disease: mutation analysis and case control association study. *Neurology.* 65: 696–700.

Panchaud, N., et al., 2013. Amino acid deprivation inhibits TORC1 through a GTPase-activating protein complex for the Rag family GTPase Gtr1. *Sci. Signal.* 6, 42.

Pankiv, S., et al., 2007. p62/SQSTM1 binds directly to Atg8/LC3 to facilitate degradation of ubiquitinated protein aggregates by autophagy. *J. Biol. Chem.* 282: 24131–24145.

Pasanen, P., et al., 2014. Novel alpha-synuclein mutation A53E associated with atypical multiple system atrophy and Parkinson’s disease-type pathology. *Neurobiol. Aging.* 35: 2180e.1–2180.e5.

Paxinos, G. and Franklin. K.B.J., 2001. The Mouse Brain in Stereotaxic Coordinates. Academic Press, San Diego.

Plowey, E.D., et al., 2008. Role of autophagy in G2019S-LRRK2-associated neurite shortening in differentiated SH-SY5Y cells. *J. Neurochem.* 105: 1048–1056.

Poewe, W., et al., 2017. Parkinson disease. *Nat. Rev. Dis. Primers* 3, 17013.

Polymeropoulos, M. H., et al., 1997. Mutation in α-synuclein gene identified in families with Parkinson's disease. *Science.* 276, 2045–2047.

Poulopoulos, M., et al., 2012. Clinical and Pathological Characteristics of *LRRK2* G2019S Patients with PD. *J. Mol. Neurosci.* 47: 139–143.

Proukakis, C., et al., 2013. A novel α-synuclein missense mutation in Parkinson disease. *Neurology.* 80: 1062–1064.

Puertollano, R., et al., 2018. The complex relationship between TFEB transcription factor phosphorylation and subcellular localization. *EMBO J.* 37, e98804.

Qiao, L., et al., 2008. Lysosomal enzyme cathepsin D protects against α-synuclein aggregation and toxicity. *Mol. Brain.* 1, 17.

Ramirez-Moreno, M. J., et al., 2019. Autophagy stimulation decreases dopaminergic neuronal death mediated by oxidative stress. *Mol. Neurobiol.* 56: 8136–8156.

Ramonet, D., et al., 2011. Dopaminergic neuronal loss, reduced neurite complexity and autophagic abnormalities in transgenic mice expressing G2019S mutant LRRK2. *PLoS One* 6, e18568.

Ramsden, N., et al., 2011. Chemoproteomics-based design of potent LRRK2-selective lead compounds that attenuate Parkinson's disease-related toxicity in human neurons. *ACS Chem. Biol.* 6: 1021–1028.

Ravikumar, B., et al., 2002. Aggregate-prone proteins with polyglutamine and polyalanine expansions are degraded by autophagy. *Hum. Mol. Genet.* 11: 1107–1117.

Ravikumar, B., et al., 2006. Rapamycin pre-treatment protects against apoptosis. *Hum. Mol. Genet.* 15: 1209–1216.

Reczek, D., et al., 2007. LIMP-2 is a receptor for lysosomal mannose-6-phosphate-independent targeting of beta-glucocerebrosidase. *Cell*. 131(4): 770–783.

Rezzani, R., et al., 2012. Morphological and biochemical studies on aging and autophagy. *Ageing Res. Rev*. 11: 10–31.

Roczniak-Ferguson, A., et al., 2012. The transcription factor TFEB links mTORC1 signaling to transcriptional control of lysosome homeostasis. *Sci. Signal.* 5, 42.

Rodriguez-Navarro, J. A., et al., 2012. Inhibitory effect of dietary lipids on chaperone-mediated autophagy. *Proc. Natl. Acad. Sci. USA*. 109: E705–E714.

Rothaug, M., et al., 2015. LAMP-2 deficiency leads to hippocampal dysfunction but normal clearance of neuronal substrates of chaperone-mediated autophagy in a mouse model for Danon disease. *Acta Neuropathol. Commun.* 3, 6.

Rubinsztein, D.C., et al*,* 2011. Autophagy and aging. *Cell*, 146: 682-695.

Saez-Atienzar, S., et al., 2014. The LRRK2 inhibitor GSK2578215A induces protective autophagy in SH-SY5Y cells: involvement of Drp-1-mediated mitochondrial fission and mitochondrial-derived ROS signaling. *Cell Death Dis.* 5, e1368.

Saftig, P., et al., 2009. Lysosome biogenesis and lysosomal membrane proteins: trafficking meets function. *Nat. Rev. Mol. Cell Biol.* 10: 623–635.

Saha, S., et al., 2015. Mutations in LRRK2 potentiate age-related impairment of autophagic flux. *Mol. Neurodegener.* 10, 26.

Samuel, F., et al., 2016. Effects of serine 129 phosphorylation on alpha-synuclein aggregation, membrane association, and internalization. *J. Biol. Chem.* 291: 4374-4385.

Sancak, Y., et al., 2008. The Rag GTPases bind raptor and mediate amino acid Signaling to mTORC1. *Science.* 1496-1501.

Sanchez-Danes, A., et al., 2012. Disease-specific phenotypes in dopamine neurons from human iPS-based models of genetic and sporadic Parkinson's disease. *EMBO Mol. Med.* 4: 380–395.

Sardiello, M., et al., 2009. A gene network regulating lysosomal biogenesis and function. *Science.* 325: 473–477.

Sato, H., et al., 2013. The role of Ser129 phosphorylation of alpha-synuclein in neurodegeneration of Parkinson's disease: a review of in vivo models. *Rev. Neurosci*. 24(2): 115-123.

Sato, S., et al., 2018. Loss of autophagy in dopaminergic neurons causes Lewy pathology and motor dysfunction in aged mice. *Sci. Rep.* 8(1), 2813.

Schapansky, J., et al., 2014. Membrane recruitment of endogenous LRRK2 precedes its potent regulation of autophagy. *Hum. Mol. Genet.* 23: 4201-4214.

Schapansky, J., et al., 2018. Familial knockin mutation of LRRK2 causes lysosomal dysfunction and accumulation of endogenous insoluble alpha-synuclein in neurons. *Neurobiol. Dis.* 111: 26-35.

Schneider, S.A., and Alcalay, R.N. (2017). Neuropathology of genetic synucleinopathies with parkinsonism: review of the literature. *Mov. Disord.* 32: 1504–1523.

Sen, S., et al., 2009. Dependence of leucine-rich repeat kinase 2 (LRRK2) kinase activity on dimerization. The J. Bio. Chem. 284(52): 36346–36356.

Seok, S., et al., 2014. Transcriptional regulation of autophagy by an FXR–CREB axis. *Nature.* 516: 108–111.

Settembre, C., et al., 2011. TFEB links autophagy to lysosomal biogenesis. *Science*. 332: 1429–1433.

Settembre, C., et al., 2012. A lysosome-to-nucleus signalling mechanism senses and regulates the lysosome via mTOR and TFEB. *EMBO J.* 31: 1095–1108.

Settembre, C., et al., 2013. Signals from the lysosome: a control Centre for cellular clearance and energy metabolism. *Nat. Rev. Mol. Cell Biol*. 14: 293–296.

Sevlever, D., et al., 2008. Cathepsin D is the main lysosomal enzyme involved in the degradation of alpha-synuclein and generation of its carboxy-terminally truncated species. *Biochem*. 47: 9678-9687.

Shackelford, D.B., and Shaw, R.J. 2009. The LKB1–AMPK pathway: metabolism and growth control in tumour suppression. *Nat. Rev. Cancer*. 9: 563–575.

Shaw, J., et al., 2008. Molecular regulation of autophagy and apoptosis during ischemic and non-ischemic cardiomyopathy. *Autophagy*. 4(4): 427-434.

Shaw, R.J., et al., 2004. The tumor suppressor LKB1 kinase directly activates AMP-activated kinase and regulates apoptosis in response to energy stress. *Proc. Natl Acad. Sci. USA*. 101: 3329–3335.

Sheng, Z., et al., 2012. Ser1292 autophosphorylation is an indicator of LRRK2 kinase activity and contributes to the cellular effects of PD mutations. *Sci. Transl. Med*. 4, 164.

Shpilka, T., et al., 2011. Atg8: an autophagy-related ubiquitin-like protein family. *Genome Biol.* 12, 226.

Sidransky, E., et al., 2009. Multicenter analysis of glucocerebrosidase mutations in Parkinson's disease. *N. Engl J. Med*. 361(17): 1651–1661.

Simonsen, A., et al., 2007. Genetic modifiers of the Drosophila *blue cheese* gene link defects in lysosomal transport with decreased life span and altered ubiquitinated-protein profiles. *Genetics*. 176(2): 1283–1297.

Singleton, A.B., et al., 2003. A-Synuclein locus triplication causes Parkinson's disease. *Science.* 302, 841.

Sitte, N., 2000a. Protein oxidation and degradation during cellular senescence of human BJ fibroblasts: part II–aging of nondividing cells. *FASEB J.* 14: 2503–2510.

Sitte, N., 2000b. Protein oxidation and degradation during cellular senescence of human BJ fibroblasts: part I–effects of proliferative senescence. *FASEB J.* 14: 2495–2502.

Smith, W.W., et al., 2006. Kinase activity of mutant LRRK2 mediates neuronal toxicity. *Nat. Neurosci*. 9,1231-1233

Sosulski, M.L., 2015. Deregulation of selective autophagy during aging and pulmonary fibrosis: the role of TGFbeta1. *Aging Cell.* 14: 774–783.

Souza, J.M., et al., 2000. Chaperone-like activity of synucleins. *FEBS Lett.*, 474: 116-119.

Stark, C., et al., 2006. BioGRID: a general repository for interaction datasets. *Nucleic Acids Res*. 34: D535–539.

Stefanis, L., et al., 2019. How is alpha-synuclein cleared from the cell? *J. Neurochem.* 150: 577–590.

Steger, M., et al., 2016. Phosphoproteomics reveals that Parkinson’s disease kinase LRRK2 regulates a subset of Rab GTPases. *eLife.* 5, e12813.

Stenmark, H. 2009. Rab GTPases as coordinators of vesicle traffic. *Nat. Rev. Mol. Cell. Biol*. 10: 513–525.

Su, Y.C., and Qi, X. 2013. Inhibition of excessive mitochondrial fission reduced aberrant autophagy and neuronal damage caused by LRRK2 G2019S mutation. *Hum. Mol. Genet.* 22: 4545–4561.

Su, Y.C., et al., 2015. Threonine 56 phosphorylation of Bcl-2 is required for LRRK2 G2019S-induced mitochondrial depolarization and autophagy. *Biochim. Biophys. Acta*. 1852: 12–21.

Tanida, I., et al., 2002. Human Apg3p/Aut1p homologue is an authentic E2 enzyme for multiple substrates, GATE-16, GABARAP, and MAP-LC3, and facilitates the conjugation of hApg12p to hApg5p. *J. Biol. Chem.* 277: 13739–13744.

Tanida, I., et al., 2004a. HsAtg4B/HsApg4B/autophagin-1 cleaves the carboxyl termini of three human Atg8 homologues and delipidates microtubule-associated protein light chain 3- and GABAA receptor-associated protein-phospholipid conjugates. *J. Biol. Chem*. 279: 36268–36276.

Tanida, I., et al., 2004b. LC3 conjugation system in mammalian autophagy. *J. Biol. Chem.* 279: 47704-47710.

Tanik, S.A., et al., 2013. Lewy body-like α-synuclein aggregates resist degradation and impair macroautophagy. *J. Biol. Chem.* 288: 15194–15210.

Tayebi, N., et al., 2001. Gaucher disease and parkinsonism: a phenotypic and genotypic characterization. *Mol. Genet. Metab.* 73: 313–321.

Tayebi, N., et al., 2003. Reciprocal and nonreciprocal recombination at the glucocerebrosidase gene region: implications for complexity in Gaucher disease. *Am. J. Hum. Genet.* 72(3): 519–534.

Tenreiro, S., et al., 2014. Phosphorylation modulates clearance of alpha-synuclein inclusions in a yeast model of Parkinson's disease. *PLoS Genet*. 10, e1004302.

Terman, A., et al., 2010. Mitochondrial turnover and aging of long-lived postmitotic cells: themitochondrial-lysosomal axis theory of aging. *Antioxid. Redox Signal*. 12: 503–535.

Theillet, F.X., et al., 2016. Structural disorder of monomeric α-synuclein persists in mammalian cells. *Nature*. 530: 45–50.

Thumm, M., et al., 1994. Isolation of auto phagocytosis mutants of *Saccharomyces cerevisiae*. *FEBS Letters.* 349: 275–280.

Tolosa, E., et al., 2020. LRRK2 in Parkinson disease: challenges of clinical trials. *Nat. Rev. Neurol.* 16: 97-107.

Tong, Y., et al., 2009. R1441C mutation in LRRK2 impairs dopaminergic neurotransmission in mice. *Proc. Natl. Acad. Sci. USA.* 106: 14622–14627.

Tong, Y., et al., 2010. Loss of leucine-rich repeat kinase 2 causes impairment of protein degradation pathways, accumulation of alpha-synuclein, and apoptotic cell death in aged mice. *Proc. Natl. Acad. Sci. USA.* 107: 9879-9884.

Tong, Y., et al., 2012. Loss of leucine-rich repeat kinase 2 causes age-dependent bi-phasic alterations of the autophagy pathway. *Mol. Neurodegener.* 7, 2.

Toth, M.L., et al., 2008. Longevity pathways converge on autophagy genes to regulate life span in *Caenorhabditis elegans*. *Autophagy*. 4: 330–338.

Tsika, E., et al., 2015. Adenoviral-mediated expression of G2019S LRRK2 induces striatal pathology in a kinase-dependent manner in a rat model of Parkinson's disease. *Neurobiol. Dis.* 77: 49–61.

Tsukada, M., and Ohsumi, Y. 1993. Isolation and characterization of autophagy defective mutants of *Saccharomyces cerevisiae*. *FEBS Letters* 333: 169–174.

Valdor, R., et al., 2014. Chaperone-mediated autophagy regulates T cell responses through targeted degradation of negative regulators of T cell activation. *Nat. Immunol.* 15: 1046–1054.

Vellai, T., et al., 2003. Genetics: influence of TOR kinase on lifespan in *C. elegans*. *Nature* 426, 620.

Venderova, K., et al., 2009. Leucine-rich repeat kinase 2 interacts with Parkin, DJ-1 and PINK-1 in a *Drosophila melanogaster* model of Parkinson's disease. *Hum. Mol. Genet.* 18(22): 4390–4404.

Viaro, R., et al., 2008. Nociceptin/orphanin FQ receptor blockade attenuates MPTP-induced parkinsonism. *Neurobiol. Dis.*, 30: 430-438.

Vidya, M.K., et al., 2018. Toll-like receptors: significance, ligands, signaling pathways, and functions in mammals. *Int. Rev. Immunol.* 37: 20–36.

Vodicka, P., et al., 2014. Assessment of chloroquine treatment for modulating autophagy flux in brain of WT and HD mice. *J. Huntington Dis.* 3: 159–174.

Vogiatzi, T., et al., 2008. Wild type α-synuclein is degraded by chaperone-mediated autophagy and macroautophagy in neuronal cells. *J. Biol. Chem.* 283: 23542–23556.

Volpicelli-Daley, L. A., et al., 2010. Phosphatidylinositol-4-phosphate 5-kinases and phosphatidylinositol 4,5-bisphosphate synthesis in the brain. *J. Biol. Chem.* 285.

Volpicelli-Daley, L.A., et al., 2016. G2019S-LRRK2 expression augments alpha-synuclein sequestration into inclusions in neurons. *J. Neurosci.*, 36: 7415-7427.

Volta, M., and Melrose, H., 2017. LRRK2 mouse models: dissecting the behavior, striatal neurochemistry and neurophysiology of PD pathogenesis. *Biochem. Soc. Trans.* 45, 113–122.

Wallings, R., et al., 2019. LRRK2 interacts with the vacuolar-type H+-ATPase pump a1 subunit to regulate lysosomal function. *Hum. Mol. Genet.* 28: 2696-2710.

Wan, W., et al., 2017. mTORC1 phosphorylates acetyltransferase p300 to regulate autophagy and lipogenesis. *Mol. Cell.* 68: 323–335.

Wang, B., et al., 2018. Autophagy of macrophages is regulated by PI3k/Akt/mTOR signalling in the development of diabetic encephalopathy. *Aging (Albany NY).*10: 2772-2782.

Wang, X., et al., 2017. Destructive cellular paths underlying familial and sporadic Parkinson disease converge on mitophagy. *Autophagy*.13: 1998–1999.

Wang, X., et al., 2012. LRRK2 regulates mitochondrial dynamics and function through direct interaction with DLP1, *Hum. Mol. Genet.* 21(9): 1931–1944.

Wang, Z., et al., 2018. Meta-analysis of human gene expression in response to *Mycobacterium tuberculosis* infection reveals potential therapeutic targets. *BMC Syst. Biol.* 12, 3.

Wauters, L., et al., 2019. Roco proteins: GTPases with a baroque structure and mechanism. *Int. J. Mol. Sci.* 20, 147.

Wauters, F., et al., 2020. LRRK2 mutations impair depolarization-induced mitophagy through inhibition of mitochondrial accumulation of RAB10. *Autophagy.* 16:2, 203-222.

Webb, J.L., et al., 2003. α-Synuclein is degraded by both autophagy and the proteasome. *J. Biol. Chem.* 278: 25009–25013.

Weng, Y.H., et al., 2016. (R1441C) LRRK2 induces the degeneration of SN dopaminergic neurons and alters the expression of genes regulating neuronal survival in a transgenic mouse model. *Exp. Neurol.* 275, 104–115.

West, A.B., et al., 2005. Parkinson's disease-associated mutations in leucine-rich repeat kinase 2 augment kinase activity. *Proc. Natl. Acad. Sci. USA.* 102: 16842–16847.

Weston, L.J., et al., 2021. Genetic deletion of polo-like kinase 2 reduces alpha-synuclein serine-129 phosphorylation in presynaptic terminals but not Lewy bodies. *J. Biol. Chem.* 100273.

Winfield, S.L., et al., 1997. Identification of three additional genes contiguous to the glucocerebrosidase locus on chromosome 1q21: implications for Gaucher disease. *Genome Res*. 7: 1020–1026.

Witoelar, A., et al., 2017. Genome-wide pleiotropy between Parkinson disease and autoimmune diseases. *JAMA Neurol.* 74: 780–792.

Xie, M., et al., 2006. A pivotal role for endogenous TGF-β-activated kinase-1 in the LKB1/AMP-activated protein kinase energy-sensor pathway. *Proc. Natl Acad. Sci. USA.* 103: 17378–17383.

Xilouri, M. and Stefanis, L. 2015. Chaperone mediated autophagy to the rescue: a new-fangled target for the treatment of neurodegenerative diseases. *Mol. Cell Neurosci.* 66: 29–36.

Xilouri, M., et al., 2009. Abberant alpha-synuclein confers toxicity to neurons in part through inhibition of chaperone-mediated autophagy. *PLoS ONE.* 4, e5515.

Xilouri, M., et al., 2013. α-Synuclein and protein degradation systems: a reciprocal relationship. *Mol. Neurobiol.* 47: 537–551.

Xiong, X., et al., 2012. The autophagy-related gene 14 (Atg14) is regulated by forkhead box O transcription factors and circadian rhythms and plays a critical role in hepatic autophagy and lipid metabolism. *J. Biol. Chem.* 287: 39107–39114.

Xiong, Y. et al. 2018. Robust kinase- and age-dependent dopaminergic and norepinephrine neurodegeneration in LRRK2 G2019S transgenic mice. *Proc. Natl. Acad. Sci. USA.* 115: 1635–1640.

Xiong, Y., et al., 2010. GTPase activity plays a key role in the pathobiology of LRRK2. *PLoS Genet.* 6: e1000902.

Xu, P., et al., 2011. JNK regulates FoxO-dependent autophagy in neurons. *Genes Dev.* 25: 310–322.

Yakhine-Diop, S.M., et al., 2014. G2019S LRRK2 mutant fibroblasts from Parkinson's disease patients show increased sensitivity to neurotoxin 1-methyl-4-phenylpyridinium dependent of autophagy. *Toxicology.* 324: 1–9.

Yang, H., et al., 2017. Mechanisms of mTORC1 activation by RHEB and inhibition by PRAS40. *Nature.* 552: 368–373.

Yao, C., et al., 2010. LRRK2-mediated neurodegeneration and dysfunction of dopaminergic neurons in a Caenorhabditis elegans model of Parkinson's disease. *Neurobiol. Dis.* 40(1): 73-81.

Yap, T.L., et al., 2008. Alpha-synuclein interacts with Glucocerebrosidase providing a molecular link between Parkinson and Gaucher diseases. *J. Biol. Chem.* 286(32): 28080–28088.

Yap, T.L., et al., 2011. Alpha-synuclein interacts with Glucocerebrosidase providing a molecular link between Parkinson and Gaucher diseases. *J. Biol. Chem*. 286, 28080-28088

Yim, W.W.Y., et al., 2020. Lysosome biology in autophagy. *Cell Discov.* 6, 6.

You, H., et al., 2006. Regulation of transactivation-independent proapoptotic activity of p53 by FOXO3a. *Proc. Natl Acad. Sci. USA.* 103: 9051–9056.

Ysselstein, D., et al., 2019. LRRK2 kinase activity regulates lysosomal glucocerebrosidase in neurons derived from Parkinson's disease patients. *Nat. Commun.* 10, 5570.

Yu, L., et al., 2010. Termination of autophagy and reformation of lysosomes regulated by mTOR. *Nature*. 465: 942–946.

Yue, M., et al., 2015. Progressive dopaminergic alterations and mitochondrial abnormalities in LRRK2 G2019S knock-in mice. *Neurobiol. Dis.* 78: 172–195.

Zarranz, J.J., et al., 2004. The new mutation, E46K, of α-synuclein causes Parkinson and Lewy body dementia. *Ann. Neurol.* 55: 164–173.

Zhang, F.R. et al., 2009. Genome wide association study of leprosy. *N. Engl. J. Med.* 361: 2609–2618.

Zhang, P., et al., 2019. Crystal structure of the WD40 domain dimer of LRRK2. *Proc. Natl. Acad. Sci. USA*. 116(5): 1579–1584.

Zhao, J., et al., 2007. FoxO3 coordinately activates protein degradation by the autophagic/lysosomal and proteasomal pathways in atrophying muscle cells. *Cell Metab*. 6: 472–483.

Zhao, H., et al., 2013. Mice deficient in *Epg5* exhibit selective neuronal vulnerability to degeneration. *J. Cell Biol.* 200(6): 731–41

Zhou, Yf., et al., 2016. Autophagy activation prevents sevoflurane-induced neurotoxicity in H4 human neuroglioma cells. *Acta Pharmacol Sin.* 37**,** 580–588.

Zhu, X., et al., 2006a. LRRK2 in Parkinson's disease and dementia with Lewy bodies. *Mol. Neurodegen.* 1, 17.

Zhu, X., et al., 2006b. LRRK2 protein is a component of lewy bodies. *Ann Neurol.* 59: 388–393.

Zimprich, A., et al., 2004. Mutations in LRRK2 cause autosomal-dominant parkinsonism with pleomorphic pathology. *Neuron.* 44: 601–607.

Zunke, F., et al., 2018. Reversible conformational conversion of alpha-synucelin into toxic assemblies by glucosylceramide. *Neuron*. 97: 92–107.

7. ABBREVIATIONS

α-syn: α-synuclein

ALP: Autophagy-lysosomal pathway

AMPK: 5'-AMP-activated protein kinase

CMA: Chaperone-mediated autophagy

CQ: Chloroquine

GCase: Glucocerebrosidase

KD: Kinase-dead

KI: Knock-in

KO: Knock-out

hα-syn: Human α-synuclein

LAMP2: Lysosomal-associated membrane protein 2

MAP1LC3: Microtubule-associated protein 1 light chain 3

LRRK1: Leucine-rich repeat kinase 1

LRRK2: Leucine-rich repeat kinase 2

MAP2: Microtubule associated protein 2

mTORC1: Mammalian target of Rapamycin Complex 1

PD: Parkinson's Disease

pSer129 α-syn: phosphoSerine129 α-synuclein

pSer1292 LRRK2: phosphoserine 1292 LRRK2

SNpc: substantia nigra *pars compacta*

TFEB: Transcription factor EB

TH: Tyrosine hydroxylase

ULK1: uncoordinated-51-like kinase 1

WB: Western Blotting

WT: Wild type

8. APPENDIX I

frontiers in Neuroscience

REVIEW
published: 17 December 2019
doi: 10.3389/fnins.2019.01352

Autophagy and LRRK2 in the Aging Brain

Federica Albanese[1†], Salvatore Novello[2†] and Michele Morari[1]*

[1] Section of Pharmacology, Department of Medical Sciences, University of Ferrara, Ferrara, Italy, [2] Laboratory of Molecular and Chemical Biology of Neurodegeneration, Brain Mind Institute, School of Life Sciences, École Polytechnique Fédérale de Lausanne, Lausanne, Switzerland

Autophagy is a highly conserved process by which long-lived macromolecules, protein aggregates and dysfunctional/damaged organelles are delivered to lysosomes for degradation. Autophagy plays a crucial role in regulating protein quality control and cell homeostasis in response to energetic needs and environmental challenges. Indeed, activation of autophagy increases the life-span of living organisms, and impairment of autophagy is associated with several human disorders, among which neurodegenerative disorders of aging, such as Parkinson's disease. These disorders are characterized by the accumulation of aggregates of aberrant or misfolded proteins that are toxic for neurons. Since aging is associated with impaired autophagy, autophagy inducers have been viewed as a strategy to counteract the age-related physiological decline in brain functions and emergence of neurodegenerative disorders. Parkinson's disease is a hypokinetic, multisystemic disorder characterized by age-related, progressive degeneration of central and peripheral neuronal populations, associated with intraneuronal accumulation of proteinaceous aggregates mainly composed by the presynaptic protein α-synuclein. α-synuclein is a substrate of macroautophagy and chaperone-mediated autophagy (two major forms of autophagy), thus impairment of its clearance might favor the process of α-synuclein seeding and spreading that trigger and sustain the progression of this disorder. Genetic factors causing Parkinson's disease have been identified, among which mutations in the LRRK2 gene, which encodes for a multidomain protein encompassing central GTPase and kinase domains, surrounded by protein-protein interaction domains. Six LRRK2 mutations have been pathogenically linked to Parkinson's disease, the most frequent being the G2019S in the kinase domain. LRRK2-associated Parkinson's disease is clinically and neuropathologically similar to idiopathic Parkinson's disease, also showing age-dependency and incomplete penetrance. Several mechanisms have been proposed through which LRRK2 mutations can lead to Parkinson's disease. The present article will focus on the evidence that LRRK2 and its mutants are associated with autophagy dysregulation. Studies in cell lines and neurons *in vitro* and in LRRK2 knock-out, knock-in, kinase-dead and transgenic animals *in vivo* will be reviewed. The role of aging in LRRK2-induced synucleinopathy will be discussed. Possible mechanisms underlying the LRRK2-mediated control over autophagy will be analyzed, and the contribution of autophagy dysregulation to the neurotoxic actions of LRRK2 will be examined.

Keywords: aging, α-synuclein, autophagy, LC3, LRRK2, lysosomes, Parkinson's disease, LAMP2A

OPEN ACCESS

Edited by:
Patrick Lewis,
University of Reading,
United Kingdom

Reviewed by:
Manish Verma,
University of Pittsburgh, United States
Luis Bonet Ponce,
NIH Clinical Center (CC),
United States

***Correspondence:**
Michele Morari
m.morari@unife.it

[†] These authors have contributed equally to this work

Specialty section:
This article was submitted to Neurodegeneration, a section of the journal Frontiers in Neuroscience

Received: *10 September 2019*
Accepted: *02 December 2019*
Published: *17 December 2019*

Citation:
Albanese F, Novello S and Morari M (2019) Autophagy and LRRK2 in the Aging Brain. Front. Neurosci. 13:1352. doi: 10.3389/fnins.2019.01352

INTRODUCTION

Autophagy is a highly conserved cellular degradation process, either bulk or selective, by which long-lived macromolecules, protein aggregates and dysfunctional/damaged organelles are delivered to lysosomes for degradation (Deter et al., 1967; Mortimore and Schworer, 1977). This constitutive physiological activity works in parallel with the UPS to implement protein quality control and maintain the integrity of cell proteome (i.e., cellular proteostasis). Recently, the involvement of autophagy in general energy homeostasis has also been proven, since autophagy can be stimulated in response to starvation-induced stress, amino acid depletion as well as cell energy needs (Puente et al., 2016; Ho et al., 2017; Olsvik et al., 2019; Sutton et al., 2019).

Dysfunctions of the ALP have been reported in aging as well as in several human disorders, including cancer, chronic inflammatory diseases, cardiomyopathies and neurodegenerative diseases (Mizushima et al., 2008; Boland et al., 2018; Deretic and Klionsky, 2018; Onorati et al., 2018; Zech et al., 2019). Notably, neurodegenerative disorders of aging such as Parkinson's disease (PD), Alzheimer's disease (AD), Huntington's disease (HD) frontotemporal dementia and amyotrophic lateral sclerosis are characterized by a common feature: accumulation of aberrant or misfolded proteins, such as α-synuclein (α-syn), Aβ, tau, mutant forms of huntingtin, TDP43, which are neurotoxic (Gal et al., 2009; Bourdenx et al., 2017; Boland et al., 2018). Furthermore, either blocking or promoting autophagy has an impact on clearance of cytotoxic proteins in different *in vitro* and *in vivo* models of aggregopathies/proteinopathies (Sarkar et al., 2008; Crews et al., 2010; Spilman et al., 2010; Ciechanover and Kwon, 2017; Moors et al., 2017).

THE AUTHOPHAGY-LYSOSOMAL PATHWAY

Macroautophagy, CMA and microautophagy are the three major forms of autophagy identified so far, although other forms such as selective and precision autophagy have been described more recently (Klionsky, 2005; Massey et al., 2006; Kimura et al., 2015; Dikic, 2017). Macroautophagy (henceforth referred to as autophagy) requires autophagosome biogenesis, a complex multi-step process regulated by the autophagy-related (ATG) gene family member proteins (Tsukada and Ohsumi, 1993; Thumm et al., 1994; Klionsky et al., 2003; Klionsky, 2012), whose transcription is driven by TFEB (Settembre et al., 2011) and many other transcription factors, such as FOXOs, E2F1, CREB, PPARγ to name a few (Fullgrabe et al., 2016). ATGs protein activity is controlled upstream by nutrient and growth signaling pathways. Autophagy starts with the formation of an isolation cup-shaped membrane (also termed phagophore) that elongates and sequesters a small portion of the cytoplasm to form the autophagosome (**Figure 1**). Then, the autophagosome fuses to the lysosomes, generating autolysosomes. Selective cargo recognition and sequestration into the autophagosome lumen require the presence of receptor-proteins, among which microtubule-associated protein 1 light chain 3 (known as MAP1LC3 or LC3). The cytosolic form of LC3, LC3I, translocates to the autophagosome membranes after being conjugated to phosphatidylethanolamine (Stolz et al., 2014; Rockenfeller et al., 2015). The abundance of LC3II, i.e., the lipidated form of LC3I, is directly correlated with the number of mature autophagosomes. LC3II partners in cargo recognition and delivery to lysosomes are a number of selective-autophagy receptor proteins such as Sequestosome 1 (SQSTM1)/p62 and other sequestosome 1-like receptors (NBR1, optineurin, NDP52, TAX1BP1, TOLLIP and ALFY/WDFY3) (Conway et al., 2019). p62, the first autophagy adaptor protein to be identified (Ishii et al., 1996), recognizes ubiquitinated proteins via its ubiquitin-associated (UBA) domain and docks onto the forming phagophore membrane through binding LC3II via the LC3-interacting region (LIR). Impaired autophagy leads to SQSTM1/p62 accumulation and aggregation of ubiquitinated proteins (Komatsu et al., 2007a). LC3I, LC3II, SQSTM1/p62 and mTOR are all validated markers of autophagy (Brown et al., 1994; Sugawara et al., 2004; Lippai and Low, 2014).

Mammalian target of rapamycin complex 1 (mTORC1) and 5′-AMP-activated kinase (AMPK) act as key upstream regulators of autophagy by modulating the serine-threonine kinase activity of ULK1/2. Upon activation, ULK1 phosphorylates and associates with ATG101, focal adhesion kinase family interacting protein of 200 kDa (FIP200) and ATG13 (Hara et al., 2008; Chan, 2009; Ganley et al., 2009) to generate the Initiation Complex. This complex acts as cellular sensor for glucose, nitrogen, growth factors, amino acids and ROS concentrations (Kim and Guan, 2015). In the presence of high levels of nutrients, mTORC1 acts as an inhibitor of autophagy by directly hyperphosphorylating ATG13 and ULK1 (at Ser757), which prevents ULK1 binding to ATG13 and AMPK (Kim and Guan, 2015; Meijer et al., 2015). Conversely, amino acids depletion suppresses mTORC1 activity. Furthermore, there is evidence that under glucose starvation or increased AMP/ATP ratio, AMPK negatively modulates mTORC1 pathway, phosphorylating (at Ser317 and Ser777) and activating ULK1 (Kim et al., 2011). Interestingly, recent studies have shown that amino acid and glucose depletion promote autophagy with different efficiencies. Indeed, amino

Abbreviations: 4E-BP, eukaryotic initiation factor 4E binding protein; α-syn: α-synuclein; AD, Alzheimer's disease; ALP, autophagy-lysosomes pathway; AMPK, 5′-AMP-activated kinase; ATG, autophagy-related gene 8; AV, autophagic vacuoles; Aβ, β amyloid; CMA, chaperone-mediated autophagy; CNS, central nervous system; COR, C-terminal of Roc; DA, dopamine; DAMPs, damage-associated molecular patterns; DKO, double knock-out; DLB, dementia with Lewy bodies; eIF4E, eukaryotic initiation factor 4E; EM, electron microscopy; ER, endoplasmic reticulum; ESCRT, endosomal sorting complexes required for transport; GCase, β-glucocerebrosidase; HD, Huntington's disease; Hsc70/HSPA8, heat shock 70 kDa protein 8; IGF-1, insulin growth factor-1; KD, kinase dead; KI, knock-in; KO, knock-out; LAMP1, lysosome-associated membrane protein 1; LAMP2A, lysosome-associated membrane protein 2 isoform A; LBs, Lewy bodies; LC3I, microtubule-associated protein 1 light chain 3 beta isoform 1; LC3II, microtubule-associated protein 1 light chain 3 beta isoform 2; LIR, LC3-interacting region; LRRK1, leucine-rich repeat kinase 1; LRRK2, leucine-rich repeat kinase 2; mtDNA, mitochondrial DNA; mTORC1, mammalian target of rapamycin complex 1; MVBs, multivesicular bodies; NFE2L2/NRF2, nuclear factor, erythroid derived 2, like 2; PD, Parkinson's Disease; PINK1, PTEN-induced putative kinase 1; ROC, Ras of complex; ROS, reactive oxygen species; SNpc, substantia nigra pars compacta; SQSTM1/p62, Sequestosome 1; TDP43, TAR DNA-binding protein 43; TFEB, transcription factor EB; TRIM, tripartite motif protein family; UBA, ubiquitin-associated domain; ULK1, uncoordinated-51-like kinase 1; UPS, ubiquitin-proteasome system; VPS34, vacuolar protein sorting 34.

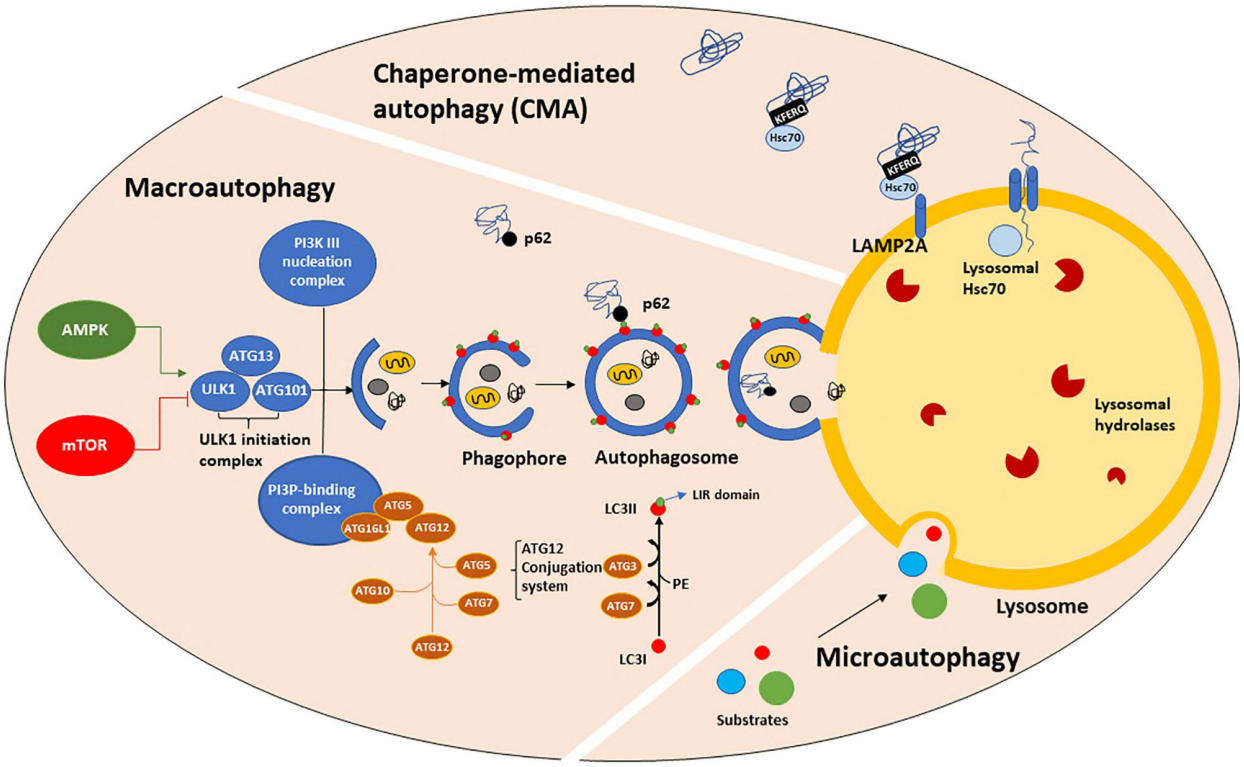

FIGURE 1 | The autophagic machinery. Three types of autophagy have been described: macroautophagy (henceforth referred to as autophagy), chaperone-mediated autophagy (CMA) and microautophagy. Autophagy is positively regulated by AMPK and negatively by mTORC1 which, in turn phosphorylates and mediates ULK1-initiation complex association and activation. The ATGs protein family, organized in three major complexes (the ULK1-initiation complex, PI3K III nucleation complex and PI3P-binding complex), mediates the formation of a cup-shaped membrane, termed phagophore. The phagophore directly engulfs a small portion of cytoplasm containing damaged organelles, misfolded or old proteins to form the autophagosome. Then, the autophagosome fuses with the lysosome, generating the autolysosome, in which autophagic substrates are degraded by lysosomal hydrolases activity and acidic environment. Substrate recognition and sequestration can also occur in a selective manner through intervention of LC3II. LC3I is a cytosolic protein, which after being conjugated to PE, translocates onto the phagophore membranes where it acts as a receptor for multiple cargo proteins, such as p62. p62 binds both LC3II (LIR domain) and ubiquitinated proteins (UBA domain), allowing their entry into the autophagosome for degradation. CMA is a one-by-one fashion type of autophagy and it is only referred to proteins bearing the KFERQ-like motif. Those proteins are directly recognized by cytosolic Hsc70, which shuttles them to the lysosomal membrane where it binds LAMP2A, a transmembrane receptor. The binding of Hsc70 to LAMP2A leads to its oligomerization, promoting the entry of CMA substrates into the lysosomal lumen. The presence of lysosomal Hsc70 is also required for cargo sequestration. Microautophagy is the least characterized form of autophagy. During microautophagy, substrates are directly engulfed by the lysosomal membrane, without an intermediate autophagosome formation.

acid starvation is able to induce ULK1-initiation complex formation and promote a great amount of autophagosomes containing LC3II and p62 whereas glucose starvation does not (Nwadike et al., 2018). In addition, amino acid but not glucose depletion, leads to lysosomal acidification, independently from autophagy and ULK1 (Nwadike et al., 2018). Furthermore, there is evidence of mTORC1 activation in a lysosomal nutrient sensing-dependent manner. In fact, amino acid depletion prevents mTORC1 recruitment and activation on the lysosomal membrane via AMPK-independent mechanisms, operated by the Rag GTPase complex, that recruits mTORC1, and by Rheb, that activates it (Lim and Zoncu, 2016). Once translocated on the lysosomal membrane, mTORC1 directly controls the subcellular localization of TFEB, a master autophagy regulator which continuously shuttles from the cytosol to the nucleus, where it mediates ATGs transcription and lysosomal biogenesis under starvation conditions (Sardiello et al., 2009; Settembre et al., 2011). mTORC1 phosphorylates TFEB in the nucleus and controls its export kinetics in a nutrient availability dependent manner (Napolitano et al., 2018). However, TFEB is able to promote autophagy gene expression not only during starvation but also during mitochondria depolarization (Nezich et al., 2015), ER stress (Martina et al., 2016) or lysosomal membrane permeabilization (Settembre et al., 2012).

CMA (**Figure 1**) is a one-by-one fashion-type of autophagy. About 30% of cytosolic proteins bear the Lys-Phe-Glu-Arg-Gln (KFERQ) sequence (Dice et al., 1986; Chiang and Dice, 1988; Chiang et al., 1989) which is recognized by cytosolic heat shock 70 kDa protein 8 (HSPA8, also known as hsc70). Then, hsc70, complexed with co-chaperones, shuttles the substrate proteins to the lysosomal membrane, where it binds to monomeric LAMP2A, a transmembrane receptor. This binding triggers LAMP2A multimerization into a translocation complex. Protein substrates must be unfolded by hsc70 and co-chaperones, and luminal hsc70 is also required to allow their translocation to the lysosomal lumen, where they are quickly hydrolyzed.

Considering that the binding to LAMP2A is the rate-limiting step for CMA and that LAMP2A-deficient lysosomes are CMA-incompetent (Cuervo et al., 1997; Kaushik and Cuervo, 2012), LAMP2A is considered a marker of CMA. In particular, LAMP2A subcellular localization has been associated with Rab11 and Rab7 function (Zhang et al., 2017). The signaling pathways that mediate the upstream modulation of CMA are still not fully understood, however, a possible crosstalk between CMA and redox stress has been proposed via NFE2L2/NRF2 (nuclear factor, erythroid derived 2, like 2) (Pajares et al., 2018). Furthermore, oxidized proteins, such as Tau and α-syn are CMA substrates (Xilouri and Stefanis, 2015; Dikic, 2017).

Microautophagy (**Figure 1**) and endosomal microautophagy are the least characterized types of autophagy. Microautophagy is a constitutive active process by which cytoplasmic content is directly engulfed into lysosomes for degradation, without an intermediate autophagosome formation (Farre and Subramani, 2004). Instead, endosomal microautophagy occurs at the surface of late endosomes following the formation of multivesicular bodies (MVBs), that ultimately fuse with lysosomal membrane (Sahu et al., 2011; Uytterhoeven et al., 2015; Mukherjee et al., 2016; Oku et al., 2017). This process is responsible for maintaining the turnover of cellular nutrients via both a selective and hsc70-mediated mechanism or bulk degradation of proteins and organelles, such as mitochondria, peroxisomes and portions of nucleus (Olsvik et al., 2019). While microautophagy requires autophagic proteins participation, endosomal microautophagy is strongly associated with endosomal trafficking, which requires ESCRT complex that together with hsc70 mediates a more selective degradation (Sahu et al., 2011; Uytterhoeven et al., 2015; Mukherjee et al., 2016; Oku et al., 2017). Thus hsc70 exerts its function in both CMA and endosomal microautophagy, depending on the interactor protein.

Recently, different studies described another autophagic pathway, named "Precision Autophagy" (Kimura et al., 2015). Precision Autophagy is a receptor-regulator-mediated type of autophagy which requires factors that are part of the tripartite motif (TRIM) protein family that can act as both receptors and regulators of autophagy at the same time. Such proteins are capable of identifying their targets, even without the need of a tag, such as ubiquitin and galectins (Stolz et al., 2014). Those proteins exert their function by first recognizing exogenous and endogenous cargos through their C-terminal domain. After substrates recognition, TRIMs, acting as a receptor, stimulate autophagy by facilitating the assembly of autophagic machinery, primarily acting on ULK1, Beclin-1, ATG16L1 in their activated status. However, TRIMs-modulated autophagy can both enhance or reduce autophagic flux. In fact, TRIM28 can either positively modulate Beclin-1 activity through VPS34 activation (Yang et al., 2013) or mediate AMPK degradation acting as an E3 ligase (Pineda et al., 2015).

AUTOPHAGY AND HEALTHY AGING

Aging is a time-mediated physiological process which carries a decline in several molecular and cellular mechanisms contributing to cellular homeostasis. Defective proteostasis has been largely reported in a plethora of *in vitro* and *in vivo* aging models (Cuervo et al., 2005; Boland and Nixon, 2006; Balch et al., 2008; Ben-Zvi et al., 2009; Bingol, 2018; Boland et al., 2018). Bergamini et al. (2004) provided the first evidence that the efficiency of autophagy and, consequently, of detoxification mechanisms, worsen along with aging in liver tissue (Donati et al., 2001; Del Roso et al., 2003). Therefore, assessing the causes of autophagic dysfunction during senescence became fundamental in order to delay age-related phenotype in both physiological and pathological conditions. Autophagic decline has been considered as one of the major contributors to the age-dependent accumulation of dysfunctional organelles, cytoplasmatic content and misfolded/aberrant proteins that might combine to form potentially cytotoxic aggregates. Furthermore, failure in replacing old organelles, especially lysosomes, mitochondria and endoplasmic reticulum (ER), has important consequences on their morphology and functions, other than cellular homeostasis. In fact, one of the morphological features associated with senescence is the presence of enlarged lysosomes containing deposited lipofuscin, i.e., a pigment formed by a highly oxidized cross-linked protein aggregates, carbohydrates and lipids, remarkably resistant to proteolytic activity of lysosomal enzymes. Moreover, lipofuscin represents an important source of ROS via the Fenton reaction. Another common feature associated with ALP deficiency is the increase number of autophagic vesicles, detected by electron microscopic (EM) and immunofluorescence in different tissues (brain, heart, muscle and kidney). This scenario is exacerbated in postmitotic cells, such as neurons, where lipofuscin accumulation is even greater due to their reduced ability to dilute it through mitotic cycles (Rezzani et al., 2012).

Dysfunctional and damaged mitochondria are responsible for increased oxidative stress and free radical production (Rezzani et al., 2012). In 1956, Harman proposed "the free radical theory" according to which ROS damage cellular functions ensuing in the characteristic aging phenotype. In senescent cells, increased ROS production as well as reduced ROS cellular detoxification can damage mtDNA, causing an accumulation of mitochondrial mutations and hypoxia in senescent tissues, such as brain (Roberts et al., 1997), heart (Pepe, 2000), and kidney (Nangaku et al., 2008). Moreover, this age-related increase in oxidative stress may lead to enhanced protein oxidation, causing unfolding, exposure of hydrophobic residues and, finally, aggregation (Miquel, 1998; Hohn et al., 2017). In particular, ALP plays a more relevant role than UPS in promoting ROS detoxification. Indeed, chronic oxidative stress causes ATGs overexpression and mTORC1 inhibition, leading to an increased autophagic, but not proteasomal, activity (Chakraborty et al., 2019). Autophagy stimulation, e.g., by rapamycin treatment, can reverse increased ROS production, promoting neuronal survival (Ramirez-Moreno et al., 2019). Trehalose is another effective autophagy enhancer that can protect against oxidative stress in an mTORC1-independent manner. Trehalose is a naturally available disaccharide that facilitates the autophagic flux and exerts anti-oxidant effects by promoting the nuclear translocation of Nrf2, and the transcription of Nrf2 target genes (Mizunoe et al., 2018).

Aging has also been associated with activation of the immune response by several DAMPs, which are molecules capable of triggering the production of proinflammatory cytokines and chemokines, growth factors and components of extracellular matrix. The circular mtDNA and some mitochondrial proteins, like *N*-formyl peptides and cardiolipin, coming from senescent mitochondria, act as DAMPs through activating Toll-like receptor 9 signaling and formyl peptide receptor-1, respectively, causing an enhanced cytokine production from cultured monocytes (Pinti et al., 2014; Jang et al., 2018).

Impaired mitophagy is another common feature of aging (Sun et al., 2016). Mitophagy is a selective form of autophagy, since it regulates the removal of old and excessive mitochondria. Mitophagy starts with the recognition and targeting of damaged mitochondria, mediated by PINK1. PINK1 accumulates at the outer membrane of damaged mitochondria, where it recruits Parkin, an E3 ubiquitin ligase, which participates to mitochondria sequestration by autophagosomes (Jin and Youle, 2012). Age-related mitophagy decline is characterized by dysfunctional, fragmented and swollen mitochondria, which is accompanied by lower PINK1 expression in murine lung tissue (Sosulski et al., 2015) and aged cells (Terman et al., 2010).

Reduced clearance of damaged/dysfunctional organelles is not the only consequence of defective autophagy, since accumulation of long-lived, misfolded, oxidized proteins also occurs during aging. In fact, ALP, and to a lesser degree UPS are impaired in senescent tissues. LAMP1 and LAMP2A levels markedly decrease over the years resulting in a defective CMA activity. In aged cells, the decrease of LAMP2A levels is initially compensated by an increase of lysosome number (Cuervo and Dice, 2000; Ott et al., 2016). In senescence, however, the compensatory increase of the number of lysosomes and chaperones fails to further sustain CMA activity rate due to the increasingly small amount of LAMP2A. As a proposed mechanism, aging can affect either LAMP2A recycling from the lysosomal lumen or its stability at the lysosomal membrane. Indeed, lysosomal membrane accumulates cholesterol during aging, which results in an enhanced fluidity, and ultimately prevents LAMP2A multimerization (Rodriguez-Navarro et al., 2012). The increased quantity of cholesterol and ceramides can also create enlarged degradation membrane domains where LAMP2A accumulates and is degraded, which further reduces its abundance (Rodriguez-Navarro et al., 2012).

Likewise, autophagy decline is associated with a decrease in either autophagosomes formation or clearance (Bergamini and Signorini, 1991). It has been reported that the decreased autophagosomes formation might be due to reduced ATGs content, whereas the decrease of autophagosome clearance may be related to impaired fusion with the lysosomes and lysosomal activity (Kenessey et al., 1989; Sitte et al., 2000a,b).

Another contributor to impaired autophagy during aging is upregulation of mTOR pathway. In fact, mTORC1 inhibition has been widely investigated as a potential mechanism to slow down aging and promote life span extension. The first evidence of the role of autophagy in life-span expansion came from studies in *C. elegans*, where mutants of *daf-2*, a gene encoding insulin growth factor (IGF-1) receptor, showed reduced longevity due to the silencing of the autophagy gene *bec-1*, the ortholog of beclin-1. This suggested for the first time that enhancing autophagy would increase life-span (Melendez et al., 2003). Indeed, knocking down key autophagy proteins dramatically reduced the life-span of *daf-2* mutants (Melendez et al., 2003; Hars et al., 2007). The most effective methods to inhibit mTORC1 signaling in order to selectively activate autophagic machinery are caloric restriction (CR) and pharmacological blockage through administration of rapamycin or similar compounds ("rapalogs") (Kapahi et al., 2010; Galluzzi et al., 2017). CR, a limiting food intake strategy without malnutrition, has been studied as a powerful anti-aging physiological intervention. CR-mediated autophagy enhancement requires activation of two energy sensors, like AMPK and Sirtuin 1, and inhibition of insulin/insulin-like growth factor (IGF) pathway, which, in turn, leads to downstream mTORC1 blockage. Abolition of high metabolic rate characterizing senescent cells is one of the accepted mechanisms by which reduced insulin/insulin-like growth factor or mTORC1 signaling promote longevity (Toth et al., 2008). Furthermore, mTORC1 plays a central role in the release of pro-inflammatory cytokines by old cells, a process named senescence-associated secretory phenotype (SASP) which is reversed by rapamycin treatment (Laberge et al., 2015). Moreover, in yeast, worms or flies CR is ineffective when mTORC1 pathway is already downregulated, demonstrating that a common signaling cascade underlies both strategies of life-span expansion (Grandison et al., 2009). Pharmacological blockade as well as genetic inhibition of mTORC1 increase life-span in several animal species, such as *C. elegans* (Vellai et al., 2003), *D. melanogaster* (Kapahi et al., 2004), *S. cereviasiae* (Kaeberlein et al., 2005), and mice (Harrison et al., 2009). On the contrary, ATG genes knockout or knockdown reverses life-span extension induced by rapamycin, suggesting that rapamycin selectively affects and enhances autophagosome formation. However, it is possible that other mechanisms come into play to extend the life-span, such as a reduced oxidative stress, as shown in rats (Moyse et al., 2019).

AUTOPHAGY AND NEURODEGENERATION

Autophagy is involved in maintaining proteostasis and general neuronal homeostasis, synaptic remodeling and activity, axo-dendritic plasticity and mitochondrial clearance in CNS. Both clinical studies and preclinical models described neuronal atrophy, reduced cargo amount, impaired autophagy and mitophagy in age-related diseases (Boland and Nixon, 2006; Menzies et al., 2017; Boland et al., 2018). To further investigate the specific role of autophagy in neuronal cell-types, several *Atg5* and *Atg7* KO models have been developed (Galluzzi et al., 2017; Boland et al., 2018). Those studies provided evidence that autophagy is essential for axonal homeostasis and that each neuronal cell type responds differently to autophagy decline due to a diverse susceptibility to cytotoxic proteins aggregation (Tsvetkov et al., 2013). *Atg5* and *Atg7* KO mice showed early onset neurodegeneration, while beclin-1 knockdown increased

susceptibility of hippocampal neurons to energy deprivation (Fekadu and Rami, 2016). Furthermore, selective and conditional genetic deletion, via Nestin-Cre technology, of *Atg5* and *Atg7* causes defective autophagy and consequent accumulation of intracellular aggregation-prone proteins in neurons and glia (Hara et al., 2006; Komatsu et al., 2006a, 2007b). Although the aged brain is accompanied by a deficiency in both general and selective types of autophagy (see above), an increased compensatory mitophagy in the later phase of neurodegenerative diseases has been observed. In fact, beyond ATP production, mitochondria are also involved in protein clearance, as proven by the intake of aggregation-prone proteins, such as amyloid-β, superoxide dismutase 1 (SOD1) variants and α-syn. Nevertheless, this compensatory process leads to a higher chance of developing mitochondria damage due to increase exposure to cytotoxic proteins, like α-syn. Therefore, enhancing PINK1-Parkin-driven mitophagy has been viewed as a strategy to improve both mitochondria quality control and protein degradation (Hertz et al., 2013; Georgakopoulos et al., 2017).

Neurodegenerative disorders of aging, such as AD, PD, and HD, have as a common feature the formation of cytotoxic aggregates. Those aggregates are made of proteins that can be oxidized, wrongly processed, misfolded or cross-linked by cellular post-translational machinery. These proteins are considered "toxic" because they lose their physiological conformation and functions, alter cellular trafficking, and block CMA or UPS, promoting their spreading throughout the CNS in a prion-like manner (Brundin et al., 2010; Brundin and Melki, 2017). Moreover, neurons are postmitotic cells, thus are not capable of diluting protein aggregates through mitotic cycles, making cells even more susceptible to their potential toxicity properties. In fact, neurons activate different compensatory mechanisms to reduce protein accumulation, for instance sequestering them in hydrophobic agglomerates or combining them with microtubules to form aggresomes (Ciechanover and Kwon, 2017). Even though this strategy can be neuroprotective in the early stages of age-related diseases, it fails to handle the increased cytotoxic burden in the later stages. As reported above, autophagy declines physiologically with senescence. In the context of neurodegenerative diseases, this age-dependent decline appears to be exacerbated because it is accompanied by the impairment of ALP machinery due to the accumulation of neurotoxic proteins. Furthermore, in most cases, neurodegenerative diseases are associated with the inheritance of mutations in genes controlling the autophagic process, suggesting that aberrant autophagy might contribute to neurodegeneration (Ravikumar et al., 2002; Berger et al., 2006; Ravikumar et al., 2006).

Autophagy and Parkinson's Disease

The neuropathological hallmarks of PD are the loss of dopamine (DA) neurons in the SNpc and the accumulation of intracellular aggregates containing α-syn, named LBs. Changes in ALP markers were reported in the human brain which are consistent with an impairment of autophagic machinery. A significant reduction of lysosomal and CMA markers, such as LAMP1, LAMP2A, Hsc70 or Cathepsin D, associated with an increase of autophagic markers LC3II and p62 levels, was reported in the whole-brain (Mamais et al., 2018) or SNpc (Chu et al., 2009; Dehay et al., 2010) of idiopathic PD patients (Xilouri and Stefanis, 2015). Moreover, LC3II has been shown to colocalize with α-syn in LBs (Alvarez-Erviti et al., 2010; Dehay et al., 2010). The patterns of ALP markers were compared in the brains of idiopathic vs. G2019S LRRK2 PD patients (Mamais et al., 2018). Interestingly, G2019S PD patients did not show the increase of LC3II, p62 and ULK-1 levels observed in idiopathic PD patients, but instead a significant reduction of LAMP1 levels. This was interpreted as being due to a different pathobiology associated with idiopathic and G2019S LRRK2 PD (Mamais et al., 2018). Consistent with this view, G2019S LRRK2 cases had lower insoluble α-syn levels compared to idiopathic PD patients, suggesting differences in the biochemical properties of aggregated α-syn (Mamais et al., 2013). In another study, an increase of LAMP2A but not LAMP1 levels was reported in the cholinergic cells of the motor nucleus of the vagal nerve in G2019S LRRK2 patients compared to non-neurological controls, which was explained as being due to either a compensation for impaired CMA or a chronic reduction in LAMP2A turnover (Orenstein et al., 2013). ALP changes were also investigated in the brains of patients suffering from dementia with LB (DLB), another type of synucleinopathy, in comparison with brains of AD patients (Crews et al., 2010; Higashi et al., 2011). In the first study, an increase of mTOR along with a reduction of ATG7 (but not beclin-1, ATG5 or ATG12) was detected in DLB vs. AD brains (Crews et al., 2010) whereas in the latter study, an increase of LC3II was observed in DLB but not AD patients, a reduction of LAMP2 levels being common (Higashi et al., 2011). These two studies suggest different roles of autophagy in these diseases.

Studies on mitophagy in PD were the first ones to elucidate the crucial role of autophagy in age-related degeneration in CNS. In fact, blocking mitochondrial complex I by administration of low doses of MPP+ is one of the most common strategies to study PD pathogenesis (Zhu et al., 2012). Early onset autosomal recessive forms of PD, also have been related to mutations in genes that encode PINK1 (Valente et al., 2004) and the E3 ubiquitin ligase Parkin (Kitada et al., 1998), both involved in recognition, targeting and degradation of damaged mitochondria. Although no behavioral changes have been observed in *Parkin*$^{-/-}$ mice (Goldberg et al., 2003; Itier et al., 2003; Perez and Palmiter, 2005), disrupted mitochondrial function, response to DA and synaptic plasticity occur in the striatum (Palacino et al., 2004; Kitada et al., 2009). Even *Pink1* deletion results in impaired mitochondrial function and increased susceptibility to oxidative stress in mice (Gautier et al., 2008). Enhancing PINK1 activity has been reported to rescue from apoptotic signals, representing a potential strategy for idiopathic PD (Petit et al., 2005; Pridgeon et al., 2007; Klinkenberg et al., 2010). Accordingly, administration of kinetin, a precursor of an ATP analog, increases PINK1 function as proven by a more abundant phosphorylated form of Bcl-xL, a protein that mediates mitochondrial-induced apoptosis (Adams and Cory, 1998; Gross et al., 1999). Moreover, kinetin can promote PINK1-dependent recruitment of Parkin on the outer depolarized mitochondrial membrane allowing mitophagy to

start (Hertz et al., 2013). Therefore, restoring mitophagy rate might be a new neuroprotective strategy to reduce DA neuron degeneration typical of PD (Park et al., 2017).

There is evidence for a causative relationship between CMA dysfunction and intracellular accumulation of α-syn, a common feature of PD. Indeed, α-syn is a qualified substrate for CMA as it bears a KFERQ-like motif. Downregulating key components of CMA pathway, such as LAMP2A in rat midbrain (Xilouri et al., 2016) and Hsc70 in neuronal cell models (Sala et al., 2016), leads to increase of α-syn intracellular content, neural loss and behavioral deficits in rats. Furthermore, either stress-mediated or PD-linked A30P and A53T mutations in the α-syn gene (SNCA) determine the production of aberrant α-syn which displays a fivefold higher affinity for LAMP2A compared to the WT protein, preventing LAMP2A translocation across the lysosomal membrane and degradation of CMA targets (Cuervo et al., 2004; Martinez-Vicente et al., 2008). Mutations in GBA, which encodes the lysosomal enzyme GCase, are major risk genetic factors for PD, since they lead to a protein loss-of-function and lysosomal dysfunction. Mutations in GBA are major genetic factors for PD, encoding the lysosomal enzyme GCase, which leads to a protein loss-of-function and lysosomal dysfunction. The GBA1 homozygous mutations, instead, cause a lysosomal storage disorder, named Gaucher Disease which is characterized by excessive accumulation of glucosylceramide, a GCase substrate, into the lysosomal lumen, with subsequent autophagy impairment. The relevance of this pathway is further strengthened by the finding that even PD patients without GBA1 mutations showed a reduced GCase activity in the same cerebral areas displaying α-syn deposition (Mazzulli et al., 2011; Murphy et al., 2014). Besides, it has been reported that chronic pharmacological blockade of GCase in A53T α-syn transgenic mice further promoted exosome-associated α-syn accumulation and secretion. This supported the view that GCase directly regulates α-syn extracellular homeostasis and might be studied as a new therapeutic target in PD (Papadopoulos et al., 2018).

LRRK2 AND AUTOPHAGY

LRRK2 is a large multidomain protein with central GTPase Ras-of-Complex (ROC) and kinase domains, surrounded by protein-protein interaction domains (Mata et al., 2006; Cookson, 2010; Mills et al., 2014). LRRK2 mutations are the most common genetic cause of familial PD (Zimprich et al., 2004; Paisan-Ruiz et al., 2005) and GWAS studies revealed LRRK2 represents a risk factor for idiopathic PD (Nalls et al., 2014). At least six pathogenic mutations of LRRK2 have been identified: two in the kinase domain (G2019S and I2020T), three (R1441C/G/H) in the GTPase/ROC domain, and one (Y1669C) in the CoR domain (Reed et al., 2019). The G2019S mutation is most frequently associated with PD, followed by R1441C/G/H (Gasser, 2009; Okubadejo et al., 2018). LRRK2-associated PD is clinically and neuropathologically indistinguishable from idiopathic PD, most cases, particularly G2019S cases, presenting with nigrostriatal dopaminergic degeneration and LBs (Marras et al., 2011; Kalia et al., 2015). The penetrance of LRRK2-mediated PD is age-dependent but incomplete. LRRK2 mutations facilitate PD through several possible mechanisms, since LRRK2 is involved in a multitude of cellular functions and pathways, among which vesicle trafficking, cytoskeletal dynamics, neurotransmitter release, synaptic plasticity, Golgi and mitochondrial function, and immune response. In addition, several studies have pointed out the role of LRRK2 in autophagy (Roosen and Cookson, 2016; Manzoni and Lewis, 2017), which will be covered in the next chapters.

In vitro Studies

The first indirect evidence of LRRK2 modulation of proteostasis came from the 2006 study of MacLeod et al. (2006) showing that primary cortical neurons overexpressing G2019S or I2020T LRRK2 had tau-positive aggregates, MVB accumulation and swollen lysosomes (**Table 1**). That LRRK2 modulates autophagy was shown for the first time by Plowey et al. (2008) in SH-SY5Y neuroblastoma cells overexpressing WT LRRK2, G2019S LRRK2 (a kinase-enhancing mutation) (West et al., 2005; Greggio et al., 2006), or K1906M LRRK2, a kinase dead (KD) mutation (**Table 1**). Cells overexpressing G2019S LRRK2 displayed neurite shortening, together with an increase in the number and size of LC3-reactive autophagic vacuoles (AV), both at the neuritic and the somatic levels. The autophagic inducer, rapamycin, further enhanced these effects whereas blocking autophagy through LC3 or *Atg7* knock-down (with RNA-interference) caused their reversal, suggesting that G2019S overexpression is associated with enhanced autophagy and neurite shortening. It is worth noting that in this model, neither WT LRRK2 nor K1906M LRRK2 overexpression altered the autophagic flux, suggesting that not the loss but the increase of kinase activity might be instrumental to LRRK2 neurotoxic effect. Other studies confirmed that G2019S or R1441C LRRK2 mutants are associated with an increased autophagy (Gomez-Suaga et al., 2012b; Bravo-San Pedro et al., 2013; Orenstein et al., 2013; Su and Qi, 2013; Yakhine-Diop et al., 2014; Su et al., 2015). Nonetheless, others *in vitro* studies in different cell lines showed that LRRK2 G2019S and/or R1441C overexpression leads to inhibition of autophagy (Alegre-Abarrategui et al., 2009; Sanchez-Danes et al., 2012; Manzoni et al., 2013a, 2016; Wallings et al., 2019). A possible difference between mutations in the Roc-COR and kinase domains in terms of response to starvation-induced autophagy was also reported (Manzoni et al., 2013b). G2019S LRRK2 overexpression was also found to inhibit specific forms of autophagy such as CMA (Orenstein et al., 2013) or mitophagy (Wauters et al., 2019); in these studies, autophagy was found to be increased (possibly to compensate for CMA blockade) (Orenstein et al., 2013) or to be unchanged (Wauters et al., 2019). The role of the kinase activity of LRRK2 was investigated using LRRK2 kinase inhibitors. LRRK2-IN1, GSK2578215A and CZC25146 were reported to increase (Manzoni et al., 2013a, 2016) or to inhibit (Saez-Atienzar et al., 2014; Schapansky et al., 2014) the autophagic flux *in vitro*. Unfortunately, first generation inhibitors were employed in these studies, which are characterized by low kinase specificity and off-target effects (West, 2017). Interestingly, however, more selective LRRK2

TABLE 1 | Synopsis of the *in vitro* studies investigating the impact of genetic and pharmacological manipulation of LRRK2 on autophagy and its markers.

	Cell type	LRRK2 manipulation	Autophagic marker	Phenotype
MacLeod et al., 2006	Primary cortical neurons	G2019S, I2020T OE	Swollen lys, vacuolized mitochondria, phospho-tau-positive aggregates, ↑ MVB	Neurite shortening
Plowey et al., 2008	SH-SY5Y	G2019S OE	↑ LC3 puncta, ↑ AV number and size ↑ autophagy	Neurite shortening, potentiated by rapamycin and reversed by LC3 or Atg7 kd but not 3-MA. Blocked by MEK-inhibitor
		WT, K1906M OE (KD)	↔	
Alegre-Abarrategui et al., 2009	HEK293T, VERO	R1441C, G2019S OE	↑ LC3 puncta, ↑ MVB and AV ↓ autophagy	Colocalization of LRRK2 with p62 and LC3 in MVB and AV, skein-like inclusions in R1441C transfected cells
		LRRK2 kd	↓ LC3II levels, ↑ LC3 turnover ↑ autophagy	Protects against BFA-induced cell death in starvation conditions
Gomez-Suaga et al., 2012b	HEK293T, PC12	WT, G2019S OE	↑ LC3 puncta, ↑ LC3II levels ↑ mature lys ↑ autophagic structures ↑ p62, ↑ autophagy	NAADP-dependent, Ca^{++}/CaMKK/AMPK-dependent. Increase cell-death triggered by an UPS inhibitor (rescued by rapamycin)
		K1906M OE (KD)	↔	
Sanchez-Danes et al., 2012	Human-derived iPSC	G2019S	↑ LC3 puncta ↑ lipid droplets, ↑ p62, ↓ LC3 flux, ↓ AV ↓ autophagic clearance	Shorter/fewer neurites
Orenstein et al., 2013	SH-SY5Y, HEK293T, human-derived iPSC, primary neurons	WT OE	↑ LAMP2A	Impaired CMA with compensatory ↑ autophagy
		G2019S OE	↑ LAMP2A ↔ LC3	
		LRRK2 kd	↔	
Bravo-San Pedro et al., 2013	Human fibroblasts	G2019S	↑ autophagic flux, ↑ AP, ↓ p62 ↑ LAMP2A, LC3, beclin-1	Inhibited by MAPK1/3 inhibitor
Manzoni et al., 2013a	H4 (neuroglioma), primary astrocytes	LRRK2 kinase inhibition: LRRK2-IN-1, GSK2578215A CZC-25146	↑ LC3I, LC3II ↑ p62 ↑ autophagic flux	mTOR-independent
Manzoni et al., 2013b	Human fibroblasts	G2019S, R1441G, Y1699C	↓ LC3II/LC3I after starvation, ↓ p62-positive in LRRK2 Y1699C and R1441G cells, ↔ p62, LAMP1 levels	mTOR-independent
Su and Qi, 2013	HEK293T	WT, G2019S OE	↑ LC3II ↑ autophagy	Drp1-dependent mitochondrial fragmentation autophagy
Saez-Atienzar et al., 2014	SH-SY5Y	LRRK2 kd LRRK2 kinase inhibition: LRRK2-IN-1, GSK2578215A	↑ LC3II, p62 ↑ autophagy ↓ AP-lys fusion ↓ autophagic flux	Induces mitochondrial fission and cell-death. Exacerbated by autophagy inhibitors
Schapansky et al., 2014	RAW264.7 (macrophages), BV2 (microglia)	LRRK2 kd, LRRK2 kinase inhibition: LRRK2-IN-1, GSK2578215A	↓ autophagic flux ↓ LC3II	↓ clearance of Q74 protein aggregates in microglial cells
Yakhine-Diop et al., 2014	Human fibroblasts	G2019S	↑ LC3II, beclin-1, LAMP2A, Cath B, Swollen lysosomes, ↑ autophagy	↑ MPP+-induced cell death, MPP+-dependent mTOR dephosphorylation
Su et al., 2015	Human fibroblasts	G2019S	↑ autophagic flux	Mitochondrial depolarization and mass loss

(Continued)

TABLE 1 | Continued

	Cell type	LRRK2 manipulation	Autophagic marker	Phenotype
	HeLa	WT, G2019S OE	↑ p62 translocation to mitochondria, ↑Bcl-2 ↑ mitophagy	Bcl-2-dependent mitophagy
Manzoni et al., 2016	H4	LRRK2 kinase inhibition: LRRK2-IN-1, GSK2578215A	↑ LC3II ↔ pULK1 ↔ pS6K	mTOR/ULK1-independent, PI3P and Beclin-1-dependent
		LRRK2 kd	↔	
	Primary astrocytes	LRRK2 KO	↑ LC3II	
Schapansky et al., 2018	Primary cortical neurons	G2019S	↓ LAMP1, LC3I ↓ autophagic flux ↑ lys pH	↑ tau phosphorylation ↑ α-syn aggregates
		LRRK2 kinase inhibition: GSK2578215A, CZC25146	↔	Rescues lys changes and reduces α-syn aggregates
Hartlova et al., 2018	Bone marrow-derived macrophages	LRRK2 kinase inhibition: GSK2578215A	↑ LC3II, ↓ p62	BFA-insensitive
		LRRK2 KO	As above	
Wallings et al., 2019	Primary rat cortical neurons	R1441C	↑ LC3II, ↔ p62, LAMP1 ↓ autophagic flux, ↓ AP-lys fusion ↓ lys protein degradation ↑ lys pH	Unresponsive to LRRK2 kinase inhibition (MLi-2, PF06447475)
		WT, G2019S	↓ autophagic flux	Reversed by LRRK2 kinase inhibition
		Non transgenic	↓ autophagic flux after LRRK2 kinase inhibitors	
		LRRK2 KO	↑ LC3II, ↔ p62, LAMP1 ↑ lys protein degradation	
Ho et al., 2019	MEF, primary neurons	R1441G	↓ lys activity ↓ LAMP2A, ↓ CMA ↔ autophagy	↓ α-syn clearance Effects rescued by CMA-activator
Wauters et al., 2019	Human fibroblasts	G2019S, R1441C	↔ LC3II ↔ autophagy	Rab10-dependent impairment of mitophagy
Bonello et al., 2019	COS7 Human fibroblasts	G2019S, R1441C	N/A	Impairs Pink1/parkin-mediated mitophagy
		D1994A (KD), LRRK2 kinase inhibition: LRRK2-IN-1		Rescues G2019S LRRK2 effects

↑ increase, ↓ decrease, ↔ no change; A, autophagosome; AV, autophagic vacuoles; BFA, bafilomycin A1; kd, knock-down; KD, kinase dead; KO, knock-out; Lys, lysosomes/lysosomal; MEF, mouse embryonic fibroblasts; MVB, multi-vesicular bodies; OE, overexpression; vmDA, ventral midbrain dopamine.

inhibitors MLi-2 and PF-06447475 increased the autophagy flux in primary cortical neurons obtained from BAC G2019S (but not R1441C) mice causing the opposite effect in non-transgenic cultures (Wallings et al., 2019). The issue of whether LRRK2 acts as negative or positive modulator of autophagy is also still unclear (**Table 1**). Neurons or macrophages obtained from LRRK2 KO mice show an increase of LC3II levels and autophagic flux, suggesting that endogenous LRRK2 inhibits autophagy (Manzoni et al., 2016; Hartlova et al., 2018; Wallings et al., 2019). However, most studies reported that WT LRRK2 overexpression increased autophagy (Gomez-Suaga et al., 2012b; Orenstein et al., 2013; Su and Qi, 2013; Roosen and Cookson, 2016), with one study (Plowey et al., 2008) reporting no effect and, another (Wallings et al., 2019), inhibition. Acute knock-down of LRRK2 was shown to be ineffective (Orenstein et al., 2013; Manzoni et al., 2016), to increase (Alegre-Abarrategui et al., 2009) or to inhibit (Schapansky et al., 2014) autophagy. Therefore, not only the regulation of autophagy operated by LRRK2 is mechanistically complex, but also experimental outcomes seem to be affected by a number of variables including the cell model, expression levels of LRRK2, LRRK2 kinase inhibitor used, autophagic markers investigated and protocols adopted (Klionsky et al., 2016). In this respect, it should be noted that although autophagy was monitored through quantification of LC3II levels, not all studies investigated the autophagic flux, i.e., fold-changes following application of autophagy inhibitors, which would allow to conclude whether the increase of LC3II levels is due to an increase of autophagosome synthesis/maturation or a blockage of their clearance.

In vivo Studies

Invertebrates

The first published evidence that LRRK2 affects autophagy *in vivo* was produced in yeasts where administration of fragments of human LRRK2 carrying mutations that impair GTPase

TABLE 2 | Changes in autosomal-lysosomal pathways in LRRK2 KO mice and rats *in vivo*.

	Strain age (mos)	Brain	Kidney	α -syn levels	Note
Tong et al., 2010	LRRK2 KO mice (20 m)	No accumulation of α-syn or ub	↓ UPS activity ↑ LC3I, ↓ LC3II ↑ p62	↑ α-syn aggregation ↑ pS129 αsyn	Age-dependent
Herzig et al., 2011	LRRK2 KO mice (14 m)	N/A	↑ Akt, TSC2, mTOR, 4E-BP1 and pT37/46 4EBP1, ↑ p62 ↔ pT308 Akt, S6, LC3I/II	↔	Mild ↑ lamellar bodies in lung type II pneumocytes
Tong et al., 2012	LRRK2 KO mice (7 m)	N/A	↓ LC3I, ↑ LC3II ↓ p62 ↑ LAMP1, LAMP2A, CathB and D	↓ α-syn insoluble fraction	Biphasic
	LRRK2 KO mice (20 m)		↑ LC3-I, LC3II ↑ LAMP1, LAMP2A, CathB and D	↑ α-syn soluble and insoluble fraction	
Hinkle et al., 2012	LRRK2 KO mice (12 m,18 m)	N/A	↑ p62	↔	
Baptista et al., 2013	LRRK2 KO rats (1–12 m)	N/A	↑ LAMP1, LAMP2A	N/A	Age-dependent
Fuji et al., 2015	LRRK2 KO mice (2–3 m)	N/A	↑ lysosomes	N/A	↑ lamellar bodies in lung type II pneumocytes
Giaime et al., 2017	LRRK KO* mice (15 m)	↑ α-syn or ub ↑ p62, ↓ LC3I, ↑ LC3II	N/A	↑ α-syn and HMW α-syn in striatum and SNpc but not CCx	Age-dependent

**Mice lacking both LRRK1 and LRRK2, i.e., double KO mice. ↑ increase, ↓ decrease, ↔ no change; AP, autophagosome; Cath, cathepsin; CCx, cerebral cortex; HMW, high molecular weight; SNpc, substantia nigra pars compacta; ub, ubiquitinated proteins.*

activity caused neuronal death, vesicle trafficking defects and AV accumulation (Xiong et al., 2010) (**Table 2**). In *Drosophila melanogaster* (Imai et al., 2008) pointed out that LRRK2 modulates protein synthesis through phosphorylation of eIF4E binding protein (4E-BP), which lies along the mTOR pathway, suggesting that LRRK2 modulates ALP. Overexpression of WT or I2020T LRRK2 hyperphosphorylated 4E-BP, which resulted in reduced 4E-BP binding to eIF4E, and deregulation of protein translation. Interestingly, however, no changes in levels or phosphorylation of mTOR were found, questioning the role of autophagy in these events (Imai et al., 2008). Later study in *Drosophila melanogaster* more convincingly proved the role of autophagy in LRRK2 toxicity, showing that activation of autophagy via pharmacological or genetic stimulation of AMPK protected against mitochondrial toxicity and DA cell loss induced by expression of human G2019S LRRK2 (Ng et al., 2012). ALP defects were also observed in follicle cells of *Drosophila melanogaster*, where the *LRRK2* homolog *Lrrk* colocalizes with, and binds to Rab7 and Lamp1 in late endosomes and lysosomes, and to a much lesser extent to Rab5 in early endosomes (Dodson et al., 2012, 2014). *Lrrk* null flies showed enlarged Rab7-positive structures containing undigested cytosolic material, increased autophagosomes and enlarged early endosomes containing monoubiquitinated proteins, consistent with the view that loss of *Lrrk* function blocks the late endosomal to lysosomal maturation, impairs the degradative properties of lysosomes and the substrate delivery to lysosomes. Interestingly, this phenotype was reversed by overexpression of WT Lrrk or G1914S Lrrk (a mutant with enhanced kinase activity equivalent to G2019S LRRK2) (Dodson et al., 2014). Studies in *C. elegans* also demonstrated that LRRK2 regulates autophagy. Saha et al. (2015) using a fluorescence gene reporter fused with lgg-1, the LC3 homolog, revealed that aging impairs the autophagic flux: hG2019S or hR1441G LRRK2 worsened this effect whereas WT LRRK2 and a LRRK2 KD mutant improved it. Nonetheless, when co-expressed with α-syn, both G2019S LRRK2 and, to a lesser extent, WT LRRK2, impaired autophagy in an age-dependent way, which was associated with a greater loss of DA neurons in older nematodes (Saha et al., 2015). Interestingly, a minimal effect of G2019S LRRK2 on the expression of the LAMP1 homolog, lmp-1, was detected, suggesting that, at variance with *Drosophila*, LRRK2 minimally altered lysosomal function (Saha et al., 2015).

Rodents

Original study in LRRK2 KO mice failed to find brain pathology (nigrostriatal degeneration and α-syn or ubiquitinated protein accumulation) and changes in brain autophagy markers in 2-year-old LRRK2 KO mice (Tong et al., 2010) (**Table 2**). Nonetheless, this study unraveled that loss of LRRK2 caused striking age-dependent pathology selectively in the kidney, which expresses the highest levels of LRRK2 in the mouse (sixfold greater than in the brain). An increase of both soluble and insoluble forms of α-syn, along with the levels of pSer129-α-syn, were found at 20 months but not at 10 weeks of age. Since α-syn is degraded by ALP and UPS, this pointed to an impairment of α-syn clearance in aged kidneys. An impairment of UPS and ALP due to the deletion of LRRK2 was further suggested by the accumulation of ubiquitinated high-molecular weight proteins and lipofuscin granules, and by the analysis of the autophagic flux, which revealed mild elevation

of LC3I, dramatic reduction of LC3II levels, and compensatory accumulation of p62.

The same groups of authors later observed (Tong et al., 2012) that changes in ALP function were actually biphasic. At 7 months, a reduction of LC3I/LC3II ratio and p62 levels was associated with a reduction of insoluble α-syn aggregates (soluble α-syn levels were undetectable), indicating an increase of ALP activity, whereas at 20 months an increase of LC3I/LC3II ratio and p62 levels was associated with elevation of both soluble and insoluble α-syn levels, indicating normalization of autophagy. Analysis of lysosomal proteins and proteases at key ages did not reveal qualitative age-dependent changes since levels of LAMP1 and LAMP2 as well as cathepsin B were found to be elevated already from the first month of age (significant elevation of cathepsin D was observed at both 7 and 20 months). However, EM analysis revealed kidney-specific age-related accumulation of autolysosomes and lipofuscin granules confirming that loss of LRRK2 is associated with lysosomes alterations. Kidney pathology in LRRK2 KO mice was substantially confirmed by Hinkle et al. (2012) and Fuji et al. (2015). These authors analyzed kidneys at 3, 12, and 18 months. Pigmentation and lipofuscin staining, already evident at 3 months, worsened with aging. p62 levels progressively increased with age, at variance with WT controls where they appeared at 12 months. Different from previous studies, however, no changes in α-syn staining was observed in these mice. Also at variance with previous data, elevated LC3II were detected in 18-month-old LRRK2 KO mice, with no difference observed at younger ages (Hinkle et al., 2012). Likewise, LRRK2 KO rats (Baptista et al., 2013) showed striking age-dependent kidney pathology, with lipofuscin accumulation and irregular hyaline droplets accumulation in kidney tubular epithelium, starting at 4 months. In the same cells, progressive increase of immunohistochemical staining for LAMP1 and LAMP2 was noted, which was overall interpreted as an impairment of lysosomal function.

Novartis group analyzed in great detail autophagy in 14-month-old LRRK2 KO mice in comparison with 5-month-old G2019S KI mice, which show enhanced kinase activity *in vivo* (Yue et al., 2015; Longo et al., 2017; Mercatelli et al., 2019), and 6-month-old KD mice, which instead show no kinase activity *in vivo* (Herzig et al., 2011; Mercatelli et al., 2019). Microvacuolization in tubular epithelial cells of LRRK2 KO mice appeared already at 1.5 months, and progressively worsened over time, with lipofuscin-like pigments appearing at 8 months. Similar changes were observed for the first time also in type II pneumocytes of lungs, other organs (brain, spleen, liver, heart) being spared, indicating a crucial role for LRRK2 in kidney and lung homeostasis. A similar pathology was observed in the kidneys of KD, but not G2019S KI, mice, consistent with the view that loss of LRRK2 or its kinase activity causes derangement of kidney homeostasis (Herzig et al., 2011). In line with this, LAMP1 or LAMP2 immunohistochemical staining was elevated in 6–9-month-old LRRK2 KO or KD mice, respectively. EM analysis revealed progressive increase in number and size of secondary lysosomes in LRRK2 KO mice, again confirming alteration in lysosome homeostasis. In keeping with Hinkle et al. (2012) and in contrast with Tong et al. (2010, 2012), no changes in α-syn levels were observed in the kidney of these mice. This study confirmed the elevation of p62 levels in the LRRK2 KO kidney (Tong et al., 2010), and compared for the first time a wider panel of autophagic and lysosomal markers using Western analysis. The resulting picture, however, was quite confusing, since the Akt/mTOR pathway was perturbed in all genotypes, but with different patterns. Akt levels were elevated in KD and LRRK2 KO mice, but not G2019S KI mice. However, TSC2 and mTOR levels were reduced in KD and elevated in LRRK2 KO and G2019S KI mice. Perhaps consistent with an overactivation of the Akt/mTOR pathway with consequent autophagy inhibition, levels of the mTOR-regulated translation initiation factor 4E-BP1 and its phosphorylated Thr37/46 forms were also elevated in LRRK2 KO mice whereas no changes were observed in G2019S KI mice. S6 kinase levels were unchanged in all genotypes. So were LC3I and LC3II levels in LRRK2 KO and KD mice (not investigated in G2019S KI mice). Kidney and lung pathology were also confirmed in 10–12 weeks LRRK2 KO mice by a Genentech study aimed at assessing the safety of two LRRK2 inhibitors (GNE-7915 and GNE-0877) (Fuji et al., 2015). This study also revealed that administration of LRRK2 kinase inhibitors did not cause vacuolization, i.e., lysosome dysregulation, in rodent tissues. At variance with rodents, however, an increase of lamellar bodies in type II pneumocytes of the lung of non-human primates, similar to those observed in LRRK2 KO mice, was shown (Fuji et al., 2015), which might be consistent with the view that inhibition of LRRK2 kinase activity impairs autophagy. The different species sensitivity was attributed to different residual LRRK2 levels after LRRK2 inhibition (Fuji et al., 2015). It therefore appears that removal of LRRK2 impairs ALP machinery in kidney and pneumocytes. Nonetheless, subtle changes observed in G2019S KI mice would not allow to rule out that also an increase of LRRK2 kinase activity might perturb autophagy, possibly indicating that ALP is physiologically regulated within a narrow range of LRRK2 kinase activity.

What also clearly emerged from these studies is that genetic deletion of LRRK2 does not impact autophagy in the brain. A more recent study, however, revealed that the functional homolog of LRRK2, i.e., LRRK1, might play a compensatory role in LRRK2 KO mice (Giaime et al., 2017). Indeed, although any changes of autophagic markers were found in mice constitutively lacking either LRRK2 or LRRK1, double KO mice showed age-dependent increase of p62 and LC3II levels, reduction of LC3I levels, and AV accumulation, indicating an impairment of autophagy (Giaime et al., 2017). Development of a selective antibody might help elucidate the role of LRRK1 in autophagy and, more in general, in cellular homeostasis.

Following the report of tau hyperphosphorylation in brain lysates of 9–10-month-old LRRK2 BAC R1441C mice (Li et al., 2009), the impact of LRRK2 mutants (i.e., LRRK2 G2019S or R1441C/G) on brain autophagy was widely investigated (**Table 3**). Autophagy abnormalities were detected in the striatum of 17–18-month-old hG2019S transgenic mice (enlarged AV and increased autophagosomes, associated with aggregated and damaged mitochondria) (Ramonet et al., 2011). Autophagy changes consistent with reduced autophagic flux were also revealed in G2019S KI mice.

TABLE 3 | Changes in autosomal-lysosomal pathways in LRRK2 mutant mice and rats *in vivo.*

	Model	Age (mos)	Brain				Kidney
				α *-syn*	*Area*	*NDG*	
Li et al., 2009	BAC R1441C mice	9–10	↑ phospho-tau	N/A	Whole brain	No	N/A
Ramonet et al., 2011	G2019S TG mice (PDGF prom)	19–20	Enlarged vacuoles, ↑ AP Mitochondrial damage	N/A	CCx	18%	N/A
	R1441C TG mice (PDGF prom)	23–24	As above but milder			No	
Herzig et al., 2011	G2019S KI mice	5	N/A	No	N/A	No	↑ TSC2, mTOR ↔ Akt, 4E-BP1 and pT37/46 4E-BP1
	Kinase-dead (D1994S KI mice)	6	N/A	No	N/A	No	↑ Akt, 4E-BP1 ↓ TSC2, mTOR ↔ pT308 Akt, S6K and pS235/236 S6K, pS240/244 S6K
Tsika et al., 2014	R1441C TG mice (DAT prom)	22	↔ LC3, p62	No	SNc	No	N/A
Liu et al., 2014	R1441G KI mice	18–22	↔ LC3, Beclin-1	No		No	N/A
Yue et al., 2015	G2019S KI mice	15	↑ LC3II, ↔ p62	No	Whole brain	No	No gross morphological changes
Schapansky et al., 2018	G2019S KI mice	20	LAMP1, LC3I	No	CCx	No	N/A
Ho et al., 2018	G2019S TG mice (PDGF prom)	12-19	↑ p62, LC3	↑	Whole brain	N/A	N/A
Ho et al., 2019	R1441G KI mice	18	↑ LAMP2A, hsc70 (m.f.) ↑ GAPDH (m.f., c.f.)	↑	CCx, STR	No	N/A
Wallings et al., 2019	BAC G2019S rats	22	↑ LC3 puncta	N/A	SN	No	N/A
	BAC R1441C rats	22	↑ LC3 puncta		CCx SN		

↑ *increase,* ↓ *decrease,* ↔ *no change; AP, autophagosomes, c.f., cytosolic fraction; m.f., membrane fraction; NDG, nigrostriatal degeneration; prom, promoter; TG, transgenic.*

Specifically, 15-month-old G2019S KI mice showed an increase of LC3II levels in a whole brain lysate (Yue et al., 2015) whereas 20-month-old G2019S KI mice, showed a reduction of LAMP1 in the cerebral cortex (Schapansky et al., 2018). This was confirmed by experiments in primary cortical neurons obtained from G2019S KI mice, where autophagy impairment was reversed by LRRK2 inhibitors (Schapansky et al., 2018). Moreover, 12–19-month-old G2019S overexpressing mice showed accumulation of LC3 and p62 levels along with levels of GRB78/BiP, an ER stress marker (Ho et al., 2018). In this study, it was shown that LRRK2 phosphorylates leucyl-tRNA synthetase, a regulator of protein translation and mTOR interactor, and that G2019S LRRK2 is associated with ER stress, accumulation of α-syn aggregates and autophagic markers. It was therefore proposed that inhibition of autophagy by G2019S LRRK2 would be secondary to ER stress and misfolded protein engulfment (Ho et al., 2018). Possibly in general agreement with previous studies, 22-month-old BAC G2019S and R1441C mice showed an increase in LC3 puncta in SNpc DA neurons, as measured by immunohistochemistry (Wallings et al., 2019). However, considering the low expression levels of LRRK2 in mouse nigral DA neurons (Biskup et al., 2006; Simon-Sanchez et al., 2006; Taymans et al., 2006; Melrose et al., 2007; West et al., 2014), it

is not clear whether these effects are truly LRRK2-dependent and, if so, if they rely on LRRK2 kinase activity or scaffold properties of LRRK2.

Autophagy abnormalities were observed also in R1441C/G LRRK2 mutants, although more inconsistently. A pattern similar to that observed in hG2019S KI mice was detected in 23–24 month-old hR1441C transgenic mice (Ramonet et al., 2011). Conversely, conditional transgenic mice expressing the R1441C mutation selectively in DA neurons, did not show accumulation of α-syn, tau or ubiquitin or even changes of p62 and LC3 levels at the age of 12–22 months (Tsika et al., 2014). This was confirmed also in R1441G KI mice, where no changes in autophagic markers LC3 and Beclin-1 were observed at 3 and 18–22 months, when compared with age-matched WT controls (Liu et al., 2014). Nonetheless, a more recent and comprehensive study in these mice at different ages spanning from 3 to 18 months, showed an age-dependent impairment of CMA (Ho et al., 2019). In particular, Western analysis revealed a significant increase in soluble α-syn and total amyloid-like α-syn oligomers in 18-month-old but not younger R1441G KI mice. Such increase of α-syn load was associated with lysosomal redistribution, with clustering of lysosomes around the nucleus of striatal neurons. Lysosomal impairment was confirmed by the (mild) increase of LAMP2A and Hsc70 levels in the membrane fraction of striatal lysates of 18-month-old mice, and by the accumulation of a typical CMA substrate, such as GAPDH. Further analysis in embryonic fibroblasts obtained from R1441G mice proved that lysosomal clearance of α-syn was indeed reduced. Interestingly, CMA activation rescued these changes, suggesting the therapeutic potential of this approach.

Mechanisms Through Which LRRK2 Regulates Autophagy

Over the years, different pathways have been identified through which LRRK2 modulates autophagy, although in most studies it is not possible to dissect out direct vs. indirect effects (**Figure 2**). LRRK2 might operate through various subsets of Rab GTPases, since Rab3A/B/C/D, Rab8A/B, Rab10, Rab12, Rab29, Rab35 and Rab43 are LRRK2 substrates (Ito et al., 2016; Steger et al., 2016, 2017) and the Rab GTPase network has been implicated in many stages of autophagy (Zoppino et al., 2010; Dou et al., 2013; Feldmann et al., 2017). Another putative pathway through which LRRK2 regulates autophagy is the MEK/ERK/Beclin-1 axis. In particular, Bravo-San Pedro et al. (2013) reported that LRRK2 G2019S increased basal autophagy in fibroblasts and the effect was reversed by the MAPK1/3 inhibitor UO126. Moreover, Manzoni et al. (2016) reported that activation of autophagy following LRRK2 kinase inhibition requires the increase of PI3P levels operated by the VPS34/Beclin-1 rather than mTOR/ULK1 pathway. Both studies are in line with the findings of Plowey et al. (2008) who showed that 3-Methyladenine, a PI3K inhibitor responsible for the mTOR-mediated activation of autophagy, did not prevent mutant LRRK2-induced neurite shortening, whereas the MAPK1/3 inhibitor U0126 did. In contrast with this view, activation of RAW264.7 macrophages or murine BV2 microglial cells via TLR4 caused phosphorylation and membrane translocation of LRRK2, inducing autophagy via an mTOR-dependent mechanism (Schapansky et al., 2014). The discrepancy on which pathway is preferentially recruited by LRRK2 for activating autophagy might be due to the different cell types employed. In fact, LRRK2 might exert a different effect on immune cells compared to other cell lines since immune cells express high levels of LRRK2 mRNA and protein, which are further enhanced in case of activation of these cells (Hakimi et al., 2011; Thevenet et al., 2011). Furthermore, cell activation and translocation of LRRK2 to the autophagosome membrane might be relevant for the physiological activity of LRRK2 but not for the pathological mechanisms underlying LRRK2-associated PD. Finally, work from Hilfiker and collaborators disclosed a link between calcium homeostasis, LRRK2 and autophagy (Gomez-Suaga and Hilfiker, 2012; Gomez-Suaga et al., 2012a,b). It is well known that cytosolic calcium regulates autophagy at different levels (Bootman et al., 2018). These authors reported that overexpression of LRRK2 or the G2019S mutant in cell lines increases the autophagosome number through an mTOR-insensitive, LRRK2 kinase-sensitive pathway (Gomez-Suaga et al., 2012b). The LRRK2 effect relied on Ca^{2+} release from ER and CaMKK/AMPK pathway activation, and was mimicked by the Ca^{2+} mobilizing compound nicotinic acid adenine nucleotide diphosphate (NAADP), acting via endolysosomal two-pore channels (TPCs). Interestingly, LRRK2 effect was occluded by an inactive mutant of TPC type 2 (TPC2) and by a pharmacological TPC2 inhibitor. Since TPC2 are expressed by lysosomes, it was proposed that LRRK2 causes the opening of TPC2 and Ca^{2+} release from lysosomes, which triggers further Ca^{2+} release from ER and induces autophagy via CaMKK/AMPK (Gomez-Suaga and Hilfiker, 2012). It remains to be established whether TPC2 opening is mediated by a direct interaction with LRRK2 or a recruitment of Rabs (e.g., Rab7).

LRRK2 seems also to play a significant role on more specific subtypes of autophagy, namely mitophagy and CMA. A link between LRRK2 and mitophagy was early suggested by two studies that showed the presence of TOM20, LC3 and active LRRK2 in the same iodixanol gradient membrane fraction of RAW264.7 macrophages and BV2 microglial cells (Schapansky et al., 2014). Moreover, pharmacological inhibition of LRRK2 kinase activity induced Drp-1 mediated mitochondrial fission in SH-SY5Y cells (Saez-Atienzar et al., 2014). More recently, Bonello et al. (2019) demonstrated that G2019S LRRK2 impairs PINK1/Parkin-mediated autophagy in human fibroblasts, and that LRRK2 kinase activity is instrumental to this effect. However, this process does not seem to be directly mediated by LRRK2 but rather by the interaction with Rab10. In normal conditions, Rab10 accumulates on depolarized mitochondria through the interaction with PINK1 and Parkin. Here, Rab10 binds to the autophagy receptor optineurin and promotes its accumulation and exposition, facilitating the degradation of depolarized mitochondria. LRRK2, in its physiological state and more prominently in the presence of kinase-enhancing mutations, phosphorylates Rab10 at the Thr73 residue, preventing its accumulation and thus inhibiting

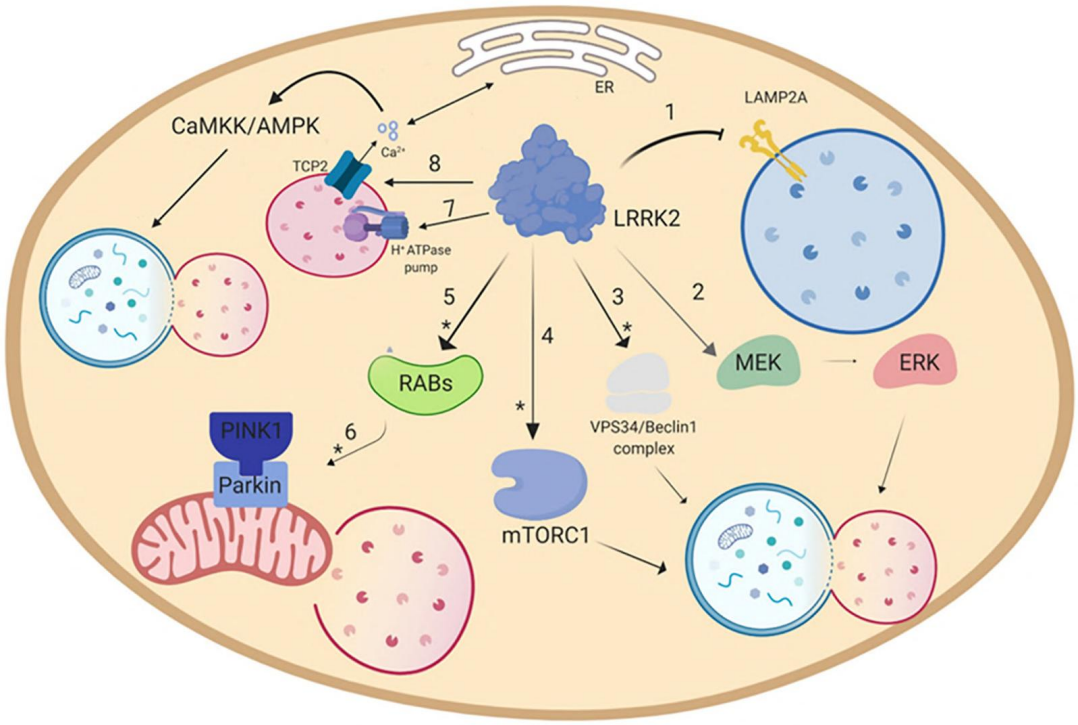

FIGURE 2 | Putative pathways through which LRRK2 modulates autophagy. **(1)** Overexpression of LRRK2 or its mutants inhibits CMA through blockade of the translocation into the lysosome operated by the LAMP2A receptor (Orenstein et al., 2013). Furthermore, LRRK2 is able to modulate autophagy by activating either **(2)** the MEK/ERK (Bravo-San Pedro et al., 2013), or the **(3)** VPS34/Beclin1 complex (Manzoni et al., 2016). Other putative pathways are **(4)** the mTORC1 pathway (Imai et al., 2008; Ho et al., 2018), or **(8)** the Ca^{2+}/CaMKK/AMPK pathway (Gomez-Suaga et al., 2012b). As for mitophagy **(5)**, LRRK2, via Rab activation (Wauters et al., 2019), is able to disrupt the **(6)** PINK1/Parkin-mediated mitophagy (Saez-Atienzar et al., 2014; Schapansky et al., 2014; Yakhine-Diop et al., 2014; Bonello et al., 2019). Furthermore, LRRK2 can regulate lysosomal pH via **(7)** lysosomal H^+-ATPase pump (Wallings et al., 2019). Asterisk (*) indicates the putative pathways modulated by pharmacological LRRK2 kinase inhibitors.

mitophagy (Wauters et al., 2019). Furthermore, such LRRK2-mediated inhibition of mitophagy makes the cell more susceptible to mitochondrial damage and subsequent cell death (Yakhine-Diop et al., 2014). A direct link between LRRK2 and lysosomal activity was recently pointed out by Wallings et al. (2019), showing that hWT LRRK2 interacts with the a1 subunit of the v-type H^+ ATPase proton pump (vATPase a1). This pump regulates the acidity of the lysosomal lumen, which is crucial for the activity of lysosomal enzymes. Primary cortical neurons obtained from LRRK2 R1441C mice showed decreased binding and protein levels of vATPase a1, with a significant more basic lysosomal pH, leading to inhibition of the lysosomal degradation activity (Wallings et al., 2019).

Regarding CMA, similar to α-syn (Cuervo et al., 2004), LRRK2 bears different KFERQ peptide motifs in its amino acid sequence that can be targeted by hsc70. Furthermore, high levels of WT or LRRK2 mutants inhibit the formation of the CMA translocation complex at the lysosomal membrane, thus blocking CMA (Orenstein et al., 2013). The LRRK2-mediated blockage of CMA induces a compensatory increase in LAMP2A and accumulation of other CMA substrates, such as α-syn (Orenstein et al., 2013). The observation that also high levels or aberrant forms of α-syn inhibits CMA (Cuervo et al., 2004), strongly points toward a synergistic role of these two proteins in neurotoxicity and protein aggregation, which has been a hot topic in the last few years.

ARE ALP CHANGES OBSERVED IN LRRK2 MODELS RELEVANT FOR LRRK2-INDUCED NEURODEGENERATION?

In vitro studies have demonstrated that not just the G2019S but also the less common LRRK2 pathogenic mutants are associated with enhanced kinase activity (Zhao and Dzamko, 2019), and that LRRK2 kinase activity is instrumental to LRRK2-mediated toxicity (West et al., 2005; Greggio et al., 2006; Plowey et al., 2008; Yao et al., 2010). On this basis, LRRK2 kinase inhibitors are being investigated as disease-modifying agents in models of LRRK2-associated and idiopathic PD (West, 2017; Zhao and Dzamko, 2019). Therefore, investigating if and to which extent the neuroprotective effect of LRRK2 inhibitors is mediated through the modulation of ALP is of great relevance and translational potential.

It was originally suggested that autophagy dysregulation contributes to the LRRK2-associated neurotoxicity *in vitro*, since removal of key autophagic proteins LC3 or ATG7 prevented G2019S-associated neurite shortening in SH-SY5Y cells, whereas autophagy activation by rapamycin worsened it (Plowey et al., 2008). In other studies, autophagy or CMA activation was shown to be protective against LRRK2-associated toxicity. In fact, rapamycin rescued the increase of cell death triggered by an UPS inhibitor in G2019S-overexpressing HEK293T cells (Gomez-Suaga et al., 2012b). Likewise, CMA activation rescued the impairment of lysosomal activity, the reduction of LAMP2A levels and the accompanying increase of α-syn in mouse embryonic fibroblasts and primary neurons obtained from R1441G KI mice (Ho et al., 2019), although whether these effects made cells more resistant to parkinsonian toxins was not reported. Consistent with the view that autophagy blockade leads to neurodegeneration (Hara et al., 2006; Komatsu et al., 2006b), Wade-Martins and collaborators reported that the autophagy inhibitor bafilomycin A1 caused cell death under starvation conditions in HEK293T cells (Alegre-Abarrategui et al., 2009). In this process, LRRK2 plays a role since LRRK2 knock-down was protective (Alegre-Abarrategui et al., 2009).

Only a few studies specifically addressed whether LRRK2 kinase inhibitors modulate ALP *in vitro,* unfortunately leading to opposite conclusions. Manzoni et al. (2013a) demonstrated that LRRK2 inhibitors LRRK2-IN1, GSK2578215A and CZC-25146 increase the autophagic flux via an mTORC1-independent pathway, either acting via the Beclin-1 or directly impacting on ULK1 (Manzoni et al., 2016, 2018). Consistent with induction of autophagy, GSK2578215A elevated LC3II and reduced p62 levels in bone-marrow-derived macrophages, although the increase of LC3II levels was minimally affected by bafilomycin A1, leading the authors to hypothesize that such increase was not related to autophagic flux changes (Hartlova et al., 2018). These studies would suggest that blocking LRRK2 kinase activity improves the proteolytic events and helps cope with misfolded proteins and damaged organelles that can drive cell death. Consistently, Schapansky et al. (2018) reported that LRRK2-IN-1 and CZC25146 reversed the lysosomal changes and reduced the accumulation of detergent-insoluble α-syn observed in primary cortical neurons obtained from G2019S KI mice. Moreover, Bonello et al. (2019) showed that GSK2578215A and LRRK2-IN-1 were able to reverse the impairment of PINK1/parkin-mediated mitophagy induced by the G2019S LRRK2 mutation. In contrast with these studies, Galindo and collaborators showed that nanomolar (i.e., LRRK2 specific) concentrations of GSK2578215A impaired the autophagic flux by altering the autophagosome/lysosome fusion, which led to mitophagy, mitochondrial fission and cytotoxicity (Saez-Atienzar et al., 2014). A reduction of the autophagic flux following LRRK2 pharmacological blockade with LRRK2-IN-1 and GSK2578215A was also observed in microglial and monocytic cells, which was associated with an impairment in clearance of Q74 protein aggregates in microglial cells (Schapansky et al., 2014). The reasons why these two sets of studies reached opposite conclusions is unclear, and might depend on cell models and protocols adopted. In addition, first generation LRRK2 inhibitors were used in these studies. Major limitation was also that none of these studies was designed to investigate whether LRRK2 inhibitors were neuroprotective.

In vivo studies did not help solve the issue. In fact, studies proving that dysregulation of autophagy is instrumental to the LRRK2-associated synucleinopathy *in vivo* are lacking. This is in part due to the general difficulty in reproducing a parkinsonian phenotype in LRRK2 KO, KI or transgenic mice (Volta and Melrose, 2017). In fact, genetic deletion of LRRK2 is not associated with nigrostriatal DA neuron degeneration whereas overexpression of hG2019S or hR1441C/G LRRK2 is inconsistently associated with late-onset nigrostriatal degeneration (Volta and Melrose, 2017). G2019S KI mice also do not show overt nigrostriatal neurodegeneration (Volta and Melrose, 2017), although functional and morphological changes at dopaminergic synapses and alterations of DA release have been reported along with aging, which might represent early sign of neuronal demise or susceptibility factors to parkinsonism (Yue et al., 2015; Longo et al., 2017; Novello et al., 2018).

Consistently, when these mice are exposed to parkinsonian toxins, they do show enhanced susceptibility to nigrostriatal degeneration. Thus, Daher et al. (2015) reported that G2019S transgenic rats were more prone than wild-type rats to develop nigrostriatal dopaminergic degeneration after AAV-mediated α-syn overexpression, whereas Karuppagounder et al. (2016) showed that G2019S transgenic mice were more sensitive to acute MPTP toxicity. Interestingly, subchronic administration of the second-generation LRRK2 kinase inhibitor PF-06447475 (West, 2017) reversed the neurotoxicity of α-syn overexpression not only in G2019S transgenic but also in wild-type rats. Although, the authors did not investigate whether this effect was due to a reduced α-syn burden mediated by an increase of the proteolytic events, this study revealed that pharmacological LRRK2 kinase inhibition could represent an appealing therapeutic approach also to idiopathic PD. This was confirmed by Greenamyre and collaborators who reported that repeated rotenone administration caused pSer1292 LRRK2 phosphorylation (index of LRRK2 activation) and pSer129 α-syn accumulation (possible early index of neurotoxicity) in SNc neurons, along with loss of nigrostriatal DA neurons which were reversed by systemic administration of the third-generation (West, 2017) LRRK2 inhibitor PF-360 (Di Maio et al., 2018; Rocha et al., 2019). Conversely, Henderson et al. (2019) failed to observe neuroprotection and clearance of α-syn aggregates in naïve mice injected with α-syn preformed fibrils (PFF), and chronically administered with the potent third-generation LRRK2 kinase inhibitor MLi-2. This would suggest that the contribution of LRRK2 to nigrostriatal degeneration might depend on the neurotoxicity pathways recruited in a specific experimental model of PD. Despite the role of LRRK2 inhibitor in idiopathic PD remains to be firmly established, these models offer the opportunity to elucidate whether ALP modulation contributes to the neuroprotection provided by LRRK2 inhibitors.

It is important to notice that these studies were performed in young-adult (i.e., 3-month-old) mice. Aged animals, however, might represent a more appropriate model to investigate the contribution of ALP to LRRK2-induced neurodegeneration. Indeed, aging is associated with autophagy and CMA impairment, and *in vivo* studies suggest that aging facilitates LRRK2-induced neurodegeneration. In fact, some studies in hG2019S and hR1441C transgenic mice reported a 18–50% loss of nigral DA neurons at old ages (16–21 months) (Ramonet et al., 2011; Chen et al., 2012; Weng et al., 2016) which were associated with morphological changes of AV and autophagosomes, reminiscent of ALP impairment (Ramonet et al., 2011). The view that aging might facilitate the onset of G2019S LRRK2 neurotoxicity might be further corroborated by the finding that virus-mediated overexpression of hG2019S LRRK2 in the striatum of C57BL/6J mice caused marked neuroinflammation associated with striatal cell loss (but not dopaminergic terminal loss) in 19-month-old but not 9–10-week-old mice (Kritzinger et al., 2018). Although quantification of these changes was not provided, qualitative analysis of microphotographs revealed that p62 accumulation was greater in aged mice, suggesting that impairment of autophagy might play a role in the underlying neurotoxic mechanisms. Changes in ALP markers (increase in LC3 puncta) were also observed in old BAC G2019S and BAC R1441C mice in the absence of overt neurodegeneration, suggesting that changes in ALP might precede neurodegeneration (Wallings et al., 2019).

Studies in G2019S KI mice carried out by Morari and collaborators pointed out an increase of α-syn pSer129 levels in the striatum and SNpc at 12 months but not earlier ages (Longo et al., 2017; Novello et al., 2018). Despite the α-syn signal is due to soluble forms of α-syn (Novello et al., 2018), it might reflect changes in proteostasis, and particularly a reduction of autophagic flux due to G2019S mutation (Schapansky et al., 2018). Consistently, when injected with an AAV2/9 overexpressing human A53T α-syn under the synapsin I promoter (Bourdenx et al., 2015; Arcuri et al., 2016), the aged animals showed a greater reduction of nigral DA neurons associated with greater accumulation of insoluble, PK-resistant α-syn and pSer129 α-syn aggregates in SNpc (Novello et al., 2018). This might reflect a reduced ability of old G2019S KI animals to cope with α-syn overload, as shown in old nematodes (Saha et al., 2015). LRRK2 mutations and aging will therefore work synergistically to inhibit ALP and, consequently, α-syn clearance, thereby facilitating disease progression and spreading; in this respect impaired autophagy has been viewed as an "aggravator" of PD (Johnson et al., 2019). These *in vivo* studies would therefore provide a rationale for pharmacological inhibition of LRRK2 kinase activity both in relation to neuroprotection and autophagy modulation.

We should also mention the careful *in vivo* work done by Giaime et al. (2017), showing that, different from LRRK2 or LRRK1 KO mice, DKO mice develop age-dependent DA neuron loss and ALP changes, which became significant at 14–15 months of age. Lack of both LRRK proteins also affected the viability of noradrenergic cells in locus coeruleus noradrenergic and striatal GABAergic medium-sized spiny neurons, and was associated with elevation of α-syn levels in striatum. Since changes in ALP markers preceded neuronal loss, these authors proposed that impairment of autophagy was instrumental to neurodegeneration (Giaime et al., 2017).

Finally, the role of impaired autophagy/CMA in PD may go beyond α-syn clearance, and changes in ALP might play a wider role in PD than hitherto imagined. Indeed, autophagy is active not only at the soma but also at the synaptic terminals, where it regulates synaptic protein quality control and synaptic activity (Hernandez et al., 2012; Vijayan and Verstreken, 2017). Soukup et al. (2016) have shown that protein quality control at synapses of *Drosophila melanogaster* is mediated by EndophilinA, a protein enriched in phagophore membranes, which is phosphorylated by LRRK2. LRRK2 phosphorylation allows the protein to create curved membranes that can harbor and recruit ATG3 to initiate autophagy (Soukup et al., 2016). Therefore, derangement of synaptic autophagy can affect synaptic homeostasis and plasticity which may increase the susceptibility to PD in the long term (Soukup et al., 2016, 2018; Vijayan and Verstreken, 2017).

CONCLUSION AND PERSPECTIVES

Autophagy is a key mechanism through which cells operate protein quality control and respond to environmental challenges. Autophagy activation can prolong the life-span of invertebrates and rodents, whereas impairment of autophagy leads to a number of disorders, among which neurodegenerative disorders of aging. A close association between autophagy and neurodegeneration has been established, although the casual link remains to be proven. In PD, ALP impairment can lead to increased levels of misfolded α-syn, accelerating its transport and spread throughout the brain. Aging, the major risk factor in PD, might facilitate this process since the efficiency of ALP machinery worsens over time. Genetic risk factors of PD, such as LRRK2 mutations, also impact on autophagy, although the control operated by LRRK2 and its mutants on ALP machinery is far from clear. *In vitro* studies offer evidence that G2019S LRRK2 causes autophagy and CMA impairment, and that autophagy activation rescues LRRK2-associated cell death or toxicity. Unfortunately, ALP changes measured in LRRK2 KO, KD and LRRK2 mutant transgenic mice are inconsistent, perhaps due the intrinsic complexity of the network through which LRRK2 controls autophagy, and the lack of standardized protocols to study autophagic flux *in vivo*. Furthermore, data obtained in transgenic mice should be taken with caution due to the obvious limitations of the models (e.g., non physiological expression levels of LRRK2, coexistence of endogenous and mutant LRRK2, neuronal pattern of LRRK2 expression). Finally, the lack of solid, progressive *in vivo* models of LRRK2-associated synucleinopathy has hindered the comprehension of the role of autophagy in LRRK2-associated parkinsonism, and discouraged the testing of potential disease-modifying agents, among which LRRK2 kinase inhibitors. The identification of early markers of neuronal demise in LRRK2 mice, among which alterations in presynaptic autophagy, will offer new opportunities for pharmacological intervention.

AUTHOR CONTRIBUTIONS

All authors listed have made a substantial, direct and intellectual contribution to the work, and approved it for publication.

FUNDING

This work was supported by a PRIN 2017 grant no. 2017LYTE9M to MM.

REFERENCES

Adams, J. M., and Cory, S. (1998). The Bcl-2 protein family: arbiters of cell survival. *Science* 281, 1322–1326. doi: 10.1126/science.281.5381.1322

Alegre-Abarrategui, J., Christian, H., Lufino, M. M., Mutihac, R., Venda, L. L., Ansorge, O., et al. (2009). LRRK2 regulates autophagic activity and localizes to specific membrane microdomains in a novel human genomic reporter cellular model. *Hum. Mol. Genet.* 18, 4022–4034. doi: 10.1093/hmg/ddp346

Alvarez-Erviti, L., Rodriguez-Oroz, M. C., Cooper, J. M., Caballero, C., Ferrer, I., Obeso, J. A., et al. (2010). Chaperone-mediated autophagy markers in Parkinson disease brains. *Arch. Neurol.* 67, 1464–1472. doi: 10.1001/archneurol.2010.198

Arcuri, L., Viaro, R., Bido, S., Longo, F., Calcagno, M., Fernagut, P. O., et al. (2016). Genetic and pharmacological evidence that endogenous nociceptin/orphanin FQ contributes to dopamine cell loss in Parkinson's disease. *Neurobiol. Dis.* 89, 55–64. doi: 10.1016/j.nbd.2016.01.016

Balch, W. E., Morimoto, R. I., Dillin, A., and Kelly, J. W. (2008). Adapting proteostasis for disease intervention. *Science* 319, 916–919. doi: 10.1126/science.1141448

Baptista, M. A., Dave, K. D., Frasier, M. A., Sherer, T. B., Greeley, M., Beck, M. J., et al. (2013). Loss of leucine-rich repeat kinase 2 (LRRK2) in rats leads to progressive abnormal phenotypes in peripheral organs. *PLoS One* 8:e80705. doi: 10.1371/journal.pone.0080705

Ben-Zvi, A., Miller, E. A., and Morimoto, R. I. (2009). Collapse of proteostasis represents an early molecular event in *Caenorhabditis elegans* aging. *Proc. Natl. Acad. Sci. U.S.A.* 106, 14914–14919. doi: 10.1073/pnas.0902882106

Bergamini, C. M., and Signorini, M. (1991). Exploring the catalytic mechanism of skeletal muscle UDP-glucose pyrophosphorylase: identification of a hyperreactive cysteine at the enzyme active site. *Int. J. Biochem.* 23, 123–127.

Bergamini, E., Cavallini, G., Donati, A., and Gori, Z. (2004). The role of macroautophagy in the ageing process, anti-ageing intervention and age-associated diseases. *Int. J. Biochem. Cell Biol.* 36, 2392–2404. doi: 10.1016/j.biocel.2004.05.007

Berger, Z., Ravikumar, B., Menzies, F. M., Oroz, L. G., Underwood, B. R., Pangalos, M. N., et al. (2006). Rapamycin alleviates toxicity of different aggregate-prone proteins. *Hum. Mol. Genet.* 15, 433–442. doi: 10.1093/hmg/ddi458

Bingol, B. (2018). Autophagy and lysosomal pathways in nervous system disorders. *Mol. Cell Neurosci.* 91, 167–208. doi: 10.1016/j.mcn.2018.04.009

Biskup, S., Moore, D. J., Celsi, F., Higashi, S., West, A. B., Andrabi, S. A., et al. (2006). Localization of LRRK2 to membranous and vesicular structures in mammalian brain. *Ann. Neurol.* 60, 557–569. doi: 10.1002/ana.21019

Boland, B., and Nixon, R. A. (2006). Neuronal macroautophagy: from development to degeneration. *Mol. Aspects Med.* 27, 503–519. doi: 10.1016/j.mam.2006.08.009

Boland, B., Yu, W. H., Corti, O., Mollereau, B., Henriques, A., Bezard, E., et al. (2018). Promoting the clearance of neurotoxic proteins in neurodegenerative disorders of ageing. *Nat. Rev. Drug Discov.* 17, 660–688. doi: 10.1038/nrd.2018.109

Bonello, F., Hassoun, S. M., Mouton-Liger, F., Shin, Y. S., Muscat, A., Tesson, C., et al. (2019). LRRK2 impairs PINK1/Parkin-dependent mitophagy via its kinase activity: pathologic insights into Parkinson's disease. *Hum. Mol. Genet.* 28, 1645–1660. doi: 10.1093/hmg/ddz004

Bootman, M. D., Chehab, T., Bultynck, G., Parys, J. B., and Rietdorf, K. (2018). The regulation of autophagy by calcium signals: do we have a consensus? *Cell Calcium* 70, 32–46. doi: 10.1016/j.ceca.2017.08.005

Bourdenx, M., Dovero, S., Engeln, M., Bido, S., Bastide, M. F., Dutheil, N., et al. (2015). Lack of additive role of ageing in nigrostriatal neurodegeneration triggered by alpha-synuclein overexpression. *Acta Neuropathol. Commun.* 3:46. doi: 10.1186/s40478-015-0222-2

Bourdenx, M., Koulakiotis, N. S., Sanoudou, D., Bezard, E., Dehay, B., and Tsarbopoulos, A. (2017). Protein aggregation and neurodegeneration in prototypical neurodegenerative diseases: examples of amyloidopathies, tauopathies and synucleinopathies. *Prog. Neurobiol.* 155, 171–193. doi: 10.1016/j.pneurobio.2015.07.003

Bravo-San Pedro, J. M., Niso-Santano, M., Gomez-Sanchez, R., Pizarro-Estrella, E., Aiastui-Pujana, A., Gorostidi, A., et al. (2013). The LRRK2 G2019S mutant exacerbates basal autophagy through activation of the MEK/ERK pathway. *Cell. Mol. Life Sci.* 70, 121–136. doi: 10.1007/s00018-012-1061-y

Brown, E. J., Albers, M. W., Shin, T. B., Ichikawa, K., Keith, C. T., Lane, W. S., et al. (1994). A mammalian protein targeted by G1-arresting rapamycin-receptor complex. *Nature* 369, 756–758. doi: 10.1038/369756a0

Brundin, P., and Melki, R. (2017). Prying into the prion hypothesis for Parkinson's disease. *J. Neurosci.* 37, 9808–9818. doi: 10.1523/JNEUROSCI.1788-16.2017

Brundin, P., Melki, R., and Kopito, R. (2010). Prion-like transmission of protein aggregates in neurodegenerative diseases. *Nat. Rev. Mol. Cell Biol.* 11, 301–307. doi: 10.1038/nrm2873

Chakraborty, D., Felzen, V., Hiebel, C., Sturner, E., Perumal, N., Manicam, C., et al. (2019). Enhanced autophagic-lysosomal activity and increased BAG3-mediated selective macroautophagy as adaptive response of neuronal cells to chronic oxidative stress. *Redox Biol.* 24:101181. doi: 10.1016/j.redox.2019.101181

Chan, E. Y. (2009). mTORC1 phosphorylates the ULK1-mAtg13-FIP200 autophagy regulatory complex. *Sci. Signal.* 2:pe51. doi: 10.1126/scisignal.284pe51

Chen, C. Y., Weng, Y. H., Chien, K. Y., Lin, K. J., Yeh, T. H., Cheng, Y. P., et al. (2012). (G2019S) LRRK2 activates MKK4-JNK pathway and causes degeneration of SN dopaminergic neurons in a transgenic mouse model of PD. *Cell Death Differ.* 19, 1623–1633. doi: 10.1038/cdd.2012.42.

Chiang, H. L., and Dice, J. F. (1988). Peptide sequences that target proteins for enhanced degradation during serum withdrawal. *J. Biol. Chem.* 263, 6797–6805.

Chiang, H. L., Terlecky, S. R., Plant, C. P., and Dice, J. F. (1989). A role for a 70-kilodalton heat shock protein in lysosomal degradation of intracellular proteins. *Science* 246, 382–385. doi: 10.1126/science.2799391

Chu, Y., Dodiya, H., Aebischer, P., Olanow, C. W., and Kordower, J. H. (2009). Alterations in lysosomal and proteasomal markers in Parkinson's disease: relationship to alpha-synuclein inclusions. *Neurobiol. Dis.* 35, 385–398. doi: 10.1016/j.nbd.2009.05.023

Ciechanover, A., and Kwon, Y. T. (2017). Protein quality control by molecular chaperones in neurodegeneration. *Front. Neurosci.* 11:185. doi: 10.3389/fnins.2017.00185

Conway, O., Akpinar, H. A., Rogov, V., and Kirkin, V. (2019). Selective autophagy receptors in neuronal health and disease. *J Mol Biol.* doi: 10.1016/j.jmb.2019.10.013 [Epub ahead of print].

Cookson, M. R. (2010). The role of leucine-rich repeat kinase 2 (LRRK2) in Parkinson's disease. *Nat. Rev. Neurosci.* 11, 791–797. doi: 10.1038/nrn2935

Crews, L., Spencer, B., Desplats, P., Patrick, C., Paulino, A., Rockenstein, E., et al. (2010). Selective molecular alterations in the autophagy pathway in patients with Lewy body disease and in models of alpha-synucleinopathy. *PLoS One* 5:e9313. doi: 10.1371/journal.pone.0009313

Cuervo, A. M., Bergamini, E., Brunk, U. T., Droge, W., Ffrench, M., and Terman, A. (2005). Autophagy and aging: the importance of maintaining "clean" cells. *Autophagy* 1, 131–140. doi: 10.4161/auto.1.3.2017

Cuervo, A. M., and Dice, J. F. (2000). Regulation of lamp2a levels in the lysosomal membrane. *Traffic* 1, 570–583.

Cuervo, A. M., Dice, J. F., and Knecht, E. (1997). A population of rat liver lysosomes responsible for the selective uptake and degradation of cytosolic proteins. *J. Biol. Chem.* 272, 5606–5615. doi: 10.1074/jbc.272.9.5606

Cuervo, A. M., Stefanis, L., Fredenburg, R., Lansbury, P. T., and Sulzer, D. (2004). Impaired degradation of mutant alpha-synuclein by chaperone-mediated autophagy. *Science* 305, 1292–1295. doi: 10.1126/science.1101738

Daher, J. P., Abdelmotilib, H. A., Hu, X., Volpicelli-Daley, L. A., Moehle, M. S., Fraser, K. B., et al. (2015). Leucine-rich repeat

kinase 2 (LRRK2) pharmacological inhibition abates alpha-synuclein gene-induced neurodegeneration. *J. Biol. Chem.* 290, 19433–19444. doi: 10.1074/jbc.M115.660001

Dehay, B., Bove, J., Rodriguez-Muela, N., Perier, C., Recasens, A., Boya, P., et al. (2010). Pathogenic lysosomal depletion in Parkinson's disease. *J. Neurosci.* 30, 12535–12544. doi: 10.1523/JNEUROSCI.1920-10.2010

Del Roso, A., Vittorini, S., Cavallini, G., Donati, A., Gori, Z., Masini, M., et al. (2003). Ageing-related changes in the in vivo function of rat liver macroautophagy and proteolysis. *Exp. Gerontol.* 38, 519–527.

Deretic, V., and Klionsky, D. J. (2018). Autophagy and inflammation: a special review issue. *Autophagy* 14, 179–180. doi: 10.1080/15548627.2017.1412229

Deter, R. L., Baudhuin, P., and De Duve, C. (1967). Participation of lysosomes in cellular autophagy induced in rat liver by glucagon. *J. Cell Biol.* 35, C11–C16. doi: 10.1083/jcb.35.2.c11

Di Maio, R., Hoffman, E. K., Rocha, E. M., Keeney, M. T., Sanders, L. H., De Miranda, B. R., et al. (2018). LRRK2 activation in idiopathic Parkinson's disease. *Sci. Transl. Med.* 10:eaar5429. doi: 10.1126/scitranslmed.aar5429

Dice, J. F., Chiang, H. L., Spencer, E. P., and Backer, J. M. (1986). Regulation of catabolism of microinjected ribonuclease A. Identification of residues 7-11 as the essential pentapeptide. *J. Biol. Chem.* 261, 6853–6859.

Dikic, I. (2017). Proteasomal and autophagic degradation systems. *Annu. Rev. Biochem.* 86, 193–224. doi: 10.1146/annurev-biochem-061516-44908

Dodson, M. W., Leung, L. K., Lone, M., Lizzio, M. A., and Guo, M. (2014). Novel ethyl methanesulfonate (EMS)-induced null alleles of the *Drosophila* homolog of LRRK2 reveal a crucial role in endolysosomal functions and autophagy in vivo. *Dis. Model. Mech.* 7, 1351–1363. doi: 10.1242/dmm.017020

Dodson, M. W., Zhang, T., Jiang, C., Chen, S., and Guo, M. (2012). Roles of the *Drosophila* LRRK2 homolog in Rab7-dependent lysosomal positioning. *Hum. Mol. Genet.* 21, 1350–1363. doi: 10.1093/hmg/ddr573

Donati, A., Cavallini, G., Paradiso, C., Vittorini, S., Pollera, M., Gori, Z., et al. (2001). Age-related changes in the autophagic proteolysis of rat isolated liver cells: effects of antiaging dietary restrictions. *J. Gerontol. A Biol. Sci. Med. Sci.* 56, B375–B383. doi: 10.1093/gerona/56.9.b375

Dou, Z., Pan, J. A., Dbouk, H. A., Ballou, L. M., DeLeon, J. L., Fan, Y., et al. (2013). Class IA PI3K p110beta subunit promotes autophagy through Rab5 small GTPase in response to growth factor limitation. *Mol. Cell* 50, 29–42. doi: 10.1016/j.molcel.2013.01.022

Farre, J. C., and Subramani, S. (2004). Peroxisome turnover by micropexophagy: an autophagy-related process. *Trends Cell Biol.* 14, 515–523. doi: 10.1016/j.tcb.2004.07.014

Fekadu, J., and Rami, A. (2016). Beclin-1 deficiency alters autophagosome formation, lysosome biogenesis and enhances neuronal vulnerability of HT22 hippocampal cells. *Mol. Neurobiol.* 53, 5500–5509. doi: 10.1007/s12035-015-9453-2

Feldmann, A., Bekbulat, F., Huesmann, H., Ulbrich, S., Tatzelt, J., Behl, C., et al. (2017). The RAB GTPase RAB18 modulates macroautophagy and proteostasis. *Biochem. Biophys. Res. Commun.* 486, 738–743. doi: 10.1016/j.bbrc.2017.03.112

Fuji, R. N., Flagella, M., Baca, M., Baptista, M. A., Brodbeck, J., Chan, B. K., et al. (2015). Effect of selective LRRK2 kinase inhibition on nonhuman primate lung. *Sci. Transl. Med.* 7:273ra215. doi: 10.1126/scitranslmed.aaa3634

Fullgrabe, J., Ghislat, G., Cho, D. H., and Rubinsztein, D. C. (2016). Transcriptional regulation of mammalian autophagy at a glance. *J. Cell Sci.* 129, 3059–3066. doi: 10.1242/jcs.188920

Gal, J., Strom, A. L., Kwinter, D. M., Kilty, R., Zhang, J., Shi, P., et al. (2009). Sequestosome 1/p62 links familial ALS mutant SOD1 to LC3 via an ubiquitin-independent mechanism. *J. Neurochem.* 111, 1062–1073. doi: 10.1111/j.1471-4159.2009.06388.x

Galluzzi, L., Bravo-San Pedro, J. M., Levine, B., Green, D. R., and Kroemer, G. (2017). Pharmacological modulation of autophagy: therapeutic potential and persisting obstacles. *Nat. Rev. Drug Discov.* 16, 487–511. doi: 10.1038/nrd.2017.22

Ganley, I. G., Lam du, H., Wang, J., Ding, X., Chen, S., and Jiang, X. (2009). ULK1.ATG13.FIP200 complex mediates mTOR signaling and is essential for autophagy. *J. Biol. Chem.* 284, 12297–12305. doi: 10.1074/jbc.M900573200

Gasser, T. (2009). Molecular pathogenesis of Parkinson disease: insights from genetic studies. *Expert Rev. Mol. Med.* 11:e22. doi: 10.1017/S1462399409001148

Gautier, C. A., Kitada, T., and Shen, J. (2008). Loss of PINK1 causes mitochondrial functional defects and increased sensitivity to oxidative stress. *Proc. Natl. Acad. Sci. U.S.A.* 105, 11364–11369. doi: 10.1073/pnas.0802076105

Georgakopoulos, N. D., Wells, G., and Campanella, M. (2017). The pharmacological regulation of cellular mitophagy. *Nat. Chem. Biol.* 13, 136–146. doi: 10.1038/nchembio.2287

Giaime, E., Tong, Y., Wagner, L. K., Yuan, Y., Huang, G., and Shen, J. (2017). Age-dependent dopaminergic neurodegeneration and impairment of the autophagy-lysosomal pathway in LRRK-deficient mice. *Neuron* 96, 796.e6–807.e6. doi: 10.1016/j.neuron.2017.09.036.

Goldberg, M. S., Fleming, S. M., Palacino, J. J., Cepeda, C., Lam, H. A., Bhatnagar, A., et al. (2003). Parkin-deficient mice exhibit nigrostriatal deficits but not loss of dopaminergic neurons. *J. Biol. Chem.* 278, 43628–43635. doi: 10.1074/jbc.M308947200.

Gomez-Suaga, P., Churchill, G. C., Patel, S., and Hilfiker, S. (2012a). A link between LRRK2, autophagy and NAADP-mediated endolysosomal calcium signalling. *Biochem. Soc. Trans.* 40, 1140–1146. doi: 10.1042/BST20120138

Gomez-Suaga, P., and Hilfiker, S. (2012). LRRK2 as a modulator of lysosomal calcium homeostasis with downstream effects on autophagy. *Autophagy* 8, 692–693. doi: 10.4161/auto.19305

Gomez-Suaga, P., Luzon-Toro, B., Churamani, D., Zhang, L., Bloor-Young, D., Patel, S., et al. (2012b). Leucine-rich repeat kinase 2 regulates autophagy through a calcium-dependent pathway involving NAADP. *Hum. Mol. Genet.* 21, 511–525. doi: 10.1093/hmg/ddr481

Grandison, R. C., Wong, R., Bass, T. M., Partridge, L., and Piper, M. D. (2009). Effect of a standardised dietary restriction protocol on multiple laboratory strains of *Drosophila melanogaster*. *PLoS One* 4:e4067. doi: 10.1371/journal.pone.0004067

Greggio, E., Jain, S., Kingsbury, A., Bandopadhyay, R., Lewis, P., Kaganovich, A., et al. (2006). Kinase activity is required for the toxic effects of mutant LRRK2/dardarin. *Neurobiol. Dis.* 23, 329–341. doi: 10.1016/j.nbd.2006.04.001

Gross, A., McDonnell, J. M., and Korsmeyer, S. J. (1999). BCL-2 family members and the mitochondria in apoptosis. *Genes Dev.* 13, 1899–1911. doi: 10.1101/gad.13.15.1899

Hakimi, M., Selvanantham, T., Swinton, E., Padmore, R. F., Tong, Y., Kabbach, G., et al. (2011). Parkinson's disease-linked LRRK2 is expressed in circulating and tissue immune cells and upregulated following recognition of microbial structures. *J. Neural Transm.* 118, 795–808. doi: 10.1007/s00702-011-0653-2

Hara, T., Nakamura, K., Matsui, M., Yamamoto, A., Nakahara, Y., Suzuki-Migishima, R., et al. (2006). Suppression of basal autophagy in neural cells causes neurodegenerative disease in mice. *Nature* 441, 885–889. doi: 10.1038/nature04724

Hara, T., Takamura, A., Kishi, C., Iemura, S., Natsume, T., Guan, J. L., et al. (2008). FIP200, a ULK-interacting protein, is required for autophagosome formation in mammalian cells. *J. Cell Biol.* 181, 497–510. doi: 10.1083/jcb.200712064

Harrison, D. E., Strong, R., Sharp, Z. D., Nelson, J. F., Astle, C. M., Flurkey, K., et al. (2009). Rapamycin fed late in life extends lifespan in genetically heterogeneous mice. *Nature* 460, 392–395. doi: 10.1038/nature08221

Hars, E. S., Qi, H., Ryazanov, A. G., Jin, S., Cai, L., Hu, C., et al. (2007). Autophagy regulates ageing in *C. elegans*. *Autophagy* 3, 93–95. doi: 10.4161/auto.3636

Hartlova, A., Herbst, S., Peltier, J., Rodgers, A., Bilkei-Gorzo, O., Fearns, A., et al. (2018). LRRK2 is a negative regulator of *Mycobacterium tuberculosis* phagosome maturation in macrophages. *EMBO J.* 37:e98694. doi: 10.15252/embj.201798694

Henderson, M. X., Sengupta, M., McGeary, I., Zhang, B., Olufemi, M. F., Brown, H., et al. (2019). LRRK2 inhibition does not impart protection from alpha-synuclein pathology and neuron death in non-transgenic mice. *Acta Neuropathol. Commun.* 7:28. doi: 10.1186/s40478-019-0679-5

Hernandez, D., Torres, C. A., Setlik, W., Cebrian, C., Mosharov, E. V., Tang, G., et al. (2012). Regulation of presynaptic neurotransmission by macroautophagy. *Neuron* 74, 277–284. doi: 10.1016/j.neuron.2012.02.020

Hertz, N. T., Berthet, A., Sos, M. L., Thorn, K. S., Burlingame, A. L., Nakamura, K., et al. (2013). A neo-substrate that amplifies catalytic activity of parkinson's-disease-related kinase PINK1. *Cell* 154, 737–747. doi: 10.1016/j.cell.2013.07.030

Herzig, M. C., Kolly, C., Persohn, E., Theil, D., Schweizer, T., Hafner, T., et al. (2011). LRRK2 protein levels are determined by kinase function and are crucial

for kidney and lung homeostasis in mice. *Hum. Mol. Genet.* 20, 4209–4223. doi: 10.1093/hmg/ddr348

Higashi, S., Moore, D. J., Minegishi, M., Kasanuki, K., Fujishiro, H., Kabuta, T., et al. (2011). Localization of MAP1-LC3 in vulnerable neurons and Lewy bodies in brains of patients with dementia with Lewy bodies. *J. Neuropathol. Exp. Neurol.* 70, 264–280. doi: 10.1097/NEN.0b013e318211c86a

Hinkle, K. M., Yue, M., Behrouz, B., Dachsel, J. C., Lincoln, S. J., Bowles, E. E., et al. (2012). LRRK2 knockout mice have an intact dopaminergic system but display alterations in exploratory and motor co-ordination behaviors. *Mol. Neurodegener.* 7:25. doi: 10.1186/1750-1326-7-25

Ho, D. H., Kim, H., Nam, D., Sim, H., Kim, J., Kim, H. G., et al. (2018). LRRK2 impairs autophagy by mediating phosphorylation of leucyl-tRNA synthetase. *Cell Biochem. Funct.* 36, 431–442. doi: 10.1002/cbf.3364

Ho, P. W., Leung, C. T., Liu, H., Pang, S. Y., Lam, C. S., Xian, J., et al. (2019). Age-dependent accumulation of oligomeric SNCA/alpha-synuclein from impaired degradation in mutant LRRK2 knockin mouse model of Parkinson disease: role for therapeutic activation of chaperone-mediated autophagy (CMA). *Autophagy* doi: 10.1080/15548627.2019.1603545 [Epub ahead of print].

Ho, T. T., Warr, M. R., Adelman, E. R., Lansinger, O. M., Flach, J., Verovskaya, E. V., et al. (2017). Autophagy maintains the metabolism and function of young and old stem cells. *Nature* 543, 205–210. doi: 10.1038/nature21388

Hohn, A., Weber, D., Jung, T., Ott, C., Hugo, M., Kochlik, B., et al. (2017). Happily (n)ever after: aging in the context of oxidative stress, proteostasis loss and cellular senescence. *Redox Biol.* 11, 482–501. doi: 10.1016/j.redox.2016.12.001

Imai, Y., Gehrke, S., Wang, H. Q., Takahashi, R., Hasegawa, K., Oota, E., et al. (2008). Phosphorylation of 4E-BP by LRRK2 affects the maintenance of dopaminergic neurons in *Drosophila*. *EMBO J.* 27, 2432–2443. doi: 10.1038/emboj.2008.163

Ishii, T., Yanagawa, T., Kawane, T., Yuki, K., Seita, J., Yoshida, H., et al. (1996). Murine peritoneal macrophages induce a novel 60-kDa protein with structural similarity to a tyrosine kinase p56lck-associated protein in response to oxidative stress. *Biochem. Biophys. Res. Commun.* 226, 456–460. doi: 10.1006/bbrc.1996.1377

Itier, J. M., Ibanez, P., Mena, M. A., Abbas, N., Cohen-Salmon, C., Bohme, G. A., et al. (2003). Parkin gene inactivation alters behaviour and dopamine neurotransmission in the mouse. *Hum. Mol. Genet.* 12, 2277–2291. doi: 10.1093/hmg/ddg239

Ito, G., Katsemonova, K., Tonelli, F., Lis, P., Baptista, M. A., Shpiro, N., et al. (2016). Phos-tag analysis of Rab10 phosphorylation by LRRK2: a powerful assay for assessing kinase function and inhibitors. *Biochem. J.* 473, 2671–2685. doi: 10.1042/BCJ20160557

Jang, J. Y., Blum, A., Liu, J., and Finkel, T. (2018). The role of mitochondria in aging. *J. Clin. Invest.* 128, 3662–3670. doi: 10.1172/JCI120842

Jin, S. M., and Youle, R. J. (2012). PINK1- and Parkin-mediated mitophagy at a glance. *J. Cell Sci.* 125(Pt 4), 795–799. doi: 10.1242/jcs.093849

Johnson, M. E., Stecher, B., Labrie, V., Brundin, L., and Brundin, P. (2019). Triggers, facilitators, and aggravators: redefining Parkinson's disease pathogenesis. *Trends Neurosci.* 42, 4–13. doi: 10.1016/j.tins.2018.09.007

Kaeberlein, M., Powers, R. W. 3rd, Steffen, K. K., Westman, E. A., Hu, D., Dang, N., et al. (2005). Regulation of yeast replicative life span by TOR and Sch9 in response to nutrients. *Science* 310, 1193–1196. doi: 10.1126/science.1115535

Kalia, L. V., Lang, A. E., Hazrati, L. N., Fujioka, S., Wszolek, Z. K., Dickson, D. W., et al. (2015). Clinical correlations with Lewy body pathology in LRRK2-related Parkinson disease. *JAMA Neurol.* 72, 100–105. doi: 10.1001/jamaneurol.2014.2704.

Kapahi, P., Chen, D., Rogers, A. N., Katewa, S. D., Li, P. W., Thomas, E. L., et al. (2010). With TOR, less is more: a key role for the conserved nutrient-sensing TOR pathway in aging. *Cell Metab.* 11, 453–465. doi: 10.1016/j.cmet.2010.05.001.

Kapahi, P., Zid, B. M., Harper, T., Koslover, D., Sapin, V., and Benzer, S. (2004). Regulation of lifespan in *Drosophila* by modulation of genes in the TOR signaling pathway. *Curr. Biol.* 14, 885–890. doi: 10.1016/j.cub.2004.03.059

Karuppagounder, S. S., Xiong, Y., Lee, Y., Lawless, M. C., Kim, D., Nordquist, E., et al. (2016). LRRK2 G2019S transgenic mice display increased susceptibility to 1-methyl-4-phenyl-1,2,3,6-tetrahydropyridine (MPTP)-mediated neurotoxicity. *J. Chem. Neuroanat.* 76(Pt B), 90–97. doi: 10.1016/j.jchemneu.2016.01.007

Kaushik, S., and Cuervo, A. M. (2012). Chaperone-mediated autophagy: a unique way to enter the lysosome world. *Trends Cell Biol.* 22, 407–417. doi: 10.1016/j.tcb.2012.05.006

Kenessey, A., Banay-Schwartz, M., DeGuzman, T., and Lajtha, A. (1989). Increase in cathepsin D activity in rat brain in aging. *J. Neurosci. Res.* 23, 454–456. doi: 10.1002/jnr.490230412

Kim, J., Kundu, M., Viollet, B., and Guan, K. L. (2011). AMPK and mTOR regulate autophagy through direct phosphorylation of Ulk1. *Nat. Cell Biol.* 13, 132–141. doi: 10.1038/ncb2152

Kim, Y. C., and Guan, K. L. (2015). mTOR: a pharmacologic target for autophagy regulation. *J. Clin. Invest.* 125, 25–32. doi: 10.1172/JCI73939

Kimura, T., Jain, A., Choi, S. W., Mandell, M. A., Schroder, K., Johansen, T., et al. (2015). TRIM-mediated precision autophagy targets cytoplasmic regulators of innate immunity. *J. Cell Biol.* 210, 973–989. doi: 10.1083/jcb.201503023

Kitada, T., Asakawa, S., Hattori, N., Matsumine, H., Yamamura, Y., Minoshima, S., et al. (1998). Mutations in the parkin gene cause autosomal recessive juvenile parkinsonism. *Nature* 392, 605–608. doi: 10.1038/33416

Kitada, T., Pisani, A., Karouani, M., Haburcak, M., Martella, G., Tscherter, A., et al. (2009). Impaired dopamine release and synaptic plasticity in the striatum of parkin-/- mice. *J. Neurochem.* 110, 613–621. doi: 10.1111/j.1471-4159.2009.06152.x

Klinkenberg, M., Thurow, N., Gispert, S., Ricciardi, F., Eich, F., Prehn, J. H., et al. (2010). Enhanced vulnerability of PARK6 patient skin fibroblasts to apoptosis induced by proteasomal stress. *Neuroscience* 166, 422–434. doi: 10.1016/j.neuroscience.2009.12.068

Klionsky, D. J. (2005). The molecular machinery of autophagy: unanswered questions. *J. Cell Sci.* 118(Pt 1), 7–18. doi: 10.1242/jcs.01620

Klionsky, D. J., Abdelmohsen, K., Abe, A., Abedin, M. J., Abeliovich, H., Acevedo Arozena, A., et al. (2016). Guidelines for the use and interpretation of assays for monitoring autophagy (3rd edition). *Autophagy* 12, 1–222. doi: 10.1080/15548627.2015.1100356

Klionsky, D. J., Cregg, J. M., Dunn, W. A. Jr, Emr, S. D., Sakai, Y., et al. (2003). A unified nomenclature for yeast autophagy-related genes. *Dev. Cell* 5, 539–545.

Klionsky, D. J. (2012). Look people, "Atg" is an abbreviation for "autophagy-related." That's it. *Autophagy* 8, 1281–1282. doi: 10.4161/auto.21812

Komatsu, M., Kominami, E., and Tanaka, K. (2006a). Autophagy and neurodegeneration. *Autophagy* 2, 315–317. doi: 10.4161/auto.2974

Komatsu, M., Waguri, S., Chiba, T., Murata, S., Iwata, J., Tanida, I., et al. (2006b). Loss of autophagy in the central nervous system causes neurodegeneration in mice. *Nature* 441, 880–884. doi: 10.1038/nature04723

Komatsu, M., Waguri, S., Koike, M., Sou, Y. S., Ueno, T., Hara, T., et al. (2007a). Homeostatic levels of p62 control cytoplasmic inclusion body formation in autophagy-deficient mice. *Cell* 131, 1149–1163. doi: 10.1016/j.cell.2007.10.035

Komatsu, M., Wang, Q. J., Holstein, G. R., Friedrich, V. L. Jr, Iwata, J., et al. (2007b). Essential role for autophagy protein Atg7 in the maintenance of axonal homeostasis and the prevention of axonal degeneration. *Proc. Natl. Acad. Sci. U.S.A.* 104, 14489–14494. doi: 10.1073/pnas.0701311104

Kritzinger, A., Ferger, B., Gillardon, F., Stierstorfer, B., Birk, G., Kochanek, S., et al. (2018). Age-related pathology after adenoviral overexpression of the leucine-rich repeat kinase 2 in the mouse striatum. *Neurobiol. Aging* 66, 97–111. doi: 10.1016/j.neurobiolaging.2018.02.008

Laberge, R. M., Sun, Y., Orjalo, A. V., Patil, C. K., Freund, A., Zhou, L., et al. (2015). MTOR regulates the pro-tumorigenic senescence-associated secretory phenotype by promoting IL1A translation. *Nat. Cell Biol.* 17, 1049–1061. doi: 10.1038/ncb3195

Li, Y., Liu, W., Oo, T. F., Wang, L., Tang, Y., Jackson-Lewis, V., et al. (2009). Mutant LRRK2(R1441G) BAC transgenic mice recapitulate cardinal features of Parkinson's disease. *Nat. Neurosci.* 12, 826–828. doi: 10.1038/nn.2349

Lim, C. Y., and Zoncu, R. (2016). The lysosome as a command-and-control center for cellular metabolism. *J. Cell Biol.* 214, 653–664. doi: 10.1083/jcb.201607005

Lippai, M., and Low, P. (2014). The role of the selective adaptor p62 and ubiquitin-like proteins in autophagy. *Biomed. Res. Int.* 2014:832704. doi: 10.1155/2014/832704.

Liu, H. F., Lu, S., Ho, P. W., Tse, H. M., Pang, S. Y., Kung, M. H., et al. (2014). LRRK2 R1441G mice are more liable to dopamine depletion and locomotor inactivity. *Ann. Clin. Transl. Neurol.* 1, 199–208. doi: 10.1002/acn3.45

Longo, F., Mercatelli, D., Novello, S., Arcuri, L., Brugnoli, A., Vincenzi, F., et al. (2017). Age-dependent dopamine transporter dysfunction and Serine129

phospho-alpha-synuclein overload in G2019S LRRK2 mice. *Acta Neuropathol. Commun.* 5:22. doi: 10.1186/s40478-017-0426-8

MacLeod, D., Dowman, J., Hammond, R., Leete, T., Inoue, K., and Abeliovich, A. (2006). The familial Parkinsonism gene LRRK2 regulates neurite process morphology. *Neuron* 52, 587–593. doi: 10.1016/j.neuron.2006.10.008

Mamais, A., Manzoni, C., Nazish, I., Arber, C., Sonustun, B., Wray, S., et al. (2018). Analysis of macroautophagy related proteins in G2019S LRRK2 Parkinson's disease brains with Lewy body pathology. *Brain Res.* 1701, 75–84. doi: 10.1016/j.brainres.2018.07.023

Mamais, A., Raja, M., Manzoni, C., Dihanich, S., Lees, A., Moore, D., et al. (2013). Divergent alpha-synuclein solubility and aggregation properties in G2019S LRRK2 Parkinson's disease brains with Lewy Body pathology compared to idiopathic cases. *Neurobiol. Dis.* 58, 183–190. doi: 10.1016/j.nbd.2013.05.017

Manzoni, C., and Lewis, P. A. (2017). LRRK2 and autophagy. *Adv. Neurobiol.* 14, 89–105. doi: 10.1007/978-3-319-49969-7_5

Manzoni, C., Mamais, A., Dihanich, S., Abeti, R., Soutar, M. P. M., Plun-Favreau, H., et al. (2013a). Inhibition of LRRK2 kinase activity stimulates macroautophagy. *Biochim. Biophys. Acta* 1833, 2900–2910. doi: 10.1016/j.bbamcr.2013.07.020

Manzoni, C., Mamais, A., Dihanich, S., McGoldrick, P., Devine, M. J., Zerle, J., et al. (2013b). Pathogenic Parkinson's disease mutations across the functional domains of LRRK2 alter the autophagic/lysosomal response to starvation. *Biochem. Biophys. Res. Commun.* 441, 862–866. doi: 10.1016/j.bbrc.2013.10.159

Manzoni, C., Mamais, A., Dihanich, S., Soutar, M. P. M., Plun-Favreau, H., Bandopadhyay, R., et al. (2018). mTOR independent alteration in ULK1 Ser758 phosphorylation following chronic LRRK2 kinase inhibition. *Biosci. Rep.* 38:BSR20171669. doi: 10.1042/BSR20171669

Manzoni, C., Mamais, A., Roosen, D. A., Dihanich, S., Soutar, M. P., Plun-Favreau, H., et al. (2016). mTOR independent regulation of macroautophagy by Leucine Rich Repeat Kinase 2 via Beclin-1. *Sci. Rep.* 6:35106. doi: 10.1038/srep35106

Marras, C., Schule, B., Munhoz, R. P., Rogaeva, E., Langston, J. W., Kasten, M., et al. (2011). Phenotype in parkinsonian and nonparkinsonian LRRK2 G2019S mutation carriers. *Neurology* 77, 325–333. doi: 10.1212/WNL.0b013e318227042d

Martina, J. A., Diab, H. I., Brady, O. A., and Puertollano, R. (2016). TFEB and TFE3 are novel components of the integrated stress response. *EMBO J.* 35, 479–495. doi: 10.15252/embj.201593428

Martinez-Vicente, M., Talloczy, Z., Kaushik, S., Massey, A. C., Mazzulli, J., Mosharov, E. V., et al. (2008). Dopamine-modified alpha-synuclein blocks chaperone-mediated autophagy. *J. Clin. Invest.* 118, 777–788. doi: 10.1172/JCI32806

Massey, A. C., Zhang, C., and Cuervo, A. M. (2006). Chaperone-mediated autophagy in aging and disease. *Curr. Top. Dev. Biol.* 73, 205–235. doi: 10.1016/S0070-215373007-6

Mata, I. F., Wedemeyer, W. J., Farrer, M. J., Taylor, J. P., and Gallo, K. A. (2006). LRRK2 in Parkinson's disease: protein domains and functional insights. *Trends Neurosci.* 29, 286–293. doi: 10.1016/j.tins.2006.03.006

Mazzulli, J. R., Xu, Y. H., Sun, Y., Knight, A. L., McLean, P. J., Caldwell, G. A., et al. (2011). Gaucher disease glucocerebrosidase and alpha-synuclein form a bidirectional pathogenic loop in synucleinopathies. *Cell* 146, 37–52. doi: 10.1016/j.cell.2011.06.001

Meijer, A. J., Lorin, S., Blommaart, E. F., and Codogno, P. (2015). Regulation of autophagy by amino acids and MTOR-dependent signal transduction. *Amino Acids* 47, 2037–2063. doi: 10.1007/s00726-014-1765-4

Melendez, A., Talloczy, Z., Seaman, M., Eskelinen, E. L., Hall, D. H., and Levine, B. (2003). Autophagy genes are essential for dauer development and life-span extension in *C. elegans*. *Science* 301, 1387–1391. doi: 10.1126/science.1087782

Melrose, H. L., Kent, C. B., Taylor, J. P., Dachsel, J. C., Hinkle, K. M., Lincoln, S. J., et al. (2007). A comparative analysis of leucine-rich repeat kinase 2 (Lrrk2) expression in mouse brain and Lewy body disease. *Neuroscience* 147, 1047–1058. doi: 10.1016/j.neuroscience.2007.05.027

Menzies, F. M., Fleming, A., Caricasole, A., Bento, C. F., Andrews, S. P., Ashkenazi, A., et al. (2017). Autophagy and neurodegeneration: pathogenic mechanisms and therapeutic opportunities. *Neuron* 93, 1015–1034. doi: 10.1016/j.neuron.2017.01.022

Mercatelli, D., Bolognesi, P., Frassineti, M., Pisano, C. A., Longo, F., Shimshek, D. R., et al. (2019). Leucine-rich repeat kinase 2 (LRRK2) inhibitors differentially modulate glutamate release and Serine935 LRRK2 phosphorylation in striatal and cerebrocortical synaptosomes. *Pharmacol. Res. Perspect.* 7:e00484. doi: 10.1002/prp2.484

Mills, R. D., Mulhern, T. D., Liu, F., Culvenor, J. G., and Cheng, H. C. (2014). Prediction of the repeat domain structures and impact of parkinsonism-associated variations on structure and function of all functional domains of leucine-rich repeat kinase 2 (LRRK2). *Hum. Mutat.* 35, 395–412. doi: 10.1002/humu.22515

Miquel, J. (1998). An update on the oxygen stress-mitochondrial mutation theory of aging: genetic and evolutionary implications. *Exp. Gerontol.* 33, 113–126.

Mizunoe, Y., Kobayashi, M., Sudo, Y., Watanabe, S., Yasukawa, H., Natori, D., et al. (2018). Trehalose protects against oxidative stress by regulating the Keap1-Nrf2 and autophagy pathways. *Redox Biol.* 15, 115–124. doi: 10.1016/j.redox.2017.09.007

Mizushima, N., Levine, B., Cuervo, A. M., and Klionsky, D. J. (2008). Autophagy fights disease through cellular self-digestion. *Nature* 451, 1069–1075. doi: 10.1038/nature06639

Moors, T. E., Hoozemans, J. J., Ingrassia, A., Beccari, T., Parnetti, L., Chartier-Harlin, M. C., et al. (2017). Therapeutic potential of autophagy-enhancing agents in Parkinson's disease. *Mol. Neurodegener.* 12:11. doi: 10.1186/s13024-017-0154-3

Mortimore, G. E., and Schworer, C. M. (1977). Induction of autophagy by amino-acid deprivation in perfused rat liver. *Nature* 270, 174–176. doi: 10.1038/270174a0

Moyse, E., Arsenault, M., Gaudreau, P., Ferland, G., and Ramassamy, C. (2019). Brain region-specific effects of long-term caloric restriction on redox balance of the aging rat. *Mech. Ageing Dev.* 179, 51–59. doi: 10.1016/j.mad.2019.01.002

Mukherjee, A., Patel, B., Koga, H., Cuervo, A. M., and Jenny, A. (2016). Selective endosomal microautophagy is starvation-inducible in *Drosophila*. *Autophagy* 12, 1984–1999. doi: 10.1080/15548627.2016.1208887

Murphy, K. E., Gysbers, A. M., Abbott, S. K., Tayebi, N., Kim, W. S., Sidransky, E., et al. (2014). Reduced glucocerebrosidase is associated with increased alpha-synuclein in sporadic Parkinson's disease. *Brain* 137(Pt 3), 834-848. doi: 10.1093/brain/awt367

Nalls, M. A., Pankratz, N., Lill, C. M., Do, C. B., Hernandez, D. G., Saad, M., et al. (2014). Large-scale meta-analysis of genome-wide association data identifies six new risk loci for Parkinson's disease. *Nat. Genet.* 46, 989–993. doi: 10.1038/ng.3043

Nangaku, M., Nishi, H., and Miyata, T. (2008). Role of chronic hypoxia and hypoxia inducible factor in kidney disease. *Chin. Med. J.* 121, 257–264.

Napolitano, G., Esposito, A., Choi, H., Matarese, M., Benedetti, V., Di Malta, C., et al. (2018). mTOR-dependent phosphorylation controls TFEB nuclear export. *Nat. Commun.* 9:3312. doi: 10.1038/s41467-018-05862-6

Nezich, C. L., Wang, C., Fogel, A. I., and Youle, R. J. (2015). MiT/TFE transcription factors are activated during mitophagy downstream of Parkin and Atg5. *J. Cell Biol.* 210, 435–450. doi: 10.1083/jcb.201501002

Ng, C. H., Guan, M. S., Koh, C., Ouyang, X., Yu, F., Tan, E. K., et al. (2012). AMP kinase activation mitigates dopaminergic dysfunction and mitochondrial abnormalities in *Drosophila* models of Parkinson's disease. *J. Neurosci.* 32, 14311–14317. doi: 10.1523/JNEUROSCI.0499-12.2012

Novello, S., Arcuri, L., Dovero, S., Dutheil, N., Shimshek, D. R., Bezard, E., et al. (2018). G2019S LRRK2 mutation facilitates alpha-synuclein neuropathology in aged mice. *Neurobiol. Dis.* 120, 21–33. doi: 10.1016/j.nbd.2018.08.018

Nwadike, C., Williamson, L. E., Gallagher, L. E., Guan, J. L., and Chan, E. Y. W. (2018). AMPK inhibits ULK1-dependent autophagosome formation and lysosomal acidification via distinct mechanisms. *Mol. Cell Biol.* 38:e00023-18. doi: 10.1128/MCB.00023-18

Oku, M., Maeda, Y., Kagohashi, Y., Kondo, T., Yamada, M., Fujimoto, T., et al. (2017). Evidence for ESCRT- and clathrin-dependent microautophagy. *J. Cell Biol.* 216, 3263–3274. doi: 10.1083/jcb.201611029

Okubadejo, N. U., Rizig, M., Ojo, O. O., Jonvik, H., Oshinaike, O., Brown, E., et al. (2018). Leucine rich repeat kinase 2 (LRRK2) GLY2019SER mutation is absent in a second cohort of Nigerian Africans with Parkinson disease. *PLoS One* 13:e0207984. doi: 10.1371/journal.pone.0207984

Olsvik, H. L., Svenning, S., Abudu, Y. P., Brech, A., Stenmark, H., Johansen, T., et al. (2019). Endosomal microautophagy is an integrated part of the autophagic response to amino acid starvation. *Autophagy* 15, 182–183. doi: 10.1080/15548627.2018.1532265

Onorati, A. V., Dyczynski, M., Ojha, R., and Amaravadi, R. K. (2018). Targeting autophagy in cancer. *Cancer* 124, 3307–3318. doi: 10.1002/cncr.31335

Orenstein, S. J., Kuo, S. H., Tasset, I., Arias, E., Koga, H., Fernandez-Carasa, I., et al. (2013). Interplay of LRRK2 with chaperone-mediated autophagy. *Nat. Neurosci.* 16, 394–406. doi: 10.1038/nn.3350

Ott, C., Konig, J., Hohn, A., Jung, T., and Grune, T. (2016). Reduced autophagy leads to an impaired ferritin turnover in senescent fibroblasts. *Free Radic. Biol. Med.* 101, 325–333. doi: 10.1016/j.freeradbiomed.2016.10.492

Paisan-Ruiz, C., Lang, A. E., Kawarai, T., Sato, C., Salehi-Rad, S., Fisman, G. K., et al. (2005). LRRK2 gene in Parkinson disease: mutation analysis and case control association study. *Neurology* 65, 696–700. doi: 10.1212/01.wnl.0000167552.79769.b3

Pajares, M., Rojo, A. I., Arias, E., Diaz-Carretero, A., Cuervo, A. M., and Cuadrado, A. (2018). Transcription factor NFE2L2/NRF2 modulates chaperone-mediated autophagy through the regulation of LAMP2A. *Autophagy* 14, 1310–1322. doi: 10.1080/15548627.2018.1474992

Palacino, J. J., Sagi, D., Goldberg, M. S., Krauss, S., Motz, C., Wacker, M., et al. (2004). Mitochondrial dysfunction and oxidative damage in parkin-deficient mice. *J. Biol. Chem.* 279, 18614–18622. doi: 10.1074/jbc.M401135200

Papadopoulos, V. E., Nikolopoulou, G., Antoniadou, I., Karachaliou, A., Arianoglou, G., Emmanouilidou, E., et al. (2018). Modulation of beta-glucocerebrosidase increases alpha-synuclein secretion and exosome release in mouse models of Parkinson's disease. *Hum. Mol. Genet.* 27, 1696–1710. doi: 10.1093/hmg/ddy075

Park, J. S., Koentjoro, B., and Sue, C. M. (2017). Commentary: nix restores mitophagy and mitochondrial function to protect against PINK1/Parkin-related Parkinson's disease. *Front. Mol. Neurosci.* 10:297. doi: 10.3389/fnmol.2017.00297

Pepe, S. (2000). Mitochondrial function in ischaemia and reperfusion of the ageing heart. *Clin. Exp. Pharmacol. Physiol.* 27, 745–750.

Perez, F. A., and Palmiter, R. D. (2005). Parkin-deficient mice are not a robust model of parkinsonism. *Proc. Natl. Acad. Sci. U.S.A.* 102, 2174–2179. doi: 10.1073/pnas.0409598102.

Petit, A., Kawarai, T., Paitel, E., Sanjo, N., Maj, M., Scheid, M., et al. (2005). Wild-type PINK1 prevents basal and induced neuronal apoptosis, a protective effect abrogated by Parkinson disease-related mutations. *J. Biol. Chem.* 280, 34025–34032. doi: 10.1074/jbc.M505143200.

Pineda, C. T., Ramanathan, S., Fon Tacer, K., Weon, J. L., Potts, M. B., Ou, Y. H., et al. (2015). Degradation of AMPK by a cancer-specific ubiquitin ligase. *Cell* 160, 715–728. doi: 10.1016/j.cell.2015.01.034

Pinti, M., Cevenini, E., Nasi, M., De Biasi, S., Salvioli, S., Monti, D., et al. (2014). Circulating mitochondrial DNA increases with age and is a familiar trait: implications for "inflamm-aging". *Eur. J. Immunol.* 44, 1552–1562. doi: 10.1002/eji.201343921

Plowey, E. D., Cherra, S. J. 3rd, Liu, Y. J., and Chu, C. T. (2008). Role of autophagy in G2019S-LRRK2-associated neurite shortening in differentiated SH-SY5Y cells. *J. Neurochem.* 105, 1048–1056. doi: 10.1111/j.1471-4159.2008.05217.x

Pridgeon, J. W., Olzmann, J. A., Chin, L. S., and Li, L. (2007). PINK1 protects against oxidative stress by phosphorylating mitochondrial chaperone TRAP1. *PLoS Biol.* 5:e172. doi: 10.1371/journal.pbio.0050172

Puente, C., Hendrickson, R. C., and Jiang, X. (2016). Nutrient-regulated phosphorylation of ATG13 inhibits starvation-induced autophagy. *J. Biol. Chem.* 291, 6026–6035. doi: 10.1074/jbc.M115.689646

Ramirez-Moreno, M. J., Duarte-Jurado, A. P., Gopar-Cuevas, Y., Gonzalez-Alcocer, A., Loera-Arias, M. J., Saucedo-Cardenas, O., et al. (2019). Autophagy stimulation decreases dopaminergic neuronal death mediated by oxidative stress. *Mol. Neurobiol.* 56, 8136–8156. doi: 10.1007/s12035-019-01654-1

Ramonet, D., Daher, J. P., Lin, B. M., Stafa, K., Kim, J., Banerjee, R., et al. (2011). Dopaminergic neuronal loss, reduced neurite complexity and autophagic abnormalities in transgenic mice expressing G2019S mutant LRRK2. *PLoS One* 6:e18568. doi: 10.1371/journal.pone.0018568

Ravikumar, B., Berger, Z., Vacher, C., O'Kane, C. J., and Rubinsztein, D. C. (2006). Rapamycin pre-treatment protects against apoptosis. *Hum. Mol. Genet.* 15, 1209–1216. doi: 10.1093/hmg/ddl036

Ravikumar, B., Duden, R., and Rubinsztein, D. C. (2002). Aggregate-prone proteins with polyglutamine and polyalanine expansions are degraded by autophagy. *Hum. Mol. Genet.* 11, 1107–1117. doi: 10.1093/hmg/11.9.1107

Reed, X., Bandres-Ciga, S., Blauwendraat, C., and Cookson, M. R. (2019). The role of monogenic genes in idiopathic Parkinson's disease. *Neurobiol. Dis.* 124, 230–239. doi: 10.1016/j.nbd.2018.11.012

Rezzani, R., Stacchiotti, A., and Rodella, L. F. (2012). Morphological and biochemical studies on aging and autophagy. *Ageing Res. Rev.* 11, 10–31. doi: 10.1016/j.arr.2011.09.001

Roberts, E. L. Jr, Chih, C. P., and Rosenthal, M. (1997). Age-related changes in brain metabolism and vulnerability to anoxia. *Adv. Exp. Med. Biol.* 411, 83–89. doi: 10.1007/978-1-4615-5865-1_10

Rocha, E. M., De Miranda, B. R., Castro, S., Drolet, R., Hatcher, N. G., Yao, L., et al. (2019). LRRK2 inhibition prevents endolysosomal deficits seen in human Parkinson's disease. *Neurobiol. Dis.* 134:104626. doi: 10.1016/j.nbd.2019.104626

Rockenfeller, P., Koska, M., Pietrocola, F., Minois, N., Knittelfelder, O., Sica, V., et al. (2015). Phosphatidylethanolamine positively regulates autophagy and longevity. *Cell Death Differ.* 22, 499–508. doi: 10.1038/cdd.2014.219

Rodriguez-Navarro, J. A., Kaushik, S., Koga, H., Dall'Armi, C., Shui, G., Wenk, M. R., et al. (2012). Inhibitory effect of dietary lipids on chaperone-mediated autophagy. *Proc. Natl. Acad. Sci. U.S.A.* 109, E705–E714. doi: 10.1073/pnas.1113036109

Roosen, D. A., and Cookson, M. R. (2016). LRRK2 at the interface of autophagosomes, endosomes and lysosomes. *Mol. Neurodegener.* 11:73. doi: 10.1186/s13024-016-0140-1

Saez-Atienzar, S., Bonet-Ponce, L., Blesa, J. R., Romero, F. J., Murphy, M. P., Jordan, J., et al. (2014). The LRRK2 inhibitor GSK2578215A induces protective autophagy in SH-SY5Y cells: involvement of Drp-1-mediated mitochondrial fission and mitochondrial-derived ROS signaling. *Cell Death Dis.* 5:e1368. doi: 10.1038/cddis.2014.320

Saha, S., Ash, P. E., Gowda, V., Liu, L., Shirihai, O., and Wolozin, B. (2015). Mutations in LRRK2 potentiate age-related impairment of autophagic flux. *Mol. Neurodegener.* 10:26. doi: 10.1186/s13024-015-0022-y.

Sahu, R., Kaushik, S., Clement, C. C., Cannizzo, E. S., Scharf, B., Follenzi, A., et al. (2011). Microautophagy of cytosolic proteins by late endosomes. *Dev. Cell* 20, 131–139. doi: 10.1016/j.devcel.2010.12.003

Sala, G., Marinig, D., Riva, C., Arosio, A., Stefanoni, G., Brighina, L., et al. (2016). Rotenone down-regulates HSPA8/hsc70 chaperone protein in vitro: a new possible toxic mechanism contributing to Parkinson's disease. *Neurotoxicology* 54, 161–169. doi: 10.1016/j.neuro.2016.04.018

Sanchez-Danes, A., Richaud-Patin, Y., Carballo-Carbajal, I., Jimenez-Delgado, S., Caig, C., Mora, S., et al. (2012). Disease-specific phenotypes in dopamine neurons from human iPS-based models of genetic and sporadic Parkinson's disease. *EMBO Mol. Med.* 4, 380–395. doi: 10.1002/emmm.201200215

Sardiello, M., Palmieri, M., di Ronza, A., Medina, D. L., Valenza, M., Gennarino, V. A., et al. (2009). A gene network regulating lysosomal biogenesis and function. *Science* 325, 473–477. doi: 10.1126/science.1174447

Sarkar, S., Krishna, G., Imarisio, S., Saiki, S., O'Kane, C. J., and Rubinsztein, D. C. (2008). A rational mechanism for combination treatment of Huntington's disease using lithium and rapamycin. *Hum. Mol. Genet.* 17, 170–178. doi: 10.1093/hmg/ddm294

Schapansky, J., Khasnavis, S., DeAndrade, M. P., Nardozzi, J. D., Falkson, S. R., Boyd, J. D., et al. (2018). Familial knockin mutation of LRRK2 causes lysosomal dysfunction and accumulation of endogenous insoluble alpha-synuclein in neurons. *Neurobiol. Dis.* 111, 26–35. doi: 10.1016/j.nbd.2017.12.005

Schapansky, J., Nardozzi, J. D., Felizia, F., and LaVoie, M. J. (2014). Membrane recruitment of endogenous LRRK2 precedes its potent regulation of autophagy. *Hum. Mol. Genet.* 23, 4201–4214. doi: 10.1093/hmg/ddu138

Settembre, C., Di Malta, C., Polito, V. A., Garcia Arencibia, M., Vetrini, F., Erdin, S., et al. (2011). TFEB links autophagy to lysosomal biogenesis. *Science* 332, 1429–1433. doi: 10.1126/science.1204592

Settembre, C., Zoncu, R., Medina, D. L., Vetrini, F., Erdin, S., Erdin, S., et al. (2012). A lysosome-to-nucleus signalling mechanism senses and regulates the lysosome via mTOR and TFEB. *EMBO J.* 31, 1095–1108. doi: 10.1038/emboj.2012.32

Simon-Sanchez, J., Herranz-Perez, V., Olucha-Bordonau, F., and Perez-Tur, J. (2006). LRRK2 is expressed in areas affected by Parkinson's disease in the adult mouse brain. *Eur. J. Neurosci.* 23, 659–666. doi: 10.1111/j.1460-9568.2006.04616.x

Sitte, N., Merker, K., Von Zglinicki, T., Davies, K. J., and Grune, T. (2000a). Protein oxidation and degradation during cellular senescence of human BJ fibroblasts:

part II–aging of nondividing cells. *FASEB J.* 14, 2503–2510. doi: 10.1096/fj.00-0210com

Sitte, N., Merker, K., Von Zglinicki, T., Grune, T., and Davies, K. J. (2000b). Protein oxidation and degradation during cellular senescence of human BJ fibroblasts: part I–effects of proliferative senescence. *FASEB J.* 14, 2495–2502. doi: 10.1096/fj.00-0209com

Sosulski, M. L., Gongora, R., Danchuk, S., Dong, C., Luo, F., and Sanchez, C. G. (2015). Deregulation of selective autophagy during aging and pulmonary fibrosis: the role of TGFbeta1. *Aging Cell* 14, 774–783. doi: 10.1111/acel.12357

Soukup, S. F., Kuenen, S., Vanhauwaert, R., Manetsberger, J., Hernandez-Diaz, S., Swerts, J., et al. (2016). A LRRK2-dependent endophilina phosphoswitch is critical for macroautophagy at presynaptic terminals. *Neuron* 92, 829–844. doi: 10.1016/j.neuron.2016.09.037

Soukup, S. F., Vanhauwaert, R., and Verstreken, P. (2018). Parkinson's disease: convergence on synaptic homeostasis. *EMBO J.* 37:e98960. doi: 10.15252/embj.201898960

Spilman, P., Podlutskaya, N., Hart, M. J., Debnath, J., Gorostiza, O., Bredesen, D., et al. (2010). Inhibition of mTOR by rapamycin abolishes cognitive deficits and reduces amyloid-beta levels in a mouse model of Alzheimer's disease. *PLoS One* 5:e9979. doi: 10.1371/journal.pone.0009979

Steger, M., Diez, F., Dhekne, H. S., Lis, P., Nirujogi, R. S., Karayel, O., et al. (2017). Systematic proteomic analysis of LRRK2-mediated Rab GTPase phosphorylation establishes a connection to ciliogenesis. *eLife* 6:e31012. doi: 10.7554/eLife.31012

Steger, M., Tonelli, F., Ito, G., Davies, P., Trost, M., Vetter, M., et al. (2016). Phosphoproteomics reveals that Parkinson's disease kinase LRRK2 regulates a subset of Rab GTPases. *eLife* 5:e12813. doi: 10.7554/eLife.12813

Stolz, A., Ernst, A., and Dikic, I. (2014). Cargo recognition and trafficking in selective autophagy. *Nat. Cell Biol.* 16, 495–501. doi: 10.1038/ncb2979

Su, Y. C., Guo, X., and Qi, X. (2015). Threonine 56 phosphorylation of Bcl-2 is required for LRRK2 G2019S-induced mitochondrial depolarization and autophagy. *Biochim. Biophys. Acta* 1852, 12–21. doi: 10.1016/j.bbadis.2014.11.009

Su, Y. C., and Qi, X. (2013). Inhibition of excessive mitochondrial fission reduced aberrant autophagy and neuronal damage caused by LRRK2 G2019S mutation. *Hum. Mol. Genet.* 22, 4545–4561. doi: 10.1093/hmg/ddt301

Sugawara, K., Suzuki, N. N., Fujioka, Y., Mizushima, N., Ohsumi, Y., and Inagaki, F. (2004). The crystal structure of microtubule-associated protein light chain 3, a mammalian homologue of *Saccharomyces cerevisiae* Atg8. *Genes Cells* 9, 611–618. doi: 10.1111/j.1356-9597.2004.00750.x

Sun, N., Youle, R. J., and Finkel, T. (2016). The mitochondrial basis of aging. *Mol. Cell* 61, 654–666. doi: 10.1016/j.molcel.2016.01.028

Sutton, M. N., Huang, G. Y., Zhou, J., Mao, W., Langley, R., Lu, Z., et al. (2019). Amino acid deprivation-induced autophagy requires upregulation of DIRAS3 through reduction of E2F1 and E2F4 transcriptional repression. *Cancers* 11:E603. doi: 10.3390/cancers11050603

Taymans, J. M., Van den Haute, C., and Baekelandt, V. (2006). Distribution of PINK1 and LRRK2 in rat and mouse brain. *J. Neurochem.* 98, 951–961. doi: 10.1111/j.1471-4159.2006.03919.x

Terman, A., Kurz, T., Navratil, M., Arriaga, E. A., and Brunk, U. T. (2010). Mitochondrial turnover and aging of long-lived postmitotic cells: the mitochondrial-lysosomal axis theory of aging. *Antioxid. Redox Signal.* 12, 503–535. doi: 10.1089/ars.2009.2598.

Thevenet, J., Pescini Gobert, R., Hooft van Huijsduijnen, R., Wiessner, C., and Sagot, Y. J. (2011). Regulation of LRRK2 expression points to a functional role in human monocyte maturation. *PLoS One* 6:e21519. doi: 10.1371/journal.pone.0021519

Thumm, M., Egner, R., Koch, B., Schlumpberger, M., Straub, M., Veenhuis, M., et al. (1994). Isolation of autophagocytosis mutants of *Saccharomyces cerevisiae*. *FEBS Lett.* 349, 275–280. doi: 10.1016/0014-579300672-5

Tong, Y., Giaime, E., Yamaguchi, H., Ichimura, T., Liu, Y., Si, H., et al. (2012). Loss of leucine-rich repeat kinase 2 causes age-dependent bi-phasic alterations of the autophagy pathway. *Mol. Neurodegener.* 7:2. doi: 10.1186/1750-1326-7-2

Tong, Y., Yamaguchi, H., Giaime, E., Boyle, S., Kopan, R., Kelleher, R. J., et al. (2010). Loss of leucine-rich repeat kinase 2 causes impairment of protein degradation pathways, accumulation of alpha-synuclein, and apoptotic cell death in aged mice. *Proc. Natl. Acad. Sci. U.S.A.* 107, 9879–9884. doi: 10.1073/pnas.1004676107

Toth, M. L., Sigmond, T., Borsos, E., Barna, J., Erdelyi, P., Takacs-Vellai, K., et al. (2008). Longevity pathways converge on autophagy genes to regulate life span in *Caenorhabditis elegans*. *Autophagy* 4, 330–338. doi: 10.4161/auto.5618

Tsika, E., Kannan, M., Foo, C. S., Dikeman, D., Glauser, L., Gellhaar, S., et al. (2014). Conditional expression of Parkinson's disease-related R1441C LRRK2 in midbrain dopaminergic neurons of mice causes nuclear abnormalities without neurodegeneration. *Neurobiol. Dis.* 71, 345–358. doi: 10.1016/j.nbd.2014.08.027

Tsukada, M., and Ohsumi, Y. (1993). Isolation and characterization of autophagy-defective mutants of *Saccharomyces cerevisiae*. *FEBS Lett.* 333, 169–174. doi: 10.1016/0014-579380398-e

Tsvetkov, A. S., Arrasate, M., Barmada, S., Ando, D. M., Sharma, P., Shaby, B. A., et al. (2013). Proteostasis of polyglutamine varies among neurons and predicts neurodegeneration. *Nat. Chem. Biol.* 9, 586–592. doi: 10.1038/nchembio.1308

Uytterhoeven, V., Lauwers, E., Maes, I., Miskiewicz, K., Melo, M. N., Swerts, J., et al. (2015). Hsc70-4 deforms membranes to promote synaptic protein turnover by endosomal microautophagy. *Neuron* 88, 735–748. doi: 10.1016/j.neuron.2015.10.012

Valente, E. M., Abou-Sleiman, P. M., Caputo, V., Muqit, M. M., Harvey, K., Gispert, S., et al. (2004). Hereditary early-onset Parkinson's disease caused by mutations in PINK1. *Science* 304, 1158–1160. doi: 10.1126/science.1096284

Vellai, T., Takacs-Vellai, K., Zhang, Y., Kovacs, A. L., Orosz, L., and Muller, F. (2003). Genetics: influence of TOR kinase on lifespan in *C. elegans*. *Nature* 426:620. doi: 10.1038/426620a

Vijayan, V., and Verstreken, P. (2017). Autophagy in the presynaptic compartment in health and disease. *J. Cell Biol.* 216, 1895–1906. doi: 10.1083/jcb.201611113

Volta, M., and Melrose, H. (2017). LRRK2 mouse models: dissecting the behavior, striatal neurochemistry and neurophysiology of PD pathogenesis. *Biochem. Soc. Trans.* 45, 113–122. doi: 10.1042/BST20160238

Wallings, R., Connor-Robson, N., and Wade-Martins, R. (2019). LRRK2 interacts with the vacuolar-type H+-ATPase pump a1 subunit to regulate lysosomal function. *Hum. Mol. Genet.* 28, 2696-2710. doi: 10.1093/hmg/ddz088

Wauters, F., Cornelissen, T., Imberechts, D., Martin, S., Koentjoro, B., Sue, C., et al. (2019). LRRK2 mutations impair depolarization-induced mitophagy through inhibition of mitochondrial accumulation of RAB10. *Autophagy* doi: 10.1080/15548627.2019.1603548 [Epub ahead of print].

Weng, Y. H., Chen, C. Y., Lin, K. J., Chen, Y. L., Yeh, T. H., Hsiao, I. T., et al. (2016). (R1441C) LRRK2 induces the degeneration of SN dopaminergic neurons and alters the expression of genes regulating neuronal survival in a transgenic mouse model. *Exp. Neurol.* 275(Pt 1), 104–115. doi: 10.1016/j.expneurol.2015.09.001

West, A. B. (2017). Achieving neuroprotection with LRRK2 kinase inhibitors in Parkinson disease. *Exp. Neurol.* 298(Pt B), 236–245. doi: 10.1016/j.expneurol.2017.07.019

West, A. B., Cowell, R. M., Daher, J. P., Moehle, M. S., Hinkle, K. M., Melrose, H. L., et al. (2014). Differential LRRK2 expression in the cortex, striatum, and substantia nigra in transgenic and nontransgenic rodents. *J. Comp. Neurol.* 522, 2465–2480. doi: 10.1002/cne.23583

West, A. B., Moore, D. J., Biskup, S., Bugayenko, A., Smith, W. W., Ross, C. A., et al. (2005). Parkinson's disease-associated mutations in leucine-rich repeat kinase 2 augment kinase activity. *Proc. Natl. Acad. Sci. U.S.A.* 102, 16842–16847. doi: 10.1073/pnas.0507360102

Xilouri, M., Brekk, O. R., Polissidis, A., Chrysanthou-Piterou, M., Kloukina, I., and Stefanis, L. (2016). Impairment of chaperone-mediated autophagy induces dopaminergic neurodegeneration in rats. *Autophagy* 12, 2230–2247. doi: 10.1080/15548627.2016.1214777

Xilouri, M., and Stefanis, L. (2015). Chaperone mediated autophagy to the rescue: a new-fangled target for the treatment of neurodegenerative diseases. *Mol. Cell Neurosci.* 66(Pt A), 29–36. doi: 10.1016/j.mcn.2015.01.003

Xiong, Y., Coombes, C. E., Kilaru, A., Li, X., Gitler, A. D., Bowers, W. J., et al. (2010). GTPase activity plays a key role in the pathobiology of LRRK2. *PLoS Genet.* 6:e1000902. doi: 10.1371/journal.pgen.1000902

Yakhine-Diop, S. M., Bravo-San Pedro, J. M., Gomez-Sanchez, R., Pizarro-Estrella, E., Rodriguez-Arribas, M., Climent, V., et al. (2014). G2019S LRRK2 mutant fibroblasts from Parkinson's disease patients show increased sensitivity to neurotoxin 1-methyl-4-phenylpyridinium dependent of autophagy. *Toxicology* 324, 1–9. doi: 10.1016/j.tox.2014.07.001

Yang, Y., Fiskus, W., Yong, B., Atadja, P., Takahashi, Y., Pandita, T. K., et al. (2013). Acetylated hsp70 and KAP1-mediated Vps34 SUMOylation is required for autophagosome creation in autophagy. *Proc. Natl. Acad. Sci. U.S.A.* 110, 6841–6846. doi: 10.1073/pnas.1217692110

Yao, C., El Khoury, R., Wang, W., Byrd, T. A., Pehek, E. A., Thacker, C., et al. (2010). LRRK2-mediated neurodegeneration and dysfunction of dopaminergic neurons in a *Caenorhabditis elegans* model of Parkinson's disease. *Neurobiol. Dis.* 40, 73–81. doi: 10.1016/j.nbd.2010.04.002

Yue, M., Hinkle, K. M., Davies, P., Trushina, E., Fiesel, F. C., Christenson, T. A., et al. (2015). Progressive dopaminergic alterations and mitochondrial abnormalities in LRRK2 G2019S knock-in mice. *Neurobiol. Dis.* 78, 172–195. doi: 10.1016/j.nbd.2015.02.031

Zech, A. T. L., Singh, S. R., Schlossarek, S., and Carrier, L. (2019). Autophagy in cardiomyopathies. *Biochim. Biophys. Acta Mol. Cell Res.* doi: 10.1016/j.bbamcr.2019.01.013 [Epub ahead of print].

Zhang, J., Johnson, J. L., He, J., Napolitano, G., Ramadass, M., Rocca, C., et al. (2017). Cystinosin, the small GTPase Rab11, and the Rab7 effector RILP regulate intracellular trafficking of the chaperone-mediated autophagy receptor LAMP2A. *J. Biol. Chem.* 292, 10328–10346. doi: 10.1074/jbc.M116.764076

Zhao, Y., and Dzamko, N. (2019). Recent developments in LRRK2-targeted therapy for Parkinson's disease. *Drugs* 79, 1037–1051. doi: 10.1007/s40265-019-01139-4

Zhu, G., Huang, Y., Chen, Y., Zhuang, Y., and Behnisch, T. (2012). MPTP modulates hippocampal synaptic transmission and activity-dependent synaptic plasticity via dopamine receptors. *J. Neurochem.* 122, 582–593. doi: 10.1111/j.1471-4159.2012.07815.x

Zimprich, A., Biskup, S., Leitner, P., Lichtner, P., Farrer, M., Lincoln, S., et al. (2004). Mutations in LRRK2 cause autosomal-dominant parkinsonism with pleomorphic pathology. *Neuron* 44, 601–607. doi: 10.1016/j.neuron.2004.11.005

Zoppino, F. C., Militello, R. D., Slavin, I., Alvarez, C., and Colombo, M. I. (2010). Autophagosome formation depends on the small GTPase Rab1 and functional ER exit sites. *Traffic* 11, 1246–1261. doi: 10.1111/j.1600-0854.2010.01086.x

Conflict of Interest: The authors declare that the research was conducted in the absence of any commercial or financial relationships that could be construed as a potential conflict of interest.

Neurobiology of Disease 159 (2021) 105487

Contents lists available at ScienceDirect

Neurobiology of Disease

journal homepage: www.elsevier.com/locate/ynbdi

Constitutive silencing of LRRK2 kinase activity leads to early glucocerebrosidase deregulation and late impairment of autophagy *in vivo*

Federica Albanese [a], Daniela Mercatelli [a,b], Luca Finetti [c], Giulia Lamonaca [d], Sara Pizzi [d], Derya R. Shimshek [e], Giovanni Bernacchia [c], Michele Morari [a,*]

[a] Department of Neuroscience and Rehabilitation, Section of Pharmacology, University of Ferrara, 44121 Ferrara, Italy
[b] Technopole of Ferrara, LTTA Laboratory for Advanced Therapies, 44121 Ferrara, Italy
[c] Department of Life Sciences and Biotechnology, University of Ferrara, 44121 Ferrara, Italy
[d] Institute for Biomedicine, Eurac Research-Affiliated Institute of the University of Lübeck, 39100 Bolzano, Italy
[e] Department of Neuroscience, Novartis Institutes for BioMedical Research, Novartis Pharma AG, 4002 Basel, Switzerland

ARTICLE INFO

Keywords:
Autophagy
Chaperone-mediated autophagy
Chloroquine
G2019S LRRK2
Glucocerebrosidase
LC3
MLi-2
pSer129 α-synuclein
Parkinson's disease
TFEB

ABSTRACT

Mutations in leucine-rich repeat kinase 2 (LRRK2) are associated with Parkinson's disease. LRRK2 modulates the autophagy-lysosome pathway (ALP), a clearance process subserving the quality control of cellular proteins and organelles. Since dysfunctional ALP might lead to α-synuclein accumulation and, hence, Parkinson's disease, LRRK2 kinase modulation of ALP, its age-dependence and relation with pSer129 α-synuclein inclusions were investigated *in vivo*. Striatal ALP markers were analyzed by Western blotting in 3, 12 and 20-month-old LRRK2 G2019S knock-in mice (bearing enhanced kinase activity), LRRK2 knock-out mice, LRRK2 D1994S knock-in (kinase-dead) mice and wild-type controls. The lysosomotropic agent chloroquine was used to investigate the autophagic flux *in vivo*. Quantitative Real-time PCR was used to quantify the transcript levels of key ALP genes. The activity of the lysosomal enzyme glucocerebrosidase was measured using enzymatic assay. Immunohistochemistry was used to co-localize LC3B puncta with pSer129 α-synuclein inclusion in striatal and nigral neurons. No genotype differences in ALP markers were observed at 3 months. Conversely, increase of LC3-I, p62, LAMP2 and GAPDH levels, decrease of p-mTOR levels and downregulation of *mTOR* and *TFEB* expression was observed in 12-month-old kinase-dead mice. The LC3-II/I ratio was reduced following administration of chloroquine, suggesting a defective autophagic flux. G2019S knock-in mice showed LAMP2 accumulation and downregulation of ALP key genes *MAP1LC3B*, *LAMP2*, *mTOR*, *TFEB* and *GBA1*. Subacute administration of the LRRK2 kinase inhibitor MLi-2 in wild-type and G2019S knock-in mice did not replicate the pattern of kinase-dead mice. Lysosomal glucocerebrosidase activity was increased in 3 and 12-month-old knock-out and kinase-dead mice. LC3B puncta accumulation and pSer129 α-synuclein inclusions were dissociated in striatal neurons of kinase-dead and G2019S knock-in mice. We conclude that constitutive LRRK2 kinase silencing results in early deregulation of GCase activity followed by late impairment of macroautophagy and chaperone-mediated autophagy.

1. Introduction

Accumulation of misfolded protein and damaged/dysfunctional organelles is a common hallmark of neurodegenerative disorders of aging, such as Parkinson's disease (PD). Several genetic factors, among which mutations in the leucine-rich repeat kinase 2 (*LRRK2)* gene,

Abbreviations: ALP, Autophagy-lysosomal pathway; CMA, Chaperone-mediated autophagy; CQ, Chloroquine; GCase, Glucocerebrosidase; KD, Kinase-dead; KI, Knock-in; KO, Knock-out; LRRK1, Leucine-rich repeat kinase 1; LRRK2, Leucine-rich repeat kinase 2; MAP2, microtubule associated protein 2; α-syn, α-synuclein; PD, Parkinson's disease; pSer129 α-syn, phosphoSerine 129 α-synuclein; pSer1292 LRRK2, phosphoSerine 1292 LRRK2; SN, substantia nigra; TFEB, Transcription factor EB; TH, Tyrosine hydroxylase; WT, Wild-type.

* Corresponding author at: Department of Neuroscience and Rehabilitation, Section of Pharmacology, University of Ferrara, via Fossato di Mortara 17-19, 44121 Ferrara, Italy.

E-mail addresses: federica.albanese@unife.it (F. Albanese), daniela.mercatelli@unife.it (D. Mercatelli), luca.finetti@unife.it (L. Finetti), giulia.lamonaca@eurac.edu (G. Lamonaca), sara.pizzi@eurac.edu (S. Pizzi), derya.shimshek@novartis.com (D.R. Shimshek), giovanni.bernacchia@unife.it (G. Bernacchia), m.morari@unife.it (M. Morari).

https://doi.org/10.1016/j.nbd.2021.105487
Received 16 July 2021; Received in revised form 13 August 2021; Accepted 16 August 2021
Available online 20 August 2021

contribute to PD pathogenesis (Cookson, 2017; Kluss et al., 2019; Poewe et al., 2017). LRRK2 is a large multidomain protein, encompassing a catalytic core with GTPase and kinase domains, flanked by protein-protein interaction motifs (Cookson, 2010; Mata et al., 2006). LRRK2-related PD is characterized by an age-dependent and incomplete penetrance. The most common mutation, p.G2019S, confers enhanced kinase activity and causes autosomal dominant PD, whereas the *LRRK2* locus is a risk factor for idiopathic PD (Berwick et al., 2019; Nalls et al., 2014). The enhancement of LRRK2 kinase activity proved neurotoxic in several *in vitro* and *in vivo* studies (Greggio et al., 2006; Heo et al., 2010; West et al., 2005; Yao et al., 2010). On the contrary, LRRK2 mutant mice harboring kinase-dead (KD) mutations, among which D1994N, exhibited a reduced age-related neuronal toxicity (Smith et al., 2006). LRRK2 plays a role in a variety of cellular functions and pathways, thus, not surprisingly, various mechanisms have been recognized or hypothesized to be involved in LRRK2-mediated neuropathology, among which the modulation of the autophagy-lysosomal pathway (ALP) (Albanese et al., 2019; Gan-Or et al., 2015; Manzoni and Lewis, 2017; Plowey and Chu, 2011; Tsika and Moore, 2012). Autophagy is a highly conserved process responsible for bulk degradation of cellular debris as well as dysfunctional/damaged organelles by delivery to lysosomes and is classically divided in three main types: macroautophagy, chaperone-mediated autophagy (CMA) and microautophagy. ALP integrates extracellular and intracellular stimuli to regulate energy balance and proteostasis (Boland et al., 2018; Galluzzi et al., 2017). However, ALP efficiency declines during physiological aging (Cuervo, 2008), resulting in impaired α-synuclein (α-syn) clearance and, possibly, sensitization to PD onset or facilitation of its progression (Johnson et al., 2019; Xilouri et al., 2008). Several studies have attempted to establish whether LRRK2 is a positive or negative modulator of ALP (Albanese et al., 2019; Madureira et al., 2020; Manzoni and Lewis, 2017; Senkevich and Gan-Or, 2020). Most studies were carried out *in vitro* and led to inconsistent data, possibly due to the different cell types and neurons used, type of LRRK2 mutant, and mutant overexpression levels. Also *in vivo* (*ex vivo*) studies did not give a conclusive picture. Indeed, original studies revealed ALP impairment in the kidney and lungs of aged LRRK2 knockout (KO) (Baptista et al., 2013; Fuji et al., 2015; Herzig et al., 2011; Hinkle et al., 2012; Tong et al., 2012; Tong et al., 2010) and KD mice (Herzig et al., 2011). An increase in autophagic markers p62 and LC3-II and a reduction in the lysosomal/endosomal marker LC3-I was found in the optical nerve (for p62 also in striatum and substantia nigra, SN) of 15-month-old mice lacking both LRRK1 and LRRK2 that were interpreted as being due to ALP inhibition (Giaime et al., 2017). Interestingly, however, the same conclusion was reached by studies performed in 15–20-month-old G2019S KI mice (Schapansky et al., 2018; Yue et al., 2015) or BAC G2019S rats (Wallings et al., 2019), showing reductions of LC3-I and LAMP1 or increase of LC3-II levels and LC3 puncta in various brain areas. Nonetheless, none of these studies analyzed the autophagic flux *in vivo*, as per accepted recommendations (Klionsky et al., 2021), making it difficult to interpret whether the increase observed in LC3-II reflec an increased or blocked autophagic flux.

The current study sought to investigate the role of LRRK2 kinase activity in the modulation of ALP *in vivo*, and how this modulation changes during aging. To this aim, G2019S KI mice (bearing enhanced kinase activity), LRRK2 D1994S KI mice (bearing a KD mutation; KD mice), LRRK2 KO mice and wild-type (WT) mice were analyzed at 3, 12 and 20 months of age. Western blotting (WB) and RT-qPCR were used to monitor the levels and expression of macroautophagy markers LC3-I, LC3-II, p62, mTOR and its Ser2448 phosphorylated, active form (hereafter referred to as p-mTOR), AMPK and its Thr172 phosphorylated, active form (hereafter referred to as p-AMPK), lysosomal marker LAMP2, and CMA marker GAPDH. The transcript levels of Transcription factor EB (*TFEB*) a master regulator of autophagy and lysosome biogenesis (Sardiello et al., 2009; Settembre et al., 2013) were also measured. Modulation of the autophagic flux *in vivo* was achieved *via* subacute administration of Chloroquine (CQ), a lysosomotropic agent that inhibits the fusion of autophagosomes with lysosomes (Klionsky et al., 2021). The hydrolytic activity of the lysosomal enzyme Glucocerebrosidase (GCase) was measured in the striatum of 3 and 12-month-old LRRK2 mutant mice. Indeed, impaired GCase activity is associated with PD (Chiasserini et al., 2015; Gegg et al., 2012; Murphy et al., 2014) and heterozygous mutations in the gene encoding for GCase, *GBA1*, are the second most common cause of genetic PD (Sidransky et al., 2009). Moreover, the impact of pharmacological inhibition of LRRK2 kinase activity on ALP was investigated *via* subacute administration of MLi-2. Lastly, to correlate ALP alterations with phosphorylation of α-syn at Serine129 (pSer129 α-syn), an early index of synucleinopathy (Oueslati, 2016), previously observed in G2019S KI mice (Longo et al., 2017; Novello et al., 2018), co-immunofluorescence analysis was conducted to visualize LC3B puncta and pSer129 α-syn inclusions in striatal microtubule associated protein 2 (MAP2) positive ($MAP2^+$) neurons and nigral tyrosine hydroxylase (TH) positive (TH^+) neurons.

2. Materials and methods

2.1. Animals

Experimental procedures involving the use of animals complied with the ARRIVE guidelines and the EU Directive 2010/63/EU for animal experiments and were approved by the Ethical Committee of the University of Ferrara and the Italian Ministry of Health (license 714/2017-PR). Female and male homozygous LRRK2 G2019S KI, KO and KD mice backcrossed for at least 9 generations on a C57BL/6 J background, were used (Longo et al., 2017; Longo et al., 2014; Mercatelli et al., 2019). Founders were obtained from Mayo Clinic (Jacksonville, FL, USA) (LRRK2 KO mice) (Hinkle et al., 2012) and from Novartis Institutes for BioMedical research (Novartis Pharma AG, Basel, Switzerland) (G2019S KI and KD mice) (Herzig et al., 2011). A colony of non-transgenic wild-type (WT) mice was initially set from heterozygous breeding of G2019S KI mice, then control WT male mice used in all experiments. Colonies were grown at the *vivarium* (LARP) of the University of Ferrara and kept under regular lighting conditions (12 h light/dark cycle), with free access to food (4RF21 standard diet; Mucedola, Settimo Milanese, Milan, Italy) and water. Animals were housed in groups of 5 for a 55x33x20 cm polycarbonate cage (Tecniplast, Buguggiate, Varese, Italy) with a Scobis Uno bedding (Mucedola, Settimo Milanese, Milan, Italy) and environmental enrichments.

2.2. Tissue processing

Mice were anesthetized with isoflurane, transcardially perfused with Phosphate Buffer Solution (PBS), then fixed with 4% paraformaldehyde (PFA) solution (pH 7.4) at 4 °C. Brains were dissected out and post-fixed in 4% PFA for 24 h. Brains were then transferred in 30% sucrose in PBS at 4 °C and then stored at −80 °C. PFA-fixed brains were sectioned at 50 μm (coronal sections) with a cryo-microtome (Leica, Buffalo Grove, Illinois, US) and stored in cryoprotective medium (30% glycerol, 30% ethylene glycol) at −20 °C.

2.3. LC3B, pSer129 α-syn and MAP2 immunofluorescence

Tissue processing and immunohistochemistry were performed on free-floating sections. Coronal sections of striatum (AP from +1.0 to −1.25 from bregma) and SN (AP from -3.16 to -3.52 from bregma) (Paxinos and Franklin, 2001) were used for all histological assays. Sections were rinsed 3 times in PBS and blocked in 5% normal goat serum (ab7481, Abcam, Cambridge, Massachusetts, US) and 0.3% TritonX-100 in PBS for 1 h. The following primary antibodies were used: LC3B (1:3000; Rb ab51520, Abcam), pSer129 α-syn (1:2000; Ms ab184674, Abcam), MAP2 (1:1000; Ck ab5392, Abcam), TH (1:1000; Ck ab76442, Abcam). After overnight incubation at 4 °C, the primary antibody staining was revealed using donkey anti-Rabbit Secondary Antibody

Alexa Fluor 488 (1:1000; A-21206, ThermoFisher Scientific, Waltham, Massachusetts, US), donkey anti-Mouse Secondary Antibody Alexa Fluor 555 (1:1000; A31570, ThermoFisher Scientific), goat Anti-Chicken IgY H&L Alexa Fluor 647 (1:1000; ab150171, Abcam). Sections were rinsed in PBS 3 times, incubated in DAPI solution, mounted onto Superfrost Plus slides (ThermoFisher Scientific) and coverslipped using antifade Fluoromount G (ThermoFisher Scientific). Images were acquired using a Leica SP8-X confocal microscope at 63× and unbiased estimations of LC3B and pSer129 α-syn in $MAP2^+$ and TH^+ cells were performed (Fiji software, NIH, Bethesda, Maryland, US and Cell Profiler software, Cambridge, Massachusetts, US) by investigators blinded to genotype and experimental conditions.

2.4. Western Blot analysis

Mice were anesthetized with isoflurane and sacrificed *via* cervical dislocation, as described (Longo et al., 2017; Longo et al., 2014; Mercatelli et al., 2019). Striatal tissue was subdissected, snap-frozen and stored at −80 °C until further use. Tissue was lysed on ice in 1× RIPA lysis buffer supplemented with 1× Halt protease and phosphatase Inhibitor Cocktail (ThermoFisher Scientific). RIPA lysates were centrifuged at 15,000*g* for 10 min at 4 °C to remove cellular debris. The pellet was discarded, and clarified lysates were quantified with a Pierce BCA protein assay (ThermoFisher Scientific). Tissue lysates were mixed with 4× LDS Sample buffer, 10× Reducing Agent, equal amounts of protein were subjected to 4–12% Bis-Trisglycine gel or 16% Trisglycine gel and transferred to PVDF membranes (Bio-Rad). Membranes were blocked with 5% milk or 5% bovine serum albumine (BSA) in tris-buffered saline with 0.1% Tween (TBST) and immunoblotted according to standard protocols. The following primary antibodies were used for the detection of endogenous LC3B (1:3000; Rb ab51520, Abcam), p62 (1:1000; Rb ab91526, Abcam), LAMP2 (1:1000; Rt ab13524, Abcam), mTOR (1:1000; Rb mAb #2983, CST), phospho-mTOR (Ser2448) (1:1000; Rb mAb #2971, CST), AMPKα (D5A2) (1:1000; Rb BK5831S CST), Phospho-AMPKα (Thr172)(1:1000; Rb mAb BK 2535S CST), phospho-S6K1 (Thr389) (1:1000; Rb BK9205S CST), S6K1 (1:1000; Rb BK9202S CST), pSer1292 LRRK2 (1:300; Rb ab203181, Abcam), LRRK2 (1:300; Rb ab133474, Abcam), β-actin (1:3000; Rb ab8227, Abcam). Following incubation at 4 °C overnight, horseradish peroxidase-conjugated secondary antibodies, goat anti-Rb (1:4000; 12–348 Merck Millipore, Burlington, Massachusetts, US) and goat anti-Rat (1:4000, AP136P, Merck Millipore), and an ECL kit (ThermoFisher Scientific) were used to detect protein signals. Multiple exposures and images were acquired using the ChemiDoc MP System (Bio-Rad, Hercules, California, US) and protein bands were quantified by densitometry using ImageLab Software (Bio-Rad). β-actin bands were used for normalization.

2.5. GCase activity assay

GCase activity was measured as described (Ambrosi et al., 2015). Mice were anesthetized with isoflurane and sacrificed *via* cervical dislocation. Mouse striata (~15 mg) were dissected out and rapidly homogenized in 150 μl and 250 μl of ice-cold RIPA buffer. Ten micrograms of protein lysates for each sample were diluted in 100 μl of Assay buffer (0.1 M sodium citrate phosphate, pH 5.6; 0.1% Triton X-100; 0.25% sodium taurocholate and 2.5 mM 4–4-Methylumbelliferyl β-D-glucopyranoside or 4-MUG). Standard curve (6-point standard curve: 25 μM - 0 μM) was also prepared by serial dilutions of 4-methylumbelliferyl (4-MU, M1381, Sigma-Aldrich, Saint Louis, Missouri, USA) in ddH_20. After incubation with the substrate for 1 h at 37 °C, the reaction was terminated adding 150 μl of stop solution (0.25 M Glycine, pH 10.4). Plates were read (Ex 360/Em 460) in Ensight Perkin Elmer (Perkin-Elmer, Boston, MA, USA), a fluorescent plate reader using Kaleido software (Perkin-Elmer). Enzymatic activity was assessed from a 4-methylumbelliferyl standard curve, whereas protein quantification was determined using a Pierce BCA assay (ThermoFisher Scientific).

2.6. Quantitative Real-time PCR analysis

Mice were anesthetized with isoflurane and sacrificed *via* cervical dislocation. Total RNA was extracted from striatal tissue (~15 mg) of 12-month-old WT, G2019S KI, KO and KD mice ($n = 8$ each) using TRI Reagent (Sigma-Aldrich). One microgram of total RNA was treated with DNase I (ThermoFisher Scientific) and used for cDNA synthesis, performed by the RevertAid First Strand cDNA Synthesis Kit (ThermoFisher Scientific), according to the manufacturer's instructions. Real-time PCR was performed using a CFX Connect Real-time PCR Detection System (Bio-Rad) in 12 μl reaction mixture containing 1.6 μl of 1:5 diluted cDNA, 6 μl SsoAdvanced Universal SYBR Green Supermix (Bio-Rad), 0.4 μl forward primer (10 μM), 0.4 μl reverse primer (10 μM) and 3.6 μl nuclease free water. Thermal cycling condition protocol was set at 95 °C for 2 min, 40 cycles at 95 °C for 15 s and 60 °C for 30 s. After the cycling protocol, a melting-curve analysis from 55 °C to 95 °C was conducted. Expression of *MAP1LC3*, *TFEB*, *mTOR*, *LAMP2*, *p62*, and *GBA1* genes was normalized using *ACTB* and *HPRT* as reference genes (Gong et al., 2016), applying QBase+ method (Hellemans et al., 2007). Gene-specific primers (Table S1) were used, and eight independent biological replicates, made in triplicate, were performed for each genotype.

2.7. CQ treatment

CQ, a validated lysosomotropic autophagy inhibitor, was administered (50 mg/kg, i.p.) once daily for three consecutive days to assess the autophagic flux (Mauthe et al., 2018). Mice were anesthetized with isoflurane and sacrificed *via* cervical dislocation at 4 or 24 h after the last CQ injection and striatal tissues were dissected out to perform WB analysis. To confirm the efficacy of this CQ administration protocol in blocking the autophagolysosomal formation, CQ was first administered to a cohort of 3-month-old WT mice ($n = 6$). After confirming LC3-II accumulation and the increase of LC3-II/I ratio, the protocol was applied to two cohorts of 12-month-old WT and KD mice (n = 6 each).

2.8. MLi-2 treatment

Two cohorts of 12-month-old WT and G2019S KI mice (n = 6 per genotype in each cohort) were subacutely treated with MLi-2 to inhibit LRRK2 kinase activity. Two protocols of MLi-2 administration were adopted: 10 mg/Kg, i.p., twice daily for seven days, or 5 mg/kg, i.p., once daily for seven days. Animals were sacrificed *via* cervical dislocation 4 h after the last injection and one striatum was collected to perform WB analysis, while the other striatum for RT-qPCR analysis.

2.9. Drugs

CQ was purchased from Sigma and was dissolved in saline solution. MLi-2 was purchased from Carbosynth (Commpton, Bershire, UK) and was dissolved in 4% DMSO and 30% hydroxyprpyl β-cyclodextrin.

2.10. Statistical analysis

Data are expressed as mean ± SEM (standard error of mean) of n mice. Statistical analysis was performed using Prism 8.0 (GraphPad Software Inc., CA, USA). For experiments with $n > 2$ groups, one-way ANOVA followed by the Bonferroni's for multiple comparisons was used. QBase+ analysis was performed to quantify fold change in gene expression (Hellemans et al., 2007), and data analyzed by one-way ANOVA followed by Dunnett's test for multiple comparisons. When only two groups of data were analyzed (*e.g.*, to assess the efficacy of CQ or MLi-2) the Student's *t*-test, two-tailed for unpaired data, was used. Statistical significance was set at $p < 0.05$.

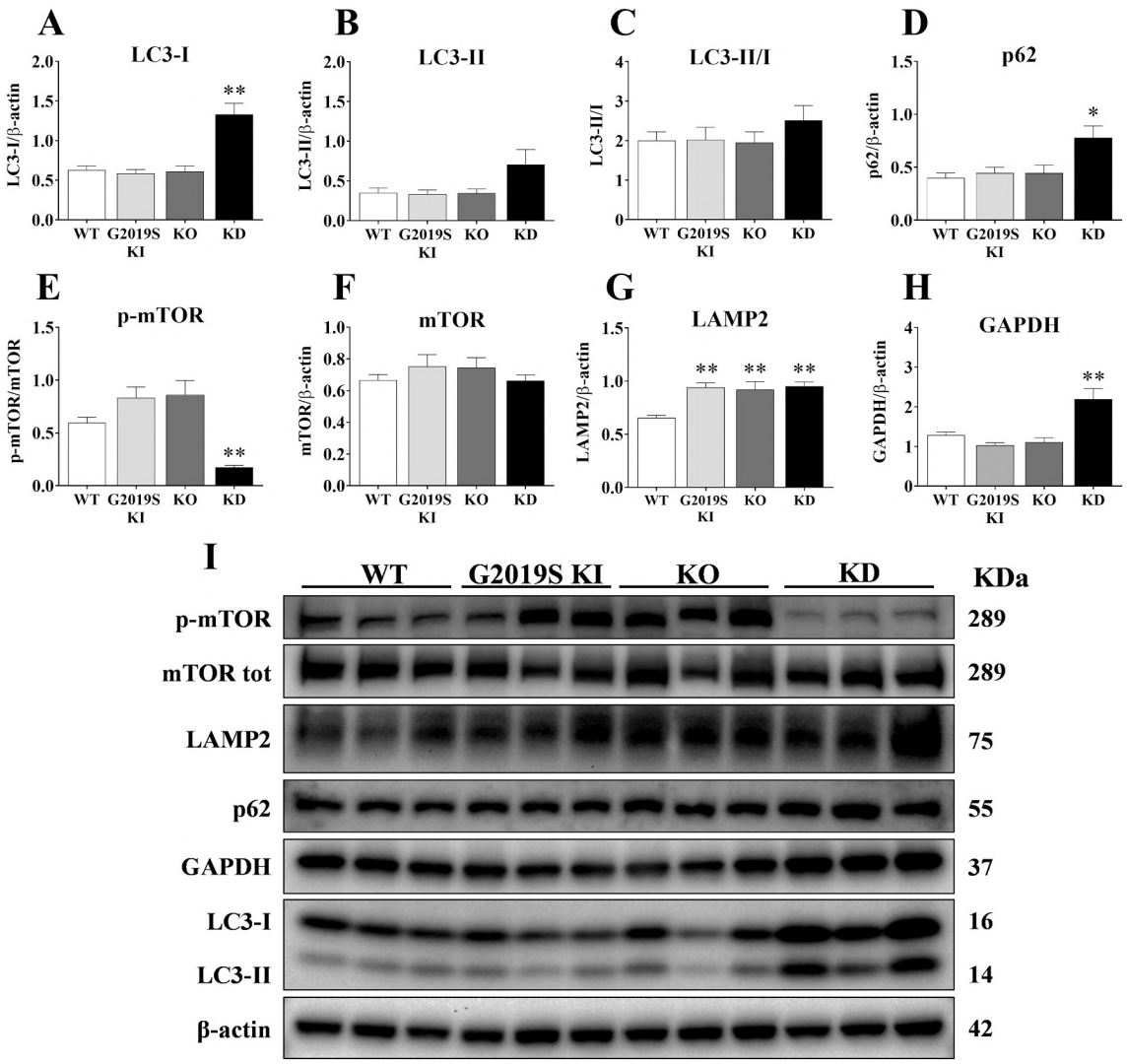

Fig. 1. Immunoblot analysis of autophagy-lysosomal pathway (ALP) markers in 12-month-old LRRK2 mice. Striatum lysates from 12-month-old WT, G2019S KI, KO and KD mice. Semi-quantitative analysis of macroautophagy markers levels: LC3-I (A), LC3-II (B), LC3-II/I (C), p62 (D), p-mTOR (normalized to total mTOR) (E) and total mTOR (F). Semi-quantitative analysis of lysosomal and CMA marker levels: LAMP2 (G) and GAPDH (H). Representative immunoblots of ALP markers in 12-month-old LRRK2-mutant mice (I). β-actin was used as housekeeping protein. Data are mean ± SEM of 8 mice per group and were analyzed using one-way ANOVA followed by the Bonferroni's test for multiple comparisons. *$p < 0.05$, **$p < 0.01$ different from WT mice.

3. Results

3.1. Effect of aging on expression of ALP markers in LRRK2 mice

To evaluate whether age-related dysfunction in striatal macroautophagy and CMA machineries is associated with LRRK2 kinase activity, WB analysis was performed in striatal tissues from 3, 12 and 20-month-old G2019S KI, KO, KD and WT mice. No marker changes across genotypes were observed in 3-month-old mice (Fig. S1). Conversely, changes of LC3-I ($F_{3,28} = 18.03$, $p < 0.0001$; Fig. 1A), LC3-II ($F_{3,28} = 2.85$, $p = 0.055$; Fig. 1B), p62 ($F_{3,20} = 5.37$, $p = 0.0071$; Fig. 1D), p-mTOR ($F_{3,28} = 12.94$, $p < 0.0001$; Fig. 1E), LAMP2 ($F_{3,28} = 8.50$, $p = 0.0004$; Fig. 1G) and GAPDH ($F_{3,20} = 11.69$, $p = 0.0001$; Fig. 1H) were detected in 12-month-old mice. KD mice showed a ~2-fold increase in the abundancy of LC3-I and p62, an 80% elevation of LC3-II and a 72% reduction of p-mTOR with respect to controls. This was associated with an increase of lysosomal marker LAMP2 (+46%) and CMA marker GAPDH (+70%). As far as KO and G2019S KI mice were concerned, a 45% increase of LAMP2 levels was only observed. As AMPK is a functional antagonist of mTOR and promotes autophagy in most systems, AMPK levels were investigated in 12-month-old mice (Fig. S2). AMPK levels were significantly affected across genotypes ($F_{3,20} = 3.62$, $p = 0.0308$), being a 50% elevation observed in KD mice.

Immunoblot analysis at 20 months (Fig. 2) showed significant changes of LC3-II ($F_{3,20} = 5.49$, $p = 0.0065$; Fig. 2B), p62 ($F_{3,20} = 8.53$, $p = 0.0008$; Fig. 2D), p-mTOR ($F_{3,20} = 8.91$, $p = 0.0006$; Fig. 2E), mTOR ($F_{3,20} = 22.28$, $p < 0.0001$; Fig. 2F) and LAMP2 ($F_{3,20} = 4.93$, $p = 0.0100$; Fig. 2G) across genotypes. Again, KD mice were most affected, showing increases of LC3-II (+30%), p62 (+80%) and mTOR (+95%) levels along with a 50% reduction of p-mTOR levels. At variance with that observed in younger mice, significant elevations of p62 (+47%), mTOR (+73%) and LAMP2 (+30%) levels were found in KO mice. Conversely, no changes in macroautophagy or lysosomal markers were observed in G2019S KI mice. To investigate whether the increase of mTOR corresponded to an increase of its activity, the phosphorylation levels of the mTOR substrate, S6K1 were investigated (Fig. S3). No changes in p-S6K1 and S6K1 levels were found (Fig. S3B, C). p-AMPK and AMPK levels were also investigated (Fig. S3D, E). Only p-AMPK levels were significantly affected across genotypes ($F_{3,20} = 6.93$, $p = 0.0022$). Both KO and KD mice showed marked increases (+443% and +

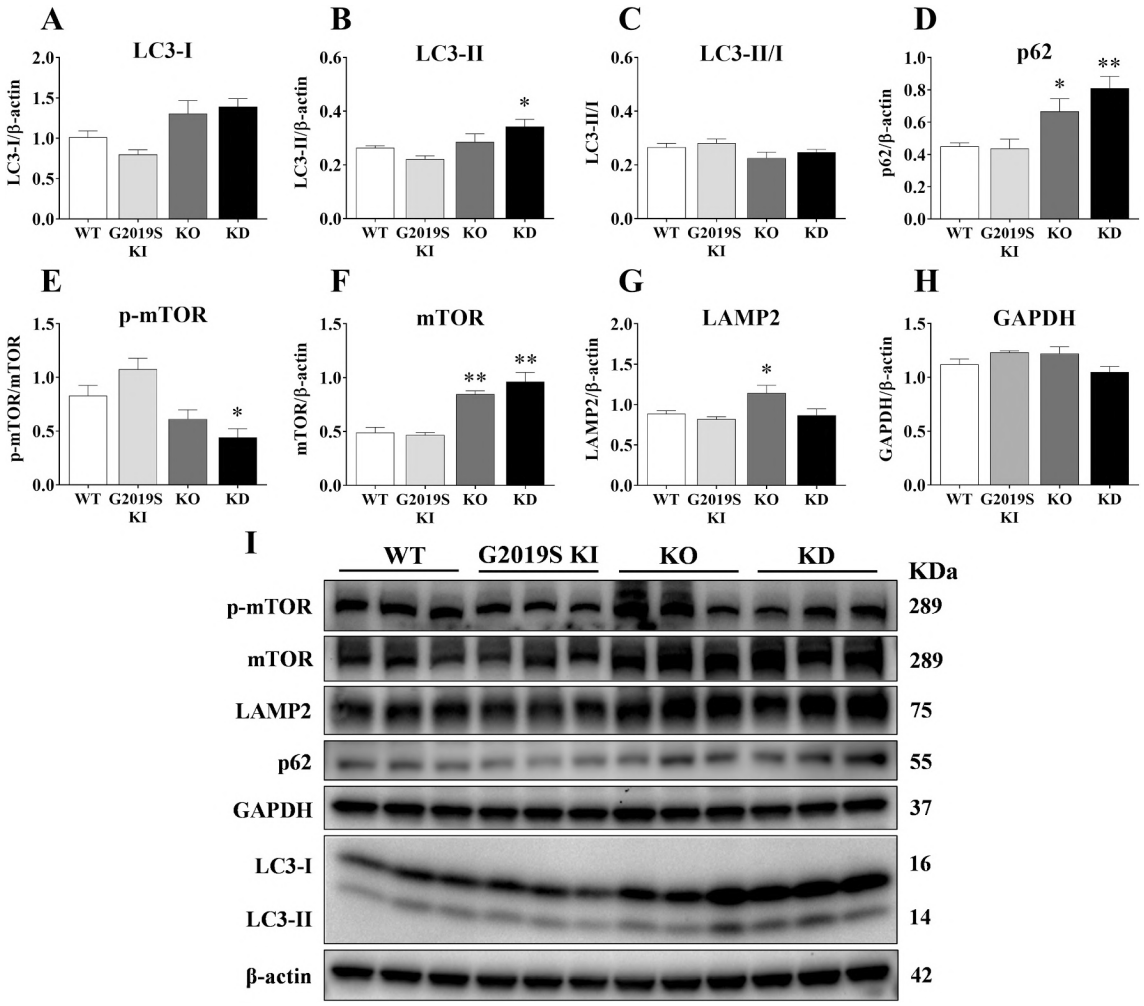

Fig. 2. Immunoblot analysis of autophagy-lysosomal pathway (ALP) markers in 20-month-old LRRK2 mice. Striatum lysates from 20-month-old WT, G2019S KI, KO and KD mice. Semi-quantitative analysis of macroautophagy marker levels: LC3-I (A), LC3-II (B), LC3-II/I (C), p62 (D), p-mTOR (normalized to total mTOR) (E) and total mTOR (F). Semi-quantitative analysis of lysosomal and CMA marker levels: LAMP2 (G) and GAPDH (H). Representative immunoblots of ALP markers in 20-month-old LRRK2-mutant mice (I). β-actin was used as housekeeping protein. Data are mean ± SEM of 8 mice per group and were analyzed using one-way ANOVA followed by Bonferroni's test for multiple comparisons. *$p < 0.05$; ** $p < 0.01$ different from WT mice.

300% respectively), being this effect just above the limit of significance in KD mice ($p = 0.059$).

3.2. Gene expression analysis of autophagy-related markers at 12 months

To investigate whether changes in protein levels correlated with changes in gene expression, RT-qPCR was performed in striatal extracts from 12-month-old mice (Fig. 3). Changes were observed in mRNA levels of *MAP1LC3B* ($F_{3,28} = 5.23$, $p = 0.0054$; Fig. 3A), *LAMP2* ($F_{3,27} = 13.44$, $p < 0.0001$; Fig. 3C), *mTOR* ($F_{3,28} = 5.39$, $p = 0.0047$; Fig. 3D) and *TFEB* ($F_{3,28} = 3.40$, $p = 0.0315$; Fig. 3E) whereas mRNA levels of *p62* were unaffected (Fig. 3B). KD mice showed a ~20% reduction of *mTOR* and *TFEB* mRNA whereas KO mice a 20% reduction of *MAP1LC3B* mRNA. Conversely, G2019S KI mice appeared largely impaired at transcriptional level due to the significant ~20% downregulation of *MAP1LC3B*, *LAMP2, TFEB* and *mTOR* gene transcripts.

3.3. Autophagic flux assessment in LRRK2 KD mice at 12 months of age

The lysosomotropic autophagy inhibitor CQ was employed to determine whether the LC3-I and LC3-II changes were due to increased or impaired ALP (Klionsky et al., 2021). To validate the administration protocol, CQ (50 mg/Kg, i.p.) (Vodicka et al., 2014) was administered daily for three consecutive days in 3-month-old WT mice, and animals were sacrificed 24 h after the last injection (Fig. S4A). A significant ~30% increase was found in LC3-II levels (df = 10, $t = 2.88$, $p = 0.0165$) and LC3-II/I ratio (df = 10, $t = 2.44$, $p = 0.0350$), which is considered an index of effective blockage of autophagosome-lysosome fusion (Fig. S4A) (Klionsky et al., 2021). CQ treatment did not alter the levels of other macroautophagy or lysosomal markers, such as p62, LAMP2, p-mTOR and mTOR in 3-month-old WT mice (Fig. S4B). The same protocol was then applied to assess the autophagic flux in 12-month-old WT, G2019S KI, KO and KD mice (Fig. S4C). CQ administration significantly reduced the levels of LC3-I (−60%, df = 10, $t = 4.20$, $p = 0.0018$), LC3-II (−80%, df = 10, $t = 5.70$, $p = 0.0002$) and p62 (−40%, df = 10, $t = 3$, $p = 0.0065$) in KD mice (Fig. S4C), and elevated LC3-I levels in WT (+60%; df = 10, $t = 3$, $p = 0.0107$) and G2019S KI (+110%; df = 10, $t = 3$, $p = 0.0110$) mice (Fig. S4C). However, the LC3-II/I ratio was significantly reduced by ~40% in G2019S KI (df = 10, $t = 6.11$, $p = 0.0001$), KO (df = 10, $t = 5.22$, $p = 0.0004$), KD (df = 10, $t = 4.66$, $p = 0.0009$) and WT (df = 10, $t = 10$, $p = 0.0040$) mice, suggesting an impairment of the autophagic flux in all genotypes (Fig. S4C). This was accompanied by a consistent elevation of p-mTOR levels across all CQ-treated LRRK2 mutants, that was most dramatic in KD mice: G2019S KI (+150%, df = 10, $t = 2.55$, $p = 0.0288$), KO mice (+110%, df = 10, $t = 3.72$, $p = 0.0040$), KD mice (+1630%; df = 10, $t = 3.74$, $p = 0.0038$). KD mice also

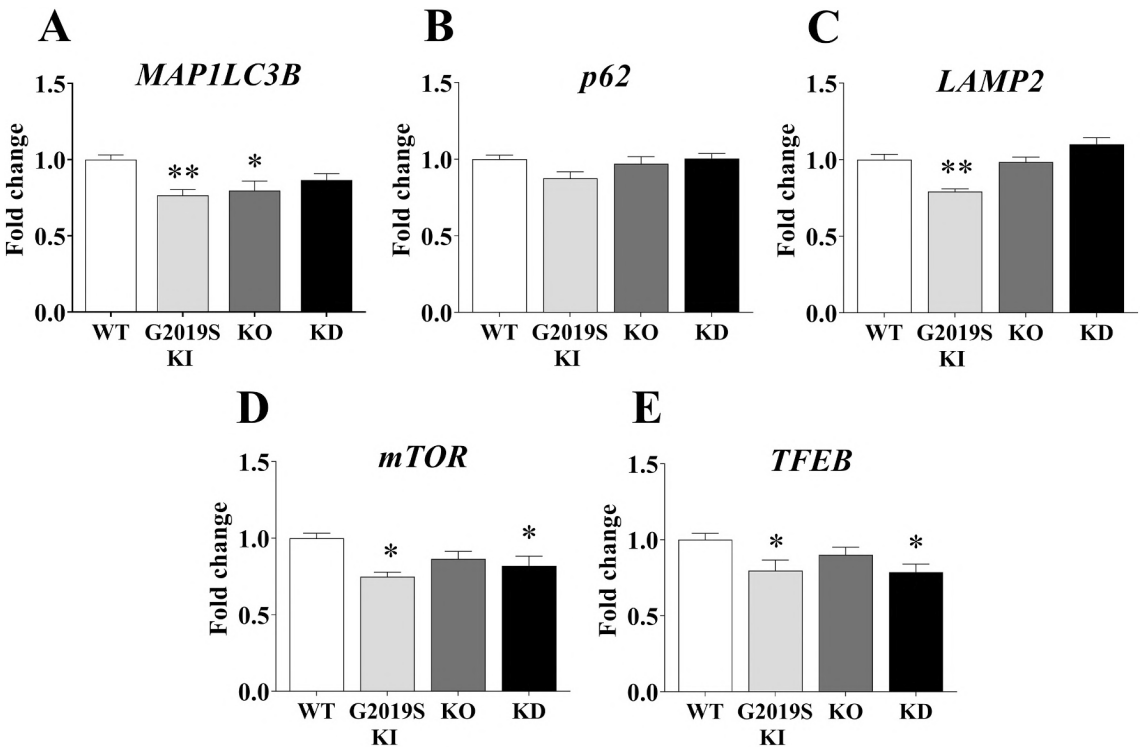

Fig. 3. RT-qPCR analysis of autophagy-related gene expression in 12-month-old LRRRK2 mice. RNAs were isolated from striatal tissue of 12-month-old WT, G2019S KI, KO and KD mice. RT-qPCR analysis was performed to analyze the mRNA expression levels of *MAP1LC3B* (A), *p62* (B), *LAMP2* (C), *mTOR* (D), *TFEB* (E) among genotypes. *ACTB* and *HPRT* were used as reference genes (Gong et al., 2016). Data are mean ± SEM of 8 mice per genotype. Statistical analysis was performed using one-way ANOVA followed by the Dunnett's test for multiple comparison. *$p < 0.05$, **$p < 0.01$ different from WT mice.

showed a 60% reduction of mTOR levels (df = 10, $t = 3.41$, $p = 0.0066$). LAMP2 levels were found 57% elevated only in WT mice after CQ treatment (df = 10, $t = 3$, $p = 0.0096$; Fig.S4C). These results, in particular the lack of an increase of LC3-II and LC3-II/I ratio in CQ-treated WT mice, led us to hypothesize that these changes were due to a tardive feedback mechanism occurring in all genotypes as a consequence of the CQ-mediated blockage of the autophagic flux, as previously reported in WT mice (Vodicka et al., 2014). Therefore, CQ administration was replicated anticipating immunoblot analysis at 4 h after the last CQ injection, *i.e.* when the ALP blockage is still effective. This new administration protocol was performed only in 12-month-old KD mice, *i.e.* the only genotype showing alterations in LC3-I and LC3-II levels. At this time-point, LC3-I levels were unchanged (Fig. 4A) whereas LC3-II levels (df = 10, $t = 5.63$, $p = 0.0002$; Fig. 4B) and the LC3-II/I ratio (df = 10, $t = 10.35$, $p < 0.0001$; Fig. 4C) were 2.5-fold elevated in WT mice, likely due to the inhibition of autolysosome formation. Conversely, CQ-treated KD mice exhibited a 30% reduction of LC3-II levels (df = 10, $t = 2.31$, $p = 0.0432$) and LC3-II/I ratio (df = 10, $t = 2.61$, $p = 0.0258$), indicating a defective autophagic flux (Fig. 4B, C). Consistently, the cargo protein p62 accumulated in CQ-treated WT mice (+78%, df = 10, $t = 4.30$, $p = 0.0016$) but not in KD mice (Fig. 4D). Conversely, p-mTOR levels were elevated by 2.5-fold in WT mice (df = 10, $t = 6.32$, $p < 0.0001$) and by 12-fold in KD mice (df = 10, $t = 19.57$, $p < 0.0001$; Fig. 4E) suggesting a marked mTOR activation in both genotypes. This enhancement of mTOR activation was coupled to a 44% reduction in total mTOR levels in KD mice (df = 9, $t = 4.18$, $p = 0.0024$; Fig. 4F). LAMP2 levels were elevated by CQ administration in both WT (+28%, df = 10, $t = 2.60$, $p = 0.0265$) and KD mice (+52% df = 10, $t = 5.89$, $p = 0.0002$; Fig. 4G).

3.4. Changes in GCase activity and GBA1 expression in LRRK2 mice

Since data pointed to a reduced autophagic flux in KD mice, we investigated whether also the activity of lysosomal GCase was affected in LRRK2 mice (Fig. 5). Significant changes were observed both at 3 months ($F_{3,20} = 8.46$, $p = 0.0008$; Fig. 5A) and 12 months ($F_{3,24} = 14.97$, $p < 0.0001$; Fig. 5B). When compared to WT controls, KD mice showed an enhancement at both ages (+80% and + 32%, respectively) whereas KO mice only at 12 months (+47%), although such increase was significant when the comparison was made against 3-month-old G2019S KI mice ($p < 0.05$). Conversely, no changes of GCase activity were detected in G2019S KI mice. RT-qPCR analysis interrogated whether changes in GCase activity were accompanied by changes of *GBA1* transcript levels in 12-month-old LRRK2-mutant mice. No significant change in *GBA1* gene expression was detected across genotypes ($F_{3,28} = 2.45$, $p = 0.0844$; Fig. 5C) although a tendency towards a reduction (15%) was observed in G2019S KI mice.

3.5. Subacute pharmacological inhibition of LRRK2 kinase activity

To test whether pharmacological LRRK2 kinase inhibition replicates the ALP impairment associated with the constitutive kinase silencing *in vivo*, MLi-2, a potent and brain penetrant LRRK2 kinase inhibitor, was administered subacutely for 7 days in 12-month-old WT and G2019S KI mice. Levels and expression of macroautophagy and lysosomal markers were evaluated 4 h after the last injection. Target engagement was confirmed by immunoblot analysis of pSer1292 LRRK2 levels, a readout of LRRK2 kinase activity (Kluss et al., 2018), in G2019S KI mice. In a pilot experiment, 10 mg/Kg (i.p.) b.i.d. for 7 days was administered, since this protocol was well tolerated in 3-month-old mice (unpublished data). After a few doses, however, lethality was observed in some 12-month-old mice of both genotypes prompting us to lower the dosage to 5 mg/Kg (i.p.), once a day for 7 days. Under these conditions, no signs of distress or mortality were noticed. WB analysis revealed a 42% reduction of pSer1292 LRRK2 levels in G2019S KI mice (Fig. S5), indicating effective targeting of LRRK2 *in vivo*. MLi-2 caused a 50% elevation

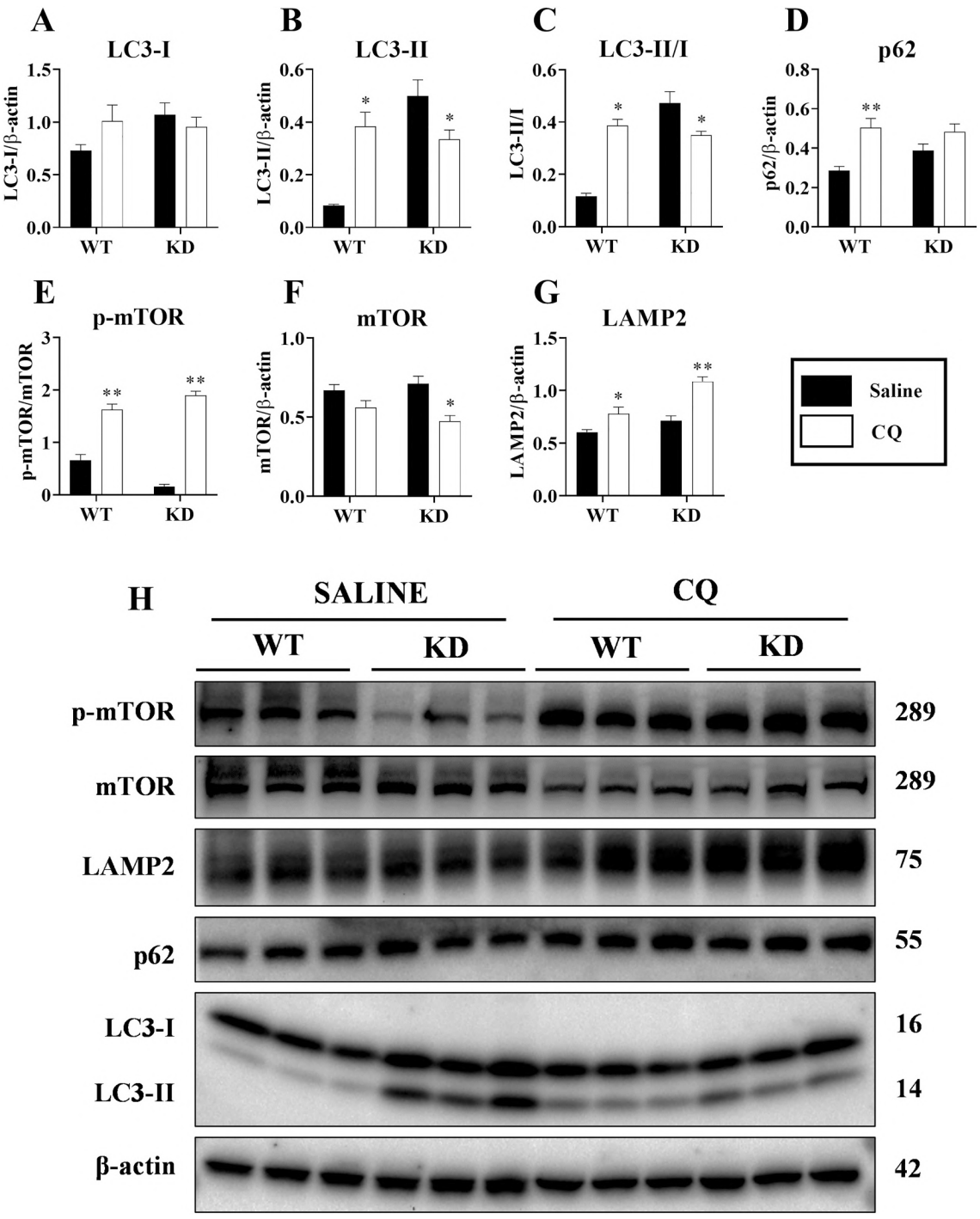

Fig. 4. Autophagic flux assessment in 12-month-old WT and KD mice. Semi-quantitative analysis of macroautophagy marker levels: LC3-I (A), LC3-II (B), LC3-II/I (C), p62 (D), p-mTOR (normalized to total mTOR) (E) and total mTOR (F). Semi-quantitative analysis of lysosomal marker levels LAMP2 (G). Representative immunoblots of macroautophagy and lysosomal markers ($n = 6$) after CQ and saline administration (H). β-actin was used as housekeeping protein. Data are mean ± SEM. Statistical analysis was performed using Student's *t*-test, two-tailed for unpaired data. *$p < 0.05$, **$p < 0.01$ different from saline-treated mice.

of LC3-I in WT mice (df = 10, $t = 2.35$, $p = 0.00406$) but not in G2019S KI mice, and no changes in LC3-II or LC3-II/I ratio in both genotypes (Fig. 6A). p62 levels were elevated in both WT and G2019S KI mice, although the increase was significant only in G2019S KI mice (+80%, df = 10, $t = 2.52$, $p = 0.0303$) whereas LAMP2 levels remained unaffected (Fig. 6A). Interestingly, p-mTOR was reduced by ~32% (df = 10, $t = 2.58$, $p = 0.00272$) and mTOR levels enhanced by ~30% (df = 10, $t = 2.51$, $p = 0.0306$; Fig. 6A) in G2019S KI mice, whereas no changes were observed in WT mice. RT-qPCR analysis showed that MLi-2 increased *MAP1LC3B* (+35%, df = 10, $t = 2.62$, $p = 0.00257$), and reduced *mTOR* (−25%, df = 10, $t = 3.66$, $p = 0.0044$) and *TFEB* (−20%, df = 10, $t = 2.71$, $p = 0.00218$) transcripts in WT mice (Fig. 6B). Moreover, MLi-2 reduced *mTOR* transcripts in G2019S KI mice (−25%, df = 10, $t = 3.86$, $p = 0.0032$) and left unaffected *p62* and *LAMP2* transcript levels in both genotypes (Fig. 6B).

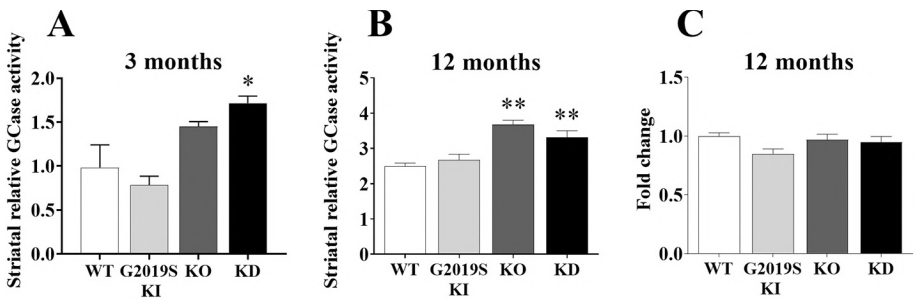

Fig. 5. Relative striatal GCase activity in 3 and 12-month-old LRRK2 mice. Striatal tissue lysates isolated from 3-month-old (A) and 12-month-old (B) WT (n = 6–8), G2019S KI (n = 6–8), KO (n = 6) and KD (n = 6) mice were used to measure relative GCase activity. Striatal *GBA1* gene expression was assessed ($n = 8$) at 12 months (C). *ACTB* and *HPRT* were used as reference genes for RT-qPCR analysis. Data are mean ± SEM of n mice per group. For GCase activity assay, data were analyzed using one-way ANOVA followed by Bonferroni's test for multiple comparisons. $^{*}p < 0.05$, $^{**}p < 0.01$ different from WT mice. For RT-qPCR analysis, data were analyzed using one-way ANOVA followed by the Dunnett's test for multiple comparison. $^{*}p < 0.05$, $^{**}p < 0.01$ different from WT mice.

3.6. Immunofluorescence analysis of LC3B puncta and pSer129 α-syn in striatum and SN

We previously reported accumulation of pSer129 α-syn soluble forms in the striatum and SN of 12-month-old G2019S KI mice (Novello et al., 2018). To investigate whether changes in ALP markers were associated with significant increase of neuronal pSer129 α-syn inclusions, immunofluorescence analysis in the striatum and SN of 12-month-old WT, KD, KO and G2019S KI mice was carried out (Fig. 7). Significant changes in LC3B puncta were observed across genotypes ($F_{3,28} = 5.40$, $p = 0.0046$). Consistent with the increase in LC3-I and LC3-II detected by WB analysis, LC3B puncta were more abundant (+78%) in striatal MAP2^{+} neurons of KD mice compared to WT mice (Fig. 7A, B) whereas no alterations were observed in KO or G2019S KI mice. On the contrary, pSer129 α-syn signal was elevated in striatal MAP2^{+} neurons of G2019S KI mice (+60%) but not KD and KO mice ($F_{3,28} = 3.68$, $p = 0.0237$) (Fig. 7A, C). LC3B changes were also detected in TH+ neurons of SN ($F_{3,29} = 12.47$, $p < 0.0001$), with KD and KO mice showing an increase (2.5-fold and 2-fold, respectively) and G2019S KI mice no change (Fig. 7D, E). However, no changes in pSer129 α-syn signal were observed in TH+ neurons across genotypes (Fig. 7F).

4. Discussion

This study aimed at investigating the role of LRRK2 in the modulation of striatal autophagy and lysosomal function *in vivo*, its kinase- and age-dependence, and relation with pSer129 α-syn inclusions in striatal and nigral neurons, using mice bearing enhanced or silenced LRRK2 kinase activity, or devoid of the full LRRK2 protein. The major finding is that constitutive silencing of LRRK2 kinase activity is associated with deregulation of GCase activity and age-dependent impairment of the autophagic flux (Fig. 8).

4.1. LRRK2 kinase silencing results in age-dependent inhibition of ALP in vivo

No differences in levels of macroautophagy and lysosomal markers were observed in the striatum of 3- month-old mice, supporting the hypothesis that no disruption of ALP machinery occurs early in life (Rubinsztein et al., 2011). Accordingly, no changes in the levels of Akt, mTOR and its substrate TSC2 were observed in the kidneys of 6-week-old G2019S KI, KO and KD mice (Herzig et al., 2011). Instead, LC3-I and the autophagosome-associated marker LC3-II (Mizushima et al., 2010) accumulated in the striatum of 12-month-old KD mice, along with LC3B-I and LC3B-II puncta in both striatal MAP2^{+} and nigral TH^{+} cells. Different lines of experimental evidence support the hypothesis that such changes reflect an impairment and not an upregulation of ALP in striatal neurons of aged mice carrying silenced LRRK2 kinase activity. First, CQ prevents lysosomal acidification causing blockage of autophagolysosome formation, and if ALP were normally active or even upregulated, an increase of LC3-II/I ratio would be expected after CQ administration (Vodicka et al., 2014), as indeed observed in WT mice. The reduction of LC3-II/I ratio, instead, indicates that CQ caused a further blockage of an already compromised autolysosome fusion step. Second, the selective autophagy receptor and autophagic clearance marker p62 accumulated in KD mice. Moreover, p62 levels were elevated in WT mice but unchanged in KD mice after CQ treatment. Third, the levels of *MAP1LC3B* and *p62* transcripts were unchanged in KD mice, suggesting that the increase of LC3-I, LC3-II and p62 protein levels was not associated with an increased synthesis, as it might be expected if autophagic flux were up-regulated. Moreover, *TFEB*, a promoter of autophagy and lysosome biogenesis (Sardiello et al., 2009; Settembre et al., 2013) was downregulated in KD mice.

If ALP is impaired in KD mice, the reduction of mTOR phosphorylated (*i.e.* active) form might reflect a compensatory mechanism to sustain a defective autophagic flux, since it is a negative regulator of ALP (Kim et al., 2011). This is also supported by the concurrent increase of AMPK levels in KD mice since AMPK and mTOR oppositely regulate the activity of the autophagy initiator ULK1 (Kim et al., 2011). The dramatic increase of p-mTOR levels in both WT and KD mice following CQ might thus reflect a general feedback mechanism aimed to inhibit ALP following lysosomal stress (Wang et al., 2018). Nonetheless, a similar reduction of p-mTOR in 20-month-old KD mice was not associated with a reduction of the phosphorylation of its substrate p-S6K1. Although we did not measure the phosphorylation levels of another mTOR substrate ElF4EBP1 and, therefore, we cannot rule out the possibility of a differential regulation, the present data would suggest that changes in mTOR phosphorylation do not translate in changes of mTOR activity. Thus, as pointed out by different *in vitro* (Manzoni et al., 2013; Manzoni et al., 2018) and *in vivo* (Herzig et al., 2011) studies it is possible that LRRK2 modulation of ALP occurs independently of mTOR, since mTOR is at the crossroad of signaling pathways involved in cellular survival, metabolism and homeostasis (Liu and Sabatini, 2020).

CMA also is likely inhibited in 12-month-old KD mice. In fact, the levels of both the lysosomal receptor LAMP2 and the CMA substrate GAPDH are elevated under basal conditions (each measure alone would not allow to draw any conclusion on CMA activity) (Cuervo et al., 2004; Kaushik and Cuervo, 2012) whereas *LAMP2* transcript levels were unchanged. These data point to lysosomal accumulation and impaired GAPDH clearance in striatum. The finding that CQ increased the striatal levels of LAMP2 in both WT and KD mice would confirm that blockade of autophagosome formation causes lysosomal overload.

At 20 months, KD mice still showed an accumulation of the macroautophagy markers LC3-II and p62, possibly confirming a long-lasting ALP impairment. This was coupled to a reduced phosphorylation of p-mTOR but not of its substrate p-S6K1, and an increase of the phosphorylated, active form of AMPK. LAMP2 and GAPDH were unchanged at this age, suggesting normalization of lysosomal activity. It is noteworthy that mild changes in ALP markers similar to those observed in KD mice, *i.e.* elevated p62 and mTOR levels associated with a slight reduction of p-mTOR levels, became evident in 20-month-old KO mice, suggesting a late ALP dysregulation also in mice devoid of LRRK2. This is

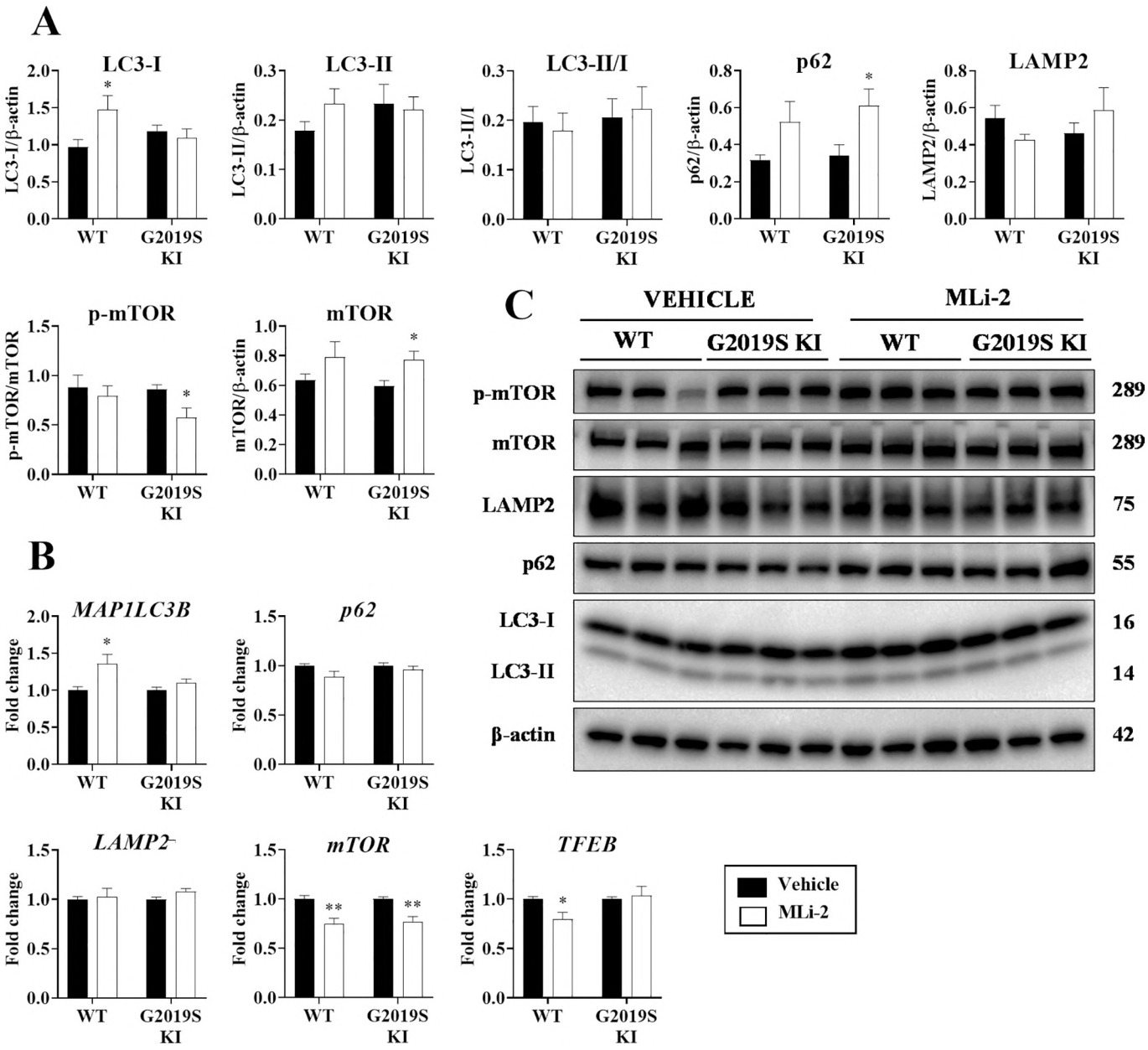

Fig. 6. Subacute pharmacological inhibition of LRRK2 kinase activity in 12-month-old WT and G2019S KI mice. Mice were subacutely administered with the LRRK2 kinase inhibitor MLi-2 (5 mg/Kg i.p., once daily for 7 days) and sacrificed 4 h after the last injection. A) Semi-quantitative analysis of macroautophagy markers (LC3-I, LC3-II, LC3-II/I ratio, p62, p-mTOR, mTOR) and lysosomal marker (LAMP2) levels, and representative immunoblots. B) RT-qPCR analysis of mRNA levels of *MAP1LC3B, p62, LAMP2, mTOR* and *TFEB* genes. β-actin was used as housekeeping protein and *ACTB* and *HPRT* were used as reference genes. Data are mean ± SEM of 6 mice per group. Protein levels were analyzed using one-way ANOVA followed by the Bonferroni's test for multiple comparisons $*p < 0.05$, $**p < 0.01$ different from saline-treated mice. Transcript levels were analyzed using one-way ANOVA followed by the Dunnett's test for multiple comparison. $*p < 0.05$, $**p < 0.01$ different from saline-treated mice.

in contrast with the lack of changes of ALP markers reported in the brain of 15-month-old LRRK2 KO mice (Giaime et al., 2017), although the different age at analysis might explain the inconsistency. Nonetheless, our data are in line with the striking age-dependent ALP and lysosomal impairment associated with kidney pathology, consistently reported in LRRK2 KO rodents *in vivo* (Baptista et al., 2013; Fuji et al., 2015; Herzig et al., 2011; Hinkle et al., 2012; Tong et al., 2012; Tong et al., 2010). The kidney pathology in KO mice, however, is characterized by an earlier onset and more severe course compared to the brain pathology. This might be due to the greater levels of LRRK2 expression in the kidney or to a LRRK1 compensatory role in the brain (Giaime et al., 2017). In fact, LRRK1 regulates autophagy in cooperation with LRRK2 (Toyofuku et al., 2015). LAMP2 levels were also significantly elevated in 20-month-old KO mice, although this was not associated with changes in GAPDH protein levels or *LAMP2* gene expression, making it impossible to draw any conclusion on the lysosomal homeostasis and CMA status in these animals. In contrast with the reduction of LC3-I and LAMP1 levels found in the cerebral cortex of 20-month-old G2019S KI mice (Schapansky et al., 2018) macroautophagy markers were unchanged in the striatum of G2019S KI mice, in line with that found in the basal ganglia of G2019S PD patients (Mamais et al., 2018). G2019S KI mice showed an increase of LAMP2 (but not GAPDH) levels at 12 months which is in partial agreement with the increase of striatal LAMP2 and GAPDH levels in aged R1441G KI mice that was proposed to reflect CMA impairment (Ho et al., 2020). The inconsistence of the GAPDH changes in the two studies might be related to the different LRRK2 mutation (Wallings et al., 2019).

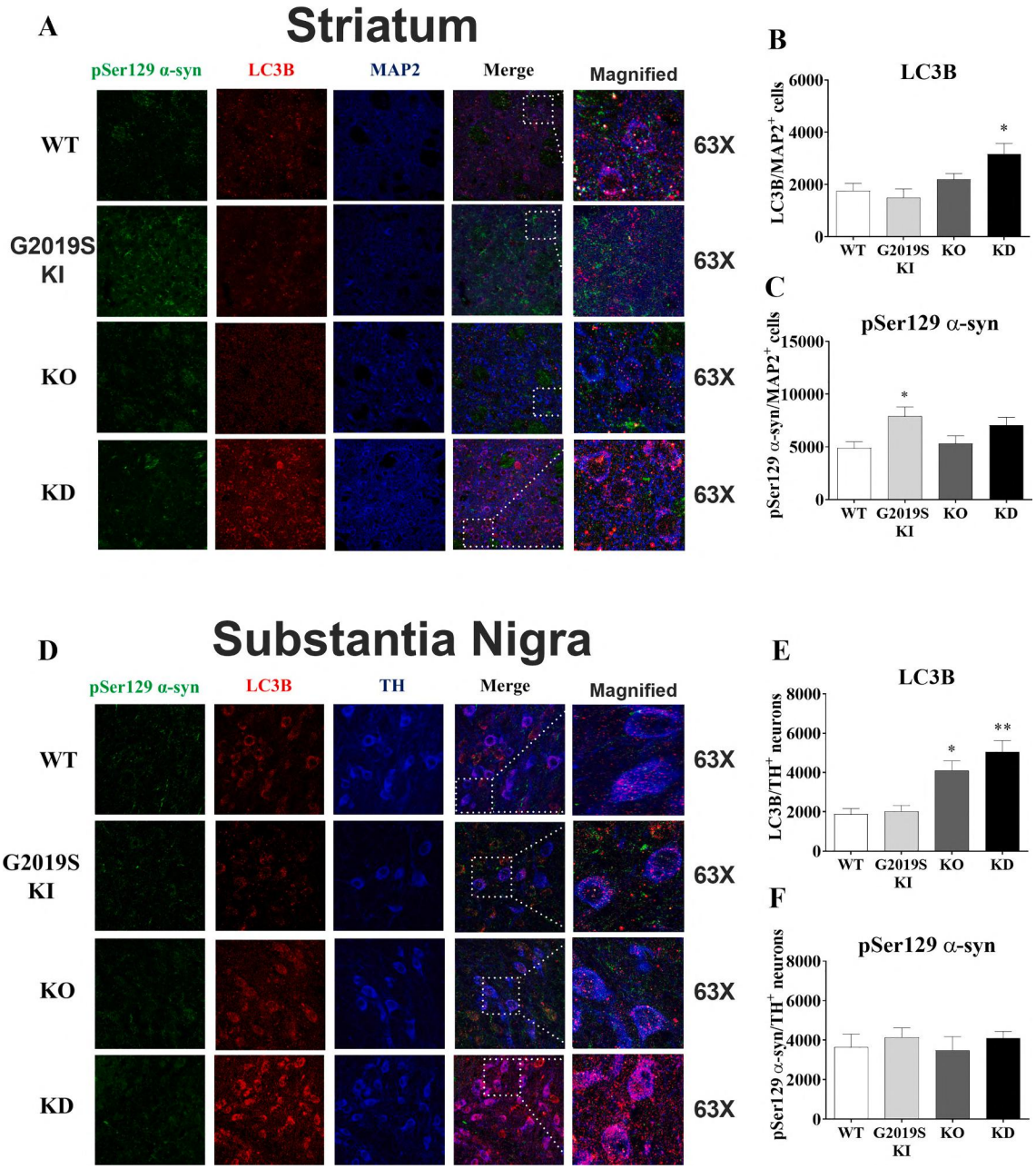

Fig. 7. Immunofluorescence analysis of LC3B puncta and pSer129 α-syn inclusions in striatal MAP2$^+$ and nigral TH$^+$ neurons of 12-month-old LRRK2 mice. A) Representative immunofluorescence images and quantification of B) LC3B expression and C) pSer129 α-syn inclusions in striatal MAP2$^+$ cells. D) Representative immunofluorescence images and quantification of E) LC3B expression and F) pSer129 α-syn inclusions in nigral TH$^+$ cells. Higher magnifications of insets drawn in merged images were also shown. The number of LC3B puncta was quantified within a mask image made by the TH or MAP2 staining. Data are mean ± SEM of 6–8 mice per group and were analyzed using one-way ANOVA followed by the Bonferroni's test for multiple comparisons. *$p < 0.05$, **$p < 0.01$ different from WT mice.

Nonetheless, significant downregulation of *MAP1LC3B*, *LAMP2*, *mTOR* and *TFEB* was observed in the striatum of 12-month-old G2019S KI mice possibly suggesting a defective transcription associated with compensatory post-translational regulation.

4.2. *LRRK2 inhibits GCase activity in vivo through its kinase function*

Consistent with the enhanced GCase hydrolytic activity in LRRK2 KO astrocytes (Ferrazza et al., 2016), the present study found elevated striatal GCase activity in LRRK2 KO and KD mice *in vivo*, indicating that striatal GCase activity is negatively regulated by LRRK2 kinase. Indeed, MLi-2 rescued the impairment of GCase activity in G2019S patient-derived fibroblasts and DA neurons (Ysselstein et al., 2019). According to this study, the increased enzymatic activity observed in both LRRK2 kinase-absent genotypes was not associated with changes of *GBA1* transcript, possibly suggesting a defective intracellular trafficking of GCase (Ysselstein et al., 2019). The lack of GCase changes in the striatum of G2019S KI mice (only a trend towards an inhibition was observed) might indicate that the inhibitory regulation is already maximal under physiological conditions so further increase of LRRK2 kinase activity associated with the G2019S mutation does not cause additional inhibition. Nonetheless, the mild reduction of *GBA1* expression observed in 12-month-old G2019S KI mice is consistent with that found in the human PD brain (Murphy et al., 2014). Elevated GCase activity was observed in 3-month-old and 12-month-old mice, suggesting that changes in lysosomal function precede changes of ALP markers observed

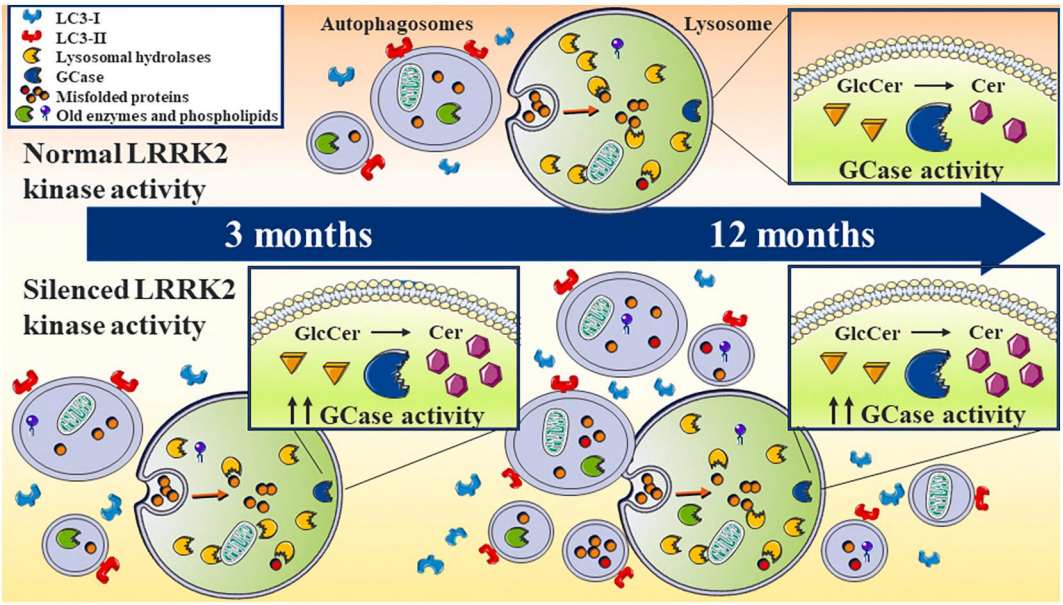

Fig. 8. Silencing LRRK2 kinase activity deregulates GCase activity and impairs the autophagy-lysosomal pathway in striatum during aging. Silencing LRRK2 kinase activity (or genetic deletion of LRRK2) results in an early (3 months of age) and sustained deregulation of the activity of the lysosomal hydrolase Glucocerebrosidase (GCase), accelerating the metabolism of Glucosylceramide (GlcCer) to Ceramide (Cer). Silencing LRRK2 kinase activity is also accompanied by a late (12 months) accumulation of autophagosomes and impaired autophagic flux.

in these genotypes.

4.3. Pharmacological inhibition of LRRK2 kinase activity

To investigate the impact of LRRK2 kinase inhibition on ALP under conditions of normal and enhanced kinase activity, subacute MLi-2 was administered in 12-month-old WT and G2019S KI mice. Aged mice were exquisitely sensitive to MLi-2 irrespective of genotype, since they did not tolerate high MLi-2 dosage causing profound inhibition of kinase activity (pSer1292 levels were reduced by ~80% in surviving G2019S KI mice, not shown). Under a safe MLi-2 dosage (associated with 42% reduction of striatal pSer1292 LRRK2), an increase of LC3-I levels and *MAP1LC3B* expression was observed in WT mice. G2019S KI mice were more affected showing an increase of p62 and mTOR and a reduction of p-mTOR levels along with a reduction of *mTOR* expression. In any genotype, subacute MLi-2 administration replicated the phenotype of 12-month-old KD mice, possibly due to adaptation phenomena accompanying constitutive silencing of LRRK2 kinase activity and/or the mild level of LRRK2 kinase inhibition achieved with the subacute protocol.

Various *in vitro* studies reported that LRRK2 kinase inhibitors, among which MLi-2, improve the autophagic flux or rescue the lysosomal defects associated with G2019S LRRK2 (Boecker et al., 2021; Manzoni et al., 2013; Obergasteiger et al., 2020; Saez-Atienzar et al., 2014; Schapansky et al., 2018; Wallings et al., 2019) whereas other showed the opposite (Schapansky et al., 2014). Our data cannot either support or confute this view, considering that elevation of p62 (not associated with changes of *p62* transcript) and reduction of *TFEB* transcript point to ALP blockade while the increase of LC3-I levels and expression suggest the opposite. Although sub-acute inhibition of LRRK2 kinase activity did not recapitulate the ALP deficits measured in 12-month-old KD mice, it can provide information on ALP targets regulated by endogenous LRRK2 control and, therefore, more sensitive to LRRK2 kinase inhibition. Indeed, the enhancement of LRRK2 kinase activity in G2019S KI mice brings mTOR function under a stronger LRRK2 control. LRRK2 inhibitors are currently under investigation as disease modifying agents in PD (Tolosa et al., 2020). Although our data cannot tell whether the MLi-2 toxicity observed in aged mice is LRRK2-related, they nonetheless confirm that dosage of LRRK2 inhibitors need to be carefully titrated in aged subjects to avoid profound inhibition of LRRK2 kinase function (Tolosa et al., 2020). Moreover, further studies are needed to ascertain the effects of long-term treatment with LRRK2 inhibitors on ALP function, particularly in aged animals.

4.4. Relationship between ALP impairment and pSer129 α-syn inclusions

Previous *in vivo* studies have shown α-syn oligomer appearance to be associated with CMA impairment in 18-month-old R1441G LRRK2 mice (Ho et al., 2020) or with autophagy impairment in 15-month-old LRRK double KO mice (Giaime et al., 2017) suggesting a link between ALP impairment and synucleinopathy. pSer129 α-syn inclusions can be viewed as an early index of synucleinopathy (Oueslati, 2016) since Ser129 phosphorylation increases the propensity of α-syn to aggregate and propagate (Samuel et al., 2016). Moreover, pSer129 α-syn co-stains with markers of Lewy body pathology in models of PD progression (Luk et al., 2012; Niu et al., 2018) and is highly enriched in Lewy Bodies (Anderson et al., 2006; Fujiwara et al., 2002). Based on previous findings that G2019S LRRK2 facilitated α-syn phosphorylation at Ser129 and nigrostriatal neurodegeneration (Novello et al., 2018; Volpicelli-Daley et al., 2016), the possibility that pSer129 α-syn inclusions were associated with ALP impairment was considered. We previously observed the development of soluble pSer129 α-syn inclusions in the striatum and SN *pars compacta* (SNc) of G2019S KI mice during aging (Longo et al., 2017; Novello et al., 2018). Here, we localize pSer129 α-syn inclusions in striatal $MAP2^+$ neurons, very likely GABAergic neurons since they represent by far (>95%) the most abundant striatal cell population (Gerfen, 1992). In line with immunoblot data, however, striatal G2019S neurons did not show altered LC3B puncta levels whereas striatal LRRK2 KD neurons showed increase in LC3B puncta but not in pSer129 α-syn inclusions. Thus, ALP impairment and pSer129 α-syn inclusions occur in different neuronal types. Based on this finding, we should conclude that the greater nigrostriatal degeneration observed in aged G2019S KI mice following virally-induced α-syn overload is due to neuronal ALP-independent mechanisms. However, there might not be a relation between pSer129 α-syn inclusions observed under basal conditions in G2019S KI mice and their enhanced susceptibility to parkinsonism. Indeed, a recent study showed that presynaptic pools of neuronal

pSer129 α-syn exist that are unrelated to Lewy Body pathology (Weston et al., 2021). This would suggest that striatal pSer129 α-syn inclusions observed in aged G2019S KI mice under basal conditions might have some bearing with the neuronal dysfunctions observed in these mice (Longo et al., 2017). On the other hand, it cannot be ruled out that the ALP impairment in KO mice also facilitates synucleinopathy in the presence of α-syn overload, due to the expected defective α-syn handling.

5. Conclusions

This study provides strong evidence that constitutive silencing of LRRK2 kinase activity results in early deregulation of GCase activity and late impairment of macroautophagy and lysosomal homeostasis (Fig. 8). Conversely, genetic deletion of LRRK2 is associated with early deregulation of GCase activity followed by an even more delayed ALP pattern reminiscent of ALP impairment, possibly indicating a contribution of LRRK2 scaffolding properties and GTPase activity or simply the loss of LRRK1 compensation. Expression of pathogenic G2019S mutation was not accompanied by changes of striatal macroautophagy markers but downregulation of key autophagy and lysosomal genes, as reported in the PD brain (Decressac et al., 2013). This might indicate that striatal ALP changes are unlike to contribute to G2019S synucleinopathy. This study contributes to shed light into the complex modulation exerted by LRRK2 over ALP *in vivo*, demonstrating that LRRK2 kinase activity is essential for a proper ALP function during aging.

Availability of supporting data

The datasets generated during and/or analyzed during the current study are available from the corresponding author on reasonable request.

Funding

This study was supported by the FAR 2020 grant from the University of Ferrara to M.M.

Declaration of Competing Interest

DRS is an employee of Novartis Pharma AG. The other authors report no competing financial interests.

Acknowledgements

N/A

Appendix A. Supplementary data

Supplementary data to this article can be found online at https://doi.org/10.1016/j.nbd.2021.105487.

References

Albanese, F., et al., 2019. Autophagy and LRRK2 in the aging brain. Front. Neurosci. 13, 1352.
Ambrosi, G., et al., 2015. Ambroxol-induced rescue of defective glucocerebrosidase is associated with increased LIMP-2 and saposin C levels in GBA1 mutant Parkinson's disease cells. Neurobiol. Dis. 82, 235–242.
Anderson, J.P., et al., 2006. Phosphorylation of Ser-129 is the dominant pathological modification of alpha-synuclein in familial and sporadic Lewy body disease. J. Biol. Chem. 281, 29739–29752.
Baptista, M.A., et al., 2013. Loss of leucine-rich repeat kinase 2 (LRRK2) in rats leads to progressive abnormal phenotypes in peripheral organs. PLoS One 8, e80705.
Berwick, D.C., et al., 2019. LRRK2 biology from structure to dysfunction: research progresses, but the themes remain the same. Mol. Neurodegener. 14, 49.
Boecker, C.A., et al., 2021. Increased LRRK2 kinase activity alters neuronal autophagy by disrupting the axonal transport of autophagosomes. Curr. Biol. 31, 2140–2154.
Boland, B., et al., 2018. Promoting the clearance of neurotoxic proteins in neurodegenerative disorders of ageing. Nat. Rev. Drug Discov. 17, 660–688.
Chiasserini, D., et al., 2015. Selective loss of glucocerebrosidase activity in sporadic Parkinson's disease and dementia with Lewy bodies. Mol. Neurodegener. 10, 15.
Cookson, M.R., 2010. The role of leucine-rich repeat kinase 2 (LRRK2) in Parkinson's disease. Nat. Rev. Neurosci. 11, 791–797.
Cookson, M.R., 2017. Mechanisms of mutant LRRK2 neurodegeneration. Adv. Neurobiol. 14, 227–239.
Cuervo, A.M., 2008. Autophagy and aging: keeping that old broom working. Trends Genet. 24, 604–612.
Cuervo, A.M., et al., 2004. Impaired degradation of mutant alpha-synuclein by chaperone-mediated autophagy. Science 305, 1292–1295.
Decressac, M., et al., 2013. TFEB-mediated autophagy rescues midbrain dopamine neurons from alpha-synuclein toxicity. Proc. Natl. Acad. Sci. U. S. A. 110, E1817–E1826.
Ferrazza, R., et al., 2016. LRRK2 deficiency impacts ceramide metabolism in brain. Biochem. Biophys. Res. Commun. 478, 1141–1146.
Fuji, R.N., et al., 2015. Effect of selective LRRK2 kinase inhibition on nonhuman primate lung. Sci. Transl. Med. 7, 273ra15.
Fujiwara, H., et al., 2002. alpha-synuclein is phosphorylated in synucleinopathy lesions. Nat. Cell Biol. 4, 160–164.
Galluzzi, L., et al., 2017. Pharmacological modulation of autophagy: therapeutic potential and persisting obstacles. Nat. Rev. Drug Discov. 16, 487–511.
Gan-Or, Z., et al., 2015. Genetic perspective on the role of the autophagy-lysosome pathway in Parkinson disease. Autophagy 11, 1443–1457.
Gegg, M.E., et al., 2012. Glucocerebrosidase deficiency in substantia nigra of parkinson disease brains. Ann. Neurol. 72, 455–463.
Gerfen, C.R., 1992. The neostriatal mosaic: multiple levels of compartmental organization. Trends Neurosci. 15, 133–139.
Giaime, E., et al., 2017. Age-dependent dopaminergic neurodegeneration and impairment of the autophagy-lysosomal pathway in LRRK-deficient mice. Neuron 96 (796–807), e6.
Gong, H., et al., 2016. Evaluation of candidate reference genes for RT-qPCR studies in three metabolism related tissues of mice after caloric restriction. Sci. Rep. 6, 38513.
Greggio, E., et al., 2006. Kinase activity is required for the toxic effects of mutant LRRK2/dardarin. Neurobiol. Dis. 23, 329–341.
Hellemans, J., et al., 2007. qBase relative quantification framework and software for management and automated analysis of real-time quantitative PCR data. Genome Biol. 8, R19.
Heo, H.Y., et al., 2010. LRRK2 enhances oxidative stress-induced neurotoxicity via its kinase activity. Exp. Cell Res. 316, 649–656.
Herzig, M.C., et al., 2011. LRRK2 protein levels are determined by kinase function and are crucial for kidney and lung homeostasis in mice. Hum. Mol. Genet. 20, 4209–4223.
Hinkle, K.M., et al., 2012. LRRK2 knockout mice have an intact dopaminergic system but display alterations in exploratory and motor co-ordination behaviors. Mol. Neurodegener. 7, 25.
Ho, P.W., et al., 2020. Age-dependent accumulation of oligomeric SNCA/alpha-synuclein from impaired degradation in mutant LRRK2 knockin mouse model of Parkinson disease: role for therapeutic activation of chaperone-mediated autophagy (CMA). Autophagy 16, 347–370.
Johnson, M.E., et al., 2019. Triggers, facilitators, and aggravators: redefining Parkinson's disease pathogenesis. Trends Neurosci. 42, 4–13.
Kaushik, S., Cuervo, A.M., 2012. Chaperone-mediated autophagy: a unique way to enter the lysosome world. Trends Cell Biol. 22, 407–417.
Kim, J., et al., 2011. AMPK and mTOR regulate autophagy through direct phosphorylation of Ulk1. Nat. Cell Biol. 13, 132–141.
Klionsky, D.J., et al., 2021. Guidelines for the use and interpretation of assays for monitoring autophagy (4th edition)(1). Autophagy 17, 1–382.
Kluss, J.H., et al., 2018. Detection of endogenous S1292 LRRK2 autophosphorylation in mouse tissue as a readout for kinase activity. NPJ Parkinson Dis. 4, 13.
Kluss, J.H., et al., 2019. LRRK2 links genetic and sporadic Parkinson's disease. Biochem. Soc. Trans. 47, 651–661.
Liu, G.Y., Sabatini, D.M., 2020. mTOR at the nexus of nutrition, growth, ageing and disease. Nat. Rev. Mol. Cell Biol. 21, 183–203.
Longo, F., et al., 2014. Genetic and pharmacological evidence that G2019S LRRK2 confers a hyperkinetic phenotype, resistant to motor decline associated with aging. Neurobiol. Dis. 71, 62–73.
Longo, F., et al., 2017. Age-dependent dopamine transporter dysfunction and Serine129 phospho-alpha-synuclein overload in G2019S LRRK2 mice. Acta. Neuropathol. Commun. 5, 22.
Luk, K.C., et al., 2012. Pathological alpha-synuclein transmission initiates Parkinson-like neurodegeneration in nontransgenic mice. Science 338, 949–953.
Madureira, M., et al., 2020. LRRK2: autophagy and lysosomal activity. Front. Neurosci. 14, 498.
Mamais, A., et al., 2018. Analysis of macroautophagy related proteins in G2019S LRRK2 Parkinson's disease brains with Lewy body pathology. Brain Res. 1701, 75–84.
Manzoni, C., Lewis, P.A., 2017. LRRK2 and autophagy. Adv. Neurobiol. 14, 89–105.
Manzoni, C., et al., 2013. Inhibition of LRRK2 kinase activity stimulates macroautophagy. Biochim. Biophys. Acta 1833, 2900–2910.
Manzoni, C., et al., 2018. mTOR independent alteration in ULK1 Ser758 phosphorylation following chronic LRRK2 kinase inhibition. Biosci. Rep. 38.
Mata, I.F., et al., 2006. LRRK2 in Parkinson's disease: protein domains and functional insights. Trends Neurosci. 29, 286–293.
Mauthe, M., et al., 2018. Chloroquine inhibits autophagic flux by decreasing autophagosome-lysosome fusion. Autophagy 14, 1435–1455.

Mercatelli, D., et al., 2019. Leucine-rich repeat kinase 2 (LRRK2) inhibitors differentially modulate glutamate release and Serine935 LRRK2 phosphorylation in striatal and cerebrocortical synaptosomes. Pharmacol. Res. Perspect. 7, e00484.
Mizushima, N., et al., 2010. Methods in mammalian autophagy research. Cell 140, 313–326.
Murphy, K.E., et al., 2014. Reduced glucocerebrosidase is associated with increased alpha-synuclein in sporadic Parkinson's disease. Brain. 137, 834–848.
Nalls, M.A., et al., 2014. Large-scale meta-analysis of genome-wide association data identifies six new risk loci for Parkinson's disease. Nat. Genet. 46, 989–993.
Niu, H., et al., 2018. Alpha-synuclein overexpression in the olfactory bulb initiates prodromal symptoms and pathology of Parkinson's disease. Transl. Neurodegener. 7, 25.
Novello, S., et al., 2018. G2019S LRRK2 mutation facilitates alpha-synuclein neuropathology in aged mice. Neurobiol. Dis. 120, 21–33.
Obergasteiger, J., et al., 2020. Kinase inhibition of G2019S-LRRK2 enhances autolysosome formation and function to reduce endogenous alpha-synuclein intracellular inclusions. Cell Death Dis. 6, 45.
Oueslati, A., 2016. Implication of alpha-synuclein phosphorylation at S129 in Synucleinopathies: what have we learned in the last decade? J. Parkinsons Dis. 6, 39–51.
Paxinos, G., Franklin, K.B.J., 2001. The Mouse Brain in Stereotaxic Coordinates. Academic Press, San Diego.
Plowey, E.D., Chu, C.T., 2011. Synaptic dysfunction in genetic models of Parkinson's disease: a role for autophagy? Neurobiol. Dis. 43, 60–67.
Poewe, W., et al., 2017. Parkinson disease. Nat. Rev. Dis. Prime. 3, 17013.
Rubinsztein, D.C., et al., 2011. Autophagy and aging. Cell 146, 682–695.
Saez-Atienzar, S., et al., 2014. The LRRK2 inhibitor GSK2578215A induces protective autophagy in SH-SY5Y cells: involvement of Drp-1-mediated mitochondrial fission and mitochondrial-derived ROS signaling. Cell Death Dis. 5, e1368.
Samuel, F., et al., 2016. Effects of serine 129 phosphorylation on alpha-synuclein aggregation, membrane association, and internalization. J. Biol. Chem. 291, 4374–4385.
Sardiello, M., et al., 2009. A gene network regulating lysosomal biogenesis and function. Science 325, 473–477.
Schapansky, J., et al., 2014. Membrane recruitment of endogenous LRRK2 precedes its potent regulation of autophagy. Hum. Mol. Genet. 23, 4201–4214.
Schapansky, J., et al., 2018. Familial knockin mutation of LRRK2 causes lysosomal dysfunction and accumulation of endogenous insoluble alpha-synuclein in neurons. Neurobiol. Dis. 111, 26–35.
Senkevich, K., Gan-Or, Z., 2020. Autophagy lysosomal pathway dysfunction in Parkinson's disease; evidence from human genetics. Parkinsonism Relat. Disord. 73, 60–71.
Settembre, C., et al., 2013. Signals from the lysosome: a control Centre for cellular clearance and energy metabolism. Nat. Rev. Mol. Cell Biol. 14, 283–296.
Sidransky, E., et al., 2009. Mutations in GBA are associated with familial Parkinson disease susceptibility and age at onset. Neurology 73, 1424–1425 (author reply 1425-6).
Smith, W.W., et al., 2006. Kinase activity of mutant LRRK2 mediates neuronal toxicity. Nat. Neurosci. 9, 1231–1233.
Tolosa, E., et al., 2020. LRRK2 in Parkinson disease: challenges of clinical trials. Nat. Rev. Neurol. 16, 97–107.
Tong, Y., et al., 2010. Loss of leucine-rich repeat kinase 2 causes impairment of protein degradation pathways, accumulation of alpha-synuclein, and apoptotic cell death in aged mice. Proc. Natl. Acad. Sci. U. S. A. 107, 9879–9884.
Tong, Y., et al., 2012. Loss of leucine-rich repeat kinase 2 causes age-dependent bi-phasic alterations of the autophagy pathway. Mol. Neurodegener. 7, 2.
Toyofuku, T., et al., 2015. Leucine-rich repeat kinase 1 regulates autophagy through turning on TBC1D2-dependent Rab7 inactivation. Mol. Cell. Biol. 35, 3044–3058.
Tsika, E., Moore, D.J., 2012. Mechanisms of LRRK2-mediated neurodegeneration. Curr. Neurol. Neurosci. Rep. 12, 251–260.
Vodicka, P., et al., 2014. Assessment of chloroquine treatment for modulating autophagy flux in brain of WT and HD mice. J. Huntington Dis. 3, 159–174.
Volpicelli-Daley, L.A., et al., 2016. G2019S-LRRK2 expression augments alpha-synuclein sequestration into inclusions in neurons. J. Neurosci. 36, 7415–7427.
Wallings, R., et al., 2019. LRRK2 interacts with the vacuolar-type H+-ATPase pump a1 subunit to regulate lysosomal function. Hum. Mol. Genet. 28, 2696–2710.
Wang, B., et al., 2018. Autophagy of macrophages is regulated by PI3k/Akt/mTOR signalling in the development of diabetic encephalopathy. Aging (Albany NY) 10, 2772–2782.
West, A.B., et al., 2005. Parkinson's disease-associated mutations in leucine-rich repeat kinase 2 augment kinase activity. Proc. Natl. Acad. Sci. U. S. A. 102, 16842–16847.
Weston, L.J., et al., 2021. Genetic deletion of polo-like kinase 2 reduces alpha-synuclein serine-129 phosphorylation in presynaptic terminals but not Lewy bodies. J. Biol. Chem. 100273.
Xilouri, M., et al., 2008. Alpha-synuclein degradation by autophagic pathways: a potential key to Parkinson's disease pathogenesis. Autophagy 4, 917–919.
Yao, C., et al., 2010. LRRK2-mediated neurodegeneration and dysfunction of dopaminergic neurons in a Caenorhabditis elegans model of Parkinson's disease. Neurobiol. Dis. 40, 73–81.
Ysselstein, D., et al., 2019. LRRK2 kinase activity regulates lysosomal glucocerebrosidase in neurons derived from Parkinson's disease patients. Nat. Commun. 10, 5570.
Yue, M., et al., 2015. Progressive dopaminergic alterations and mitochondrial abnormalities in LRRK2 G2019S knock-in mice. Neurobiol. Dis. 78, 172–195.